Spring 2001

Adsorption of Inorganic and Organic Ligands Onto Aluminum Hydroxide and Its Effect in Water Treatment

Peter Pommerenk
Old Dominion University

ADSORPTION OF INORGANIC AND ORGANIC LIGANDS ONTO ALUMINUM HYDROXIDE AND ITS EFFECT IN WATER TREATMENT

by

Peter Pommerenk
Dipl.Ing.(univ.), December 1989, Universität der Bundeswehr München
M.S., December 1996, Old Dominion University

A Dissertation Submitted to the Faculty of
Old Dominion University in Partial Fulfillment of the
Requirement for the Degree of

DOCTOR OF PHILOSOPHY

ENVIRONMENTAL ENGINEERING

OLD DOMINION UNIVERSITY
May 2001

Approved by:

Gary C. Schafran (Director)

William A. Drewry (Member)

John R. Donat (Member)

ABSTRACT

ADSORPTION OF INORGANIC AND ORGANIC LIGANDS ONTO ALUMINUM HYDROXIDE AND ITS EFFECT IN WATER TREATMENT

Peter Pommerenk
Old Dominion University, 2001
Director: Dr. Gary C. Schafran

The inorganic anions fluoride, sulfate, and orthophosphate are ubiquitous substances in aqueous environments. These chemicals are also applied in drinking water treatment processes where fluoridation, coagulation with sulfate-based metal salts, or the use of passivating corrosion inhibitors or sequestering agents is practiced. If these ions are present at elevated levels in raw waters or added in the treatment train at points other than directly before entering a finished water reservoir, they can exert a negative influence on the removal of particles and natural organic matter.

Although the water chemistry of these inorganic ions seems to be well understood, their potential effects on the surface chemistry of coagulated particles and their ability to compete with organic anions for aluminum hydrolysis products in water treatment has not received much attention.

In the present work, bench and pilot-scale studies were conducted that indicated that removal of particles and natural organic matter by coagulation with alum is substantially decreased when fluoride is present in the raw water or added at concentrations typically used in water treatment plants. The application of fluoride in this manner also resulted in a tenfold increase in finished water aluminum concentrations. Batch adsorption experiments and surface complexation modeling showed that fluoride does not directly impact particle charge suggesting that its primary influence is the ability to form soluble complexes with aluminum.

Although the batch adsorption experiments indicated that sulfate can compete with organic acids for adsorption to positively charged aluminum floc, jar tests did not yield conclusive evidence that this ion has a considerable influence on turbidity and natural or-

ganic matter removal. Sulfate primarily interacts with aluminum hydroxide by electrostatic attraction which has the beneficial effect of limiting the positive surface charge of aluminum hydroxide particles.

Orthophosphate was found to form negatively charged surface complexes on aluminum hydroxide and can thus affect particle charge and stability. It also competed strongly with organic matter for adsorption sites, where both fluoride and sulfate at similar concentrations did not have any perceptible influence.

A surface complexation model was developed from experimental data that enables prediction of the effects that inorganic and organic anions exert during coagulation with alum. The model simulated the effects of orthophosphate and fluoride well but overpredicted the influence of sulfate on the adsorption of organic acids to aluminum hydroxide.

ACKNOWLEDGMENTS

Grateful appreciation is expressed to my advisor, Dr. Gary Schafran, for his interest in my development and for providing invaluable guidance and encouragement throughout my graduate career at Old Dominion University.

I am also thankful to the members of my dissertation committee, Dr. William Drewry and Dr. John Donat, for reviewing this manuscript and for their valuable suggestions. Dr. Raymond Letterman at Syracuse University contributed worthy ideas for this research. Discussions with Dr. Tesfa Tekleab were also instrumental in this work.

I would like to thank Newport News Water Works for allowing me to utilize their pilot facility, and Mr. Randolph Hawkins for his assistance during the studies.

The financial support provided through departmental research assistantships, tuition scholarships, and funding by Dr. Robert Cushing at Carollo Engineers, P.C. is appreciated.

This dissertation is dedicated to my wife, Laura, and my sons, Sebastian and Alexander, without whose patience and sacrifice of valuable playtime, this work would not have been completed.

TABLE OF CONTENTS

LIST OF TABLES

LIST OF FIGURES

1. INTRODUCTION

1.1. Motivation

It has been more than two decades since it was discovered that organic substances in raw water supplies can form potentially carcinogenic compounds upon chlorination during the water purification process. Ever since, the focus on coagulation by researchers, regulators, engineers, and operators has shifted from primarily particle removal to a situation where the removal of natural organic matter (NOM), a poorly defined group of organic compounds that originate from the decay of plant and animal matter, is also a primary concern. Although the development of alternative treatment technologies to prevent disinfection by-product (DBP) formation has been rapid, the most popular and cost-effective choice to eliminate these DBP-precursors remains the coagulation process.

It has been well recognized that the application of metal salt coagulants, such as aluminum sulfate or ferric chloride, is an effective means of removing NOM. The need to optimize this process with regard to NOM removal resulted in "enhanced coagulation" requirements that were included in the 1994 proposed rule for DBPs and are now incorporated in the recently published final rule (U.S. Environmental Protection Agency, 1998). Concurrently, the water research community responded with numerous publications about the effectiveness of different coagulants for NOM-removal, ways to characterize natural organic substances, the development of empirical models to predict DBP-precursor removal, and several other related topics.

In a recent paper by Edwards (1997), a mathematical model was presented that allows prediction of total organic carbon (TOC) removal during coagulation in water treatment, requiring input of coagulant type and dose, treatment pH, raw water TOC, and UV-absorbance at 254 nm. This model was derived from fitting data to an empirical, nonlinear model. Such an approach is not without merit, as it may allow an estimate of NOM-removal, which can be helpful in preliminary engineering design and regulatory issues. However, this

*This document was typeset with LaTeX 2ε using the style of the journal *Water Research*. Bibliographical references were generated by BibTeX.

model has certain shortcomings when used as a research tool: Empirical models permit only little mechanistic interpretation of the underlying processes, and most importantly, they neglect the influence of source water characteristics and treatment parameters aside from those required for input. In addition, models that solely predict TOC removal cannot forecast the effects of raw water and treatment parameters on colloidal stability and thus the removal of particulate contaminants, which, despite the efforts to prevent DBP-formation, must remain a primary goal of water treatment.

Developing a mechanistic model that enables prediction of NOM and particle removal is a formidable task because the physicochemical treatment of natural waters is a highly complex process. This complexity arises not only from the variability in source water composition, but also from the multitude of process configurations and treatment conditions. However, it is possible to quantify certain effects in water treatment by applying well accepted theories and without the excessive use of fitting parameters. The work of Iyer (1984) provides a good example. Based on chemical equilibria that include surface complexation reactions and principles that govern colloid stability and aggregation kinetics, he developed a method to predict the effects of coagulant concentration on flocculation kinetics. Although his work covers only a small aspect of water treatment, it provides a framework to incorporate *any* chemical reaction with known thermodynamic constants. As such, it does not impose restrictions for simultaneously modeling the removal of organic substances by adsorption (i.e., surface complexation) and particle destabilization. If the data for verification were available, his model could also be used to study effects of physical variables, for example, temperature or mixing conditions.

There are numerous possibilities to expand on or complement research on fundamental processes in physicochemical water treatment with metal salt coagulants. One of the research opportunities that seem to have received little attention include the chemical interactions of substances other than organic matter with the coagulant. It it obvious that differences in the inorganic composition of a water have quantifiable effects on the treatment process (and NOM removal), if one realizes that the "master variable" pH essentially represents the concentration of the inorganic ligand OH^-. This work focused on the effects of some less "obvious" inorganic anions that may be present in the raw water or that are added

during the treatment process. Treatment chemicals that introduce potentially interfering ions to the water include, for example, lime (Ca^{2+}), hydrofluosilicic acid ($Si(OH)_4, F^-$), zinc orthophosphate (Zn^{2+}, PO_4^{3-}), and the metal salt coagulant itself (SO_4^{2-} for aluminum or ferric sulfate).

Research goals associated with this work include quantifying the effects of some inorganic anions in bench- and pilot scale studies and describing the basic mechanisms in terms of chemical reactions by applying chemical equilibrium models to data collected from carefully controlled laboratory experiments. It is hoped that this research will help provide a better understanding of the chemistry of conventional water treatment and that utilities, consultants, and researchers, who consider the use of alternative technologies, including various coagulation strategies, can utilize this knowledge to optimize the existing process to meet the desired treatment goals.

In the following sections, an overview of the physicochemical processes that control particle and NOM removal during coagulation and a review of literature relevant to this work is provided.

1.2. Overview of Metal Salt Coagulation

Coagulation is a suitable process to remove both particulate and dissolved contaminants from water. Although a distinction between "solid" (particulate) and "dissolved" can be made on the basis of thermodynamics, it is often difficult to practically determine because aquatic materials span a wide size spectrum and the separation of the phases is typically accomplished by filtration through a membrane of arbitrary size cutoff, e.g., 0.45 μm or 0.2 μm. This operational definition can lead to situations where, for example, large metal-organic complexes that can exhibit both solute and colloid characteristics are retained by the membrane, whereas true solids, e.g., colloidal oxides, pass.

Solids typically found in natural waters consist predominantly of inorganic particles, e.g., clays, metal oxides and carbonates, and organic colloidal matter of detrital origin, as well as living microorganisms. "Solid-phase" organic matter also includes organic molecules that are adsorbed to inorganic surfaces. Under conditions typical for natural waters, almost complete surface coverage can be expected for certain minerals (Davis, 1982). The "dis-

solved" portion of natural organic matter, determined by membrane separation, constitutes mainly organic macromolecules, including those that are complexed with metal cations.

Based on the distinction between dissolved and solid contaminants, the removal mechanisms in water treatment can be explained in terms of the solid-water interface and solution chemistry: When a metal salt coagulant is added to the water during the treatment process, the hydrated metal cation forms monomeric and possibly polymeric hydroxo complexes, and it precipitates as an amorphous metal hydroxide, when the pH-dependent solubility is exceeded. These various hydrolysis products have a tendency to attach to the inorganic and organic solids present in the water and destabilize these particles by surface charge neutralization or enmeshment in the precipitate. The chemically destabilized particles can then be removed by flocculation and solid-liquid separation (sedimentation or floatation) or direct filtration.

The removal of inorganic and organic materials from solution during coagulation with metal salt coagulants can be the consequence of different primary mechanisms. Randtke (1988) distinguished between precipitation and coprecipitation of molecules and further defines different modes of coprecipitation, namely, isomorphic and nonisomorphic inclusion, occlusion, and surface adsorption. Direct precipitation leads to the formation of insoluble complexes, e.g. $AlPO_4(s)$ (Hsu, 1975) or basic aluminum humates and fulvates (Hall and Packham, 1965). This is believed to be a predominant process at pH$<$ 5 (Randtke, 1988). Coprecipitation by inclusion and occlusion can be thought of as the formation of a mixed salt/hydroxide or solid solution, e.g., $Al(H_xPO_4)_y(s)$ (Hayden, 1971). The latter processes and direct precipitation can be considered "three-dimensional" mechanisms, whereas the adsorption to a "preformed" surface is "two-dimensional" (Corey, 1981). These distinct mechanisms can potentially result in different removal efficiencies for dissolved substances, i.e., during the "three-dimensional" process, the contaminant anion may have access to more binding sites than during pure surface adsorption. However, there is considerable disagreement among researchers about the relative significance of these mechanisms.

1.3. Mechanisms of NOM-removal

The mechanisms that cause the removal of NOM from waters undergoing coagulation with metal salts can be explained based on the distinction that is made between dissolved and particulate organic matter as indicated previously. Dissolved organic carbon (DOC) is typically identified as the fraction that is smaller than 0.45 μm and generally accounts for 90% of the total organic carbon in natural waters (Thurman, 1985). A large fraction of the DOC consists of non-identifiable organic compounds (humic substances and hydrophilic acids) that contain many of the same functional groups (e.g. carboxylic, phenolic) as simple organic acids as shown in Figure 1.1. Carboxylic functional groups (–COOH) are found in almost all DOC, and they are completely deprotonated at the pH of most natural waters. Thus, they contribute aqueous solubility and acidity to the organic molecule and also provide sites for complexation of metal cations. Other important functional groups include the phenolic and hydroxyl groups (–OH) that also cause natural organic matter to behave similarly to simple organic acids with respect to ion exchange and complexation.

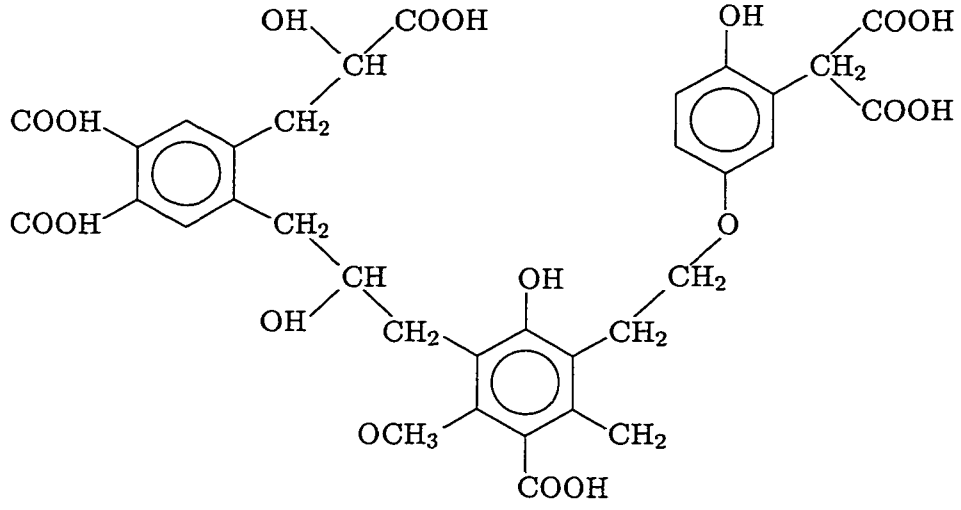

Figure 1.1. Functional groups on natural organic matter (Modified from Thurman (1985)).

The dissolved organic fraction is thought to be removed during coagulation by two general mechanisms: Adsorption to metal hydroxide floc or formation of insoluble metal

organic complexes. In early studies with humic and fulvic acids (Hall and Packham, 1965) it was suggested that the latter mechanism, i.e., precipitation of humates and fulvates, is dominant and observed over a wide pH range. They utilized aluminum chloride instead of alum in their work which may have caused the formation of polymeric aluminum species. These highly charged cations are known to exhibit different coagulating behavior than alum precipitates (Van Benschoten and Edzwald, 1990a). Narkis and Rebhun (1977) also suggested that humic and fulvic acids are precipitated by cationic aluminum species, whereas Semmens and Fields (1980) were able to explain their data only in terms of an adsorption mechanism. Jekel (1986) states that interactions of humic acid and aluminum salts at neutral pH are primarily a surface complexation on in situ formed $Al(OH)_3$. Randtke (1988) proposed a compromise, indicating that both mechanisms may operate but are restricted to different pH regions and also depend on the whether the organic material is in true solution or in colloidal form. He also noted that NOM molecules do not have the proper size and chemical characteristics to be incorporated in the lattice structure of the metal hydroxides and that they are most likely removed by adsorption to the surface of the precipitates as they form. Therefore, precipitation kinetics and transport may play an important role. Dempsey (1989) also entered the discourse and found that over a wide pH range the adsorption of fulvic acid to aluminum hydroxide is a much stronger reaction than the formation of aluminum fulvate complexes.

The importance of precipitate formation for NOM removal in water treatment has led to several studies, where the adsorption of organic substances onto preformed aluminum hydroxide was investigated. Mazet *et al.* (1990) conducted studies that consisted of mixing known amounts of humic or fulvic acid to alum coagulated kaolinite suspensions. Based on their ζ-potential measurements, these authors hypothesized that electrostatic interactions and a ligand exchange process occur simultaneously when humics adsorb to preformed floc. Julien *et al.* (1994) studied the adsorption of organic acids to preformed hydroxide flocs and found a correlation between removal efficiency and the number and ionization of functional groups. Generally, removal increased with a greater number of functional groups, and thus greater molecular weight. They also observed the reversal of electrokinetic potential of the floc and attributed it to the formation of negatively charged surface complexes on

the hydrous oxide surface. Research on the influence of the number and arrangement of carboxylic and phenolic groups on the removal of simple aromatic and aliphatic acids by metal salt coagulants has also been conducted by Lefebvre and Legube (1993). Their results suggest that aromatic acids with two or more adjacent carboxyl or phenol groups are easily removed by coagulation. They proposed reaction mechanisms for organic acid adsorption (surface complexation) to hydrous oxide surfaces similar to those suggested by Kummert and Stumm (1980). Lefebvre and Legube (1993) however did not address the effect of ionization of functional groups on adsorption. Bose and Reckhow (1998) have conducted studies on fractionated NOM and found that humic and fulvic acid were removed to a greater extent than other fractions, presumably because of their size. Higher charge density (i.e., greater carboxylic acidity) did not necessarily cause greater NOM-removal.

Although many of these researchers provide a mechanistic explanation for their observations, only few attempted to apply surface complexation models to their data. This may partly be due to uncertainties in the characteristics of the surfaces that provide adsorption sites, but also the many unknowns regarding natural organic adsorbates as well. In contrast, as discussed in the following section, surface complexation modeling has found widespread application in the processes involving adsorption of inorganic and complex organic substances to well characterized, crystalline oxide particles.

1.4. Adsorption to Oxide Surfaces

The interaction of dissolved substances with metal oxy-hydroxide surfaces has long been recognized as an important process in regulating the fate of contaminants in natural aquatic environments and has been studied extensively. In the past three decades great advances have been made in explaining adsorption from aqueous solution assuming the formation of surface complexes that can be described with coordination chemistry models. Table 1.1 summarizes the surface complexation reactions for oxide surfaces.

The formation of surface complexes is conceptualized similarly to the way solute interactions are written; i.e., a solute reacts stoichiometrically with one or more discrete hydroxyl groups (S–OH) on the oxide surface (S–) if it is thermodynamically favorable. It has been shown that the application of the surface acid/base reactions explain the protolytic behav-

Table 1.1. Surface complexation reactions.

Reaction Type	Example
Surface Acidity	$S\text{–}OH + H^+ \rightleftharpoons S\text{–}OH_2^+$
	$S\text{–}OH \rightleftharpoons S\text{–}O^- + H^+$
Metal Binding	$S\text{–}OH + Pb^{2+} \rightleftharpoons S\text{–}OPb^+ + H^+$
	$2S\text{–}OH + Pb^{2+} \rightleftharpoons (S\text{–}O)_2Pb + 2H^+$
Ligand Exchange	$S\text{–}OH + F^- \rightleftharpoons S\text{–}F + OH^-$
Ternary Surface Complex Formation	$S\text{–}OH + L^- + Cu^{2+} \rightleftharpoons S\text{–}L\text{–}Cu^{2+} + OH^-$

ior of many different oxides, such as α-FeOOH, γ-Al_2O_3, TiO_2, SiO_2(am) and δ-MnO_2 (Schindler, 1981). The reaction schemes for metal binding have also been used to successfully demonstrate the interactions of lead with alumina (Hohl and Stumm, 1976), and more recently the adsorption of trivalent cations to silica and alumina (Kosmulski, 1997a; Lin *et al.*, 1997). The ligand exchange reaction was proposed by Hingston *et al.* (1972) and has been applied in this manner by others to simple and complex anions (Hao and Huang, 1986; Cheng and Huang, 1996). Many researchers have been able to elucidate the effects of (organic) complexing ligands on trace metal adsorption when considering the formation of ternary surface complexes (Davis and Leckie, 1978a; Dalang *et al.*, 1984; Bowers and Huang, 1987; Nowack and Sigg, 1996).

The mass action laws for surface complexation reactions are treated similarly to those involving solute-solute interactions. However, the free energy of adsorption includes an electrostatic term to account for the effects of repulsion or attraction by equal or opposite charges that accumulate at the interface. The incorporation of the electrostatic term in surface complexation modeling (i.e., the representation of the electric double layer) relies on the theories of Gouy-Chapman and Stern-Grahame and limiting cases thereof (Stumm and Morgan, 1996). It is the inclusion of the electrostatic term that allows studying the effects of adsorption on particle stability using surface complexation modeling.

With the development of surface complexation models, many researchers have been able

to predict adsorption in simple systems. In particular, the adsorption of inorganic ions to goethite, has been investigated in many studies, and recently Dzombak and Morel (1990) published a compilation of surface complex formation constants derived from applying the "double-layer model" to the data collected from numerous sources. However, no such extensive research has been conducted on the adsorption onto freshly precipitated aluminum hydroxide, although many papers have been published that address ion adsorption onto alumina and gibbsite. Due to the chemical composition, freshly prepared aluminum hydroxide precipitate can be expected to behave similarly to these crystalline solids. However, there are also differences, e.g., the thermodynamically stable, crystalline phase is less soluble than the amorphous precipitate formed under water treatment conditions (Snoeyink and Jenkins, 1980).

With respect to studying and modeling adsorption to metal hydroxide surfaces, many questions remain unanswered in the literature. First of all, little research has been conducted to investigate whether modeling parameters derived from single solute experiments can be applied to multisorbate systems, such as those encountered in water treatment. Secondly, although abundant work has been conducted in modeling adsorption of trace metals onto hydrous oxides in natural systems (Stumm and Morgan (1996) and references therein), there seems to be a need to increase these efforts and study anionic substances, and in particular, the adsorption of organic acids and their conjugate bases under water treatment conditions. Published work that addresses sorption of simple organic acids to metal oxides in natural systems can serve as a guide to understanding NOM-removal by coagulation. One of the earlier studies involving modeling the adsorption of simple organic acids onto oxide surfaces was conducted by Kummert and Stumm (1980). These researchers demonstrated that the extent of adsorption and the residual surface charge can be predicted as a function of pH and other solution variables using experimentally determined equilibrium constants. They also observed that the tendency to form coordinate complexes in solution is a good indicator that inner-sphere complexes are formed on the surface as well. Interactions of simple organic acids with oxide surfaces have been addressed and refined subsequently by many other researchers. Person *et al.* (1998) studied the surface complexation of orthophthalic acid, an aromatic acid with two adjacent carboxyl groups, to boehmite, alumina, and goethite.

These authors identified two dominating phthalate surface complexes, one outer-sphere and one inner-sphere complex. Evanko and Dzombak (1998) focussed on studying the influence of structural features on the sorption of organic acids onto goethite and recently published their modeling results (Evanko and Dzombak, 1999). They found that Suwannee River fulvic acid exhibited adsorption behavior similar to a simple tetracarboxylic acid, whereas the sorption of Aldrich humic acid appeared to be influenced by hydrophobic interactions and required introducing additional surface complexes to the model. Interestingly, their results for the adsorption of phthalic acid did not agree with those from Person *et al.* (1998), although the same procedure for the preparation of goethite was followed.

Fewer studies have been devoted to competitive interactions of simple organic acids and inorganic anions. Hawke *et al.* (1989) applied the surface complexation model to account for the interactions of phosphate, fluoride, humic acid, and the major seawater ions with goethite. Ali and Dzombak (1996a) were successful in modeling the effects of sulfate on the adsorption of chelidamic and phthalic acid and Mesuere and Fish (1992) could adequately predict surface complexation in a binary chromate-oxalate system. These results are promising with regard to the ability to model complex adsorbent-adsorbate systems, such as those encountered in water treatment.

Under the premise that adsorption to amorphous aluminum hydroxide is the dominant process, it should be possible to utilize surface complexation models to study the influence of competing ions on organic matter removal during coagulation with alum. It has to be remembered that the chemical processes at the solid-solution interface also play an important role in particle-particle interactions, i.e., that conditions that result in optimal NOM-removal in water treatment may not be favorable for particle removal. Therefore, it is equally important to document the effects of competitive solutes on particle destabilization as well as NOM removal through coagulation.

1.5. Influence of Adsorption on Particle Stability

The development of electric charge on solid particle surfaces can be caused by lattice imperfections and chemical reactions at the surface that are well documented (Stumm and Morgan, 1996). These reactions include the ionization of surface hydroxyl groups (S–OH)

and the coordinative binding of cations and anions as illustrated in Table 1.1. The accumulated charge at the surface has to be counterbalanced by a diffuse ion swarm in order to maintain electroneutrality. This spatial distribution of ions near the surface (the "electric double layer" or EDL) results in an electrostatic potential between the particle surface and the bulk solution and therefore causes a repulsive force when particles with similar surface characteristics and charge approach each other.

A colloidal suspension is stable when the repulsive forces between particles exceed attractive forces, i.e., van der Waals forces, preventing particle aggregation. The objective of particle removal in water treatment is to overcome these repulsive forces by "quenching" the surface charge, i.e., minimizing the electrostatic potential and inducing accumulation (aggregation) of the particles. Naturally occurring particles are typically negatively charged (Amirtharajah and O'Melia, 1990) and in conventional water treatment, their destabilization is usually accomplished by addition of a hydrolyzing metal salt coagulant. Positively charged hydrolysis products are typically formed under most coagulation conditions and they specifically bind to the particle surface. The extent of charge neutralization depends on coagulant dose, particle surface area, and the amount of substances competing for surface sites and the metal cation. Particle stability (and removal efficiency) is therefore intimately linked to surface complexation reactions.

In water treatment, electrophoretic mobility measurements are commonly used to estimate the electrostatic potential near the particle surface, or more precisely at the hydrodynamic shear plane. The electrostatic potential at the shear plane is generally referred to as the ζ-potential and is often used to qualitatively predict turbidity removal. Where particle removal occurs by charge neutralization (destabilization), measured ζ-potentials near zero are good indicators of the potential for particle aggregation.

Numerous studies have been conducted that illustrate the relationship between ζ-potential and adsorption of hydrolyzed metal species to inorganic particles (Black and Willems, 1961; Letterman *et al.*, 1982) and the effects of competing anions on particle stability and flocculation kinetics (Letterman and Vanderbrook, 1983; Iyer, 1984; Sricharoenchaikit and Letterman, 1987). ζ-potential data derived from electrokinetic measurements have also been used to calibrate surface complexation models that correct for electrostatic effects

and enable calculation of the diffuse layer potential (Iyer, 1984; Hansmann and Anderson, 1985; Crawford *et al.*, 1996). In these studies, the unknowns were determined by fitting the measured ζ-potential to the calculated diffuse layer potential. Commonly, surface complexation model parameters are determined from fitting acid-base titration and adsorption data (Stumm and Morgan, 1996). However, no work has been published where these models have been verified by comparing calculated diffuse layer potentials and measured ζ-potentials. In order to predict coagulation efficiency with respect to NOM and particle removal, it is necessary to utilize both adsorption and electrokinetic data for model calibration and verification.

1.6. Potential Effects of Selected Inorganic Ions in Water Treatment

An inorganic anion present in water can be considered as interfering with coagulation if it forms soluble and insoluble complexes with the metal ions supplied by the coagulant. The formation of soluble, non-adsorbable metal-ligand complexes can potentially decrease the amount of metal hydroxide precipitate and correspondingly decrease the number of available surface sites for adsorption of organics. The affinity of some inorganic ions for surfaces can also result in competition for complexation sites and changes in particle surface charge and stability. The possible interferences for some inorganic anions are outlined below.

Fluoride is an inorganic anion that generally occurs in natural waters at levels below 1 mg/L (Snoeyink and Jenkins, 1980). At higher solution pH values (pH>8), fluoride is generally present in water in the free, ionic state (F^-) but at lower pH values can significantly complex with metal cations or adsorb to precipitated metal oxy-hydroxides. The ability to form soluble, inorganic complexes with aluminum is known for waters undergoing coagulation with aluminum salts (Sung and Rezania, 1985; Driscoll and Letterman, 1988; Van Benschoten and Edzwald, 1990a; Letterman and Driscoll, 1994) and in aqueous solutions in general (Roberson and Hem, 1969; Schafran and Driscoll, 1987). It has also been recognized that fluoride strongly adheres to mineral surfaces and freshly precipitated aluminum hydroxide (Bower and Hatcher, 1967; Hingston *et al.*, 1972; Bar-Yosef *et al.*, 1988) and that it forms soluble aluminum-fluoro complexes that are non-adsorbable (Matijević *et al.*, 1969). Sorption onto precipitated aluminum hydroxide and activated alumina is an

important and widely accepted treatment procedure for the removal of fluoride in raw waters elevated in fluoride (Choi and Chen, 1979; Montgomery, 1985; Hao and Huang, 1986).

Sulfate is widely distributed in nature and may be present in natural waters in concentrations ranging from a few to several thousand milligrams per liter. Sulfate can be introduced to the water treatment process through the addition of aluminum sulfate (alum) or iron sulfate coagulants. In aqueous solution under ambient conditions, sulfate is generally present in the free divalent state (SO_4^{2-}) and it forms only weak complexes with polyvalent cations. It can however specifically adsorb to oxyhydroxide surfaces through ligand exchange (Hingston *et al.*, 1972; Zachara *et al.*, 1987; Ali and Dzombak, 1996b). The effects of sulfate on particle stability in water treatment have been well studied in part because of the widespread use of alum (aluminum sulfate) as a primary coagulant. In early studies, it was observed that sulfate displaces the "optimum" pH of sweep floc coagulation. Hanna and Rubin (1970) and Hayden (1971) showed that sulfate induces rapid formation of a settleable aluminum hydroxide floc and they attributed this observation to the formation of insoluble hydroxosulfato aluminum complexes. Some researchers have suggested that sulfate catalyzes the precipitation of $Al(OH)_3$ by inhibiting the formation of soluble polymeric aluminum hydroxo complexes (Snodgrass *et al.*, 1984; Bottero and Bersillon, 1989). Letterman *et al.* (1982) conducted extensive electrokinetic studies that indicated that sulfate decreases the electrophoretic mobility of aluminum hydroxide coated particles by surface complexation. Interestingly, the influence of sulfate on NOM removal has not been addressed in the recent literature. Although it is well known that sulfate can suppress adsorption of inorganic and organic anions to oxyhydroxides (Zachara *et al.*, 1987; Ali and Dzombak, 1996b), its effects in water treatment seem to be obscure. Maulding and Harris (1968) noted its influence when they reported that "the presence of SO_4^{2-} has a deleterious effect on color removal." Jekel (1986) also observed a decrease in adsorption of humate to $Al(OH)_3$ in the presence of sodium sulfate. Nevertheless, these effects have not been addressed in published studies involving the comparison of sulfate-based versus non-sulfate based coagulants (Van Benschoten and Edzwald, 1990b; Julien *et al.*, 1994; Crozes *et al.*, 1995).

Phosphate is present in unpolluted natural waters usually at concentrations below

0.05 mg/L P (Snoeyink and Jenkins, 1980). In water treatment plants it is added as zinc orthophosphate, a corrosion inhibitor. Also, condensed phosphates, like hexametaphosphate, are used to sequester iron in drinking water and these compounds tend to hydrolyze and revert to orthophosphate (Snoeyink and Jenkins, 1980). (Ortho-) Phosphate has a strong affinity for polyvalent metal cations and is believed to inhibit mobilization of lead in finished waters. It is therefore not unlikely that it can compete with hydroxyl ions for aluminum during the water treatment process. Hanna and Rubin (1970) observed that increasing doses of orthophosphate displaced the zone in which an aluminum nitrate solution rapidly precipitated to more acidic pH values. They explained this effect by the formation of an aluminum phosphate solid. On the other hand, Hsu (1975) concluded that a pure $AlPO_4(s)$ phase occurs only when a large excess of phosphate is present. Under water treatment conditions, where PO_4/Al ratios were low, phosphate was removed completely, which was most likely due to adsorption to aluminum hydroxide flocs. These properties are favorable and have been used for phosphorus removal in wastewater treatment (Boller, 1984). Phosphate can strongly adhere to hydrous oxides and aluminosilicate minerals (Lijklema, 1980; Ioannou and Dimirkou, 1997) and has the potential to influence trace metal adsorption to goethite (Venema *et al.*, 1997). Boisvert *et al.* (1997) studied monophosphate adsorption to aluminum hydroxide flocs and they observed a decrease in ζ-potential with increasing PO_4-dose, which indicates that interferences with particle destabilization are possible. Davis (1982) noted that natural organic compounds compete with orthophosphate for sites on alumina. Therefore, the specific interaction of orthophosphate with the metal hydroxide flocs is also likely to impact adsorption of organic acids.

1.7. Research Goals

The solution characteristics that control the removal of natural organic matter from waters undergoing coagulation are not well known. Recent water treatment research has focussed on studying the properties of NOM that affect its removability, the effectiveness of various coagulants in removing NOM, the influence of some treatment options, such as ozonation, and the effects of treatment (coagulation) pH. Indicators, such as "specific UV absorbance" have been developed to predict the adsorbability of NOM; however, such indicators are

likely to fail when two waters of different origin, but with equal specific UV absorbance are treated. One factor heretofore not well acknowledged (or known?) is the presence of other (inorganic) substances, that can be present at elevated concentrations in the source water or that are added prior to or during the coagulation process. In order to gain a better understanding about the factors that govern the effectiveness of water treatment processes, fundamental knowledge of the interferences by these substances is necessary. Previous efforts to predict treatment efficiency with respect to NOM removal are purely empirical and neglect the potentially masking effects of common water constituents that are present in the raw water or added during the coagulation process. The goal of this research was to quantify the effects of selected inorganic anions on organic matter removal and particle stability in waters undergoing coagulation with alum. Data, collected from laboratory- and pilot-scale studies, was interpreted in terms of competitive chemical reactions on the aluminum hydroxide surface. In particular, these studies were designed to:

- Quantify the influence of the inorganic anions fluoride, sulfate, and orthophosphate applied at typical doses in water treatment processes, or at concentrations present in natural waters, on NOM-removal and particle stability during alum coagulation.
- Elucidate mechanisms that explain the competitive adsorption of inorganic and organic anions to amorphous aluminum hydroxide.
- Determine whether surface complexation models adequately describe the effects of these inorganic anions on organic matter removal and particle stability.

2. BENCH-SCALE TESTS ON THE INFLUENCE OF SELECTED INORGANIC ANIONS ON COAGULATION

2.1. Introduction

This study was initiated a few years after it was discovered that raw water reservoirs in southeastern Virginia when augmented with ground water from the lower Potomac aquifer contained elevated levels of fluoride. Water quality monitoring revealed that fluoride concentrations increased from background levels to between 1 and 2 mg/l during drought conditions. Knowing that fluoride can strongly complex aluminum in aqueous solution and that aluminum sulfate (alum) is the most widely used coagulant in the U.S. and elsewhere, it was suspected that elevated fluoride levels could adversely impact conventional water treatment when aluminum salts are used as the primary coagulant. In addition to elevated fluoride concentrations in source waters, it was suspected that some treatment plants might introduce fluoride in the process train at a point where it could interfere with particle and NOM removal. A review of the literature conducted for this work did not reveal any publications where these impacts were addressed. However, an examination of water treatment plant schematics collected under the Information Collection Rule (U.S. Environmental Protection Agency, 1996) revealed that a number of utilities added fluoride prior to filtration.

It is well recognized that fluoride can increase the soluble fraction of aluminum in waters coagulated with alum. This assertion has been made following experimental studies (Sung and Rezania, 1985), and the effect can also be readily calculated from known thermodynamic constants. Soluble aluminum concentrations as a function of pH and at three different fluoride concentrations were computed using PHREEQC* (Parkhurst and Appelo, 1999) and are graphically represented in Figure 2.1. The solution and solid species considered in this computation and their equilibrium constants are listed in Table 2.1.

Utilizing these graphs, it can be concluded that the impact of fluoride on the dissolved aluminum fraction is most pronounced in the pH range from approximately 5 to about 7. This interval covers the pH range commonly encountered in waters undergoing coagulation

*Chemical equilibrium computer programs used in this work are described in Appendix A

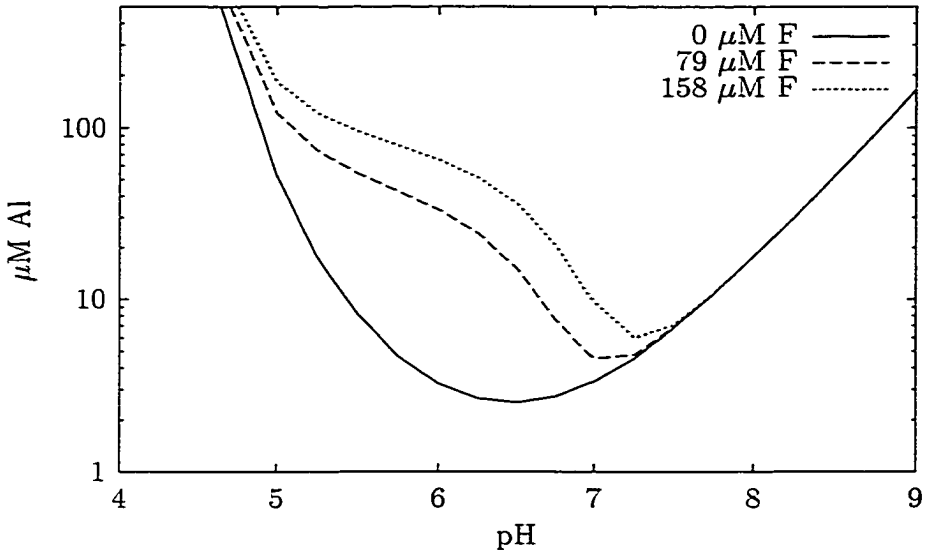

Figure 2.1. Soluble aluminum as a function of pH and fluoride dose.

Table 2.1. Solid and dissolved aluminum species. Equilibrium constants are taken from the PHREEQC thermodynamic database (Parkhurst and Appelo, 1999).

Reaction	$\log K$
$Al^{3+} + H_2O \rightleftharpoons AlOH^{2+} + H^+$	-4.99
$Al^{3+} + 2H_2O \rightleftharpoons Al(OH)_2^+ + 2H^+$	-10.1
$Al^{3+} + 3H_2O \rightleftharpoons Al(OH)_3^0 + 3H^+$	-16
$Al^{3+} + 4H_2O \rightleftharpoons Al(OH)_4^- + 4H^+$	-23
$Al^{3+} + F^- \rightleftharpoons AlF^{2+}$	7.01
$Al^{3+} + 2F^- \rightleftharpoons AlF_2^+$	12.75
$Al^{3+} + 3F^- \rightleftharpoons AlF_3$	17.02
$Al^{3+} + 4F^- \rightleftharpoons AlF_4^-$	19.72
$Al(OH)_3(s) + 3H^+ \rightleftharpoons Al^{3+} + 3H_2O$	10.2

with alum. For example, at pH 6, the concentration of soluble aluminum is approximately 3 μM as Al in the absence of fluoride, and it is 30 μM as Al at a total fluoride concentration of 79 μM (1.5 mg/l as F). If a water was treated with an alum dose of 100 μM as Al ($\approx$ 30 mg/l as alum, $Al_2(SO_4)_3 \cdot 14\,H_2O$), the presence of fluoride at concentrations similar to those in Figure 2.1 would cause a substantial decrease of the the amount of $Al(OH)_3$ precipitate formed. Considering the importance of this amorphous phase for particle removal and adsorption of natural organic matter (NOM) as described in Section 1, it is therefore likely that fluoride can interfere with particle and organic matter removal during water treatment. It is also apparent that this effect may be dependent on treatment pH and the applied alum dose. The appropriate factorial experimental design to test this conjecture would therefore include both variable pH and coagulant doses.

If the influence of fluoride on aluminum solubility is indeed the main cause of negative impacts in water treatment with alum, one would expect smaller or no effects when a metal salt coagulant is added where the active coagulating species are more stable than metal-fluoride complexes. This may be the case for iron-based and prehydrolyzed aluminum-based coagulants. Effects of fluoride on the solubility of amorphous iron hydroxide can be demonstrated in the same manner as for aluminum by utilizing chemical equilibria (not shown). This analysis would reveal that fluoride complexes ferric iron only weakly at pH greater than 4.

In contrast to alum, where hydrolysis occurs in situ, prehydrolyzed aluminum coagulants (e.g., polyaluminum chloride) contain polynuclear species and do not cause precipitation of an amorphous phase (Van Benschoten and Edzwald, 1990a). There is considerable disagreement among researchers about the structure of the polymeric species and their stability constants. Therefore, the effect of fluoride on aluminum speciation cannot be readily assessed. Because these polymers are preformed (i.e., hydrolysis is completed), the effects of fluoride on aluminum solubility may depend on the rate of a reaction such as

$$Al_p(OH)_q^{3p-q} + pF^- \rightleftharpoons pAlF^{2+} + qOH^-$$

to form aluminum-fluoride complexes. This process may be slow compared to the reactions involving the free aluminum ion and one or more fluoride ions shown in Table 2.1. These

considerations also apply to the case where fluoride is added to a water that has already been coagulated with alum, i.e., an amorphous solid phase has been formed. In treatment plants, such a situation could occur when a water is fluoridated at a point downstream of the coagulant introduction and upstream of solid-liquid separation. This type of process can be simulated in batch experiments by varying the order of fluoride addition.

To investigate the effects of variable concentrations of fluoride on coagulation, jar test experiments were conducted using natural and synthetic waters made to variable and well controlled concentrations of NOM, particles, inorganic cations and anions, and ionic strength. To a limited extent, experiments were also performed using ferric chloride and a prehydrolyzed aluminum coagulant.

When studying competitive effects on coagulation with alum, consideration should also be given to sulfate. This inorganic ion is introduced by the coagulant itself and it can also be present in raw water. Letterman *et al.* (1982) and Letterman and Vanderbrook (1983) performed extensive jar tests with aluminum salt coagulants and they described four distinct regions of particle stability that are a function of aluminum and sulfate concentration, pH and initial particle volume. They contended that particles are destabilized when positively charged aluminum hydrolysis products adsorb to a negatively charged particle surface. Their findings suggest that at $pH < 7.5$ and low background sulfate concentrations ($\approx 10^{-5}$M) there is the potential that particles become restabilized unless the alum dose is increased to a point where a sufficient amount of sulfate coadsorbs and "quenches" the excess positive charge. At elevated sulfate concentrations ($> 10^{-4}$M) and $pH < 7.5$, the restabilization effect was not discernible. Although these researchers greatly contributed to elucidating the role of sulfate in water treatment, little is known about whether this anion affects NOM removal.

Maulding and Harris (1968) investigated how the presence of calcium, magnesium, and sodium affects color removal, electrophoretic mobility and residual metal concentration in a water undergoing coagulation with ferric sulfate. They observed substantial effects on these parameters when a metal-sulfate salt was used instead of the chloride salt. They concluded that the formation of soluble iron-sulfate ion pairs caused a decrease in the amount of iron available to coagulate the "color particles." However, it is not known whether sulfato

complexes have a noticeable influence on NOM removal when aluminum salts are used under typical water treatment conditions. As pointed out in Section 1, sulfate has also the tendency to compete with other (organic) anions for sites on oxyhydroxide surfaces. Therefore, inhibition of NOM removal due to the presence of excess sulfate can also be caused by competitive adsorption to amorphous aluminum hydroxide. As a limited subset of this study, jar tests were conducted to examine these effects.

2.2. Materials and Methods

2.2.1. Raw Water

Synthetic waters were prepared by diluting water collected from the Northwest River in southeastern Virginia. The Northwest River drains from the Great Dismal Swamp and typically contains dissolved organic carbon (DOC) at concentrations ranging from 15 to 50 mg C/l. Immediately after collection, the raw water was passed through a 0.45 μm cartridge filter (Gelman Sciences, AquaPrep^{TM}600) using a peristaltic pump (Cole-Parmer) and then diluted with distilled, deionized water to the desired DOC concentration. The ionic strength was adjusted to approximately 0.01 M by addition of reagent grade sodium nitrate or sodium chloride (Fisher Scientific). The resulting solution was then augmented with either reagent grade kaolin clay (Fisher Scientific) or silica particles (MIN-U-SIL 10, U.S. Silica). For the experiment with a prehydrolyzed aluminum coagulant, a solution was prepared with commercially available humic acid (Aldrich Chemical) and kaolin clay as the organic matter and particle sources, respectively. Selected tests were also conducted using water from Lake Ontario collected at the raw water intake of the Metropolitan Water Board Treatment Plant in Oswego, New York. In contrast to Northwest River water, this water was very low in turbidity and natural organic matter content and moderately high in alkalinity (116 mg/l as $CaCO_3$). Selected water quality parameters including ultraviolet light absorbance at 254 nm (UV_{254}) for the waters tested is this study are summarized in Table 2.2. Where applicable, specific ultraviolet absorbance (SUVA) was calculated by dividing UV_{254} [m^{-1}] by DOC [mg C/l]. SUVA has recently been identified as a good predictor for the amenability of NOM to removal by coagulation (White *et al.*, 1997).

Table 2.2. Raw water characteristics.

Source	Northwest River		Humic Acid	Lake Ontario
UV_{254} [cm^{-1}]	0.2	0.5	0.2	0.02
DOC [mg C/l]	6	10	not analyzed	2
SUVA [l/mg·m]	3.3	5.0	n/a	1.0
Particle Source	Kaolin	MIN-U-SIL	Kaolin	n/a
Turbidity [NTU]	16	9	not analyzed	2.1
Electrolyte	$NaNO_3$	NaCl	none	n/a

2.2.2. Jar Test Procedure

A standard six paddle gang stirrer (Phipps & Bird) and two-liter square jars were utilized for the jar tests conducted in this study. The water to be tested was transferred to the jars and the coagulant was injected under vigorous mixing. When necessary, a predetermined amount of reagent grade sodium hydroxide or hydrochloric acid (Fisher Scientific) was added prior to coagulant addition to attain a finished water pH in the range of 4.5 to 7.5. Fluoride or sulfate was also added before the coagulant, except in the experiments where the effects of the order of addition were studied. Here, fluoride was also injected immediately after the two minute rapid mix period. After 15 minutes of flocculation, the suspension was allowed to settle for 30 minutes. A portion of the sample withdrawn at the sample port was immediately passed through a 0.45 μm polycarbonate membrane (Osmonics) using a vacuum filtration apparatus (Gelman Sciences). The filtered aliquot was retained for the analysis of nonpurgeable organic carbon (NPOC), UV_{254}, total dissolved metals and total dissolved fluoride. Filtered NPOC concentrations were assumed to represent the amount of organic carbon in solution (DOC). Preliminary work indicated that the membranes did not leach organic material or adsorb measurable quantities of the analyte. The unfiltered sample portion was used to determine turbidity and/or particle size distribution and pH. Electrophoretic mobility was determined using a sample that was withdrawn with a syringe immediately after the rapid mix phase.

Table 2.3. Coagulant properties.

Product	Manufacturer	Concentration	Specific Gravity
Alum	General Chemical Corp.	8.3 % Al_2O_3	1.33
Westchlor FA700S	Westwood Corp.	10.22 % Al_2O_3	1.20
Ferric Chloride	Midland Resources, Inc.	13.61 % Fe	1.421

2.2.3. Reagents

The chemicals used in this study were of reagent grade unless otherwise noted. A fluoride standard stock solution was prepared by dissolving 2.210 g of sodium fluoride (Fisher Scientific) in distilled, deionized water and diluting to 1000 ml. A 200 ml 0.5 M sulfate stock solution was made up from 17.426 g potassium sulfate (Fisher Scientific) and distilled, deionized water. Hydrochloric acid and sodium hydroxide solutions were prepared and standardized according to Standard Methods (Eaton *et al.*, 1995).

The coagulants used in this study were of commodity grade; selected properties and their origins are listed in Table 2.3.

2.2.4. Analytical Methods

All analyses were performed in accordance with Standard Methods (Eaton *et al.*, 1995) unless otherwise noted. The methods utilized during this study are described in greater detail in Appendix B.

Turbidity was measured using a Monitek TA1 nephelometer calibrated to cover a range from 2 to 20 NTU. In the experiment with Lake Ontario water, total particle count was analyzed in lieu of turbidity. The analysis of the particle size distribution was performed immediately after the jar tests with a multichannel particle counter (Coulter Multisizer II). Electrophoretic mobility was determined with a Zeta Meter ZM-77 according to the manufacturer's operating instructions.

Samples filtered through a 0.45 μm polycarbonate membrane (Osmonics) were analyzed for non-purgeable organic carbon and UV-absorbance at 254 nm. Samples for organic carbon analysis were acidified to pH 2 with hydrochloric acid.

Aluminum concentrations were measured by atomic absorption spectroscopy (Perkin-Elmer). Sample aliquots were acidified with trace metal grade nitric acid to pH < 2 at least 12 hours prior to analysis. The nitrous oxide-acetylene flame technique was utilized on all samples. Those with concentrations below $10\,\mu$M (0.3 mg/l Al) were reanalyzed using the graphite furnace technique. Fluoride was determined potentiometrically. Where aluminum concentrations were found to be in excess of $40\,\mu$M ($\approx$ 1 mg/l Al), a standard addition technique was employed to minimize interference.

2.3. Results and Discussion

2.3.1. Effects of Fluoride on Coagulation with Alum

Experimental results from the tests with synthetic water coagulated with alum at varying concentrations of fluoride are graphically represented in Figures 2.2 through 2.5. In these experiments, it was attempted to attain a settled water pH of 5, 5.5 or 6.2. The corresponding actual pH values were 4.9 ± 0.2, 5.5 ± 0.1, and 6.2 ± 0.2 ($\bar{x} \pm \sigma$), respectively. Alum concentrations ranged from 0 to $168\,\mu$M as Al (0 to 50 mg/l as $Al_2(SO_4)_3 \cdot 14\,H_2O$).

The graphs representing settled water turbidity and electrophoretic mobility versus alum dose in the absence of fluoride (Figure 2.2) exhibit trends typical for a water moderately high in turbidity and organic matter. Independent of pH, a slight increase in turbidity (upper plot) can be observed at the lowest coagulant dose. Electrophoretic mobility increased correspondingly (lower plot) which suggests that aluminum hydrolysis products adsorbed to the particles. This may have resulted in an enlargement of the solids and caused an increase in scattered light intensity. The alum dose of $34\,\mu$M as Al resulted in mobility values no greater than $-1\,\mu$m cm/(V s) and was apparently too low to destabilize the particles and induce effective flocculation. A further increase to a dose of $67\,\mu$M as Al led to an obvious improvement in settled water turbidity. It appears that the magnitude of the drop depended on the treatment pH, with the highest pH providing the best particle removal based on turbidity. At all pH, electrophoretic mobility increased linearly with alum dose. However, at concentrations greater than $101\,\mu$M as Al, the flocs became positively charged and turbidity decreased no further. The small differences in electrophoretic mobility due to

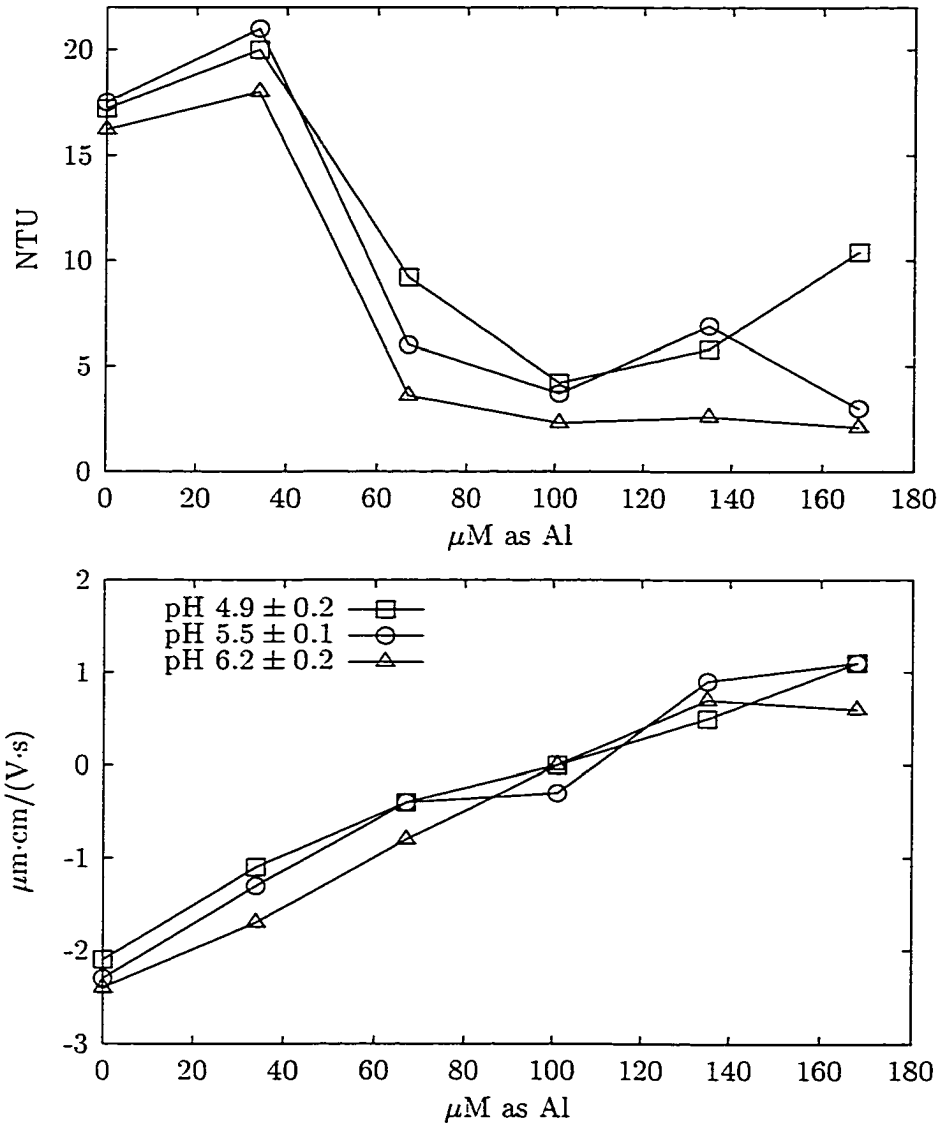

Figure 2.2. Settled water turbidity and electrophoretic mobility as a function of alum dose and pH without fluoride for coagulation of synthetic Northwest River water.

pH did not seem to have a great influence on particle removal. At a dose of 168 μM Al, the settled water turbidity at pH 4.9 was noticeably greater compared to the tests conducted at higher pH. Although electrophoretic mobility was not higher than at pH 5.5, it is possible that the adsorbed aluminum species caused restabilization of the floc. This suggests that adsorption and charge neutralization governed particle removal at the lowest pH, whereas "sweep-floc" coagulation may have been predominant at the highest pH. Restabilization may have also caused the evident increase in turbidity at pH 5.5 and an alum dose of 135 μM as Al. In summary, in the absence of fluoride in the raw water, coagulation at pH 6.2 appeared to provide the best particle removal.

The results from the jar tests where fluoride was added are displayed in Figures 2.3 and 2.4. As in the previous test series, electrophoretic mobility increased linearly with alum dose and substantial turbidity removal occurred generally when a value of $-1\,\mu\mathrm{m\,cm/(V\,s)}$ was exceeded. In contrast to the experiment without fluoride, it appears that this threshold was strongly dependent on pH. The critical coagulant concentrations (CCC), i.e., the doses necessary to destabilize the suspension and achieve substantial turbidity removal, were clearly higher when fluoride was added to the raw water. These data are summarized in Table 2.4.

Table 2.4. Critical coagulant concentration (μM as Al) as a function of pH and fluoride dose.

	0 μM F	79 μM F	158 μM F
pH 4.9 $\pm$ 0.2	67	168	$>$ 168
pH 5.5 $\pm$ 0.1	67	135	168
pH 6.2 $\pm$ 0.2	67	101	135

Generally, critical coagulant concentrations increased with decreasing pH and increasing fluoride dose. In the absence of fluoride the CCC was not dependent on pH. Utilizing the reactions listed in Table 2.1, a more detailed analysis of the observed effects can be performed by computing the speciation of aluminum at the CCC. Matijević *et al.* (1969) employed a similar approach when studying the coagulation of silver halide sols in the presence of alu-

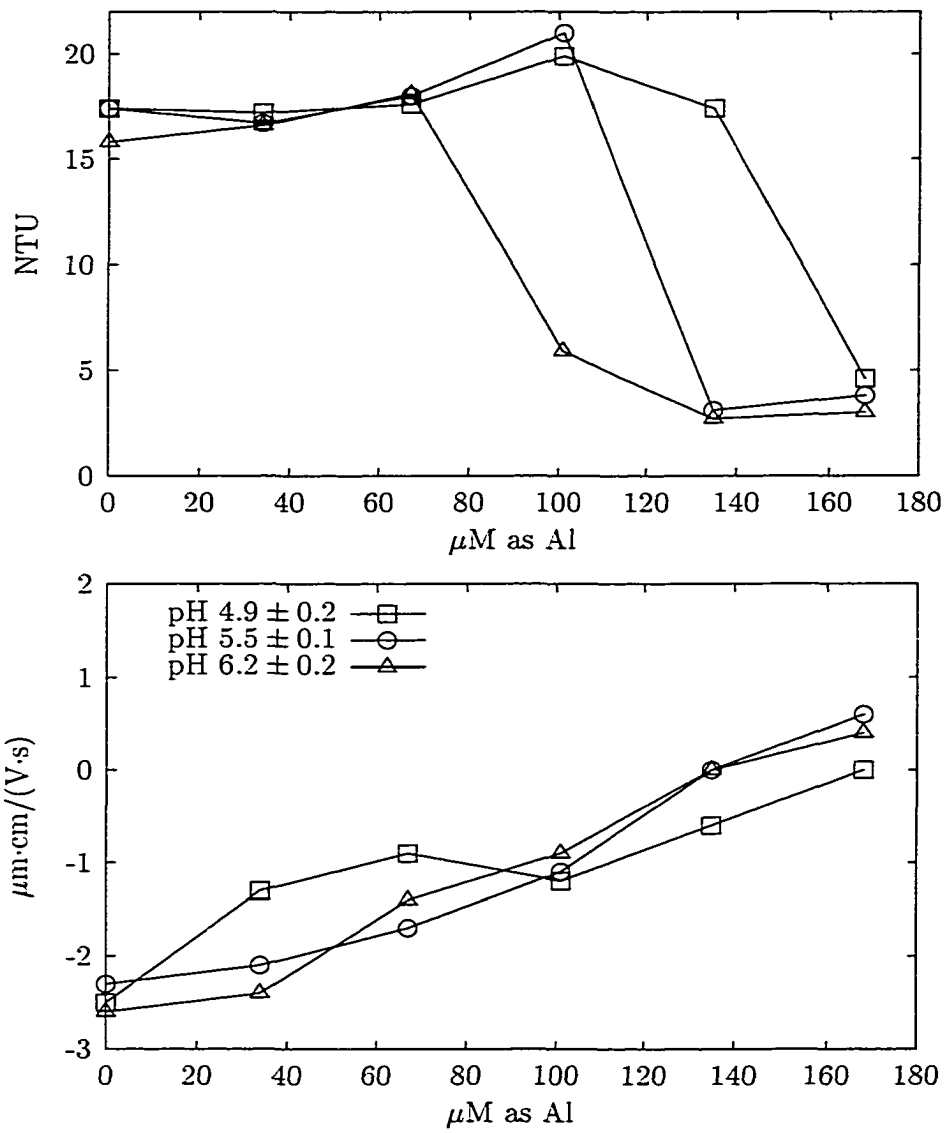

Figure 2.3. Settled water turbidity and electrophoretic mobility as a function of alum dose and pH at a fluoride concentration of 79μM (1.5 mg F/l.)

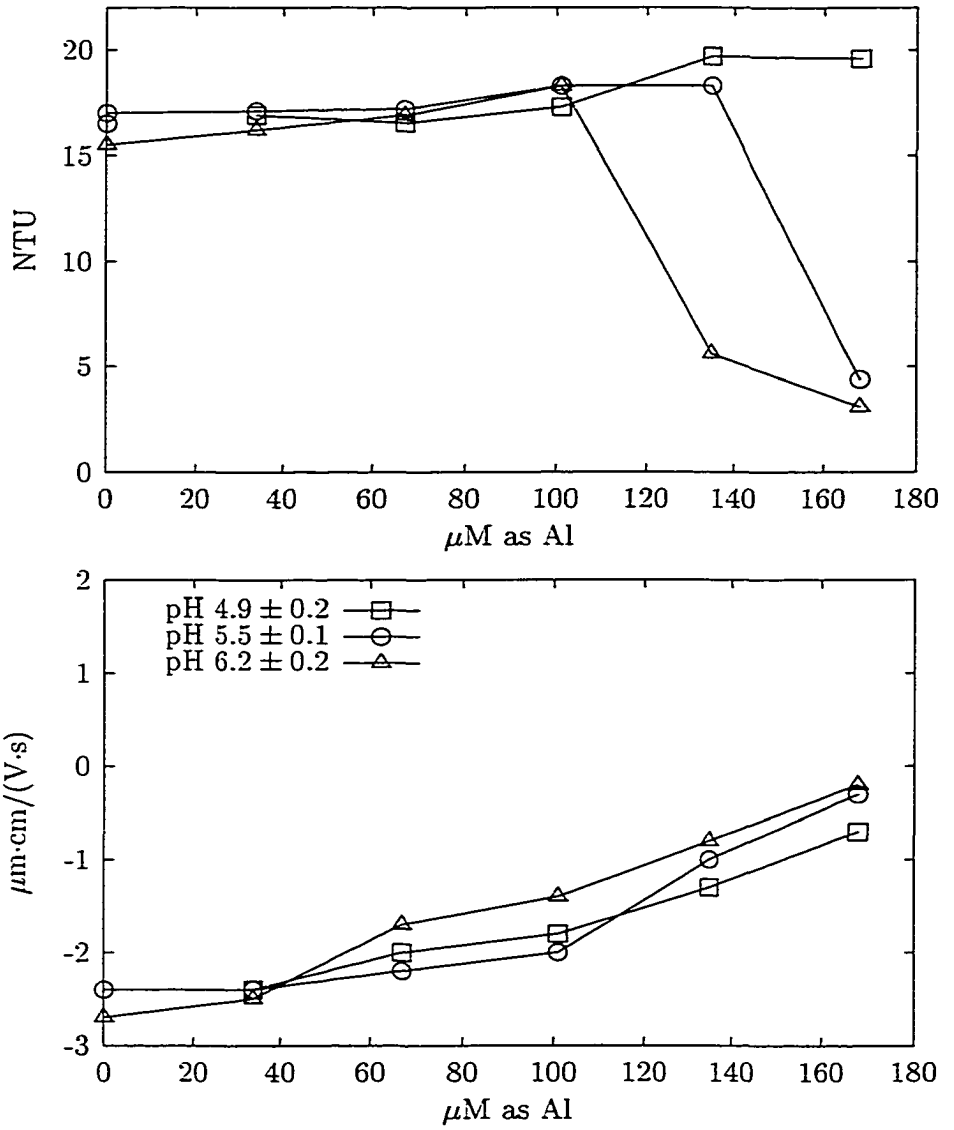

Figure 2.4. Settled water turbidity and electrophoretic mobility as a function of alum dose and pH at a fluoride concentration of 158 μM (3.0 mg F/l.)

minum ions and fluoride. This analysis, however, should be considered semi-quantitative, because due to the lack of thermodynamic data, the interactions of aluminum with the NOM are not included. There is also some uncertainty about the solubility product of $Al(OH)_3$. The computer program PHREEQC was utilized to compute the sum of fluoroaluminum complexes ($\sum AlF_p; p = 1, \ldots, 4$), the sum of hydroxoaluminum complexes including the hexaaquoaluminum(III) ion ($\sum Al(OH)_q; q = 0, \ldots, 4$), and the amount of aluminum precipitated as amorphous $Al(OH)_3$(s). The CCC in Table 2.4 and the corresponding pH measured during the experiment were used in the computer model as the total aluminum concentration and hydrogen ion activity, respectively. Polymeric aluminum species were not included, because they are unlikely to be present in waters undergoing coagulation with alum (Van Benschoten and Edzwald, 1990a). The results of this calculation are shown in Table 2.5.

Table 2.5. Speciation of aluminum at the CCC in the presence of fluoride (Concentrations are in μM as Al; numbers in parentheses denote the total charge of the species in μeq/l).

		0 μM F		79 μM F		158 μM F	
pH 4.9	$\sum AlF_p$	0	(0)	74	(144)	129	(230)
	$\sum Al(OH)_q$	67	(167)	94	(235)	39	(92)
	$Al(OH)_3$(s)	0	(0)	0	(0)	0	(0)
pH 5.5	$\sum AlF_p$	0	(0)	45	(60)	93	(123)
	$\sum Al(OH)_q$	10	(13)	8	(9)	11	(14)
	$Al(OH)_3$(s)	57	(0)	82	(0)	65	(0)
pH 6.2	$\sum AlF_p$	0	(0)	27	(21)	62	(48)
	$\sum Al(OH)_q$	3	(0)	3	(1)	3	(1)
	$Al(OH)_3$(s)	64	(0)	71	(0)	70	(0)

These data suggest that in the absence of fluoride at pH 4.9, adsorption of monomeric aluminum species caused the destabilization of the particles, whereas at the highest pH enmeshment in the amorphous precipitate ("sweep floc") occurred. This contention confirms the earlier conclusion about the different coagulation mechanisms. Based on the computational results, both adsorption of monomeric species and precipitation of aluminum hydrolysis products caused particle removal at pH 5.5.

It is observed that a similar partitioning between soluble and amorphous aluminum hydrolysis products occurs with or without fluoride in solution at a given pH value (Table 2.5). Although the charged aluminum-fluoride complexes contributed substantially to the total aluminum concentration, in most cases, the sum of the concentrations of hydroxoaluminum complexes and the precipitate add up to values between 73 and 94 μM as Al. These doses are similar to the coagulant concentration that led to substantial turbidity removal in the absence of fluoride and independent of pH (67 μM Al). This observation suggests that positively charged fluoroaluminum complexes did not cause destabilization of the particles in the synthetic water. Matijević *et al.* (1969) arrived at a similar conclusion.

At pH 4.9 and 79 μM of fluoride, the sum of the concentrations of hydroxoaluminum complexes and the precipitate was much higher than 67 μM. If a dose resulting in approximately 67 μM of "active" coagulant were required, theoretically, 135 μM of alum would not have been sufficient for turbidity removal in this experiment. At the highest fluoride dose and at pH 4.9, no particles were removed when adding 168 μM Al, however, the calculation was performed to confirm that the added alum dose did not yield the required concentration of "active" species. PHREEQC predicted that a slightly higher alum dose (202 μM, 60 mg/l as $Al_2(SO_4)_3 \cdot 14\,H_2O$) would have resulted in $\sum Al(OH)_q = 66\,\mu M$.

A comparison to the measured concentrations in samples filtered through a 0.45 μm membrane showed that PHREEQC overpredicted dissolved aluminum concentrations at low pH by up to 70 μM. Decreasing the solubility product for $Al(OH)_3(s)$ by two orders of magnitude did not improve the fit substantially. This discrepancy could have been caused by formation of (insoluble) aluminum-organic complexes that were not included in the calculation. Also, for the computation it was assumed that fluoride did not adsorb to the aluminum hydroxide precipitate. However, a substantial amount of the added fluoride may

not have been available to form dissolved complexes. A more quantitative analysis would therefore require including surface complexes in the computer model.

The effects of fluoride on NOM removal in these experiments are graphically represented in Figure 2.5. The initial DOC concentration was slightly below 6 mg C/l. The raw water SUVA of 3.3 l/mg·m suggests that the water contained a considerable amount of natural organic matter of non-humic origin (Edzwald *et al.*, 1985) and that only moderate reduction in DOC can be achieved by alum coagulation (White *et al.*, 1997).

In some instances, an incremental increase in alum dose did not yield a decrease in settled water DOC. Because the target pH was not always attained exactly, it happened that the pH values at two adjacent data points differed by as much as 0.4 units. Despite this inconsistency, a negative influence of fluoride on DOC removal is well discernible. Noticeable DOC removal occurred without fluoride even at the lowest alum doses, whereas a coagulant dose of at least 67 μM Al was needed in the presence of fluoride. To achieve the same DOC removal, up to five times more coagulant was necessary where 158 μM fluoride was added compared to the nonfluoridated water.

The graphs reveal that the effect of fluoride diminished with increasing alum dose and that the settled water DOC concentration asymptotically approached a value near 2 mg C/l. Apparently, the raw water contained a substantial amount of NOM that was not amenable to removal by coagulation with alum. Irrespective of the fluoride dose, highest TOC removals were achieved at pH near 6.2. Considering that at this pH aluminum is least soluble, these data suggest that under these experimental conditions the adsorption of NOM to $Al(OH)_3(s)$ was favored over the formation of insoluble aluminum-NOM complexes. The impact of fluoride also appeared to be least pronounced at this pH. A qualitative interpretation of this result can be readily made utilizing the solubility diagram in Figure 2.1. These model calculations show that even in the presence of fluoride, the amount of precipitate formed increases with increasing pH up to approximately pH 7.

Based on these observations, the influence of fluoride on particle and NOM removal should be less detrimental under conditions were the formation of metal-fluoride complexes is unfavorable. This may be the case where coagulation with alum is practiced at pH greater than 7, and, as indicated earlier, where a coagulant is used whose actively coagulating

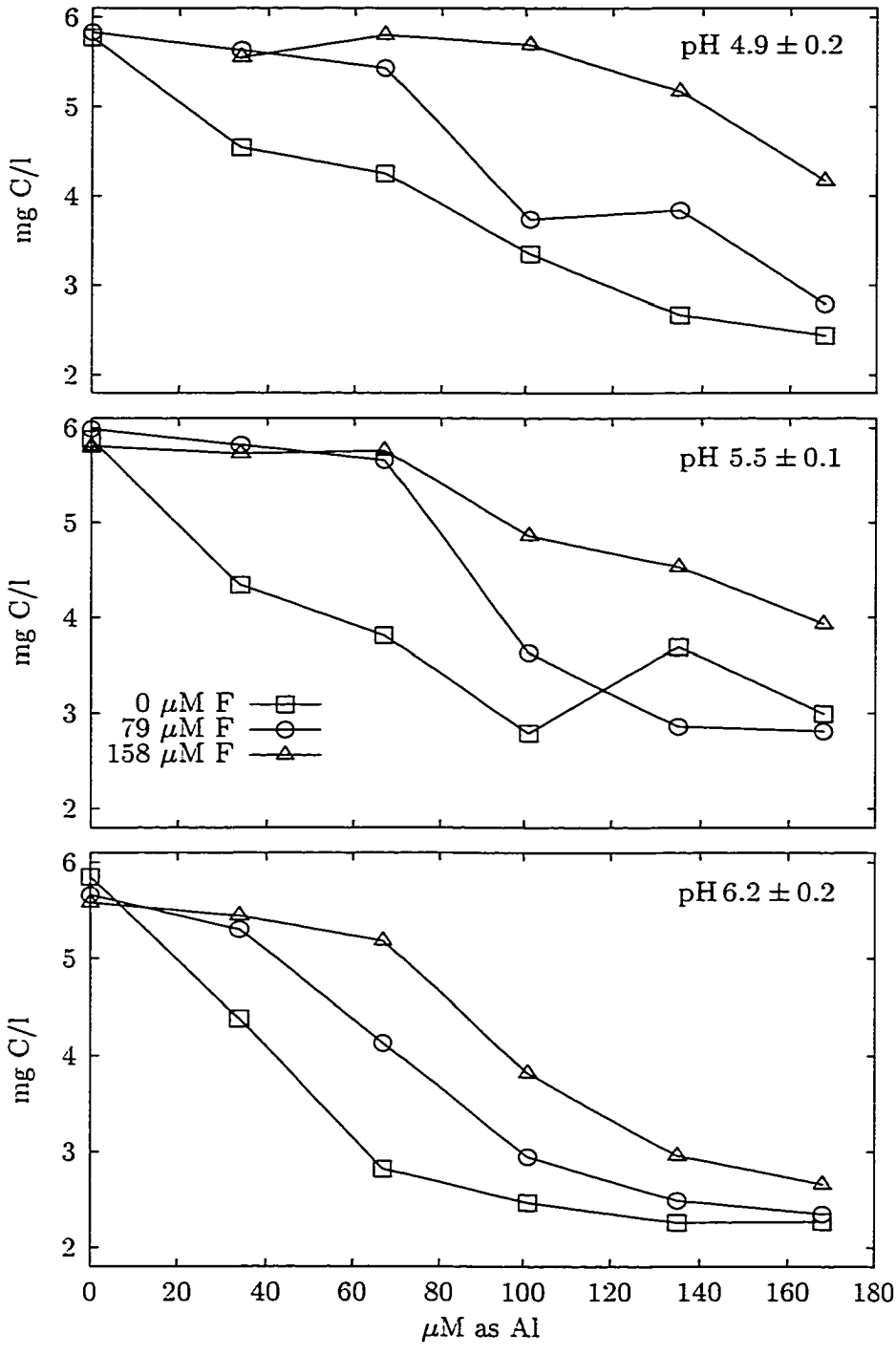

Figure 2.5. Settled water DOC as a function of alum dose, fluoride concentration, and pH.

species do not complex fluoride to a great extent. For these reasons, additional jar tests were conducted on high-alkalinity water and using prehydrolyzed and iron-based coagulants.

2.3.2. Effects of Fluoride on Coagulation of a High Alkalinity – Low DOC Water

In a separate effort, the impacts of fluoride on coagulation of a natural water (Lake Ontario) were studied. This source water was very low in turbidity and DOC and moderately high in alkalinity. The extreme low specific UV_{254} absorbance indicated that the NOM contained in this water was largely hydrophillic and difficult to remove by coagulation (Edzwald *et al.*, 1985; White *et al.*, 1997). These experiments were conducted with and without pH adjustment, resulting in settled water pH of 6.4 ± 0.2 and 7.4 ± 0.2, respectively. Alum doses ranged from 0 to 50 μM as Al and fluoride was added at concentrations of 0 and 79 μM. Instead of turbidity and DOC, particle concentration and UV_{254} were used to characterize the impacts of fluoride.

The results of the study with Lake Ontario water are presented in Figures 2.6 and 2.7. Without acid addition, alum caused only a small decrease in pH from 7.7 to approximately 7.4. Regardless of whether fluoride was added to the raw water, particle removal occurred at the lowest alum dose. A substantial decline in particle concentration at higher doses was not observed. At an alum dose of 34 μM, fluoride had a small, but measurable impact on particle removal. There was essentially no difference in settled water UV_{254} due to prefluoridation. Dissolved aluminum concentrations measured following the tests at pH 7.4 spanned a narrow range between 5 and 10 μM Al. The good agreement with the values predicted by chemical equilibrium computations (Figure 2.1) suggests that the lack of fluoroaluminum complex formation caused the almost negligible effects on NOM and particle removal.

When the coagulation pH was adjusted to 6.4 (using hydrochloric acid) the addition of fluoride to the raw water had a far greater effect (Figure 2.7). At this pH, a higher alum dose was required to attain a settled water particle concentration of 10^5/ml when no fluoride was added, whereas no particle removal was achieved at any dose after prefluoridation. There were also noticeable differences in removal of UV-absorbing substances and in dissolved aluminum concentrations (not shown). In the absence of fluoride, approximately 2 μM Al remained in solution at this pH, whereas the soluble aluminum fraction was in the range

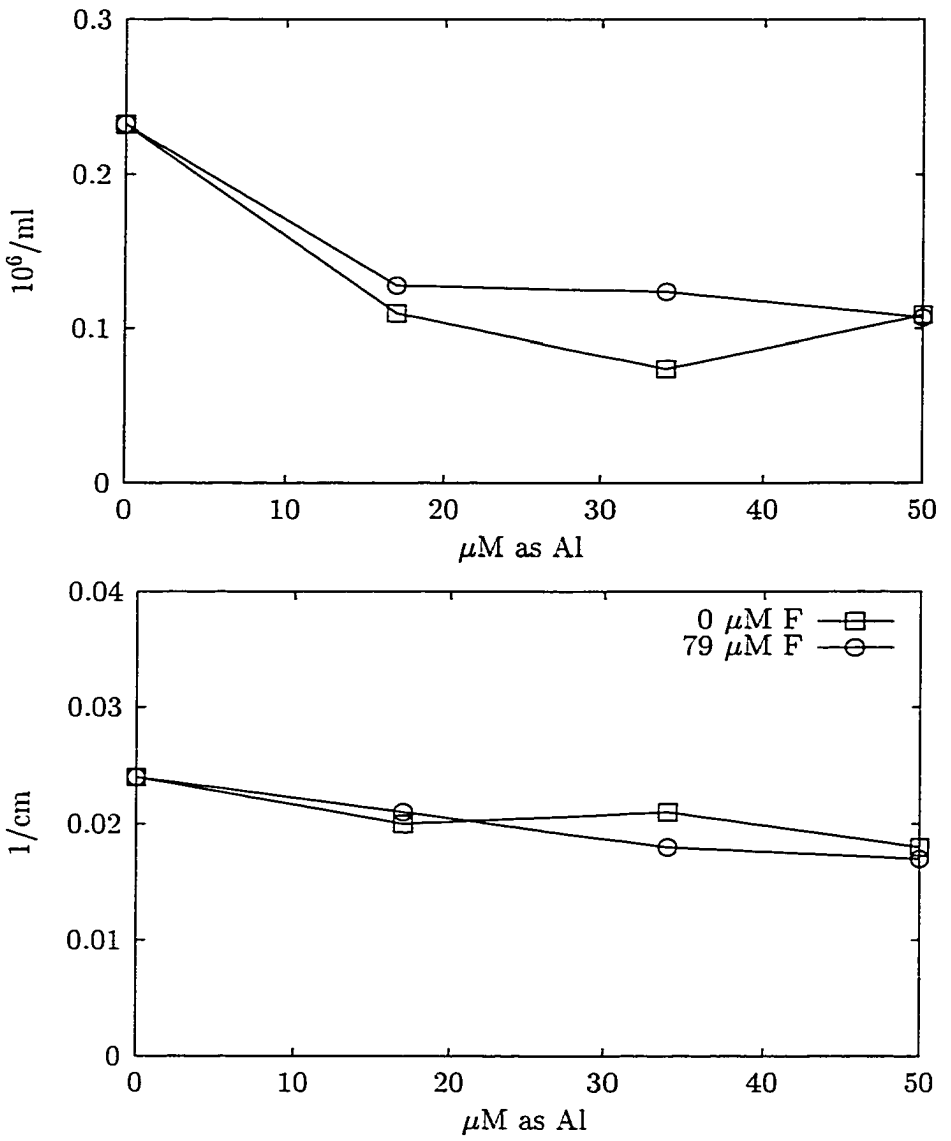

Figure 2.6. Particle Concentration and UV_{254} as a function of alum and fluoride dose at pH 7.4 ± 0.2 for Lake Ontario water.

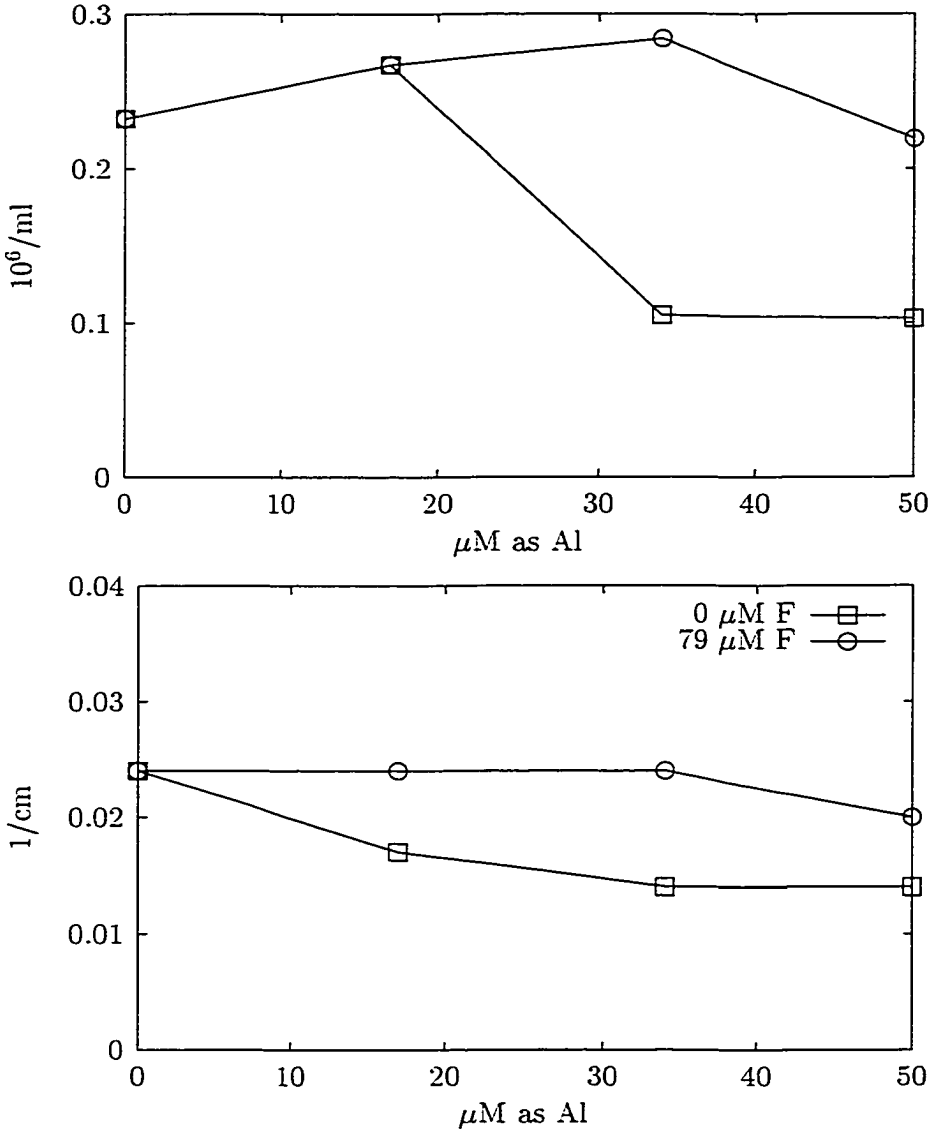

Figure 2.7. Particle Concentration and UV_{254} as a function of alum and fluoride dose at pH 6.4 ± 0.2 for Lake Ontario water.

between 22 and 27 μM Al at a total fluoride concentration of 79 μM. These findings further illustrate that the aqueous chemistry of fluoride and aluminum was the major cause for the negative effects on NOM and particle removal observed in this study.

2.3.3. Effects of Fluoride on Coagulation with Ferric Chloride

The influence of fluoride on particle and NOM removal may be less detrimental when a iron-based coagulants are used. As noted earlier, preliminary chemical equilibrium modeling indicated that iron does not complex fluoride to a great extent at typical treatment pH values. Therefore, coagulation jar tests with ferric chloride were conducted to confirm that the affinity of aluminum to fluoride caused the negative impacts on particle and NOM removal in the previous tests and not reactions directly between fluoride and particles and NOM. The same synthetic raw water used with alum was coagulated at equimolar metal concentrations (0 to 168 μM as Fe) and at three different pH values (4.5 ± 0.4, 5.5 ± 0.2, and 6.1 ± 0.1). Coagulation with ferric chloride is generally practiced at lower pH compared to alum. Fluoride was added to result in concentrations of 0, 79, and 158 μM. The results from electrophoretic mobility (EM) and turbidity measurements are shown in Figures 2.8 through 2.10.

Generally, the influence of coagulation pH on turbidity removal was greater than in the tests with alum. The corresponding electrophoretic mobilities indicate that the charge of the coagulated particles decreased with increasing pH, regardless of the applied fluoride dose. In some instances (Figure 2.8, 0 μM F, pH 5.5 and 6.1) the onset of turbidity removal occurred at EM values as little as $-1.5\,\mu\mathrm{m\,cm/(V\,s)}$. At the lowest pH, the settled water turbidity increased with doses greater than 101 μM Fe. This effect was likely due to charge reversal and was less pronounced in the presence of fluoride (Figures 2.9, 2.10), suggesting that fluoride interacted with the coagulant/coagulated particles. The critical coagulant concentrations (CCC) for these experiments were determined based on the lowest dose at which substantial turbidity removal occurred and the values are listed in Table 2.6. A missing data point prevented an accurate estimate of the CCC for pH 4.5 and 79 μM F.

These data show that a greater ferric chloride dose was necessary to destabilize the suspension when fluoride was added. However, the coagulation pH appeared to be the

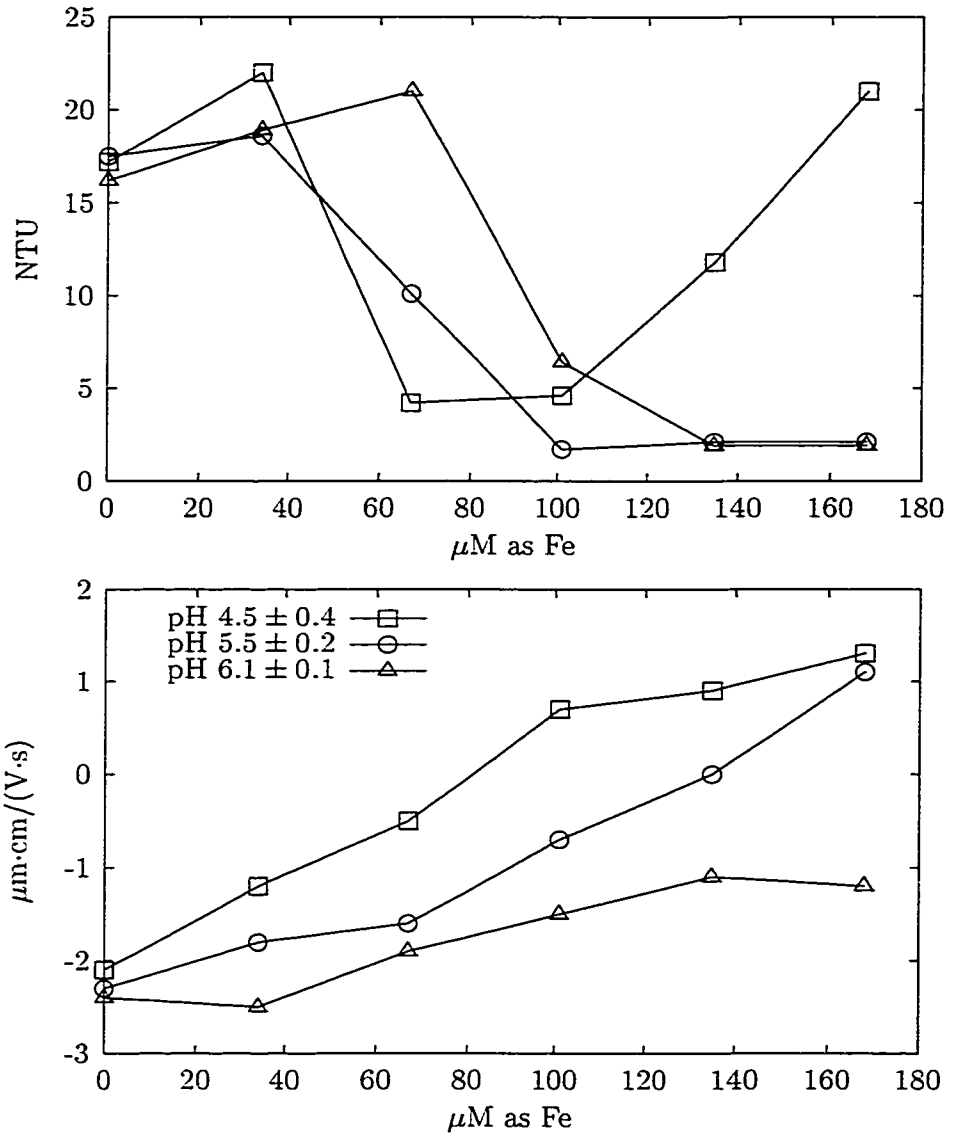

Figure 2.8. Settled water turbidity and electrophoretic mobility as a function of ferric chloride dose and pH without fluoride.

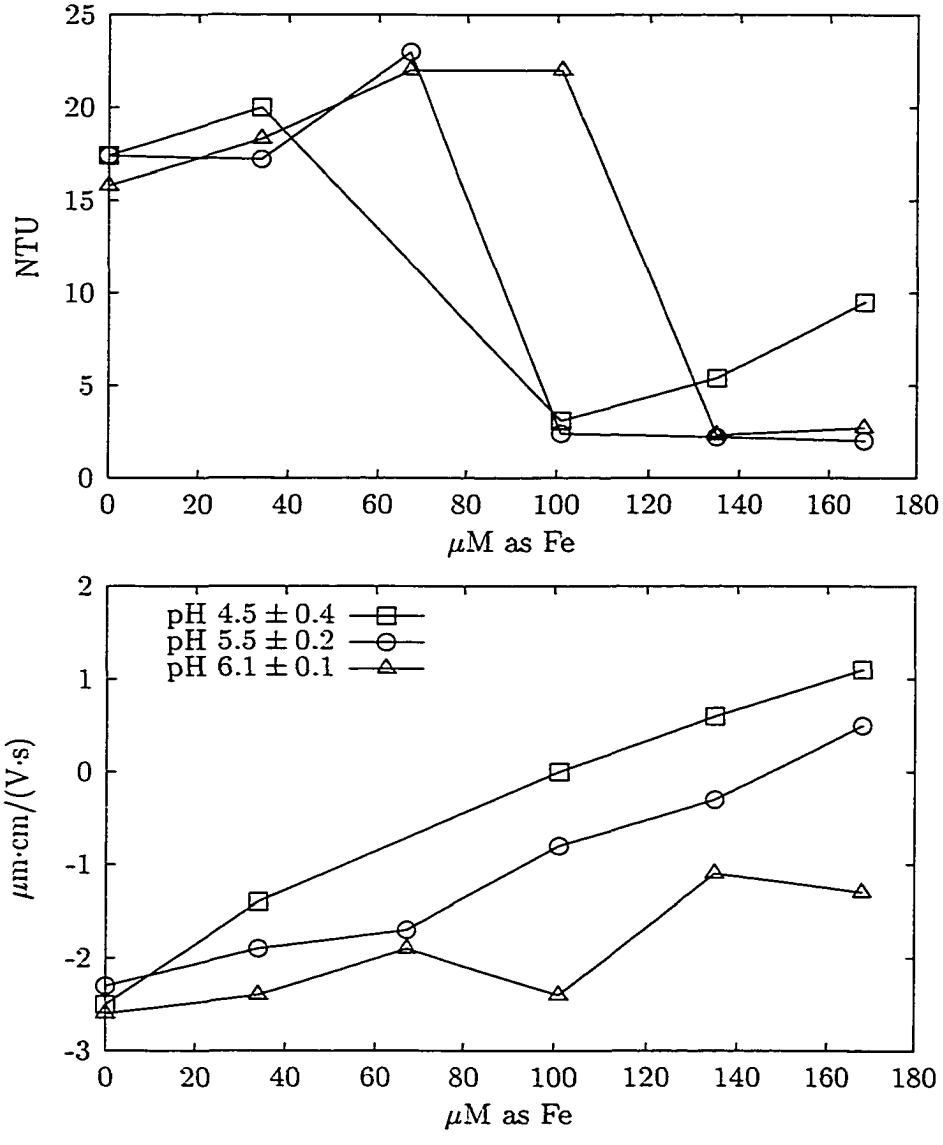

Figure 2.9. Settled water turbidity and electrophoretic mobility as a function of ferric chloride dose and pH at a fluoride concentration of 79μM (1.5 mg F/l.)

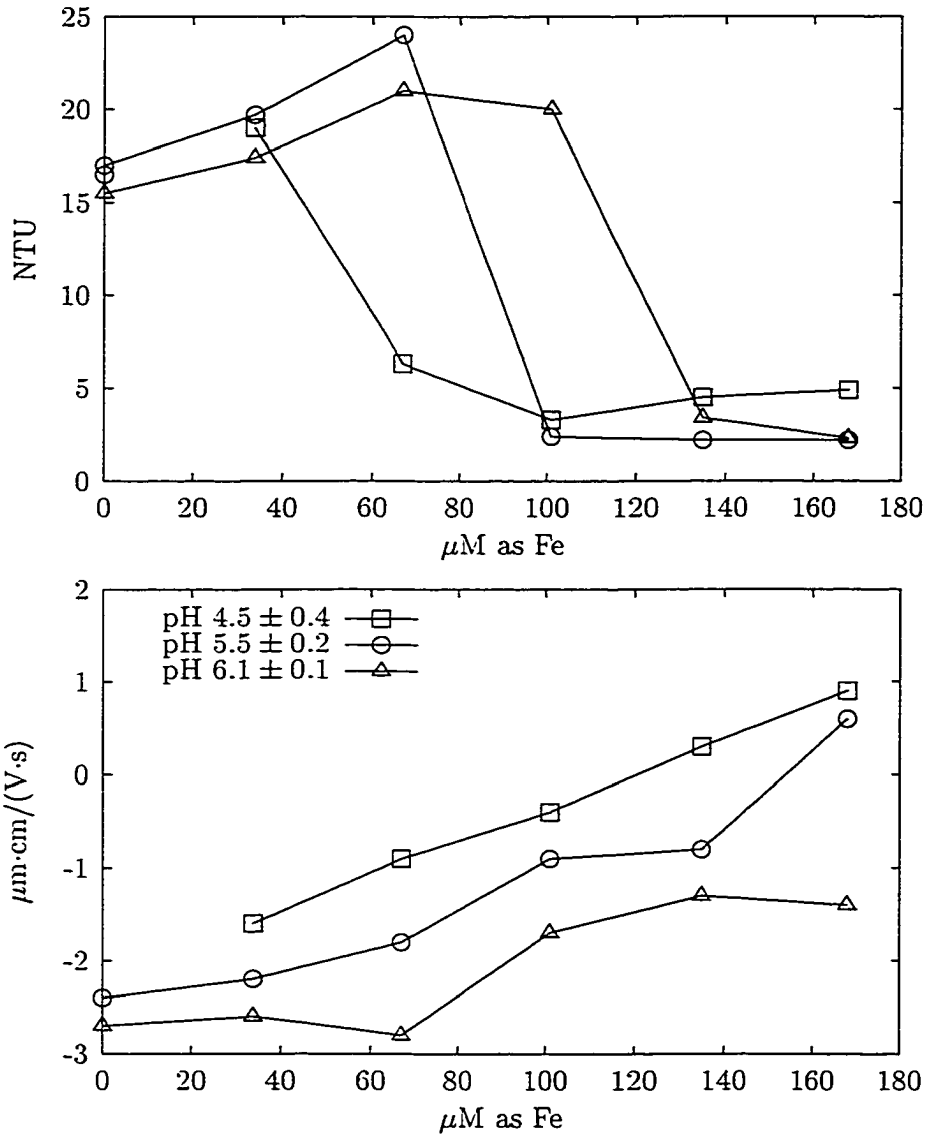

Figure 2.10. Settled water turbidity and electrophoretic mobility as a function of ferric chloride dose and pH at a fluoride concentration of 158μM (3 mg F/l.)

Table 2.6. Critical coagulant concentration (μM as Fe) as a function of pH and fluoride dose.

	0 μM F	79 μM F	158 μM F
pH 4.5 $\pm$ 0.4	67	-	67
pH 5.5 $\pm$ 0.2	67	101	101
pH 6.1 $\pm$ 0.1	101	135	135

dominating factor for particle removal. As opposed to the experiments with alum, the CCC increased with increasing pH and doubling the fluoride concentration did not have any impact. The importance of pH in these experiments also becomes apparent when examining the EM as a function of pH and the corresponding minimum coagulant dose that resulted in turbidity removal at all fluoride concentrations. These data are shown in Table 2.7.

Table 2.7. Electrophoretic mobility as a function of pH, ferric chloride and fluoride dose (μm cm/(V s)).

	0 μM F	79 μM F	158 μM F
pH 4.5 $\pm$ 0.4, 67 μM Fe	-0.5	-	-0.9
pH 5.5 $\pm$ 0.2, 101 μM Fe	-0.7	-0.8	-0.9
pH 6.1 $\pm$ 0.1, 135 μM Fe	-1.1	-1.1	-1.3

There was a small decrease in mobility with increasing fluoride concentration at the same ferric chloride dose, which indicates that iron-fluoride complexes were formed. This interaction possibly occurred at the particle-water interface, because soluble iron-fluoride complexes are not very stable under the tested conditions as indicated earlier. Although higher doses of ferric chloride were applied to achieve turbidity removal at increasing pH, the particle mobilities were more negative. Apparently, the speciation of iron hydrolysis products that led to destabilization of the suspension varied significantly in the examined pH range.

Settled water DOC concentrations as a function of ferric chloride dose, fluoride con-

centration, and pH are shown in Figure 2.11. These data indicate that fluoride did not affect NOM removal noticeably when the iron coagulant was used. Coagulation at pH 4.5 provided the greatest reduction in DOC with finished water concentrations slightly lower than those obtained when alum was used.

In summary, the limited effects of fluoride on coagulation with ferric chloride support the hypothesis that the formation of soluble fluoroaluminum complexes is the main cause for negative impacts on chemical treatment with alum.

2.3.4. Effects of the Order of Fluoride Addition on Coagulation With Alum

In an effort to determine how the point of fluoride addition would affect particle and NOM removal in treatment processes with alum, additional jar tests were conducted. The three test series conducted involved coagulation of synthetic water (Northwest River water with MIN-U-SIL) without fluoride, after addition of 79 μM fluoride to the raw water (premix), and addition of 79 μM fluoride after the two-minute rapid mix period (postmix). The alum dose was varied between 0 and 269 μM as Al and the appropriate amount of NaOH was added to the raw water to attain approximately pH 6 in the settled water. The obtained pH values ranged from 6.0 to 6.4 with the exception of the postmix-fluoridation experiments in which the three highest alum doses were applied (pH 5.6–5.8). The synthetic water had a DOC concentration of 10 mg/l C and a SUVA of 5.0 l/mg·m indicating that a large fraction of the NOM was humic substances and that substantial removal could be achieved. In these experiments, UV absorbance at 254 nm (UV_{254}) after filtration through a 0.45 μm membrane was utilized as a surrogate parameter for the dissolved organic carbon concentration.

The results from turbidity and UV-measurements in these experiments are presented in Figure 2.12. These data show that the addition of fluoride to the untreated water required a substantially higher alum dose for removal of particles than coagulation without fluoridation. In contrast, when fluoride was added immediately after the rapid mix period, there was no effect on settled water turbidity. The bottom plot in Figure 2.12 reveals that at alum doses required for particle removal, a substantial reduction in UV_{254} was achieved. Premix-fluoridation impeded NOM removal although these effects were not as detrimental as observed in earlier experiments. Although particle removal was unaffected

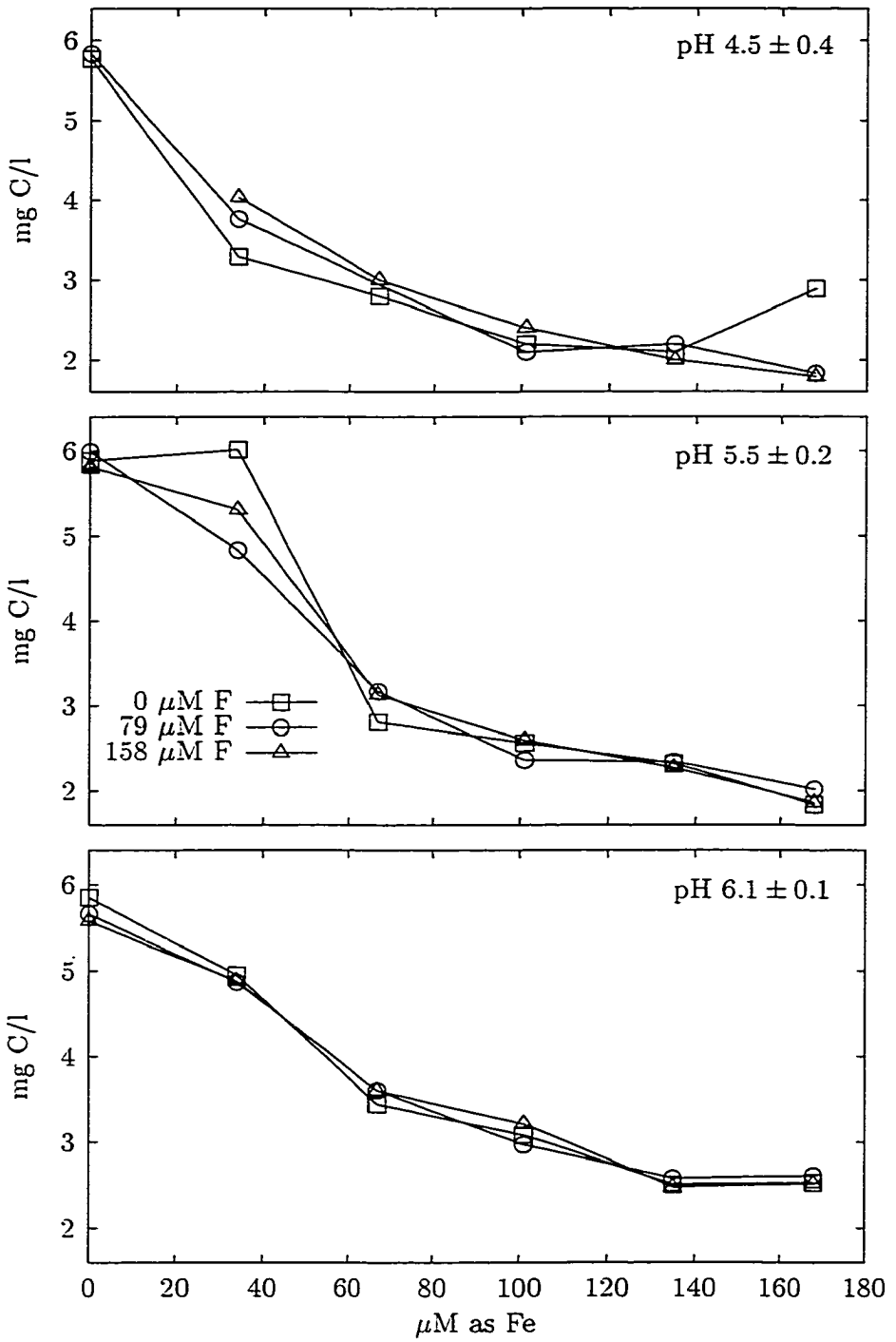

Figure 2.11. Settled water DOC as a function of ferric chloride dose, fluoride concentration, and pH.

by the addition of fluoride *after* mixing, there was a measurable influence on UV_{254}. This observation suggests that fluoride affects the mechanisms that are responsible for NOM removal and particle destabilization differently.

Examination of the total dissolved aluminum and fluoride concentrations depicted in Figure 2.13 may help explain the observed differences. In the experiments with the lowest alum dose, all the added aluminum was dissolved and turbidity and UV_{254} remained at their initial values regardless of fluoride addition. In the examined pH range, the theoretical solubility of $Al(OH)_3$ (considering only inorganic complexes) is exceeded at this dose. It is possible that aluminum formed soluble Al-NOM complexes that prevented the formation of a (filtrable) precipitate. The solution also may have been supersaturated with respect to $Al(OH)_3(s)$, however, the silica particles in the synthetic water should have provided sufficient nucleation sites for precipitation to occur.

At a dose of 67 μM Al, there was a substantial difference in dissolved aluminum concentrations among treatments. Where fluoride was added just prior to the coagulant, all the aluminum remained in solution to satisfy the demand exerted by fluoride and NOM to form soluble compounds; turbidity and UV_{254} did not change. Under the other treatment conditions, a substantial drop in dissolved aluminum concentration and UV_{254} occurred. Apparently, the increased dose induced precipitation of $Al(OH)_3$ and coadsorption of organic matter and caused a small increase in turbidity. Where fluoride was added after mixing, its residual concentration decreased noticeably. This further supports the conclusion that an amorphous precipitate had formed during the rapid mix phase and provided adsorption sites for anions. However, the dissolved aluminum concentration is slightly greater compared to the unfluoridated water, which indicates that the amorphous phase had partially dissolved. This dissolution process must have been slow considering the difference in dissolved aluminum to the premix experiment and the elapsed time between fluoride addition and sample filtration of approximately one hour.

At alum doses higher than 67 μM Al, precipitate was also formed in the premix-fluoridation tests as evidenced by the onset of removal of UV-absorbing substances, fluoride, and aluminum from solution. At an alum dose of 151 μM Al, no removal of turbidity occurred when fluoride was added to the raw water. Despite the fact that at this dose, pH,

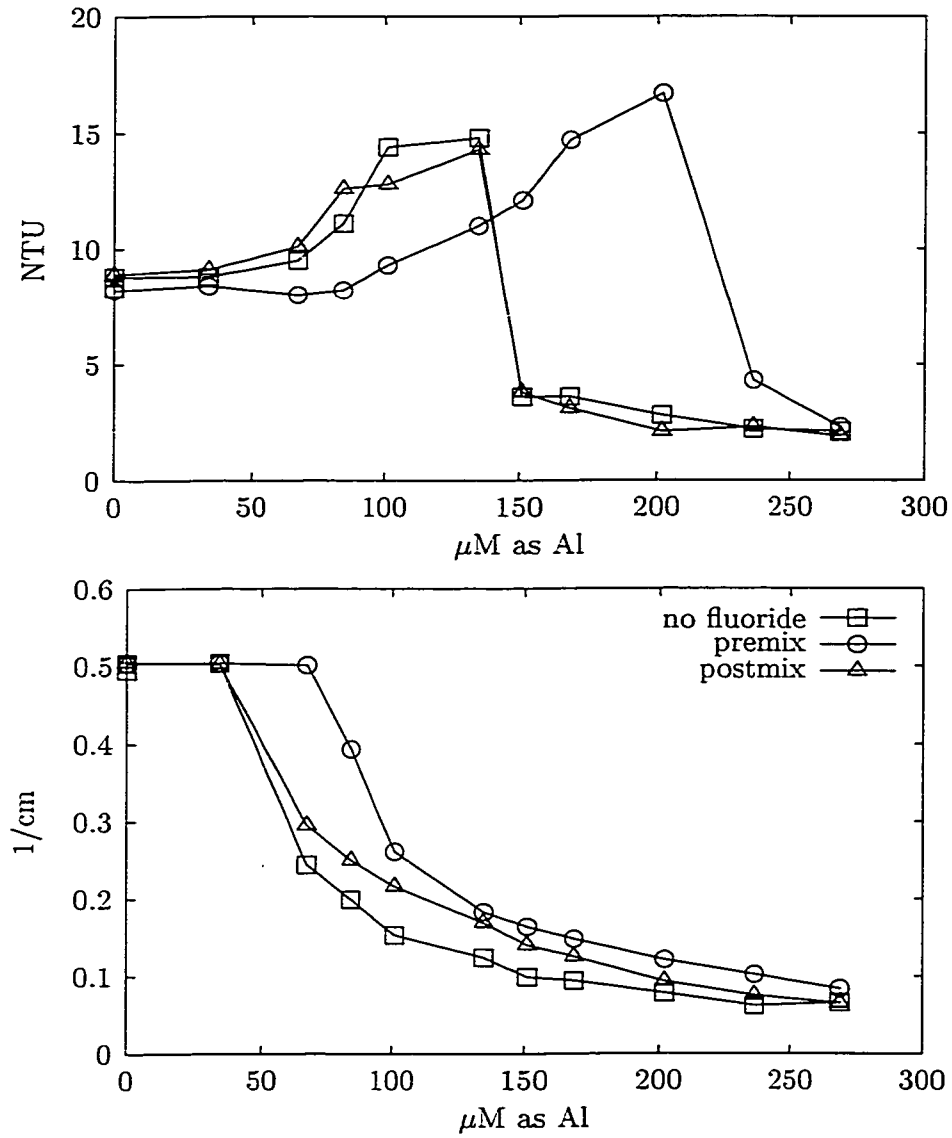

Figure 2.12. Effect of the point of fluoride addition on turbidity and UV_{254} as a function of alum dose (fluoride concentration = 79 μM, pH$\approx$ 6).

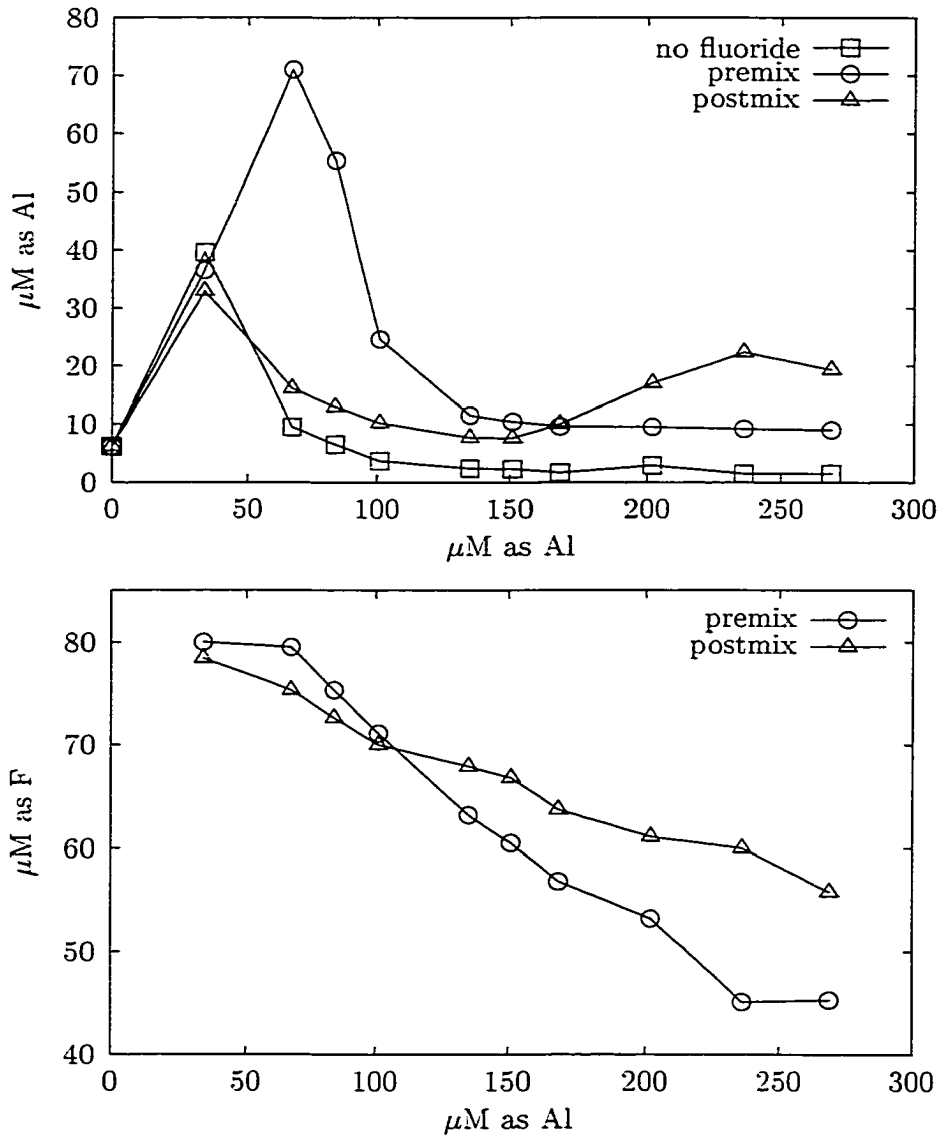

Figure 2.13. Effect of the point of fluoride addition on total dissolved aluminum and fluoride concentrations as a function of alum dose (pH≈ 6).

UV_{254}, dissolved aluminum and fluoride concentration were nearly identical to the postmix experiment, turbidity exhibited a further increase. It appears that although the addition of fluoride after the rapid mix period caused resolubilization of aluminum, this process was too slow to cause breakup of already aggregated particles and may have only remobilized natural organic molecules that were adsorbed.

The apparent differences in removal of fluoride from solution suggest that more adsorption sites were available when fluoride was added prior to the rapid mix. Consequently, the dissimilar structural features of the precipitate may have also contributed to the differences in particle and NOM removal.

Based on these observations, it can be concluded that fluoride has the most negative impact on coagulation with alum when added at a point before aluminum hydrolysis occurs. A limited set of tests involving coagulation of a humic acid suspension using a prehydrolyzed aluminum coagulant confirmed this finding (not shown).

2.3.5. Effects of Sulfate on Coagulation with Alum

To examine whether elevated sulfate concentrations can affect NOM removal in waters coagulated with alum, a limited series of jar tests were conducted utilizing a portion of the synthetic water prepared for studying the effect of the point of fluoride addition. Alum doses were varied between 0 and 269 μM as Al and the pH was adjusted with sodium hydroxide to result in a settled water pH of 6.0 ± 0.3. Sulfate was added to the raw water at concentrations of 1.5 mM and 3.0 mM as SO_4. The results from turbidity and dissolved aluminum measurements are presented in Figure 2.14.

At alum doses smaller than the CCC, both sulfate doses resulted in a similar increase in turbidity compared to the control. At greater coagulant concentrations, only the 3.0 mM spike had a noticeable influence with higher turbidity values at 150-235 μM Al. It is unlikely that these effects were due to formation of aluminum sulfate ion pairs and inhibition of $Al(OH)_3$ precipitation, because one would expect general trends as observed in the presence of fluoride. Snodgrass *et al.* (1984) studied particle formation and growth in dilute aluminum solutions and suggested that sulfate primarily affected nucleation kinetics and influenced the rate of particle aggregation to a smaller extent. Although these researchers only examined

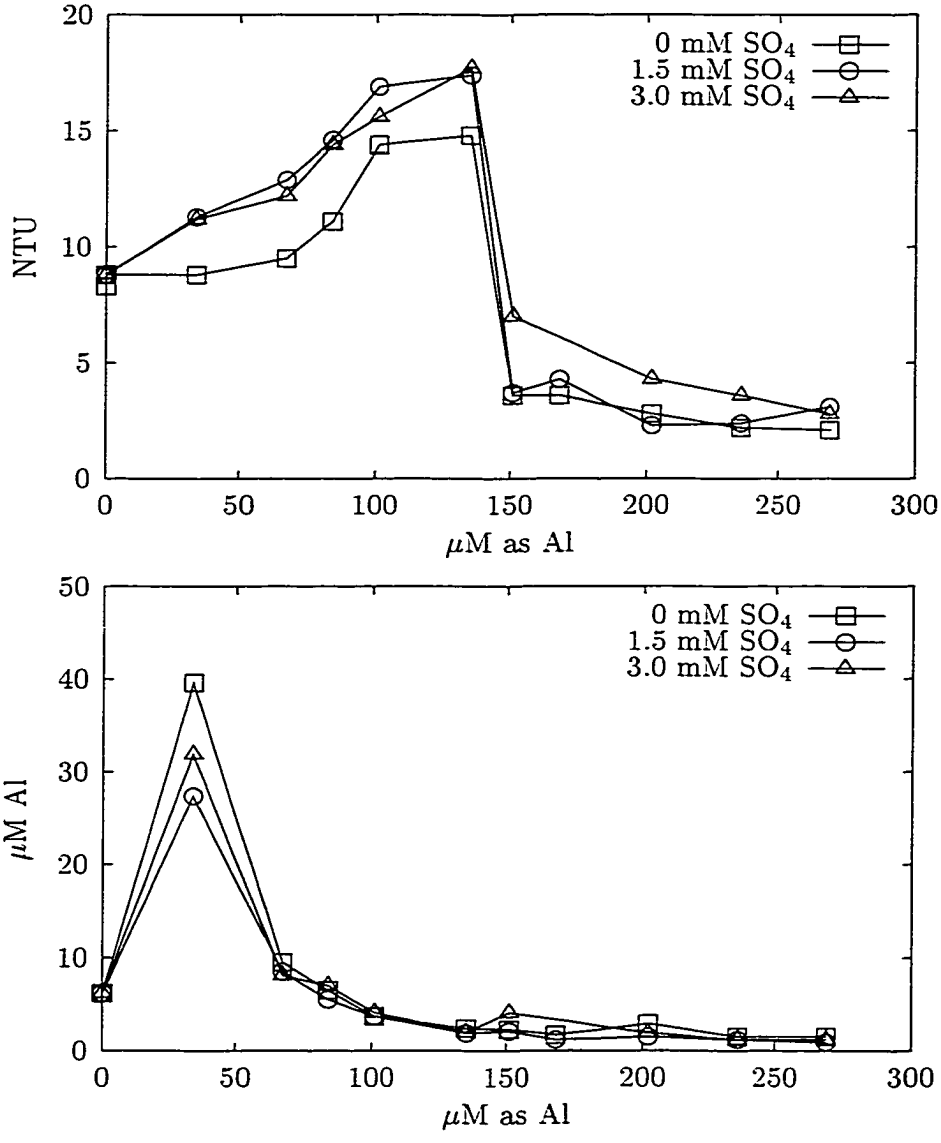

Figure 2.14. Turbidity and total dissolved aluminum as a function of alum and sulfate dose.

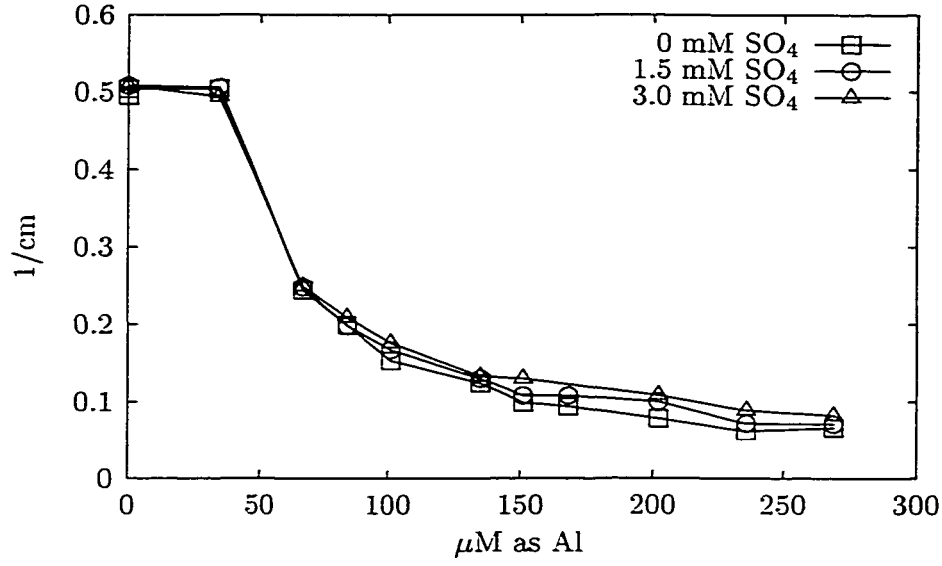

Figure 2.15. UV_{254} as a function of alum and sulfate dose.

aluminum-to-sulfate ratios of Al : SO_4 > 1 : 1.5, the slight increase in turbidity observed here may be related to an increase in non-aggregating aluminum hydroxide nuclei. This assertion is supported by the fact that at the lowest alum dose, dissolved aluminum slightly decreased when excess sulfate was present (Figure 2.14). At higher alum doses, there were essentially no differences in residual aluminum concentrations due to sulfate.

The graphs in Figure 2.15 show that sulfate had a negligible effect on removal of UV-absorbing substances. These results contrast the observations by Maulding and Harris (1968), who observed "deleterious effects" on color removal at similar metal-to-sulfate ratios. However, these researchers conducted their experiments at pH < 4, where ion-pairing may be more favorable due to the low concentration of competing hydroxyl ions. Based on the SUVA of the synthetic water used in these tests and the efficient removal of UV_{254} following coagulation with alum, it can be concluded that the NOM strongly complexed to aluminum. Thus, if sulfate influences removal of organic substances, this effect should be more pronounced in low SUVA waters.

2.4. Influence of Inorganic Anions on Coagulation

The investigations of the effects of two common anions on coagulation showed that fluoride can, under certain circumstances, significantly impact the removal of particles and natural

organic matter in conventional water treatment. These findings are important because fluoride can impair efforts to maintain an effective barrier against pathogenic microorganisms and to minimize the formation of disinfection byproducts. To offset these effects and achieve removals equal to those in the absence of fluoride, higher coagulant doses were needed. If fluoride is added for dental caries prophylaxis, these potential effects can be avoided by discontinuing the use of fluoridation or by moving the point of application. However, there are both surface and groundwaters that naturally contain fluoride at levels often exceeding several hundred micromols per liter. In these cases, solutions for mitigating the negative impacts are often not straightforward.

On the other hand, sulfate, which can be introduced to the treatment process through the use of alum (or ferric sulfate), seemed to have little influence even when added at (molar) concentrations more than ten times as high as the aluminum dose. On the contrary, work by other researchers has shown that sulfate has the beneficial effect of preventing formation of highly charged polymeric hydroxoaluminum complexes during hydrolysis, inducing rapid precipitation of a settable $Al(OH)_3(s)$-floc (Hanna and Rubin, 1970; Hayden, 1971). This significant difference in effectiveness to influence the treatment process is a consequence of the ability of the anion to chemically interact with the metal ion. Fluoride, a strong lewis base, has a strong affinity to form covalent bonds with aluminum, whereas the interaction of sulfate with Al^{3+} is largely electrostatic (Snodgrass *et al.*, 1984).

Based on the results from the experiments conducted for this work, the effects of fluoride on coagulation depend on type of coagulant and dose, point of application, and pH. A substantial impact on the treatment process can be expected when the active coagulant species are in-situ hydrolyzed aluminum monomers. This is typically the case when aluminum sulfate (alum) is applied in conventional water treatment at pH 5–7. In the process of mixing this chemical with the raw water, fluoride, which may be already present or which is being added concurrently, can effectively compete with hydroxyl ions for the aluminum cation, inhibiting the formation of the hydrolysis products that are responsible for destabilizing particles and adsorbing or coprecipitating natural organic matter. Limited experiments confirmed that the use of an aluminum-based coagulant that consists of prehydrolyzed hydroxoaluminum complexes (e.g., polyaluminum chloride) can mitigate the

deleterious effects that were observed with alum. Because the aluminum cation has undergone hydrolysis prior to application to the water, a rapid formation of AlF_x complexes can not occur. In fact, the reversal of the hydrolysis reactions may be a required step in the formation of fluoroaluminum complexes, and this process may be too slow to detect any immediate influence of fluoride. Jar tests with ferric chloride demonstrated that utilizing an iron-based coagulant may also help control the negative influence of elevated fluoride concentrations in raw waters. Ferric iron can complex fluoride appreciably; however, this interaction is typically restricted to pH values below the range where coagulation with iron-based coagulants is practiced (pH < 4).

In the experiments with alum, it was also observed that the effects of fluoride diminish with increasing coagulant dose. It is apparent that once the fluoride "demand" is overcome, an increase in alum dose allows hydrolysis products to form. Flouride can also be removed from solution by adsorption to the aluminum hydroxide precipitate. Therefore, the relative influence of flouride decreases with increasing dose. However, at an alum dose where adequate particle and NOM removal is achieved, a significant amount of fluoride may remain in solution. In the pH range where alum coagulation is typically practiced, fluoride is largely present as AlF_x. Consequently, the residual fluoride can not only lead to exceeding regulatory levels for aluminum in the finished water, but also result in precipitation of $Al(OH)_3(s)$ in the distribution system. To avoid high finished water aluminum concentrations and postprecipitation, the coagulant dose would have to be increased to maximize fluoride removal.

The point of fluoride addition plays a significant role in the effectiveness of this anion to affect coagulation with alum. The addition of fluoride *after* the coagulant affected the removal of particles and NOM substantially less than during prefluoridation. The critical coagulant concentration in the experiment where fluoride was added two minutes after coagulant was identical to that whene no fluoride was applied. Similar to the case with polymeric aluminum coagulants, it is likely that the formation of fluoroaluminum complexes is kinetically not favored after hydroxoaluminum monomers or precipitates have formed. In particular, in pH regions where $Al(OH)_3(s)$ is predominant, the adsorption to and dissolution of the solid may have to precede formation of dissolved AlF_x species. Similarly, fluoride

may exert only a small effect on Al-NOM surface complexes and/or precipitates that have already formed. However, the experimental evidence suggested that some dissolution may occur, mobilizing previously adsorbed organic matter. Therefore, even when added downstream of the mixing basin where the aluminum hydrolysis product has formed, fluoride may exert an influence on downstream processes, e.g., granular media filtration.

The coagulation pH has a major influence on the effect of fluoride on particle and NOM remvoval, because fluoroaluminum complexes are most stable at pH < 7.5. Initial chemical equilibrium calculations were confirmed in experiments with high-alkalinity water, and based on these results, coagulation practiced at pH values above 7.5 is likely not to be affected by the presence of fluoride. Waters that are high in alkalinity (and pH, i.e., hydroxyl ion concentration) often also contain elevated concentrations hardness ions (calcium, magnesium, iron, etc.), which may also help alleviate the impact of fluoride by competing with aluminum. In practice, a utility may choose to coagulate at higher pH to avoid the detrimental effects of fluoride. However, because the solubility of $Al(OH)_3(s)$ increases with increasing pH > 6.5 (Figure 2.1), the effects of elevated dissolved aluminum concentrations in the finished water as mentioned above need to be considered.

The comparison of the effects of fluoride and sulfate showed that the knowledge of the affinity of the anion for the coagulant metal ion may help predict the negative consequences the anion may have in water treatment. Consequently, negative influences may also occur in other systems with strong metal-ion interactions. These may include effects due to sequestering agents (e.g., condensed phosphates and ferric iron), corrosion inhibitors (orthophosphate), or in the softening process (e.g., fluoride and calcium).

2.5. Summary

Jar tests were conducted to investigate the effect of fluoridation on removal of particles and natural organic matter by alum and ferric chloride coagulation. The results indicated that the efficiency of the coagulation process is substantially decreased when fluoride is added to the raw water at concentrations typically used in water treatment plants. This effect was negligible or at least less pronounced at pH > 7 and when ferric chloride was used. Chemical equilibrium calculations predicted that aluminum forms strong complexes with

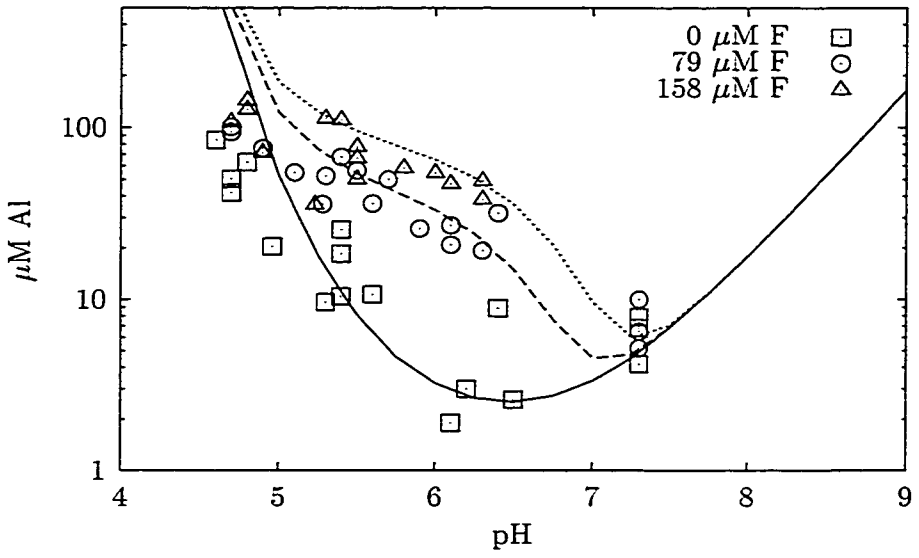

Figure 2.16. Model predicted and measured dissolved aluminum concentration as a function of pH and fluoride dose.

fluoride only at pH < 7.5, whereas iron-fluoride complexes are stable at pH < 4. Therefore, it was concluded that the observed detrimental effects were primarily due to the affinity of aluminum to strongly bond with fluoride, which decreases the amount of aluminum hydrolysis product available for charge neutralization and precipitation. Despite the fact that interactions of aluminum and NOM as well as adsorption of fluoride to aluminum hydroxide were not included in the chemical equilibrium model, dissolved aluminum concentrations were in general agreement with predicted values and supported this conclusion. These data are shown in Figure 2.16.

Variation of the order of chemical addition in the jar tests revealed that the judicious selection of the point of fluoridation can mitigate the deleterious effects on particle and NOM-removal in coagulation treatment with alum. The experimental results suggested that addition of fluoride immediately after the rapid mix period did not affect particle removal and decreased NOM-removal only to a small extent. It was concluded that the dissolution of $Al(OH)_3(s)$ (and other preformed aluminum species) by fluoride is not favored kinetically. In these tests, it was also observed that substantial fluoride removal occurs irrespective of the point of addition. Therefore, aside from the aspect of water quality, addition of fluoride to the raw water can incur increased chemical costs for a water utility.

Contrary to reports by earlier researchers, sulfate did not have a considerable influence on turbidity and DOC removal when added to a synthetic water prior to coagulation with alum at pH 6.

3. THE EFFECTS OF FLUORIDATION IN PILOT-SCALE WATER TREATMENT WITH ALUMINUM SULFATE

3.1. Introduction

The addition of fluoride in potable waters is practiced by many utilities in the United States due to its effect for reducing dental caries (cavities). Approximately 62% of the US population currently receives water that is fluoridated and it is likely in the future that this number will rise, in part driven by legislation (American Dental Association, 1995).

The generally recognized conventional point of addition of fluoride in water treatment plants in the United States is after water has passed through a plant's physicochemical process train and shortly before entering a clearwell or finished-water reservoir. When added in this manner, fluoride is likely to have no influence on the treatment processes occurring upstream. An exception might be where fluoridated water is used for backwashing filters, a practice necessary to remove material, that has accumulated within the filter bed and can cause excessive headloss and turbidity breakthrough. Backwashing is usually accomplished by reversing the flow through the filter at a rate sufficiently high to fluidize the granular medium. Typically, treated, and oftentimes chlorinated and fluoridated water is injected at the bottom of the filter for either a specified time or until the backwash effluent turbidity has decreased below a preset value.

In an effort to assess how fluoridation is commonly practiced at large treatment facilities, a review of plant schematics collected for the Information Collection Rule (U.S. Environmental Protection Agency, 1996) was conducted. This examination revealed that many treatment plants in the US add fluoride at locations other than immediately before a clearwell and that these other points of addition may indeed influence the treatment process, particularly the removal of particles and natural organic matter (NOM). Of the approximately 400 treatment plants that were involved in monitoring under the Information Collection Rule (surface water plants serving >100,000 and groundwater plants serving >50,000 population), thirty-nine were characterized as adding fluoride at or before the point of coagulant addition. The combined (design) flow rate of these plants exceeds 22×10^6 m^3/d.

Another thirty-three treatment plants were described as adding fluoride between the rapid mix and filtration stages and the (design) flow rates of these plants exceeds 11×10^6 m^3/d. These statistics illustrate that a significant volume of water in the United States is treated where fluoride addition occurs somewhere in the midst of the unit processes that target particle and NOM removal.

Prefluoridation (i.e., the addition of fluoride prior to filtration) may also be widely implemented in small and medium-sized facilities. This conclusion can be made because certain states in the U.S. actually require that "unless otherwise approved, fluoride shall be applied to the raw water" (Virginia Department of Health, 1995, Waterworks Regulations).

An assessment of how many treatment facilities utilize fluoridated water for the purpose of filter backwashing, cannot be made a priori. However, because many treatment plants are likely to have just a single storage facility for finished (and fluoridated) water, from which backwash water is withdrawn, it can be expected that this practice is fairly common.

The bench-scale study results presented in Section 2 indicated that fluoride considerably impaired particle and NOM removal when added prior to the coagulant. To confirm these findings, further studies were conducted utilizing a pilot-scale facility specifically designed to mimic a "real" treatment plant. As a minor subset of this work, it was also examined whether the use of fluoridated backwash water has an impact on filter performance. It is well known that deep bed filtration requires proper chemical pretreatment to facilitate attachment of particles to the filter media (Cleasby, 1990). Following backwashing, filter effluent turbidity typically exhibits an initial peak and decreases slowly while the backwash water is displaced and destabilized particles accumulate in the filter aiding in the collection of more particles. Considering the impact of fluoride on the solution chemistry of aluminum and the stability of alum coagulated particles as described in Section 2, it was suspected that utilizing fluoridated backwash water can affect the filter performance in two ways. First, during backwashing fluoride could dissolve precipitated aluminum resulting in a "cleaner" filter bed than that where alum floc was removed by fluid shear alone. Second, because after backwashing fluoride is still present in the filter – either dissolved in the residual backwash water or possibly adsorbed to the granular material – there is the potential that after filter startup particles are not as effectively retained resulting in a prolonged ripening period.

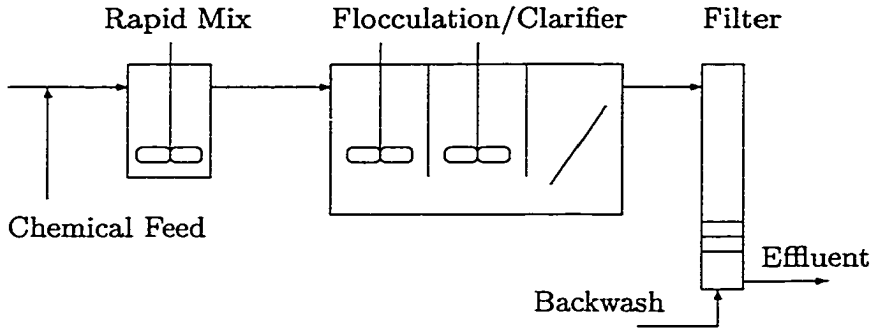

Figure 3.1. Harwood's Mill pilot plant.

If the pilot-scale studies confirm that fluoride indeed has a role in influencing particle and organic matter removal in conventional water treatment, then these findings could have significant ramifications relative to efforts to optimize treatment to ensure removal of Cryptosporidium oocysts and NOM that serves as disinfection by-product precursor material.

3.2. Materials and Methods

3.2.1. Pilot Plant Operation

A short duration (17 days) pilot study to assess the impact of prefluoridation was conducted utilizing the permanent pilot plant at the Harwood's Mill water treatment facility that is continuously operated by Newport News Waterworks, Virginia. The 6.8 m^3/h plant consists of the unit processes mixing, flocculation, upflow sludge blanket clarification, and multimedia filtration. Two filters were operated at a loading rate of 9.8 m/h and the media consisted of 76 mm of gravel, 230 mm of sand, and 610 mm of anthracite coal. The plant – a schematic is shown in Figure 3.1 – was monitored for 150 hours without fluoride addition followed by addition of commodity grade hydrofluosilicic acid fed to the rapid mix for a period of 150 hours to result in a fluoride concentration of approximately 80 μM (1.5 mg F/l). After turning off the fluoride feed, the water quality was monitored for an additional 90 hours. During the study, the coagulation pH was not controlled and remained

at pH 6 ± 0.1. The alum dose was 150 μM as Al (45 mg/l as $Al_2(SO_4)_3 \cdot 14\,H_2O$). To mimic the conditions at the full scale facility, an organic polymer (Allied Colloids, Percol LT22S) was fed at a dose of 0.8 mg/l (as product). The filters were backwashed for ten minutes when the head overlying the filters exceeded 2.4 m. During the study period, between one and three samples were taken daily from the raw water influent, clarifier effluent and filter effluent. Both filtered (0.45 μm) and unfiltered sample portions were analyzed for organic carbon, UV absorbance at 254 nm (UV_{254}), fluoride and aluminum concentrations. Turbidity and filter head were recorded at regular intervals at least five times every day. UV_{254} and dissolved organic carbon (DOC) measurements were used to calculate specific ultraviolet absorbance (SUVA) values during the study using the relationship

$$\text{SUVA}\ \left[\frac{\text{l}}{\text{m}\cdot\text{mg}}\right] = \frac{UV_{254}\ [\text{m}^{-1}]}{\text{DOC}\ [\text{mg C/l}]}$$

In a separate effort (conducted 26 months after the pilot-scale prefluoridation study), the effects of utilizing fluoridated water for filter backwashing were studied. The pilot plant was operated under the same conditions as described above without prefluoridation, with the exception that both filters were backwashed every 72 hours regardless of headloss. For one of the two filters that were monitored, fluoridated water (79 μM F, 1.5 mg/l) was utilized for the backwash, whereas the other filter received unfluoridated water. Filtered water from the pilot plant stored in polyethylene tanks was used as a backwash water source. During the 10-minute interval up to six samples were collected from the backwash wastewater. Immediately after the filters were put back online, samples were taken at short intervals from each filter effluent and retained for aluminum and fluoride analysis. At the same time, filter effluent turbidity was recorded using the installed online turbidity meters. Filter head data were collected periodically throughout the filter cycle. Samples taken from the backwash water were split and one aliquot was passed through a 0.45 μm polycarbonate membrane. Both portions were retained for aluminum and fluoride analysis; the turbidity of the unfiltered sample aliquot was measured upon return to the laboratory.

3.2.2. Analytical Methods

The online turbidimeters (HACH 1720C) were calibrated and operated according to the manufacturer's instructions. Laboratory analyses were performed following the procedures outlined in *Standard Methods* (Eaton *et al.*, 1995) and are described in greater detail in Appendix B.

3.3. Results and Discussion

3.3.1. Treatment Performance During Prefluoridation

The major goals associated with the prefluoridation pilot-plant study were to determine if prefluoridation could negatively impact the removal of particles and organic matter and cause an increase in the aluminum concentrations in treated water.

The values for turbidity during the study period in the raw water and at points following clarification and filtration are illustrated in Figures 3.2 and 3.3. Where appropriate, the beginning and the end of the fluoridation period are indicated by vertical dashed lines. During the study period raw water turbidity remained fairly constant at slightly below 4 NTU except for higher turbidity values for three days near 300 hours. Dissolved organic carbon concentrations ranged from 5.4 to 7.1 mg C/l ($\bar{x} \pm \sigma = 5.9 \pm 0.5$ mg C/l). Considering that the coagulant dose necessary for "optimum" organic matter removal usually exceeds that to achieve turbidity removal (Hall and Packham, 1965; Semmens and Fields, 1980), the variation in raw water turbidity was not expected to have any impact on treatment efficiency.

It is apparent that after the fluoride feed was started after 150 hours, the clarifier turbidity values increased from at or below 0.3 NTU to over 0.3 NTU and up to 0.45 NTU. When the fluoride feed was discontinued at 300 hours an immediate drop from 0.4 to 0.25 NTU in postclarifier turbidity occurred. Statistical analysis of the two sets of data collected during and outside the prefluoridation period revealed that the difference in mean clarifier effluent turbidity of 0.1 NTU was significant (one-sided t-test, $P \ll 0.01$). The spike in turbidity just prior to prefluoridation may have been due to a disturbance of the sludge blanket and was classified as a statistical outlier, because this data point was located

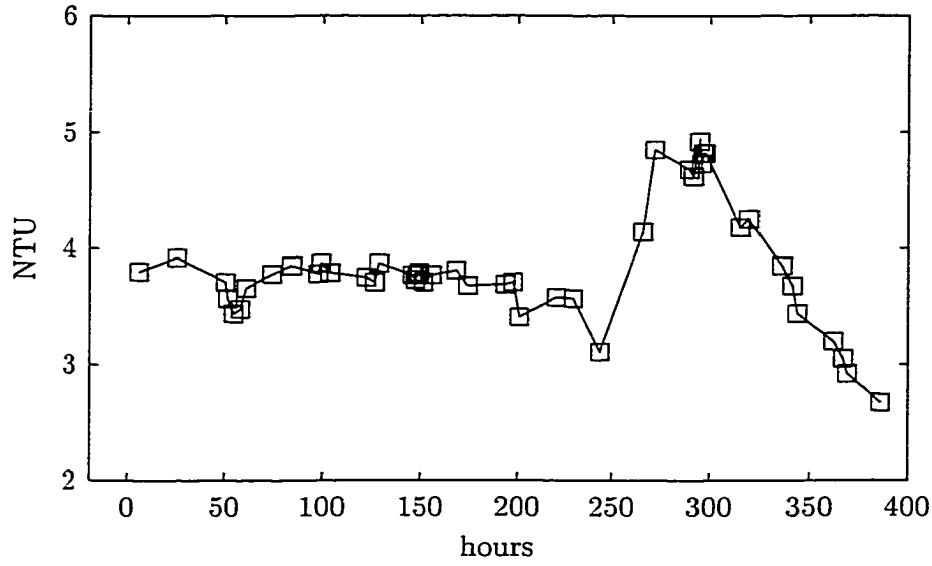

Figure 3.2. Raw water turbidity versus time.

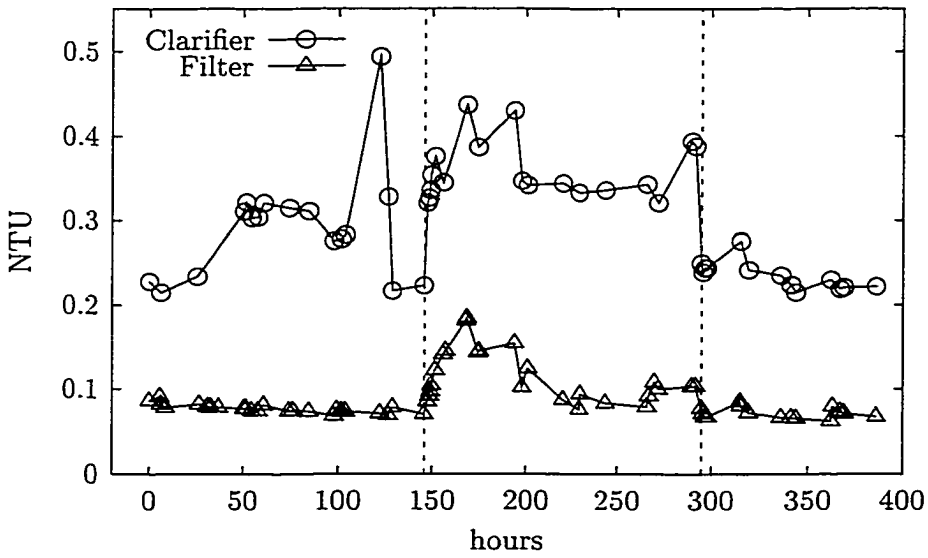

Figure 3.3. Clarifier and filter effluent turbidity versus time.

more than 1.5 times the interquartile range above the 75th percentile. There was a similar trend in filtered water turbidity. After the start of prefluoridation the turbidity instantly increased from below 0.1 NTU to 0.2 NTU. This breakthrough may have been due not only to increased particle loading from the clarifier but it may have also resulted from detachment of particles from the filter media, that were restabilized upon the change in solution chemistry. There was also a subtle drop in turbidity at the end of the prefluoridation period. As with clarifier turbidity, the observed difference of 0.03 NTU, based on the mean turbidity with and without the presence of fluoride is statistically significant (one-sided t-test, $P \ll 0.01$). Box-and-whisker plots of the filter effluent turbidity data collected during the periods with and without prefluoridation provide visual confirmation of the statistically significant differences in performance (Figure 3.4).

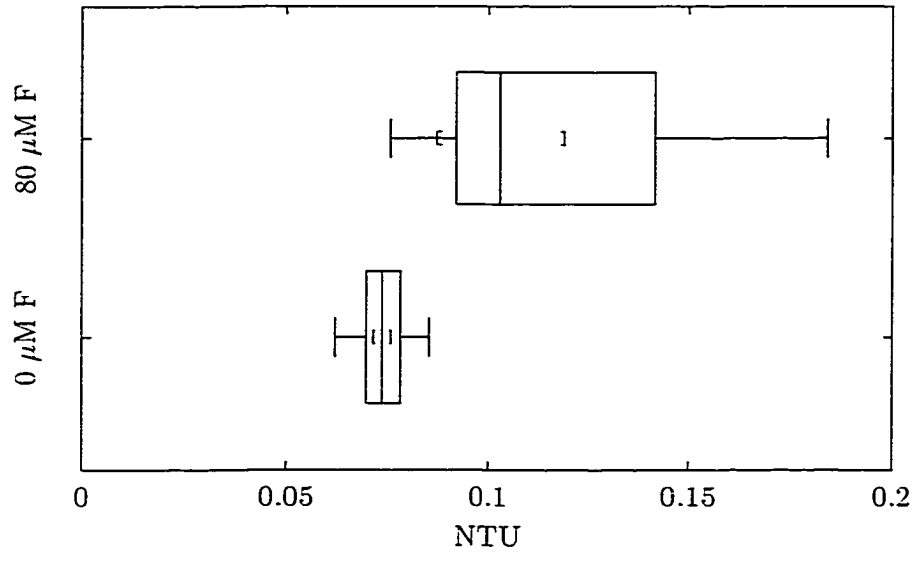

Figure 3.4. Filtered water turbidity as a function of fluoride dose.

As noted previously, the decreased turbidity removal efficiency of the clarifier resulted in higher particle loading to the filter. It was suspected that an increase in particle loading may not only have led to turbidity breakthrough but also could have adversely affected filter run times. Analysis of the hydraulic data shows that the head over the filters during prefluoridation conditions exceeded the head development during periods when fluoride was not fed (Figure 3.5). The solid and the dashed lines represent least squares fits of the data and are provided to illustrate the different head development trends. Filters were generally

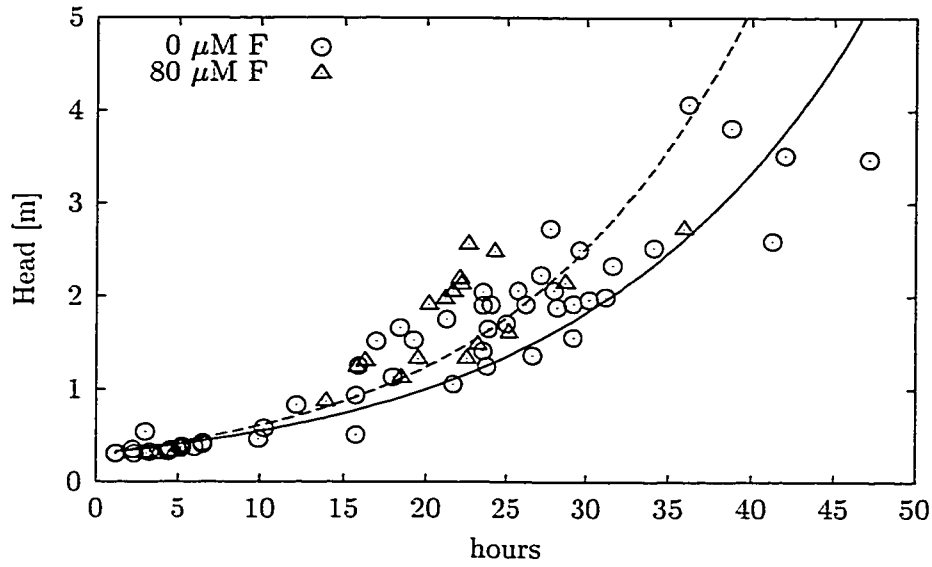

Figure 3.5. Head as a function of filter run time and fluoride dose.

backwashed when the head exceeded 2.4 m; whereas filter run times were generally greater than 25 hours without fluoride addition, they seldom exceeded 25 hours while the raw water was fluoridated. This trend is particularly discernible, when only the data from the filter cycles immediately prior to and after start of the fluoride feed are plotted (not shown).

The impact of prefluoridation on TOC removal is depicted in Figure 3.6. In general, TOC-removal data exhibited greater scatter than turbidity data. However, it is clear that for both clarifier and filter, TOC removal exceeded 40% (fraction removed > 0.40) when no fluoride was added to the head of the plant, whereas during prefluoridation the performance was significantly lower ($P \ll 0.01$) with TOC removals of approximately 35%. To illustrate the statistical difference in performance graphically, a box-and-whisker plot of the two datasets is provided in Figure 3.7. A Student's t-test revealed also that there was no significant difference in clarifier and filter performance during prefluoridation with respect to overall TOC-removal at a 95% confidence level ($P = 0.09$). This analysis suggests that TOC removal predominantly occurred in the sludge blanket clarifier and no additional TOC was removed by the filter.

To rule out whether temporal changes in raw water quality could have caused the adverse affects on NOM removal during prefluoridation, the variation of raw water specific UV absorbance (SUVA) was analyzed. Specific UV absorbance is generally accepted as an

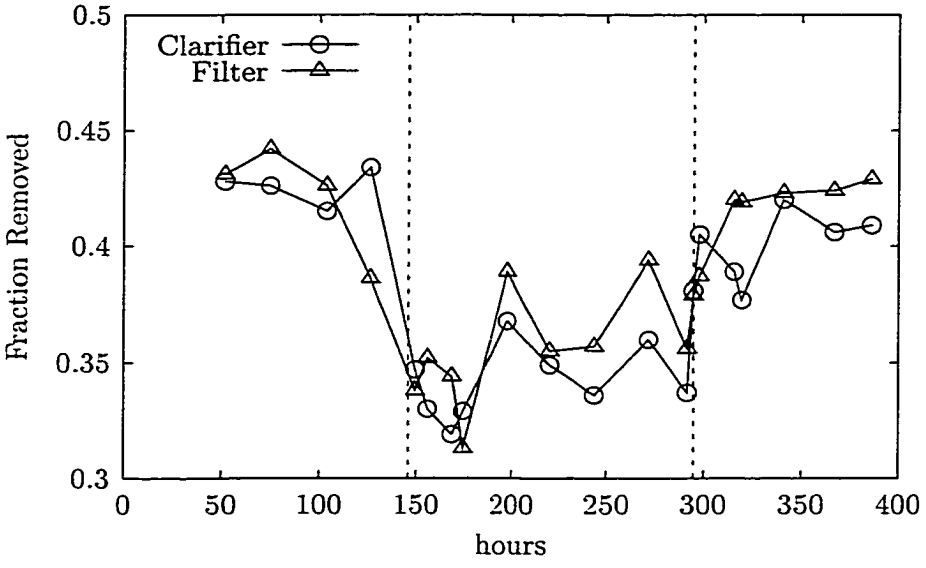

Figure 3.6. Clarifier and filter effluent TOC versus time.

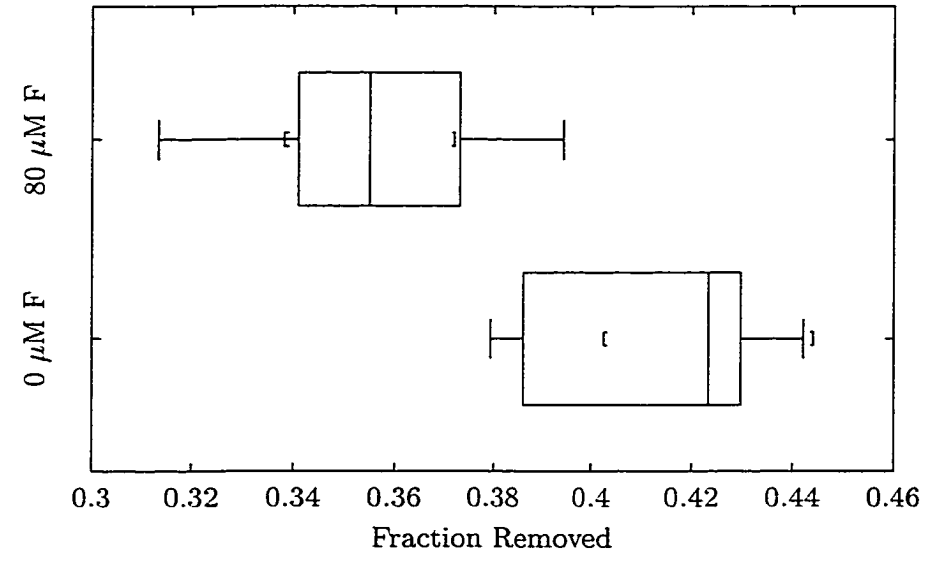

Figure 3.7. TOC removal as a function of fluoride dose.

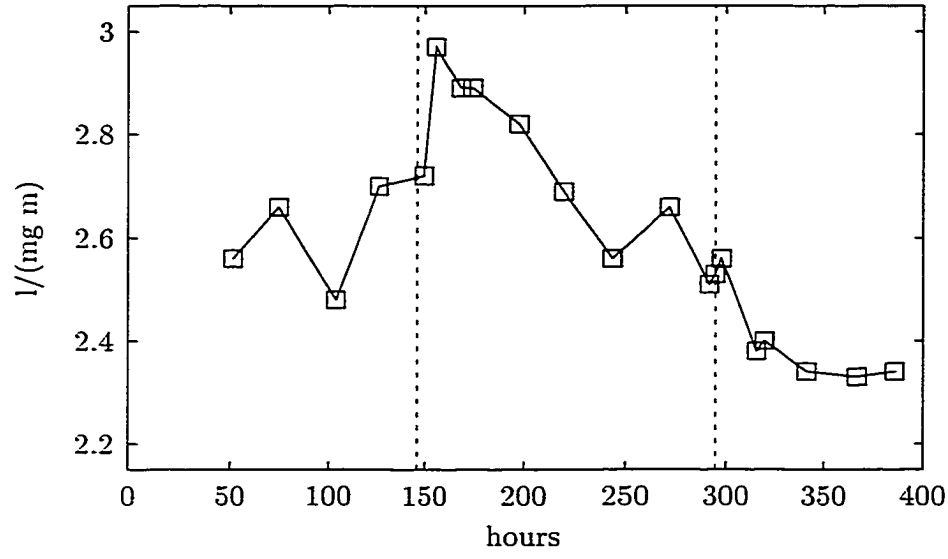

Figure 3.8. Raw water specific UV absorbance versus time.

indicator of the hydrophobic nature of natural organic matter (Edzwald *et al.*, 1985). The natural organic substances in waters with high SUVA (of 4 and greater) are thought to have a large fraction of hydrophobic functional groups and are more easily removed by coagulation. In contrast, waters with low SUVA (< 2) are thought to contain mainly hydrophilic, non-humic organic material that is more difficult to remove by coagulation (White *et al.*, 1997). If the changes in raw water SUVA, as indicated in Figure 3.8, were dictating TOC removal efficiency, one would expect that, due to the increase in SUVA at the startup of prefluoridation, improved NOM removal would have been observed. Similarly, at the time when prefluoridation was discontinued, raw water SUVA exhibited a downward trend, whereas there was a clear improvement in NOM removal at the plant. Therefore, the decrease in NOM removal during prefluoridation was not due to changes in raw NOM characteristics and it is possible that, had the raw water SUVA remained constant, the impact of prefluoridation would have been even greater than observed during the study.

Changes in total aluminum concentration during the pilot study were also observed and directly related to the presence of fluoride (Figure 3.9). The postfilter and postclarifier aluminum concentrations increased by an order of magnitude; from values near 4 μM to up to 40 μM Al during the period of prefluoridation. This variation was in reasonably good agreement with dissolved aluminum concentrations predicted by chemical equilibrium cal-

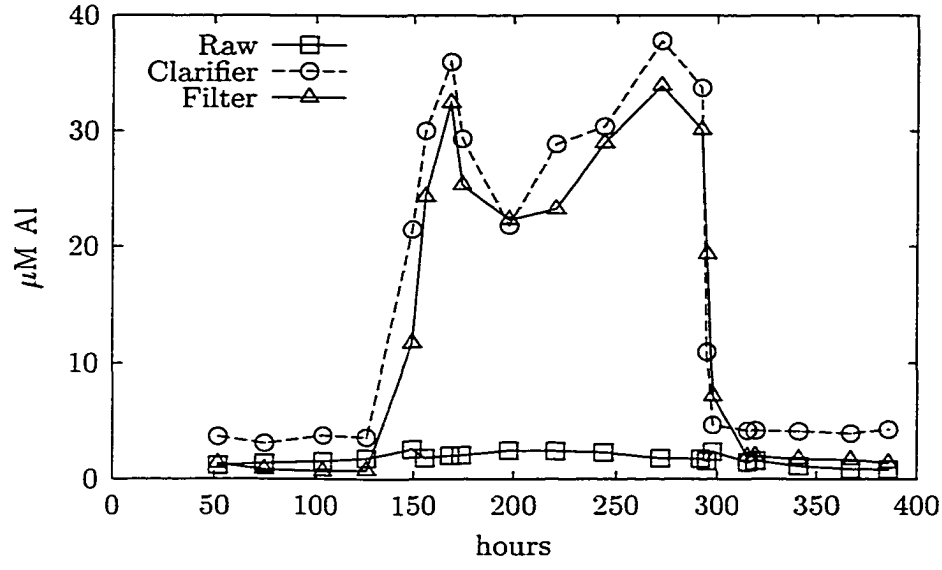

Figure 3.9. Total aluminum concentration versus time.

culations (refer to Section 2). The 0.45 μm filtered aluminum concentrations (not shown), were in good agreement with the total aluminum concentrations suggesting that the majority of aluminum was dissolved in solution. There are currently no enforceable maximum contaminant limits for aluminum in drinking water in the United States despite the ongoing controversy about the link between aluminum in drinking water and the occurrence of Alzheimer's disease. If finished water aluminum concentrations were regulated at 0.2 mg/l (7.4 μM Al), as in Germany for example, this limit would have been grossly exceeded in this study while fluoride was applied. It is also worth noting that prior to and after the prefluoridation period, the aluminum concentration in the clarifier effluent was significantly higher than in the filter effluent (Figure 3.9), indicating that a measurable amount of aluminum is retained by the filter.

Another negative aspect of prefluoridation was discovered when fluoride concentrations in the clarifier effluent were compared to the applied fluoride dose as shown in Figure 3.10: The applied dose was approximately 80 μM, but only 60 μM was recovered after the clarifier. Even in the absence of prefluoridation, it was apparent that raw water fluoride concentrations were being lowered by approximately 30%. The likely reason for this observation was the removal of fluoride by adsorption to aluminum hydroxide floc, which had also been observed during bench-scale studies (Section 2). It is clear, based on these studies and

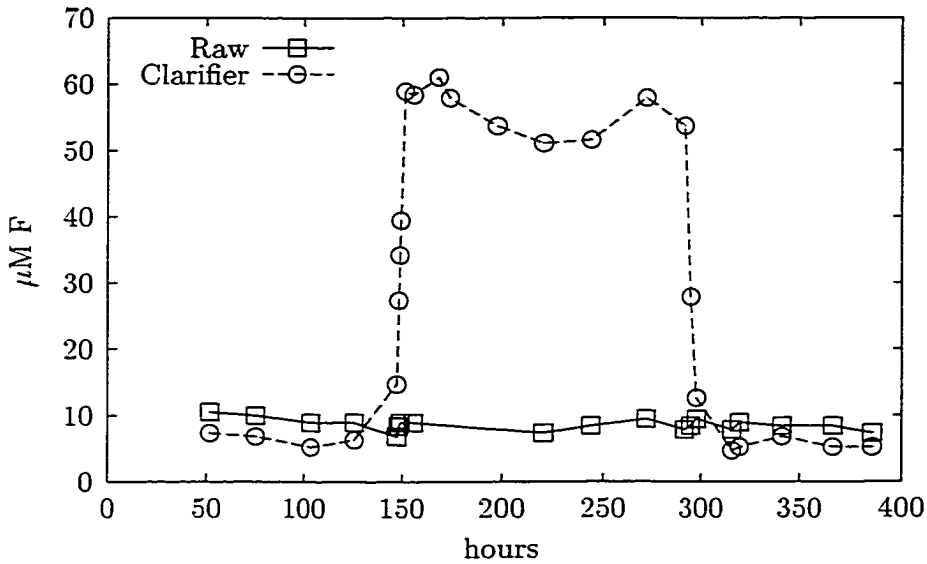

Figure 3.10. Total fluoride concentration versus time.

chemical equilibrium modeling, that for raw waters undergoing treatment with alum, fluoride will negatively affect NOM and particle removal. Therefore, the application of fluoride to the raw water has not only the potential for deleterious effects on plant performance, but can also result in additional chemical costs.

3.3.2. Effects of Fluoridated Backwash Water

In this subset of the pilot-scale study, data collected during three filter cycles were examined to assess the influence of utilizing fluoridated water for backwashing. This experiment was conducted because it was suspected a priori that fluoride might influence the removal of aluminum accumulated within the filter bed during backwashing and the retention of aluminum hydrolysis products during ripening, i.e., when a filter is placed back online. This influence was suspected because it was earlier shown (Section 2) that fluoride can form soluble AlF_x complexes that can increase the solubility of aluminum below pH 7. It was also believed that the use of fluoridated backwash water might lead to increased sorption of fluoride on the aluminum coated filter media after backwashing, affecting the surface chemistry of the media and leading to performance differences compared to utilizing nonfluoridated backwash water. Another potential influence would be enhanced aluminum leaching during ripening as fluoride retained on the media during backwash reversibly desorbs (with con-

comitant Al solubilization) when low fluoride water is applied to the filter. It should be noted that the relatively short duration of this study may mask or overemphasize some of the differences between the two conditions that might be observed over a longer period of time.

In contrast to the results from the prefluoridation study, the observed differences in headloss development and filter effluent turbidity between the two filters were not closely correlated to the use of fluoridated or nonfluoridated backwash water (not shown). Although a systematic relationship for these parameters could not be established, some notable observations were made.

Total aluminum concentrations in samples taken from the backwash effluent typically decreased within five minutes from several millimols per liter to values less than 100 μM Al. Generally, there was no difference in these trends when fluoridated backwash water was utilized as shown in Figure 3.11. This plot also shows that the dissolved fluoride concentration in the wastewater approached the influent value of 80 μM at the end of the 10-minute backwash period, although several bed volumes of fluoridated water passed through the column based on the backwash flow rate. Apparently, fluoride adsorbed to the alum floc that was removed from the filter grains. After the bulk of the material in the filter was removed, no more adsorption occurred.

The backwash water turbidity usually exhibited the same trends as total aluminum concentrations as evidenced by the linear correlation between these parameters shown in Figure 3.12. This relationship suggests that the accumulated particulate matter in the filter was enmeshed in the aluminum precipitate.

Although no effects on headloss development and filtered water turbidity were observed, the use of fluoridated backwash water affected finished water aluminum concentrations that were monitored following two backwash events (November 11 and 15). These data indicate that the finished water aluminum concentrations were slightly higher in the effluent of the filter that had been backwashed with fluoridated water (Figure 3.13). Typically, the aluminum concentration reached a maximum thirty minutes after this filter was put back online and then slowly declined. This time period corresponded to the approximate detention time between the top of the filter media and the sample port as determined by tracer

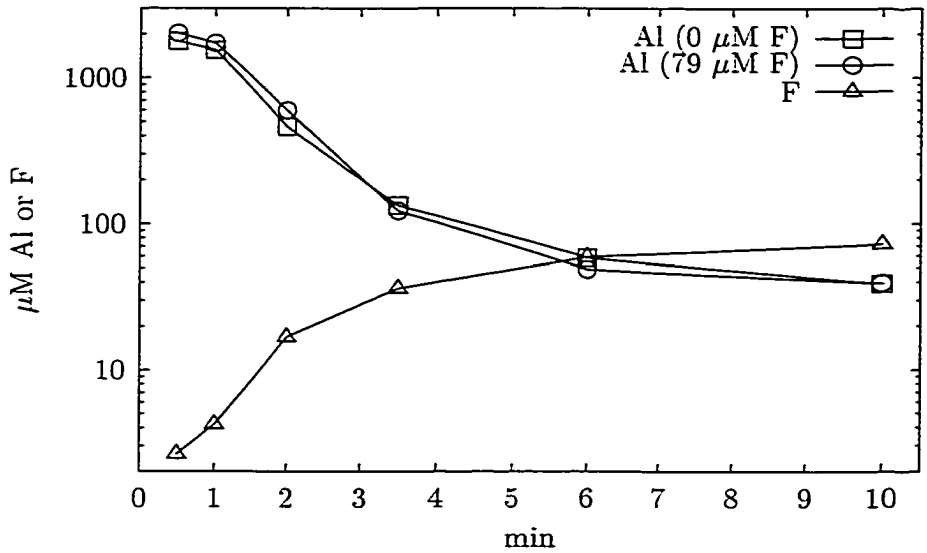

Figure 3.11. Total aluminum and dissolved fluoride concentration in filter backwash effluent as a function of time and influent fluoride concentration.

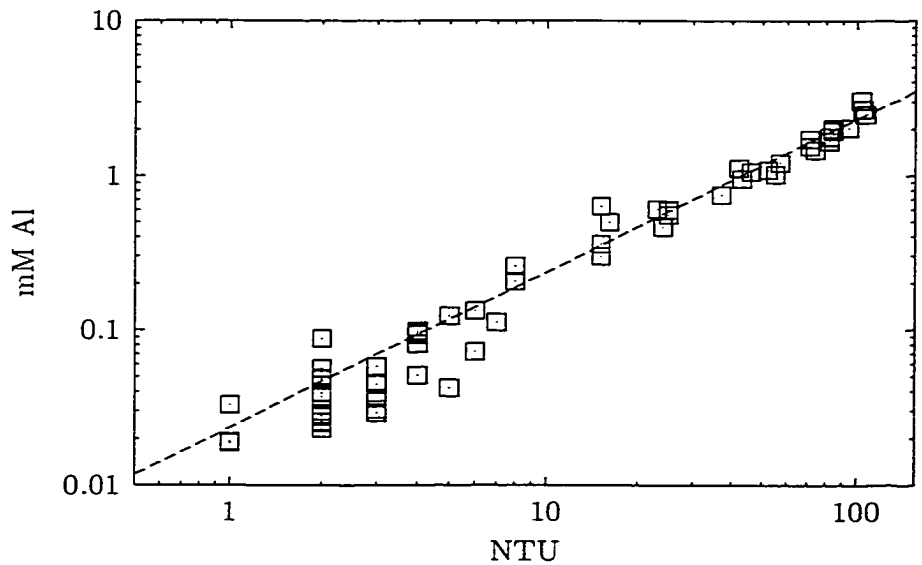

Figure 3.12. Total aluminum concentration versus turbidity in filter backwash water on November 8.

studies. (Tracer tests were conducted using sodium chloride; detention time was based on the elapsed time to reach 90% of the influent conductivity). Aluminum concentrations in the effluent of the filter that did not receive fluoridated backwash water slowly decreased from approximately 2 μM to 1 μM. After six hours there was no detectable difference between the two filters in the amount of aluminum discharged. A comparison of these data with the total fluoride concentrations in the filtered water effluent measured at the same time (Figure 3.14), reveals that there is a high correlation between these two parameters. After approximately five hours after the filter that received fluoridated backwash water was put back in service, no fluoride was detectable in the filter effluent. After this period of time, there was also no difference in finished water aluminum concentration between the filters, suggesting that fluoride was indeed retained within the media and solubilized aluminum hydrolysis product. However, considering the time between backwashing and the magnitude of the aluminum concentrations leaving the filters, it seems unlikely that the use of fluoridated backwash water would have a measurable impact on the quality of the distributed water. In addition, treatment plant operators that are aware of the effects of filter ripening, typically flush the filter after backwashing to avoid that the initially high turbidity water enters the distribution system ("filter-to-waste").

3.4. Discussion

The data gathered during a prefluoridation study using a pilot-scale facility that mimics a full-scale plant clearly confirm the findings from bench-scale experiments (Section 2). The addition of fluoride to the raw water at doses typically used in water treatment resulted in a significant decrease in turbidity and TOC removal by the clarifier, because complexation with fluoride inhibits formation of aluminum hydrolysis products that destabilize particles and adsorb or precipitate natural organic matter. The filtration process was also affected because the increased particle loading on the filters required more frequent backwashing. It was also observed that the filters exhibited turbidity breakthrough at the beginning of the prefluoridation period, indicating the the change in solution chemistry affected the surface chemistry of the filter media.

These effects can be offset by increasing the alum dose to a point at which all fluoride is

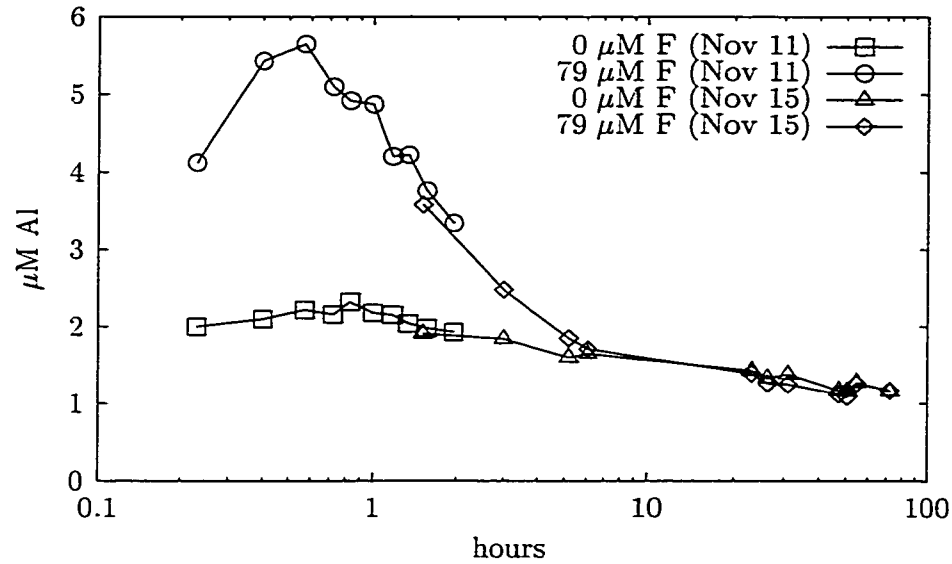

Figure 3.13. Total aluminum in filter effluent as a function of time and fluoride concentration in backwash water.

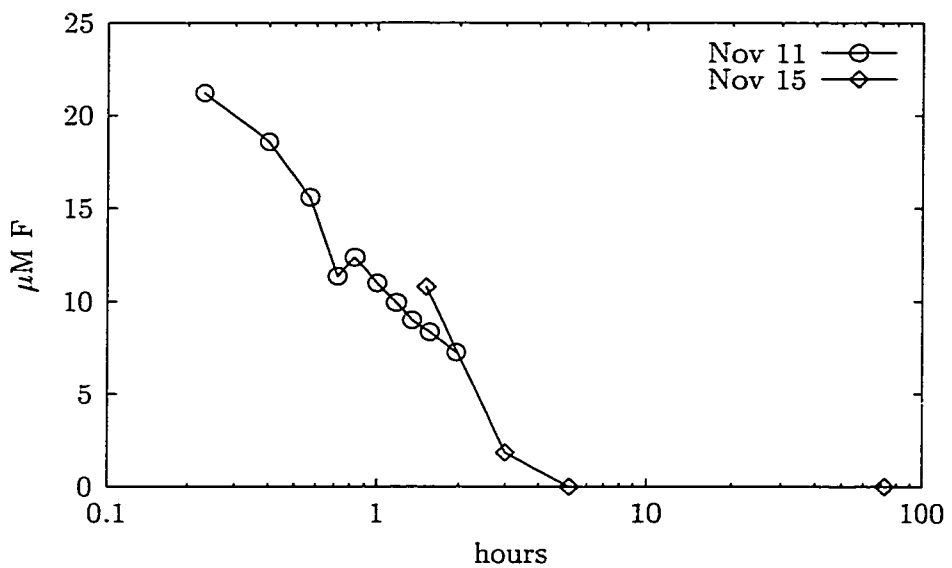

Figure 3.14. Total fluoride in filter effluent as a function of time.

complexed and adequate particle and NOM removal is obtained. This approach is satisfactory if the raw water concentration of fluoride and other coagulant-demanding substances is constant. Because this is rarely the case with surface waters, a treatment plant operator will typically adjust the alum dose in response to changing water quality conditions, which may be problematic if the effect of fluoride is not considered. The raw water fluoride concentration may rapidly change not only when prefluoridation is started, but also when a supplemental raw water source is put in service that is elevated in fluoride. Sudden changes in fluoride concentration may also occur when spent backwash water is recycled to the coagulation process. (However, in the U.S., regulations are proposed to minimize these recycle streams (U.S. Environmental Protection Agency, 2000)). If these rapid changes are infrequent and result in decreased NOM removal only for short periods of time, regulatory compliance is likely not to be affected. However, only a single breakthrough of turbidity can introduce pathogenic microorganisms into the distribution system and pose an acute public health risk (Fox and Lytle, 1996).

Neglecting the effects of fluoride can also lead to underestimating the correct alum dose when it is determined through jar testing. If the full-scale facility practices prefluoridation, then the jar test protocol must incorporate this treatment step. Otherwise, the jar test would yield lower coagulant doses than required to meet the treatment goals.

Even if the alum dose is adjusted to meet the treatment objectives, a substantial amount of dissolved aluminum passes through the plant, which can lead to undesirable long-term effects, such as post-precipitation upon changes in pH at the point of entry or within the distribution system. For example, utilizing the solubility diagram in Figure 2.1, a change in pH from 6 to 7.5 in the presence of 79 μM F, can result in precipitation of approximately 25 μM of $Al(OH)_3(s)$. This material can accumulate in water pipes, decrease the networks' carrying capacity, and be remobilized under adverse condition degrading the visual appearance and palatability of the water. Elevated aluminum concentrations do not only affect the aesthetic quality of the water, but there are also potential health effects, which are currently not addressed in U.S. regulations. Particularly, if no pH changes occur, the aluminum that has passed through the treatment plant remains complexed as AlF_x, which may increase the bioavailability and neurotoxicity of fluoride (Varner *et al.*, 1998).

3.5. Summary

The results from pilot scale studies involving conventional water treatment with alum provide compelling evidence that fluoride can have significant deleterious effects on plant performance if it is added at points in the treatment train that target particle and NOM removal. Under conditions that are typical for treatment plants practicing enhanced coagulation, it was observed that the application of fluoride to the raw water caused

- a significant decrease in TOC-removal,
- a significant decrease in clarifier performance,
- a significant increase in filter effluent turbidity,
- a decrease in filter run times due to increased particle loading,
- a tenfold increase in finished water aluminum concentration, and
- loss of up to 40% of the applied fluoride dose due to sorption to flocs.

These findings can have a strong impact on the water industry, because there are a large number of plants that apply fluoride in a manner where it can interfere with plant performance. The use of fluoridated backwash water resulted in higher aluminum concentrations for a short time after putting the filter back online but did not appear to affect head development or effluent turbidity.

4. LIGAND ADSORPTION ONTO ALUMINUM HYDROXIDE

4.1. Introduction

Processes at the solid-water interface play an important role in many geochemical processes, and it has also been recognized that adsorption to hydrous metal oxides may be a dominant mechanism for the removal of organic contaminants in drinking water treatment with metal salt coagulants (Randtke, 1988). There is general agreement among researchers that this process is influenced by coordinative reactions (Stumm and Morgan, 1996), for example

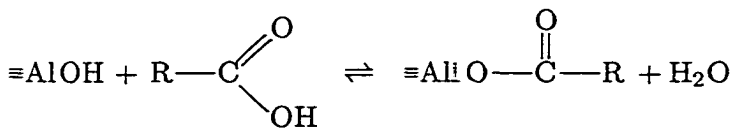

where ≡AlOH is a functional group at the aluminum oxide-water interface and R–COOH represents an organic molecule carrying a carboxylic functional group. Where organic ligands react in this manner, adsorption can be conceptualized in the same manner as ligand exchange reactions involving inorganic anions (Hingston *et al.*, 1972). It is believed that during a ligand exchange reaction a surface hydroxyl group is replaced by a strongly adsorbing anion to form a coordinative or "inner-sphere" complex. Adsorption of a weakly bound anion is thought to be largely the consequence of electrostatic attraction between charged surface species and the ion (or dipole) in solution. These reactions are usually ionic-strength dependent and the adsorbing anion retains its hydration sheath to form an "outer-sphere" complex. Organic anions may also interact with oxide surfaces through hydrophobic expulsion (Stumm and Morgan, 1996). Adsorption due to electrostatic or chemical interaction is due to attractive forces, whereas hydrophobic interactions are driven by the incompatibility of nonpolar compounds or nonpolar moieties within a molecule with water. Hydrophobic substances are usually only sparingly soluble in water and seek to reduce the contact with water by accumulating at surfaces.

In the past, these interactions with simple and complex organic acids have been studied extensively. However, fundamental research has largely focused on interactions with crystalline oxide particles (Kummert and Stumm, 1980; Rohmann and Sontheimer, 1982;

Davis, 1982; Balistrieri and Murray, 1987; Ali and Dzombak, 1996a,b; Person *et al.*, 1998; Evanko and Dzombak, 1998), whereas there have been only few efforts to study the adsorption of organic ligands to freshly precipitated metal hydroxide floc in well defined solutions (Jekel, 1986; Bose and Reckhow, 1998). The results from studies with well characterized, crystalline aluminum oxide solids can potentially aid in explaining interfacial phenomena involving amorphous aluminum hydroxide because these substances may be equivalent with regard to the reactivity of their surface functional groups. However, there may be significant differences in specific surface area and/or surface site density. The specific surface area for γ-Al_2O_3 is typically reported to be near $100\,m^2/g$ (Hohl and Stumm, 1976; Kummert and Stumm, 1980; Cheng and Huang, 1996), whereas that of aluminum hydroxide floc can range from 600 to $1100\,m^2/g$ (Bottero and Bersillon, 1989). The thermodynamically stable, crystalline phase, $Al(OH)_3(s)$, is also less soluble than the amorphous precipitate formed under water treatment conditions (Snoeyink and Jenkins, 1980).

During the literature review conducted for this work it became apparent that among the many studies involving the removal of organic substances by treatment with aluminum based coagulants, none have been conducted to elucidate the adsorption mechanisms to preformed floc over a wide pH-range, including the effects of competitive ions. Jekel (1986) studied the effects of calcium and sulfate on the adsorption of humate and some simple organic acids to in-situ precipitated aluminum hydroxide but confined the experiments to pH 7. Other research aimed at defining the role of the functional groups of NOM during removal by adsorption onto metal hydroxides (Lefebvre and Legube, 1993; Julien *et al.*, 1994). These works were either limited to a narrow pH-range or focused mainly on iron-based coagulants. Therefore, there is a need for studying organic contaminant removal by adsorption to amorphous aluminum hydroxide, including variation of pH, competition by common ions, utilization of simple organic acids as NOM surrogates, and electrokinetic measurements. The rationale for this experimental design is described below.

It is well known that the "master-variable" pH influences the speciation of surface hydroxyl groups on oxide particles, the protolysis of (potentially adsorbing) weak acids, and the dissolution and precipitation of the adsorbent, $Al(OH)_3(s)$. In studies with crystalline oxides, the concentration of the adsorbent is usually considered constant over a wide pH

range. However, due to the higher solubility of freshly precipitated aluminum hydroxide (compared to crystalline aluminum oxide) and the lower solid concentrations encountered in water treatment, the variation of pH can greatly affect the mass of precipitate formed and thus the available surface area for solutes to adsorb. It also has to be recognized that pH affects the speciation of aluminum in solution, which can compete with the surface hydroxyl groups for inorganic and organic ligands. For example, Hao and Huang (1986) suggested that the formation of fluoroaluminum complexes in solution affects the adsorption of fluoride to alumina at low pH.

Because natural waters can seldom be considered solutions with single solutes, it is prudent to study the effects of competing ligands during adsorption to aluminum hydroxide. There is ample evidence that common inorganic anions interfere with the removal of inorganic and organic substances by adsorption to crystalline oxides (Hawke *et al.*, 1989; Mesuere and Fish, 1992; Ali and Dzombak, 1996a) and these interactions are also of great importance in water treatment. For example, Meng *et al.* (2000) recently showed that silicate strongly impaired removal of arsenate and arsenite by ferric chloride. However, this literature review revealed that the effects of anions such as fluoride, sulfate, and phosphate on NOM-removal are rarely considered. For instance, the potential effects of sulfate are often neglected when comparing the performance of alum or ferric sulfate to ferric chloride.

Simple aliphatic and aromatic acids have been used extensively as NOM surrogates, because they carry the same functional groups as natural organic substances. Despite the structural complexity of natural organic matter, it has been found that, for example, pyromellitic acid mimics the adsorption of Suwannee Fulvic Acid to goethite (Evanko and Dzombak, 1999), and that gallic acid and pyrogallic acid behave similarly to humic substances when coagulated with ferric chloride (Lefebvre and Legube, 1993). The utilization of simple organic acids as NOM-surrogates not only allows determining the role of organic functional groups, but can also greatly simplify laboratory experiments, because batch adsorption studies involving natural organic substances often involve elaborate preparations, e.g. extractions or resin separations. This method has the advantage that the process can be easily reproduced, whereas it is virtually impossible to obtain a natural water with identical NOM characteristics for replicate tests. In the present study, the organic acids

listed in Table 4.1 were chosen as NOM-surrogates. The behavior of these substances has been previously investigated in adsorption tests with crystalline aluminum and iron oxides (Kummert and Stumm, 1980; Rohmann and Sontheimer, 1982; Mesuere and Fish, 1992; Ali and Dzombak, 1996a; Evanko and Dzombak, 1999) and coagulation experiments with metal salt coagulants (Lefebvre and Legube, 1993; Julien *et al.*, 1994).

The acidity constants listed in Table 4.1 were taken from Martell and Smith (1977, 1982) and are given at infinite dilution and 25°C. The values for pyrogallic acid in the literature source were not available at $I = 0$ M and were therefore extrapolated using Davies' equation (Morel and Hering, 1993). The selected compounds exhibit markedly different acid-base properties as a result of the number and arrangement of carboxylic and phenolic functional groups. These differences are likely to impart different adsorption properties, which can be compared to those of natural organic substances. Two organic acids of natural origin tested in this work included Aldrich humic acid (AHA) and Dismal Swamp organic matter (DSOM).

In addition to determining the extent of adsorption of single or competing ions to aluminum hydroxide in this work, attention was paid to measuring the change in electrophoretic mobility of the suspension upon adsorption. Electrophoretic mobility measurements allow estimating the potential difference across the hydrodynamic shear plane at the particle-water interface, the ζ-potential. The relationship of electrophoretic mobility to ζ-potential strictly applies only to particles of simple geometries (Hunter, 1981). However, the isoelectric point pH_{iep} (i.e., the pH, at which the electrophoretic mobility is zero) can be determined unambiguously. This parameter is important in the optimization of water treatment processes because particle suspensions rapidly coagulate near the pH_{iep}. ζ-potential measurements can also provide useful information about the nature of adsorbate-solid interactions because the displacement of the pH_{iep} due to adsorption can be interpreted as a result of the formation of inner-sphere complexes at the oxide or hydroxide surface (Hunter, 1981).

Collectively, the results from these experiments can provide valuable insight into the mechanisms for removal of organic substances by adsorption to amorphous aluminum hydroxide, the effects of competing solutes, and the impacts on particle stability.

Table 4.1. Simple organic acids.

Compound	Structural Formula	$\log K_a$
Oxalic Acid (OxA)	HOOC—COOH	-1.252 -4.266
Phthalic Acid (PhtA)	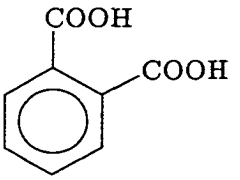	-2.95 -4.93
Salicylic Acid (SalA)	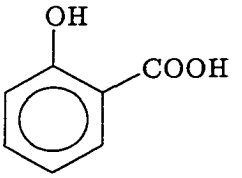	-2.97 -13.74
Pyrogallic Acid (PygA)	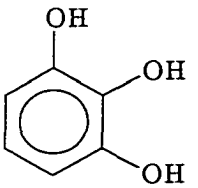	-9.2 -11.5 -14.6
Pyromellitic Acid (PymA)	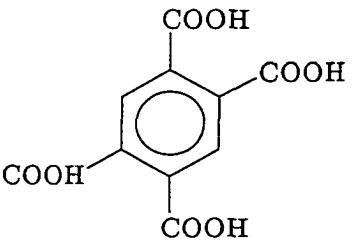	-1.70 -3.12 -4.92 -6.23

4.2. Materials and Methods

4.2.1. Experimental Procedure

Amorphous aluminum hydroxide was prepared by slowly adding 6 M NaOH to a continuously stirred and N_2-sparged solution containing 1.0 mM reagent grade aluminum chloride until a pH of 8.3 ± 0.2 was reached. Similar procedures for the preparation of metal hydroxides have been utilized by other researchers (Davis and Leckie, 1978a; Zachara *et al.*, 1987; Anderson and Benjamin, 1990b). The sparging of the solution was necessary to avoid undesirable changes in pH due to the transfer of carbon dioxide into or out of solution. The adsorption of carbonate to amorphous metal hydroxide has also been found to cause a shift of the pH-edge of other anions (Zachara *et al.*, 1987) and a decrease of the pH_{iep} (Chowdhury *et al.*, 1991). The high aluminum concentration was selected in order to keep the amount of precipitate formed fairly constant over a wide pH range, i.e., the complexation of aluminum with the solutes would not affect the concentration of sorbent to a great extent.

The freshly prepared aluminum hydroxide suspension was allowed to equilibrate for two hours while the pH was held constant by adding NaOH as needed. After this period of time, the adsorbate was added under vigorous mixing provided by nitrogen sparging and a magnetic stirrer. In the binary adsorbate experiments, the two reagents (adsorbates) were added simultaneously. The pH was then adjusted using 2 M HCl and after each incremental addition, a 40 ml aliquot was withdrawn, transferred to a polyethylene centrifuge tube, and agitated for two hours on a reciprocating shaker. For the determination of the electrophoretic mobility of the aluminum hydroxide particles, 5 ml of the suspension were then withdrawn using a syringe. The remainder of the sample was centrifuged for twenty minutes at 3,400 g. The pH of the supernatant was measured before it was passed through a 0.2 μm polycarbonate membrane (Osmonics) using a vacuum filtration device (Gelman Sciences) and retained for the analysis of adsorbate and aluminum concentrations. The fraction of the analyte that had adsorbed to aluminum hydroxide was calculated from the difference in the amount added and the concentration remaining in the filtered sample normalized to the total concentration.

4.2.2. Inorganic Reagents

All the inorganic reagents used in this study were reagent grade (Fisher Scientific) and prepared by dissolution in deionized, distilled water. Phosphate and sulfate stock solutions were prepared using their monopotassium and dipotassium salts, respectively. A fluoride stock solution was made using sodium fluoride.

4.2.3. Simple Organic Acids

Simple organic acid stock solutions were prepared from pure, water-soluble chemicals. Phthalic and salicylic acid solutions were made up using the monopotassium and monosodium salt, respectively (Fisher Scientific). Pyrogallic and oxalic acid were in their fully protonated form (Fisher Scientific). To completely dissolve the pyromellitic acid (Aldrich Chemical Company) in water, it was necessary to adjust the stock solution pH to approximately pH 8 using 6 M sodium hydroxide. The concentrations of the simple organic acid stock solutions were verified by titration against a standardized base and comparison of the experimental titration curve with that calculated from published acidity constants (Martell and Smith, 1977, 1982) using a computer program for calculating chemical equilibria (Parkhurst and Appelo, 1999). The experimental measurements and modeled titration curve for pyrogallic acid are shown in Figure 4.1. Data for the other organic acids fit their predicted values equally well.

4.2.4. Organic Acids of Natural Origin

Humic acid was prepared by dissolving a commercially available humic acid sodium salt (Aldrich Chemical Company) in distilled, deionized water to result in a concentration of 4100 mg C/l.

Natural organic matter was extracted from water collected in a drainage ditch in the Great Dismal Swamp in southeastern Virginia. Upon arrival in the laboratory, the water was passed through a 0.45 μm cartridge filter (Gelman Sciences, AquaPrep^{TM}600) using a peristaltic pump (Cole-Parmer) to remove particulate matter. At the time of collection the dissolved organic carbon concentration was 14 mg C/l; UV-light absorption at 254 nm (UV_{254}) was 0.70 cm^{-1}. The filtrate was then applied to a strongly acidic cation exchanger

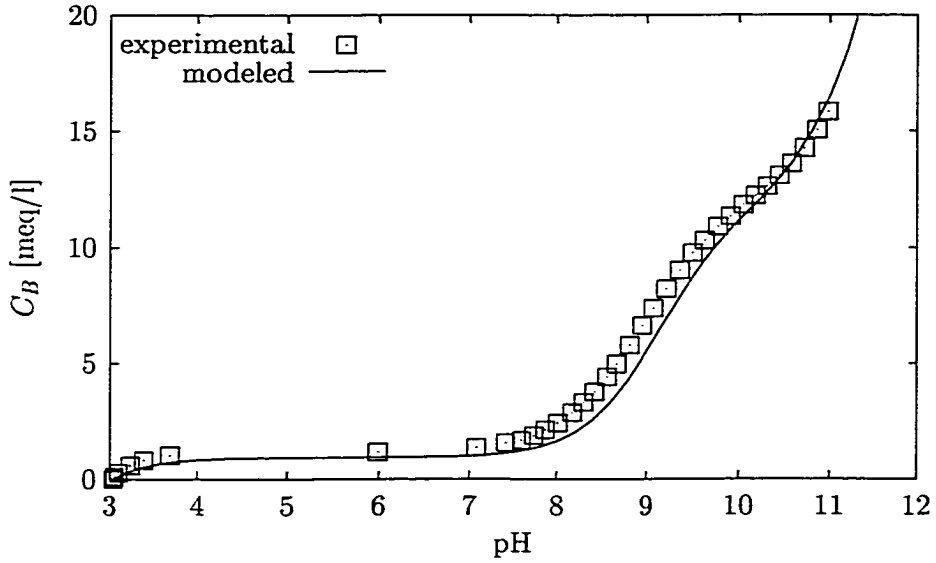

Figure 4.1. Titration of 11.1 mM pyrogallic acid.

(Amberlite IR-118H, Sigma Chemical Company) to remove major cations. Preliminary tests with varying flow rates and pH adjustment of the filtrate were conducted to find the conditions under which maximum cation removal occurred while maintaining the initial organic carbon content as measured by UV_{254}. It was observed that UV absorption was generally lower when the filtrate was adjusted to pH 4 and that it slightly decreased with decreasing flow rate. Sodium, potassium, calcium, and magnesium were virtually completely removed by the resin under all tested conditions, whereas iron remained largely in solution, possibly because it was complexed to the organic substances. Strong correlation of UV_{254} to the residual iron concentration in the resin effluent at different flow rates and pH appeared to confirm this suspicion. The concentration of manganese was below the analytical detection limit. Based on these observations the filtered water was applied to the resin without prior pH adjustment and at the highest practical flow rate.

To prepare a stock solution from which working solutions could be prepared, the filtered and pretreated Dismal Swamp water was next concentrated by vacuum distillation under moderate heat ($T < 45°C$) and neutralized to pH 7 with sodium hydroxide. The final concentration of the Dismal Swamp organic matter concentrate (DSOM) was 462 mg C/l. The UV-spectrum of the raw water was then compared to that of the concentrate rediluted to the initial concentration to evaluate whether significant changes in NOM characteristics

occurred during extraction. Nearly identical spectra were observed and suggest that the procedure did not greatly alter the characteristics of the natural organic matter.

To further characterize the Aldrich Humic Acid (AHA) and the Dismal Swamp extract, dilute solutions were prepared from the stocks, acidified to pH < 4 and titrated to pH > 10 with 1.0 N NaOH. It was then attempted to represent the titration data as if the natural organic matter were composed of a mixture of three monoprotic acids. This approach has previously been successfully applied to characterize NOM from various natural waters (Oliver *et al.*, 1983). The amounts and acidity constants of these acids were determined using FITEQL (Herbelin and Westall, 1996). The experimental data and the fitted titration curves are shown in Figure 4.2 and 4.3. The acidity values normalized to the organic carbon concentration and the acidity constants are listed in Table 4.2.

Table 4.2. Model Parameters for Aldrich humic acid and Dismal Swamp organic matter extract represented as a mixture of three monoprotic acids.

NOM	Acidity [meq/g C]	$\log K_a$
DSOM	18.2	-3.22
	9.8	-5.97
	16.2	-9.67
HA	4.9	-4.18
	3.0	-6.21
	1.8	-8.65

The carboxylic acidity of Aldrich Humic Acid of 7.9 meq/g C (i.e., the sum of the acids with pK_a less than 8) is generally in good agreement with literature values for NOM from various source waters (Thurman, 1985), whereas that of the DSOM extract (28 meq/g C) is significantly higher. However, this value agrees favorably with charge balance calculations that yielded 27 meq/g C. The charge imbalance was calculated based on the raw water concentrations of the ions listed in Table 4.3 and utilizing PHREEQC. Because alkalinity and inorganic carbon were not measured, it was assumed that the water was in equilibrium with the atmosphere ($P_{CO_2} = 10^{-3.5}$atm). The estimated total inorganic carbon concentration,

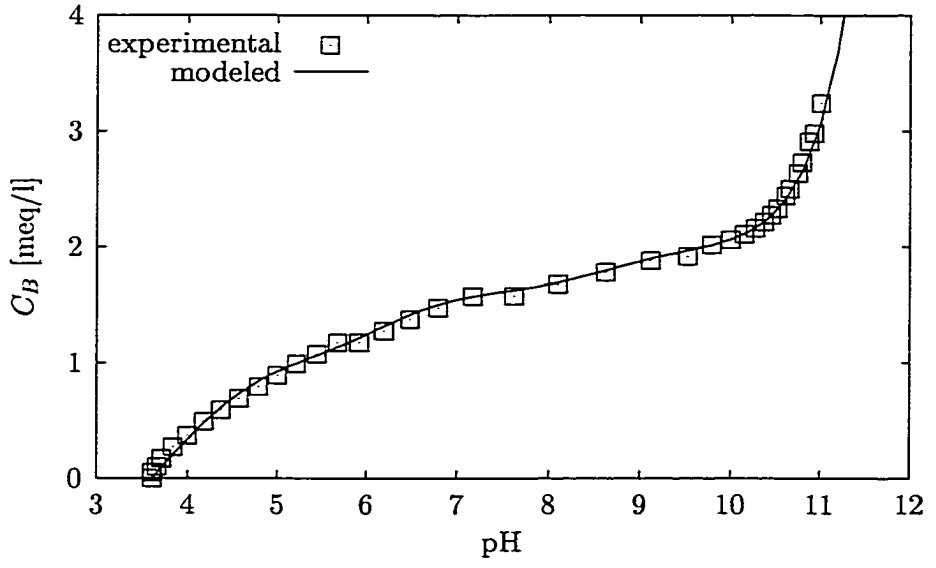

Figure 4.2. Titration of Aldrich humic acid (200 mg C/l).

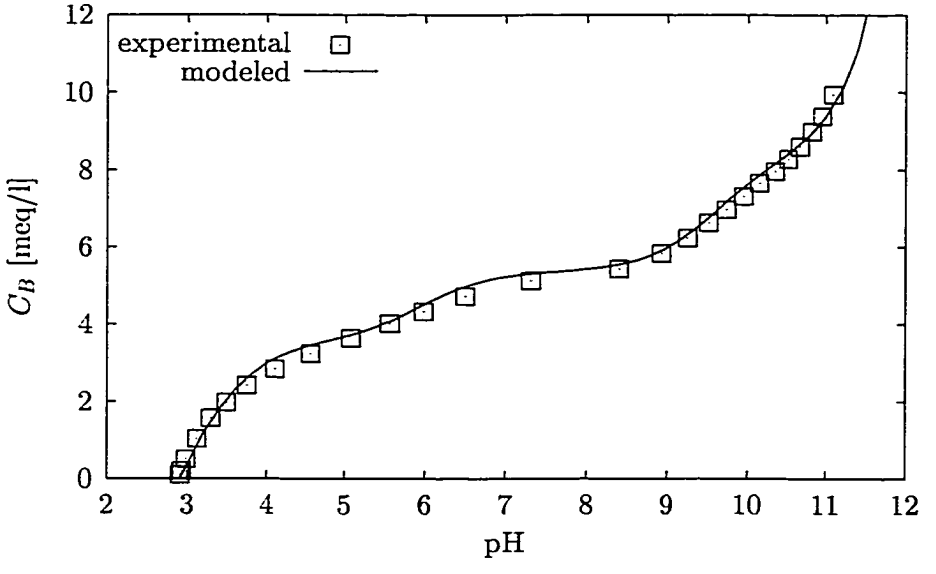

Figure 4.3. Titration of DSOM (185 mg C/l).

T_{CO_3}, was 30 μM.

Table 4.3. Ionic composition of Dismal Swamp water.

Cations	[μM]	Anions	[μM]
Na^+	263	Cl^-	280
K^+	65	NO_3^-	5
Ca^{2+}	134	SO_4^{2-}	58
Mg^{2+}	76	T_{CO_3}	30
Fe^{3+}	27	pH	6.6

4.2.5. Analytical Methods

All analyses of inorganic substances and measurement of non-purgeable organic carbon (NPOC) conformed with Standard Methods (Eaton *et al.*, 1995). The analytical methods utilized in this study are described in greater detail in Appendix B.

Aluminum

Filtered sample aliquots, acidified to pH < 2, were analyzed for aluminum using nitrous oxide flame atomic absorption spectroscopy. The measured values were subtracted from the total aluminum concentration to determine the amount of precipitate $Al(OH)_3(s)$.

Inorganic Anions

Filtered sample aliquots were analyzed for sulfate, fluoride, or orthophosphate. Sulfate analysis was performed by ion chromatography with a carbonate/bicarbonate eluent. Fluoride was determined potentiometrically using equal amounts of sample and ionic strength adjustment buffer. Orthophosphate was measured colorimetrically utilizing the ascorbic acid reduction method.

Organic Substances

UV spectroscopy was found to be a rapid, yet reliable, analytical method to quantify most of the organic substances used in this study. Concentrations obtained from non-purgeable organic carbon measurements generally correlated well to those from UV spectroscopy. However, NPOC data exhibited large variation at concentrations less than 1 mg C/l and therefore the UV light absorption method was utilized for most organic analytes. In preliminary tests, solutions with variable aluminum and organic acid concentrations and pH were scanned in the wavelength region between 200 and 360 nm in order to find the conditions under which the method was most sensitive to the analyte, while being least susceptible to interference. It was suspected that interferences could not only arise from the presence of inorganic ions, but also from the formation of aluminum-organic acid complexes. The displacement of the peak wavelength due to complexation can occur and has previously been used to study the interactions of aluminum and simple organic acids in aqueous solution (Rakotonarivo *et al.*, 1989; Sikora and McBride, 1989; Cathalifaud *et al.*, 1997).

pH effects on the UV spectra of the simple organic acids were generally noticeable in the immediate vicinity of their pK_a. The presence of aluminum at a molar aluminum : organic acid ratio of up to 16:1 was least perceptible when the acids were in their fully protonated forms, i.e., at pH values less than the lowest pK_a. Figures 4.4 and 4.5 illustrate the lack of an aluminum influence at pH 2. Based on these observations, the UV analysis was conducted after acidification to pH 2. Samples from the experiments involving Aldrich Humic Acid were acidified to pH 3 to avoid precipitation. The molar extinction coefficients ϵ (molar absorbtivity), that relate absorbance to concentration according to Beer's Law, were determined by ordinary linear regression of the calibration data. The wavelengths used and the calculated molar extinction coefficients are listed in Table 4.4. The value for Aldrich Humic Acid is given in liters per mol C·cm.

Because UV measurements for pyrogallic acid were found to yield irreproducible results during the experiments, the NPOC results were used. NPOC results are also reported for the experiments involving the Dismal Swamp organic matter extract. Oxalic acid was strongly affected by the presence of aluminum and acidification to pH < 1.2 was not feasible, therefore this compound was analyzed by ion chromatography. The same analytical method used for

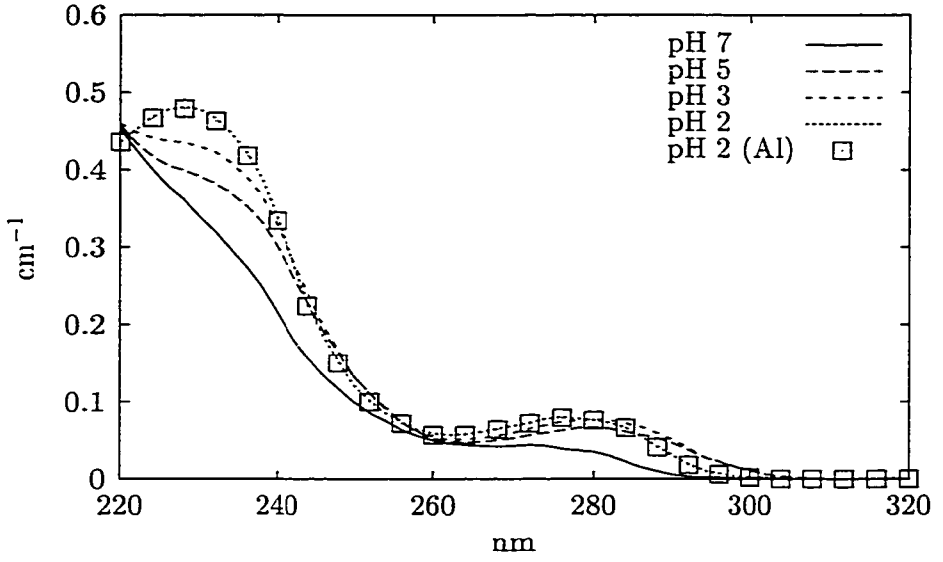

Figure 4.4. UV-spectrum of phthalic acid (63 μM) as a function of pH and in the presence of 1 mM Aluminum at pH 2.

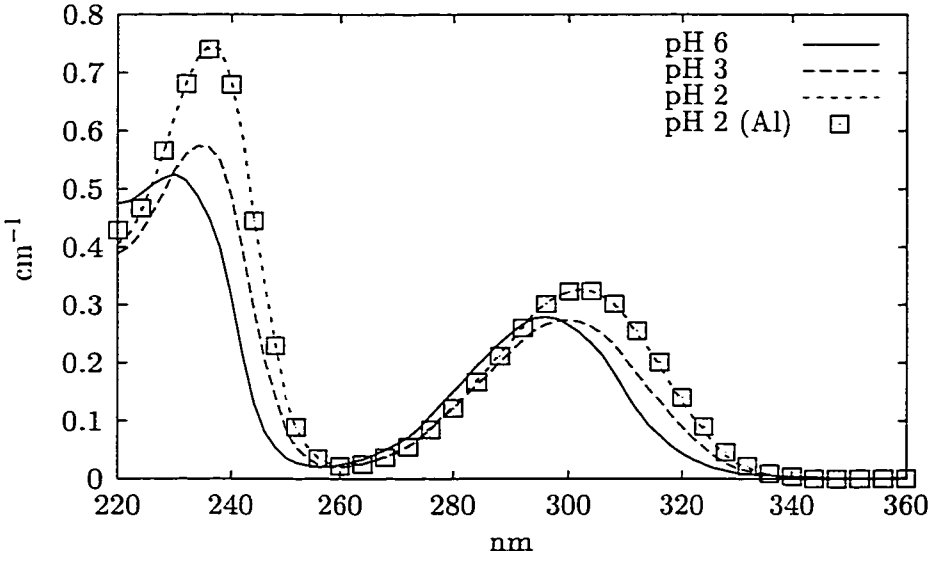

Figure 4.5. UV-spectrum of salicylic acid (82 μM) as a function of pH and in the presence of 1 mM Aluminum at pH 2.

Table 4.4. Molar extinction coefficients.

Organic Substance	Wavelength [nm]	ϵ [l/(mol·cm)]
Phthalic Acid	228	7375
Salicylic Acid	300	3491
Pyromellitic Acid	292	2211
Aldrich Humic Acid	254	1063

sulfate was utilized and provided sufficient reprocibility and sensitivity (Appendix B).

ζ-Potential

Particle electrophoretic mobility was determined by laser doppler velocimetry. To minimize analytical errors, at least five measurements at different depths of the sample cell were conducted. The electrophoretic mobility was then determined from the profile of apparent mobility versus depth. The instrument's software converted electrophoretic mobility to ζ-potential using Smoluchowski's equation.

4.3. Results and Discussion

4.3.1. Solubility and Electrokinetic Properties of Aluminum Hydroxide

Measurement of the aluminum concentration in the centrifuged and filtered samples after conclusion of each experiment indicated that between pH 5 and 8 more than 90% of the added aluminum was in particulate form (Figure 4.6). The solid line in Figure 4.6 represents the solubility of aluminum hydroxide computed using PHREEQC and considering only monomeric hydroxo aluminum species as in Section 2 (Table 2.1). A solubility constant for $Al(OH)_3(s)$ of 10.6 provided a good fit, which is only slightly greater than the value available in the thermodynamic database of the program. The good correlation of measured to computed aluminum concentrations indicates that the solids formed during the experiment consisted predominantly of amorphous aluminum hydroxide and that the various solutes used did not noticeably alter the solubility of the precipitate.

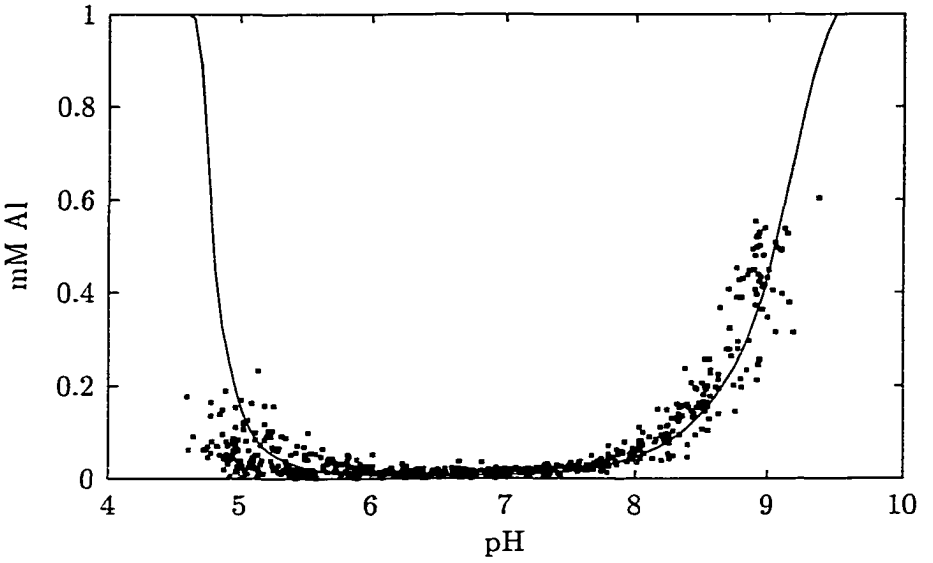

Figure 4.6. Dissolved aluminum concentration as a function of pH. Solid line calculated using PHREEQC.

Replicate experiments were conducted to characterize the electrokinetic properties of the pure aluminum hydroxide precipitate and to establish a reference to which results from subsequent tests with ions other than the electrolyte ions could be compared. The results from the ζ-potential measurements are shown in Figure 4.7. The dashed line represents a least squares fitted polynomial and is included to illustrate the trend of the data.

The data indicate that the aluminum hydroxide precipitate has a positive ζ-potential over the studied pH-range suggesting that positively charged surface groups $\equiv AlOH_2^+$ predominate over negatively charged sites $\equiv AlO^-$. The ζ-potential is roughly constant up to pH 7 and then decreases with increasing pH which is apparently due to the deprotonation of the surface hydroxyl groups, i.e., $\equiv AlOH_2^+ \rightleftharpoons \equiv AlOH + H^+$. Based on these data, the point at which the ζ-potential is zero cannot be determined exactly. However, it appears that the pH_{iep} is at a pH slightly greater than 9. This observation agrees favorably with published work by many other researchers. Matijević *et al.* (1971) determined the electrophoretic mobility of aluminum hydroxide particles over a wide pH range and their results are very similar to those obtained in this work (Figure 4.7). Letterman *et al.* (1982) found a pH_{iep} of 9.2 for aluminum hydroxide coated silica particles and Anderson and Benjamin (1990b) reported a value of pH 8.9 for the isoelectric point of a pure precipitate prepared from

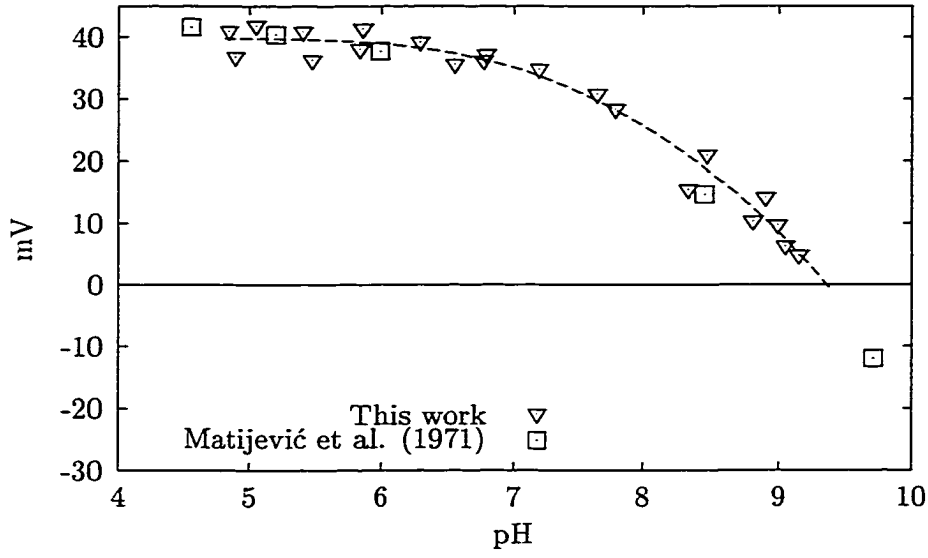

Figure 4.7. ζ-potential of aluminum hydroxide as a function of pH.

aluminum nitrate under conditions similar to this work.

4.3.2. Adsorption of Inorganic Anions

The graphs of fractional adsorption and ζ-potential as a function of pH for the inorganic ions studied in this work are shown in Figures 4.8 through 4.15. Sulfate follows a trend typical for anions, where adsorption decreases with increasing pH (Figure 4.8). At all total sulfate concentrations sorption of SO_4^{2-} seems to diminish to negligible levels near the pH_{iep} (beyond which the aluminum hydroxide surface is negatively charged). This observation suggests that electrostatic forces at the surface-water interface play an important role in sulfate adsorption. At a total concentration of 0.10 mM at pH 5 sulfate was completely removed and the adsorption density, i.e., mol of adsorbed sulfate per mol of (total) aluminum, was approximately 0.1 mol SO_4/mol Al. With increasing sulfate concentrations, fractional adsorption decreased, whereas adsorption density increased. For example at pH 5 and 0.50 mM SO_4, the adsorption density increased to approximately 0.25 mol SO_4/mol Al. At the highest sulfate dose, the adsorption density remained at this value, suggesting that the surface of the aluminum hydroxide precipitate was "saturated."

Sulfate significantly decreased the ζ-potential of the precipitate particles in these experiments as shown in Figure 4.9. However, it did not greatly influence the pH_{iep} nor did it

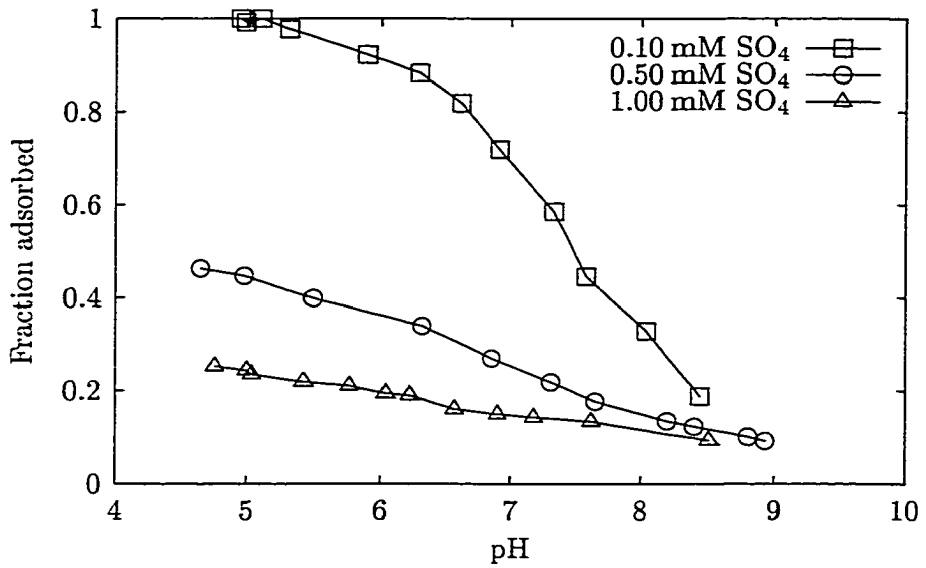

Figure 4.8. Fraction of sulfate adsorbed as a function of pH and total concentration.

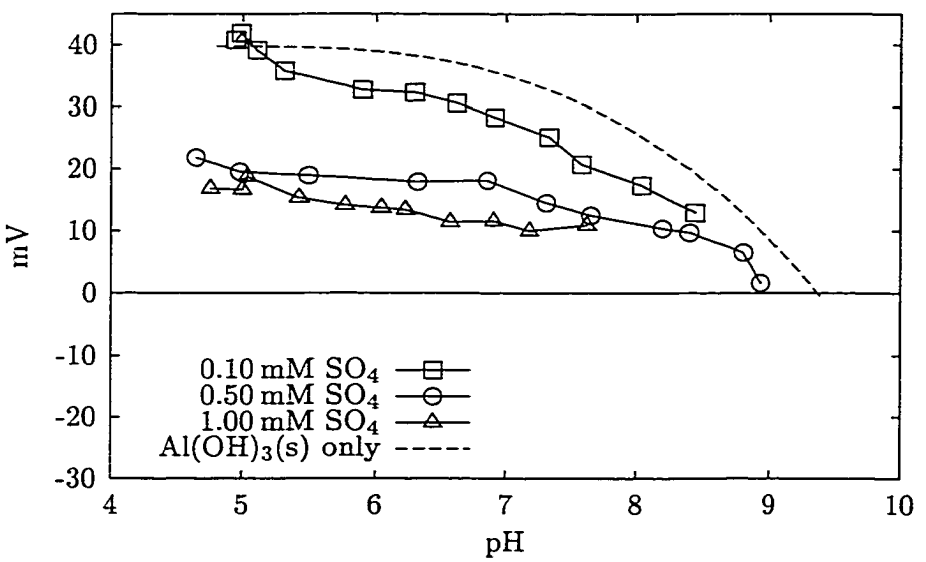

Figure 4.9. ζ-potential as a function of pH and total sulfate concentration.

cause a reversal in ζ-potential. This effect is typically due to *specifically adsorbed* ions forming inner-sphere complexes, i.e., the process involving adsorption to the surface by forces other than electrical potential (e.g., covalent bonding) (Hunter, 1981). With increasing sulfate dose the ζ-potential appears to approach a finite value at any given pH. It is possible that because the increased adsorption of the divalent ion lowers the charge near the surface (to less positive values), less electrostatic attraction for negative ions may exist. Therefore, it appears that under these experimental conditions and with respect to its effects on the electrokinetic properties of the particles, sulfate acts like a weakly adsorbing electrolyte ion. This weak interaction with the aluminum hydroxide surface can be expected when considering that sulfate only forms weak ion pairs with aluminum in solution.

A more quantitative analysis of the data that may provide information about the nature of the surface complex, can be obtained by relating the ζ-potential measurements to the amount of sulfate adsorbed. Under certain assumptions, the change in surface charge upon adsorption can be calculated from ζ-potentials based on Gouy and Chapman's theory. The solution of the Poisson-Boltzmann equation for the diffuse layer charge σ_d in the presence of a mono-charged electrolyte is (Davis and Kent, 1990):

$$\sigma_d = -\sqrt{8RT\epsilon\epsilon_0 I 10^3}\sinh\left(\frac{\psi_d F}{2RT}\right)$$

where R is the molar gas constant ($8.314\,\mathrm{J\,mol^{-1}K^{-1}}$), T the absolute Temperature, ϵ the relative dielectric constant (78.5 at 25°C), ϵ_0 the permittivity of free space ($8.854 \cdot 10^{-12}$ F/m), and F is Faraday's constant ($96485\,\mathrm{C/m^2}$). For the ionic strength, I, a value of 0.005 M was used in the subsequent calculations. Under the assumption that the hydrodynamic shear plane of the particles coincides with the outer Helmholtz plane (i.e., the closest plane of approach of the counter ions), the diffuse layer potential ψ_d can be approximated by the measured ζ-potential (Hunter, 1981). Because the surface charge σ_0 has to be balanced by the diffuse layer charge σ_d, the charge of the hydroxide particles as a function of pH can therefore be readily computed using the above equation. The difference in charge of the pure particles and those modified in the presence of a ligand $\Delta\sigma$ divided by the amount adsorbed is thus a measure that allows comparison of different adsorbing ligands at variable doses.

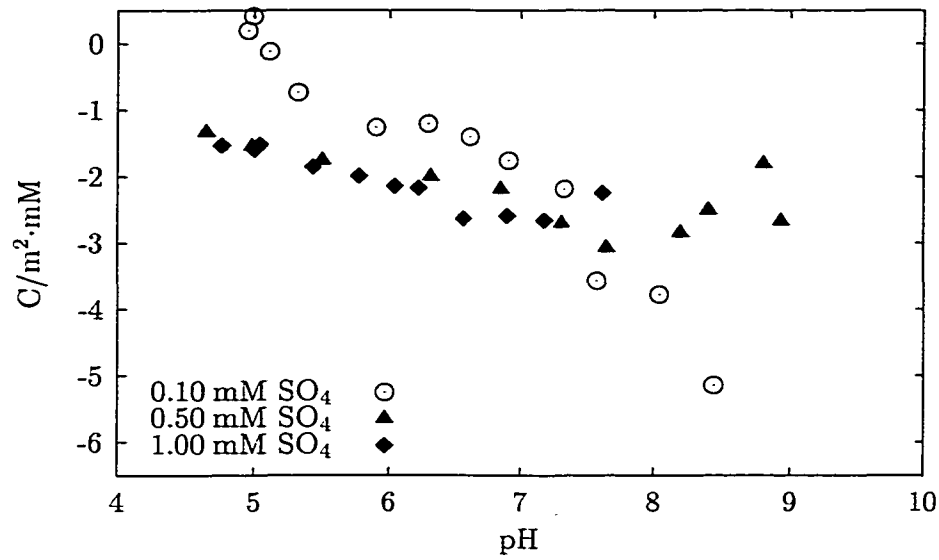

Figure 4.10. Change of surface charge per mM sulfate adsorbed as a function of pH.

To obtain paired values at the same pH, the ζ-potential of the "pure" $Al(OH)_3(s)$ particles was approximated by fitting a third-order polynomial to the measured data (shown as a dashed line in Figure 4.7). The calculated change in surface charge per mM adsorbed sulfate ($\Delta\sigma/[SO_4]_{ads}$) versus pH is shown in Figure 4.10.

The plot reveals a discernible difference in the effects on surface charge between the 0.10 mM and the higher sulfate doses. Between 0.5 mM and 1.00 mM, the change in surface charge is essentially indistinguishable. Thus, at these doses, the surface charge of the precipitate decreases proportionally with sulfate adsorption density and the impact appears to be greater at higher pH. Generally, at pH > 8 the data exhibited more scatter, possibly because the low surface concentrations and low (absolute) ζ-potentials were easier affected by random errors. A steeper slope of the $\Delta\sigma/[SO_4]_{ads}$ versus pH-curve at pH > 8 could also be expected because due to dissolution of the sorbent, the adsorbed charge has to be distributed over a smaller surface area and thus exerts a greater influence on surface charge density. The linear decrease in $\Delta\sigma/[SO_4]_{ads}$ with increasing pH suggests that the surface complex becomes more negatively charged by releasing protons. The data from the experiment with the 0.10 mM dose do not follow the same trend. Because the impact on ζ-potential at this dose was small, these differences could be a result of random error. However,

they could also indicate that at pH < 7, a different mechanism may affect adsorption of sulfate at low total concentrations. Considering that sulfate was completely removed near pH 5, it is possible that at low surface coverage sulfate ion may adsorb by ligand exchange according to the following reactions (in the order of increasing pH):

$$\equiv AlOH_2^+ + H^+ + SO_4^{2-} \rightleftharpoons \equiv AlHSO_4 + H_2O$$

$$\equiv AlOH_2^+ + SO_4^{2-} \rightleftharpoons \equiv AlSO_4^- + H_2O$$

whereas at higher doses, increasing site saturation favors adsorption predominated by electrostatic attraction as shown below. The reactions may affect surface charge differently than the ligand exchange mechanism.

$$\equiv AlOH_2^+ + H^+ + SO_4^{2-} \rightleftharpoons \equiv AlOH_2^+HSO_4^-$$

$$\equiv AlOH_2^+ + SO_4^{2-} \rightleftharpoons \equiv AlOH_2^+SO_4^{2-}$$

According to these reactions, adsorption of negatively charged sulfate ions occurs only when the surface is positively charged, i.e., $\equiv AlOH_2^+$ sites predominate over neutral or negatively charged surface hydroxyl groups. This also implies that no sulfate is removed at pH > pH_{iep} as was observed in the experiments. Thus, sulfate adsorbs either by exchange with $-OH_2^+$ or by electrostatic attraction to $-OH_2^+$. This is in agreement with the work by Hingston *et al.* (1972) who suggested that completely dissociated acids adsorb only to positively charged surfaces, because protons are required for the exchange of –OHgroups. Because sulfate fully ionizes at pH > 2, it can therefore not remove neutral or negatively charged surface hydroxyl groups (–OH, $-O^-$) to provide a site for complexation.

The data from these experiments demonstrate the ability of sulfate to "quench" the surface charge while not reversing the ζ-potential over a wide pH-range. This is a well known fact and has great advantages in water treatment. Aluminum sulfate (alum) is the most widely used metal salt coagulant and it contains 1.5 mol of SO_4^{2-} per mol of Al. Because of this stoichiometry, even when the coagulant is "overdosed," charge reversal (i.e., an increase of particle charge from near zero to more positive values with increasing dose) and particle restabilization is inhibited due to the coadsorption of the negatively charged sulfate ion. Rapid coagulation of oxide particles typically occurs at values of $|\zeta| < 14 \pm 4$ mV

(Hunter, 1981); based on these experimental data (Figure 4.9), the ζ-potential of aluminum hydroxide particles prepared from alum can be expected to fall within this range. Therefore, once the "coagulant demand" of a water is satisfied, any excess alum added will probably not cause the ζ-potential to exceed a threshold value, where electrostatic repulsion between particles occurs and formation of a settleable floc is impaired. In fact, this behavior has been well established in work by other researchers (Hanna and Rubin, 1970; Hayden, 1971; Letterman and Vanderbrook, 1983). This work also confirms that the charge of aluminum hydroxide particles in the presence of sulfate is pH-dependent and that the likelihood for charge reversal due to overdosing with alum decreases with increasing pH.

The adsorption data gathered from the experiments with orthophosphate are depicted in Figure 4.11. At a dose of 0.01 mM PO_4 (not shown), no phosphate was detectable in solution, indicating that it had adsorbed completely to the aluminum hydroxide precipitate. At 0.10 mM complete removal occurred in the pH range between 5 and 8. This trend is consistent with the observations made by Anderson and Benjamin (1990a). When comparing the adsorption envelope with the solubility data for $Al(OH)_3(s)$ in Figure 4.6, it appears that phosphate adsorption is limited by the amount of precipitate present at pH > 8. This is indicated by the dashed line in Figure 4.11 representing the fraction of aluminum present as $Al(OH)_3(s)$ as computed with PHREEQC using a solubility constant of $\log K = 10.6$. The correlation of solids concentration to fractional removal is very high and indicates that the maximum adsorption density in this pH-range is approximately 0.1 mol PO_4 per mol Al. Phosphate strongly adsorbed at the pH_{iep} suggesting that electrostatic attraction plays a minor role and that inner-sphere surface complex formation may be the dominant sorption mechanism. This conclusion becomes more evident when considering the ζ-potential data shown in Figure 4.12. At the low dose, phosphate does not appear to greatly influence the electrophoretic mobility of the particles. However, at the increased concentration, charge reversal has occurred and the point at which $\zeta = 0$ has moved to pH ≈ 8.

Although complete removal of phosphate occurred at pH 5 and 8, the effect on ζ-potential is remarkably different at these pH values. At pH 8, phosphate has neutralized the charge of the precipitate particles, whereas there is only a small effect at pH 5. This behavior can be understood considering the solution chemistry of orthophosphate. Within the examined

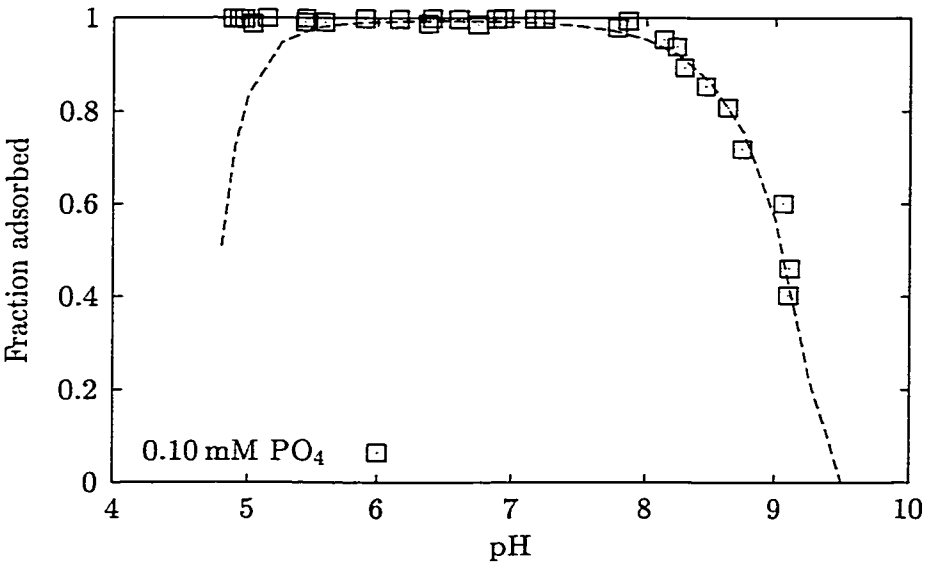

Figure 4.11. Fraction of orthophosphate adsorbed as a function of pH and total concentration. Dashed line indicates the fraction of aluminum precipitated.

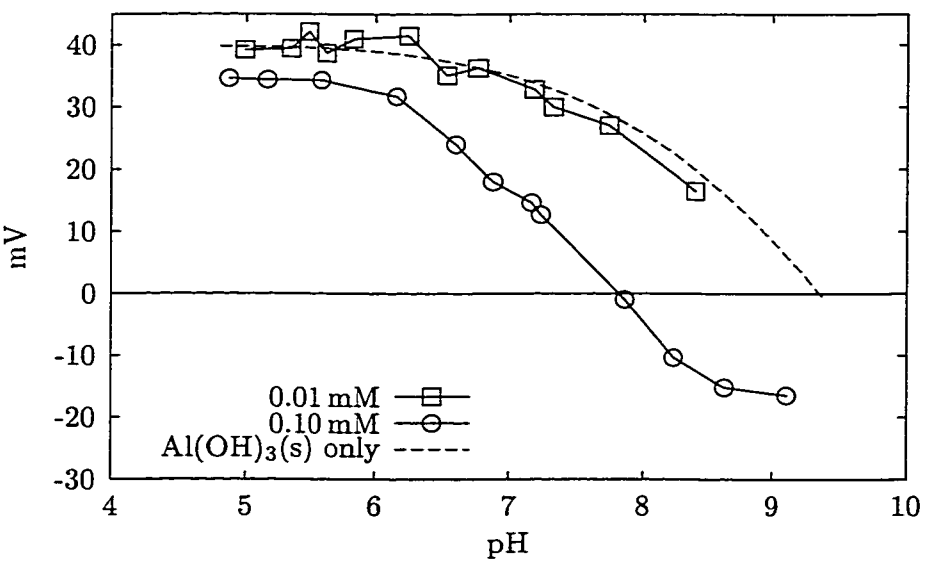

Figure 4.12. ζ-potential as a function of pH and total orthophosphate concentration.

pH-range, the singly charged species $H_2PO_4^-$ dominates at pH $< pK_{a,2} \approx 7.2$; HPO_4^{2-} is dominant at pH $> pK_{a,2}$. Although there is a difference in ζ-potential between pH 5 and 8 for the pure precipitate, the adsorption of the lower charged orthophosphate species has apparently a smaller effect on ζ-potential than the divalent ion. An analysis of the effect on surface charge per mol adsorbed phosphate (as previously conducted for sulfate) also suggests that a more negatively charged surface complex forms at elevated pH (Figure 4.13). Because the trend of the data exhibits an inflection to a more negative slope near pH 6, it appears that the deprotonation of the orthophosphate ion in solution indeed affects the type of surface complex formed. Similar observations were made by Boisvert *et al.* (1997). Therefore, the following reactions may occur at pH < 7.2, where the dihydrogenphosphate ion predominates:

$$\equiv AlOH_2^+ + H_2PO_4^- \rightleftharpoons \equiv AlH_2PO_4 + H_2O$$

$$\equiv AlOH + H_2PO_4^- \rightleftharpoons \equiv AlHPO_4^- + H_2O$$

and at pH > 7.2, where the divalent orthophosphate species occurs:

$$\equiv AlOH_2^+ + HPO_4^{2-} \rightleftharpoons \equiv AlHPO_4^- + H_2O$$

$$\equiv AlOH + HPO_4^{2-} \rightleftharpoons \equiv AlPO_4^{2-} + H_2O$$

Compared to the effect of sulfate (shown in Figure 4.10), phosphate exerts a far greater decrease in surface charge per mol anion adsorbed (Figure 4.13). This is particularly discernible at pH greater than 7, where both orthophosphate and sulfate are present as a divalent ion in solution. As shown in the reactions above, orthophosphate adsorption may be accompanied by release of a proton to form a surface complex and H_2O. As indicated previously, the proton release is required to exchange –OH groups. Therefore, the weak acidity of an anion seems to be of greater importance for adsorption and the effect on surface charge than the ionic charge.

Although orthophosphate occurs only at low concentrations in unpolluted raw waters, this work shows that only low concentrations are required to induce charge reversal on aluminum hydroxide particles. Therefore, there is the possibility that it can interfere with the coagulation process in water treatment where orthophosphate-based corrosion inhibitors are

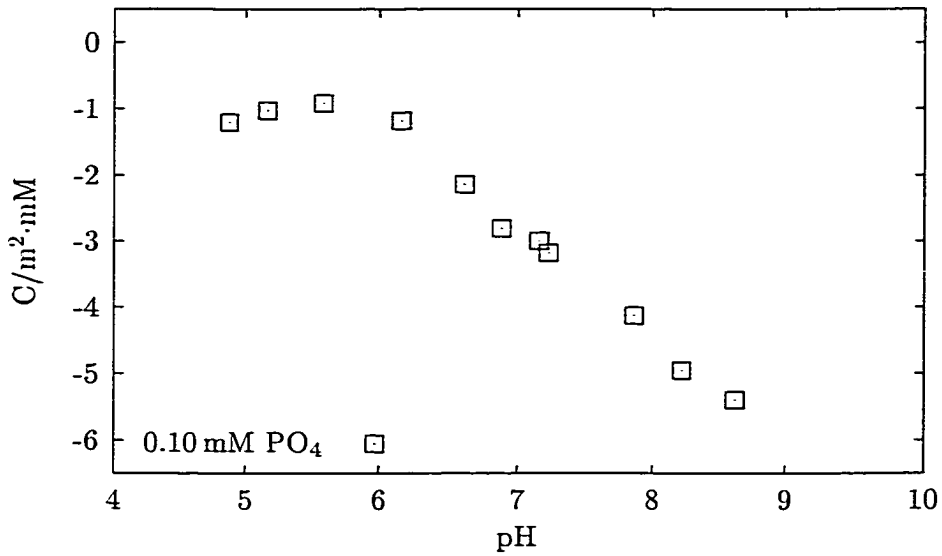

Figure 4.13. Change of surface charge per mM orthophosphate adsorbed as a function of pH.

used. It is not known whether there are utilities that add inhibitors at the point of coagulant addition. However, where orthophosphate treated water is used for backwashing granular media filters, it may be reintroduced to the treatment train through wastewater recycling (i.e., after sludge dewatering and decanting). This may be particularly true if no provisions are made for flow equalization and dilution, allowing a sudden change in water chemistry to occur. The coadsorption of orthophosphate to particles during the coagulation process can inhibit charge neutralization and thus hamper formation of a settable floc. Because proper chemical treatment is also required for effective filtration, particle breakthrough may occur. Consequently, orthophosphate may also adversely affect filter ripening. The findings from the experiment also confirm that treatment with aluminum salts is very effective for removing orthophosphate from solution.

Fractional adsorption of fluoride to freshly precipitated aluminum hydroxide is depicted in Figure 4.14. The pH-dependent removal of fluoride is remarkably different from that of sulfate or phosphate. Fractional removal was nearly identical for both tested concentrations and even at the lower concentration of 0.05 mM, a measurable fraction remains in solution. Fluoride also exhibited a broad maximum in adsorption near pH 6 decreasing steeply above pH 7.5 and below pH 5.5. As opposed to sulfate and phosphate, fluoride forms strong com-

plexes with aluminum in solution, which may account for the observed behavior. These fluoroaluminum complexes (AlF^{2+}, AlF_2^+, AlF_3^0) predominate in the acidic pH-region and are likely to exhibit due to their cationic charge a different adsorption behavior than the "free" anion, which would explain the decrease in adsorption with decreasing pH at pH < 5.5. If this behavior were due only to the dissolution of $Al(OH)_3(s)$, the measured dissolved aluminum concentrations in this region would have been much higher than observed. The pH-dependent adsorption of fluoride to hydrous alumina was also investigated by Hao and Huang (1986), who compared their data to those of previous researchers. In all these works, an optimum pH between 5 and 6 was reported, which agrees well with the data presented here.

The experimental results do not clearly indicate which adsorption mechanism governs the observed behavior. Fluoride removal decreased to negligible levels near the pH_{iep} and exerted only a small influence on ζ-potential (Figure 4.15) over the examined pH-range. The effects of higher fluoride concentrations were not tested because it would have affected the amount of precipitate formed as earlier experiments (Section 2) indicated. However, the strong affinity of fluoride to aluminum is well known and it is most likely that a ligand exchange reaction according to

$$\equiv AlOH_2^+ + F^- \rightleftharpoons \equiv AlF + H_2O$$

as proposed by Hao and Huang (1986) describes the adsorption onto aluminum hydroxide. In this scenario, the ligand exchange reaction occurs when the surface is positively charged to result in a neutrally charged surface complex. Fluoride may also complex uncharged sites despite the belief that completely dissociated acids including fluoride ($pK_a = 3.16$) adsorb only to positively charged surfaces (Hingston *et al.*, 1972). However, because fluoride is a stronger Lewis base than hydroxyl ion (Stumm and Morgan, 1996), it may undergo ligand exchange without being protonated. The formation of uncharged surface complexes would explain the lack of impact on surface charge which is illustrated in Figure 4.16. The change in surface charge per mM adsorbed fluoride does not vary with pH and its absolute value is generally smaller than 1 C/(m^2mM). Sulfate and phosphate which decreased the surface charge by 1-6 C/(m^2mM), may form mono- or divalent surface complexes. This comparison

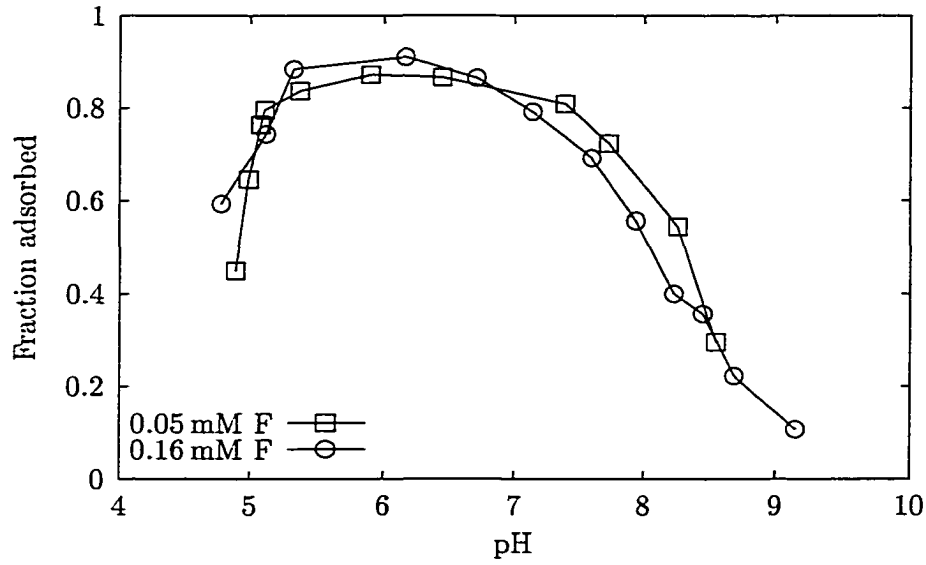

Figure 4.14. Fraction of fluoride adsorbed as a function of pH and total concentration.

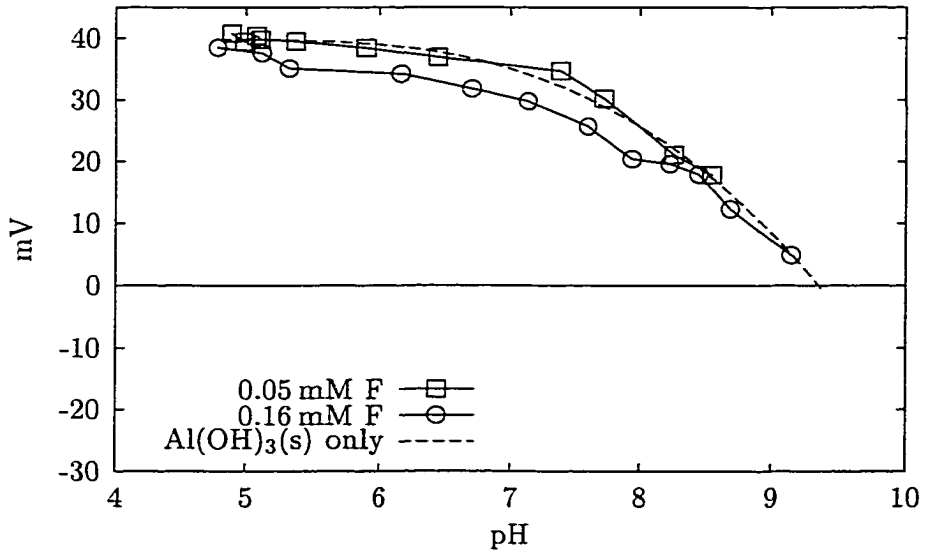

Figure 4.15. ζ-potential as a function of pH and total fluoride concentration.

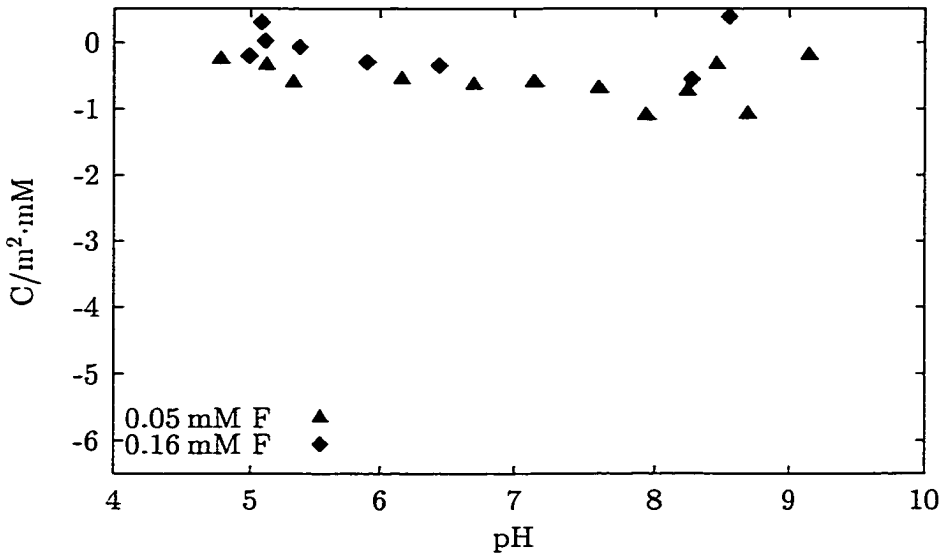

Figure 4.16. Change of surface charge per mM fluoride adsorbed as a function of pH.

thus supports that fluoride adsorbs in a manner where it has little impact on ζ-potential. Similar conclusions were reached by other researchers for the adsorption of fluoride onto hydrous iron oxide. Davis and Kent (1990) state that "extensive adsorption of F^- is promoted by the strength of the resulting Fe-F bond, small size of F^-, its strong nucleophilic character, and the lack of increase in surface charge resulting from F^- adsorption."

The negative effects of fluoride in water treatment with alum have been clearly demonstrated and the results from the batch test presented here supplement these earlier findings (Section 2, 3): If ligand exchange governs the direct complexation of fluoride to the precipitate, it will not greatly influence particle stability but rather the detrimental effects on turbidity removal during coagulation with alum would be mostly caused by the formation of fluoroaluminum complexes in solution and a concurrent decrease in aluminum hydrolysis product available to interact with particles.

4.3.3. Adsorption of Simple Diprotic Organic Acids

Five simple organic acids that vary in number and type of functional groups were examined in this work. A comparison of the fractional adsorption of organic acids with two functional groups (oxalic, phthalic, and salicylic acid), is provided in Figures 4.17 and 4.18.

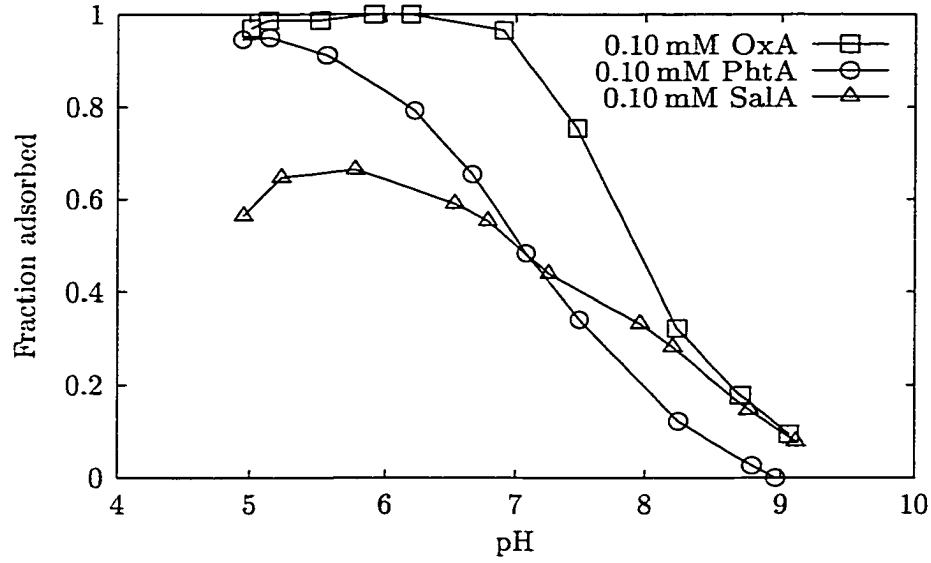

Figure 4.17. Adsorption of oxalic, phthalic, and salicylic acid as a function of pH (Concentration of each acid = 0.10 mM).

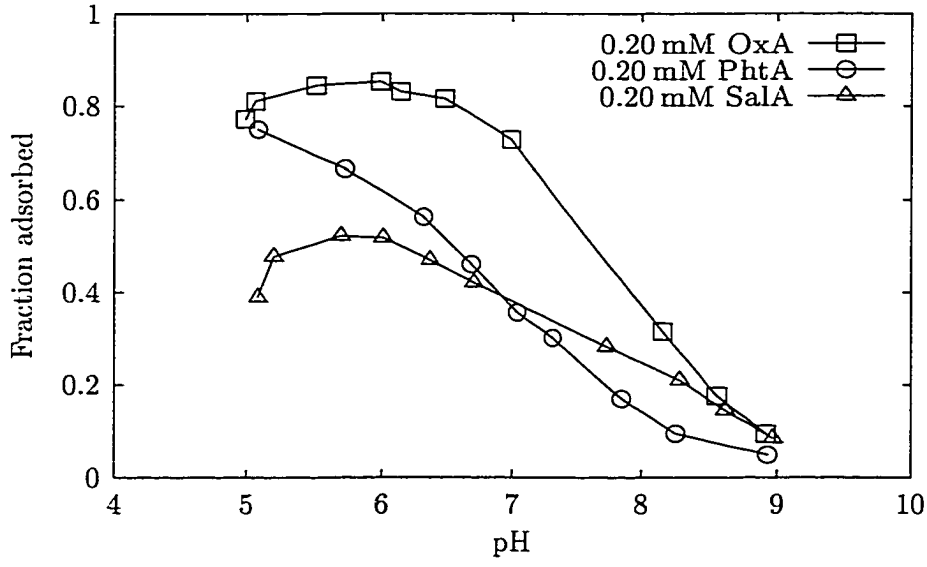

Figure 4.18. Adsorption of oxalic, phthalic, and salicylic acid as a function of pH (Concentration of each acid = 0.20 mM).

Generally, these compounds exhibited adsorption behavior to aluminum hydroxide similar to inorganic anions with a maximum adsorption density near pH 5 and negligible removal near the pH_{iep}. Oxalic and salicylic acid exhibit a slight decrease in adsorption with pH < 5.5. Both oxalic and phthalic acid carry two carboxyl groups which, based on their pK_a values listed in Table 4.1, are predominantly ionized at pH > 5. Several factors could be responsible for the difference in pH-dependent adsorption of these two compounds that have similar functional groups. Oxalic acid has lower pK_a values and thus at any pH more ionized carboxyl groups are available to interact with positively charged surface functional groups. It is also much lower in molecular mass and therefore specific charge density. The strong carboxylic acidity of oxalic acid is 83.3 meq/g C, whereas that of phthalic acid is only 20.8 meq/g C. These differences may affect the structure of a possible surface complex. A variety of bonding configurations for the adsorption of diprotic organic acids to oxides have been proposed in recent research (Kummert and Stumm, 1980; Biber and Stumm, 1994; Evanko and Dzombak, 1998). Following these examples, it can be envisaged that oxalate may form a bidentate surface complex in a five-membered ring structure on aluminum hydroxide (Figure 4.19). At higher surface loadings, a monodentate complex may predominate. Due to its smaller charge density, phthalic acid may not have the tendency to form a surface "chelate" and a monodentate surface complex would predominate even if the second carboxyl group ionizes (Figure 4.19).

The pH edge of salicylic acid is significantly different from that of oxalic and phthalic acid. Even at the low total concentration of 0.10 mM, complete removal did not occur. However, at pH > 7, it appears that it adsorbed to aluminum hydroxide to a greater extent than phthalic acid. Salicylic acid has a lower carboxylic acidity (11.9 meq/g C) and differs structurally from phthalic acid in that it has a phenolic group in the *ortho*-position. Biber and Stumm (1994) indicated that salicylic acid binds with aluminum in an inner-sphere complex in solution. They also suggested that the phenolic functional group is not directly involved in aluminum-salicylate complexation in solution. However, Biber and Stumm (1994) hypothesized that at the surface of aluminum oxide, a hydrogen bond due to the phenolic group is involved in the inner-sphere surface complex. The behavior observed here also indicates that both functional groups participate at least indirectly in the adsorption

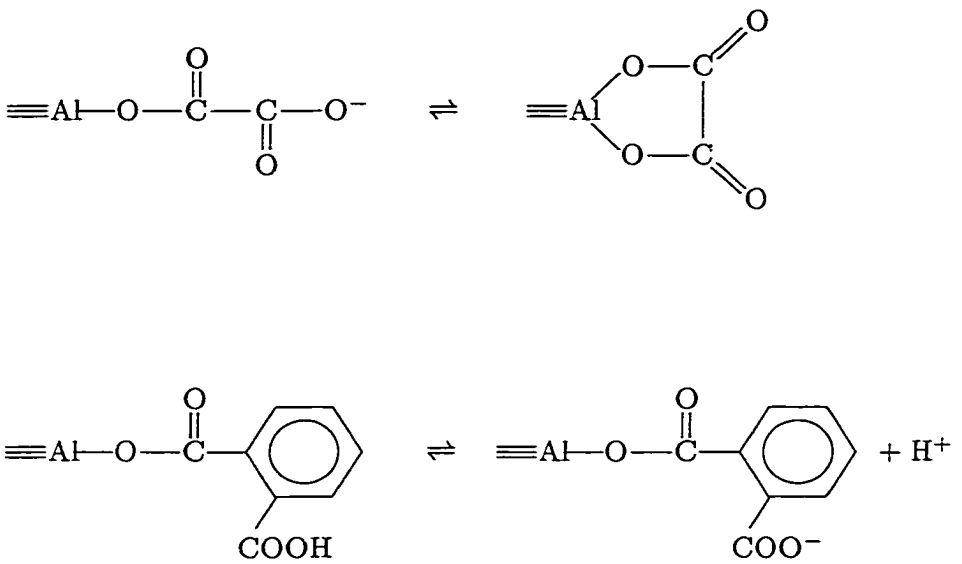

Figure 4.19. Possible surface structures for oxalic and phthalic acid.

reaction. Comparison of the pH edges of phthalic and salicylic acid suggests that a second carboxylic group on the benzene ring in the *ortho*-position enhances removal in the low pH range, whereas an additional phenolic group increases adsorption at elevated pH. If the phenolic group reacted with uncharged surface hydroxyl groups in a manner similar to orthophosphate, it would undergo a ligand exchange reaction such as

$$\equiv \mathrm{AlOH} + \mathrm{R-OH} \rightleftharpoons \equiv \mathrm{AlO-R} + \mathrm{H_2O}$$

However, the pK_{a2} of salicylic acid of 13.7 suggests that deprotonation of the phenolic group is not favored in the pH range examined here.

Oxalic and salicylic acid exhibit a maximum in adsorption density near pH 5.5. With oxalic acid it may reflect the deprotonation of one carboxyl group. However, as with fluoride, this behavior may be caused by formation of non-sorbable dissolved complexes and/or partial dissolution of the precipitate. Utilizing known stability constants, the speciation of dissolved aluminum in the presence of these three organic acids under these experimental conditions can be readily estimated. The stability constants in Table 4.5 were taken from Martell and Smith (1977) and extrapolated to $I = 0$ M using Davies' equation.

The fraction of 1 mM aluminum complexed to 0.10 mM phthalic, salicylic, or oxalic acid

Table 4.5. Stability constants of aluminum-organic acid complexes.

Ligand	$\log \beta_1$	$\log \beta_2$	$\log \beta_3$
Phthalic Acid	4.8	8.5	
Oxalic Acid	7.3	12.7	16.3
Salicylic Acid	14.2	24.9	31.1

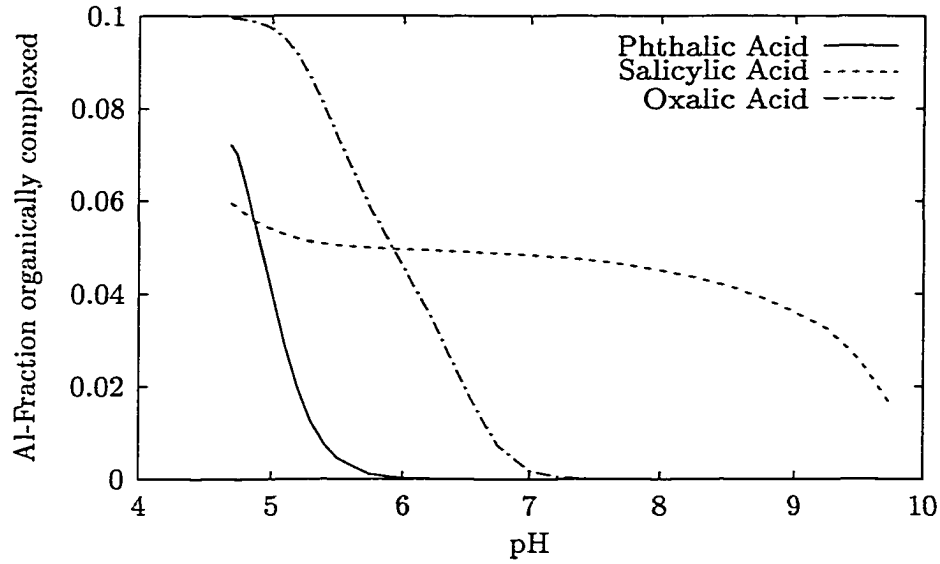

Figure 4.20. Fraction of 1 mM aluminum complexed to oxalic, phthalic and salicylic acid as a function of pH

in solution versus pH as calculated with PHREEQC is shown in Figure 4.20. At pH < 5 the affinity for aluminum in solution increases in the order salicylic $<$ phthalic $<$ oxalic acid. At pH > 5.5, only a negligible fraction of phthalic acid is complexed to aluminum. Therefore, it appears that the formation of soluble complexes may indeed influence the adsorption of oxalic and salicylic acid. Kummert and Stumm (1980) found that the tendency of organic ligands to form surface complexes on γ-Al_2O_3 is related to their tendency to form complexes with aluminum in solution. Generally, the adsorption data follow this tendency; however, the pH at which salicylic and phthalic acid complex aluminum equally is at a higher pH in the adsorption plot.

The effect of adsorption of oxalic, phthalic, and oxalic acid on the ζ-potential of the aluminum hydroxide particles is shown in Figures 4.21 and 4.22.

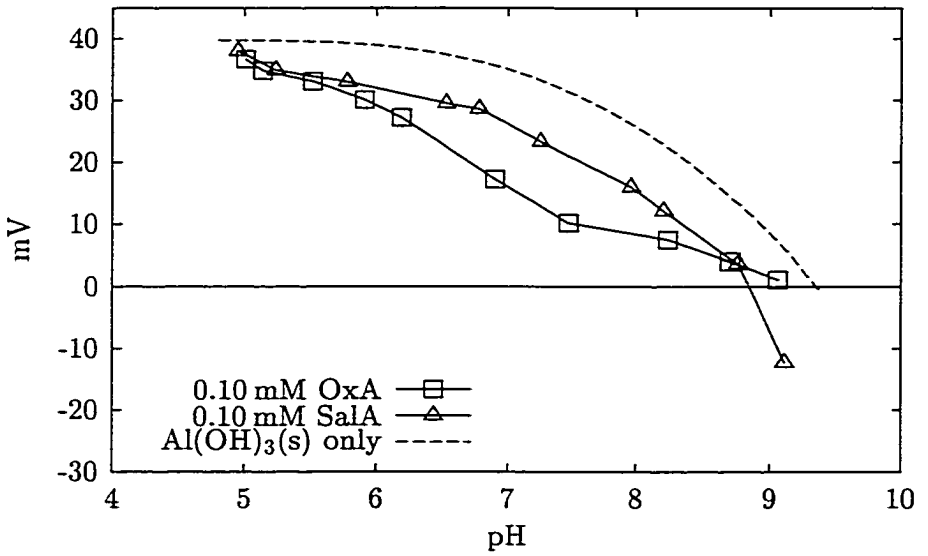

Figure 4.21. Effect of adsorption of oxalic, phthalic and salicylic acid on ζ-potential as a function of pH (Total concentration = 0.10 mM).

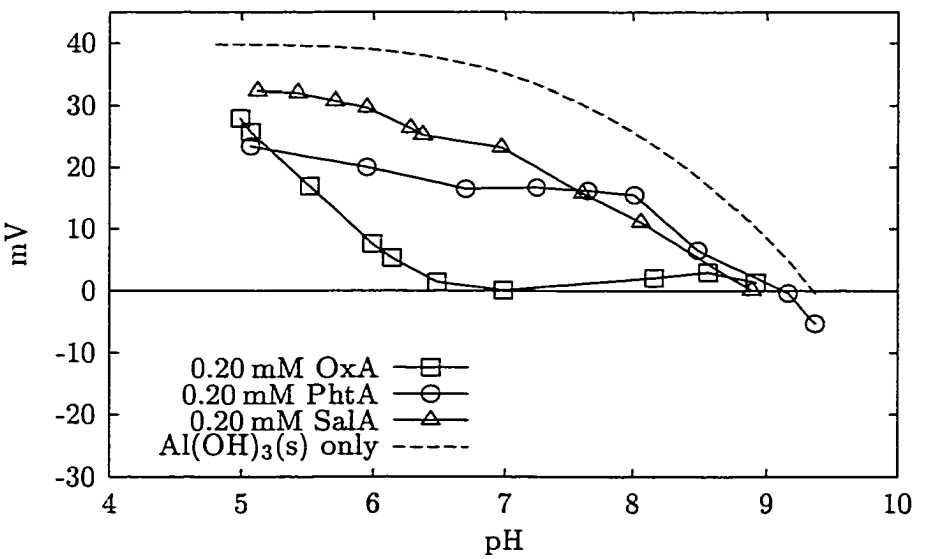

Figure 4.22. Effect of adsorption of oxalic, phthalic and salicylic acid on ζ-potential as a function of pH (Total concentration = 0.20 mM).

Generally, the more strongly adsorbing ions caused greater decrease in ζ-potential. Oxalic acid has a far greater influence than the two aromatic compounds. This is particularly discernible at pH > 7. The decrease in ζ-potential is small near pH 5, suggesting that a more negatively charged surface complex may predominate at higher pH. At a total concentration of 0.20 mM, oxalate decreased the ζ-potential to 0.1 mV at pH 7. Although it did not induce charge reversal of the particles, this is a strong indication that oxalic acid forms an inner-sphere complex at the solid-water interface. Its strong affinity to aluminum in solution seems to support this assertion.

At both doses, the ζ-potential decreased only slightly upon adsorption of salicylic acid and the location of the pH_{iep} was essentially not affected. If salicylate indeed forms an inner-sphere complex at (hydrous) aluminum oxide surfaces as suggested by Biber and Stumm (1994) then the small effect on ζ-potential indicates that the resulting surface complex is uncharged.

Phthalic acid exerts a greater effect than salicylic acid. Electrophoretic mobility measurements were not conducted for the experiment with the 0.10 mM dose. The data resemble those for sulfate which also did not affect the pH_{iep} but caused a considerable decrease in ζ-potential near pH 5. This suggests that phthalic acid predominantly adsorbs through electrostatic attraction to the aluminum hydroxide surface. Person *et al.* (1998) noted that phthalic acid adsorption to γ-Al_2O_3 is not affected by ionic strength at low pH, and concluded that an inner-sphere complex forms, whereas only at high pH > 7 the interaction is dominated by coulombic forces. These experimental results cannot confirm their "inner-sphere" observation.

4.3.4. Adsorption of Simple Polyprotic Organic Acids

Of the organic acids that were examined in this work, pyromellitic and pyrogallic acid carry more than two functional groups. Although the acidity constants of these compounds have been established (Table 4.1), no thermodynamic data have been published with respect to the interaction with aluminum in aqueous solution. The adsorption of these substances to aluminum hydroxide versus pH is shown in Figures 4.23 and 4.24.

Like the other acids with carboxyl groups, pyromellitic acid reached its maximum ad-

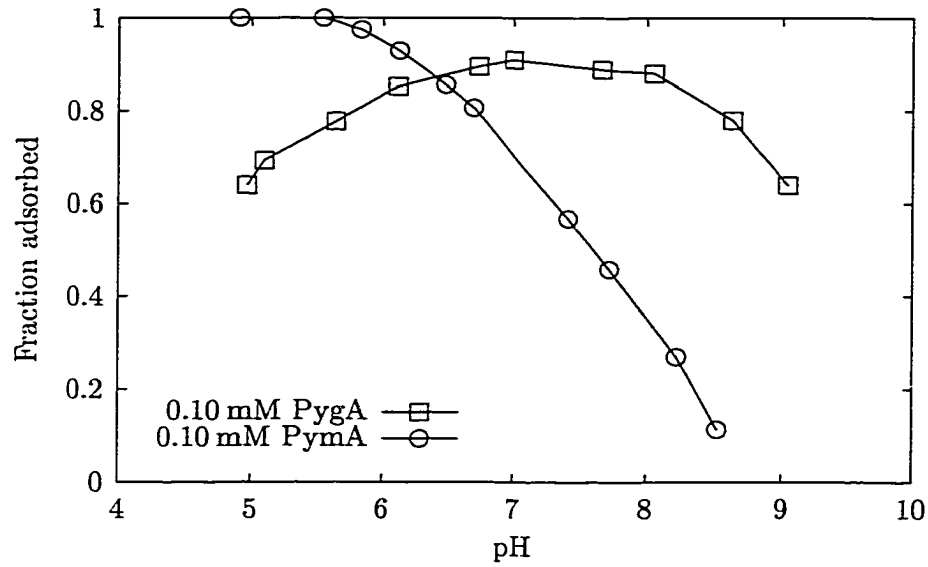

Figure 4.23. Adsorption of pyromellitic and pyrogallic acid as a function of pH (Concentration of each acid = 0.10 mM).

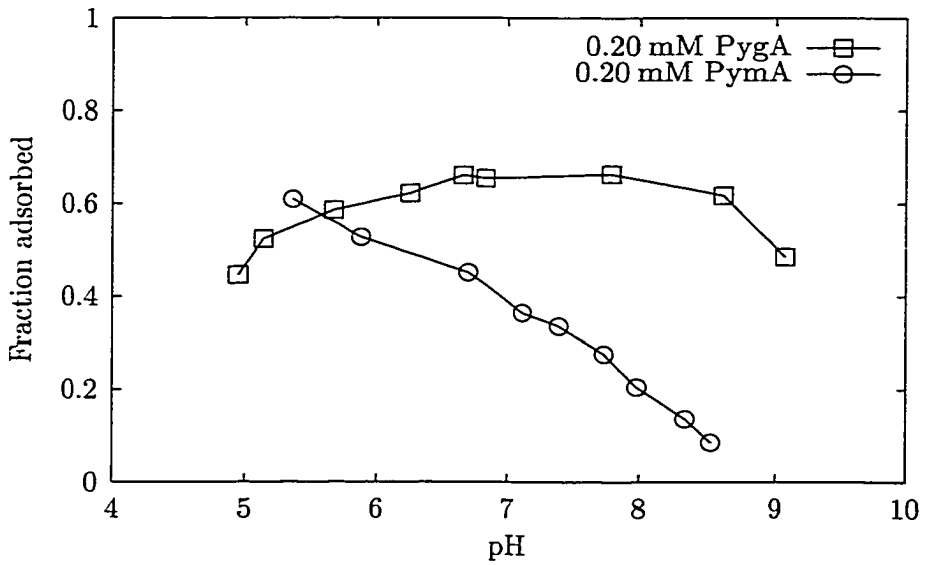

Figure 4.24. Adsorption of pyromellitic and pyrogallic acid as a function of pH (Concentration of each acid = 0.20 mM).

sorption density at the lower pH and little or no removal occurred at the pH_{iep}. The latter observation is consistent with that made for fully dissociated inorganic acids in that positively charged surface hydroxyl groups have to be present for adsorption to occur. At the 0.10 mM dose, it was removed to a greater extent than phthalic acid (refer to Figure 4.17). However, at the 0.20 mM dose, the adsorption of phthalic acid was greater despite the fact that pyromellitic acid has a higher charge density (33 meq/g C), more carboxylic functional groups, and significantly lower pK_a-values. These observations suggest that the additional carboxyl groups enhance removal of pyromellitic acid at low concentrations by occupying more binding sites on the hydroxide surface. On the other hand, the formation of polynuclear surface complexes may lead to surface saturation at a lower total sorbate concentration compared to a compound that occupies fewer surface sites.

Pyrogallic acid, an aromatic compound with three adjacent phenolic groups, exhibited a greatly different adsorption behavior. Its adsorption density reached a broad maximum around pH $\approx$ 7 and it was strongly bound to the precipitate at the pH_{iep}. If electrostatic interactions were dominant, the decrease in adsorption with decreasing pH may be related to greater repulsion of the uncharged phenolic groups by the increasingly positive surface hydroxyl groups. However, it can be assumed that pyrogallic acid behaves similarly to catechol, an aromatic acid with two adjacent phenol groups, that has been found to form strong surface complexes on iron oxide surfaces (Evanko and Dzombak, 1998). Therefore it is also possible that protons compete with surface aluminum ions for the phenolic oxygen atoms at low pH and cause the decrease in adsorption of pyrogallic acid with decreasing pH. At pH $>$ 7, adsorption decreased with increasing pH and it may be limited by the amount of precipitate formed. Pyrogallic acid also exhibited a great decrease in adsorption density at higher total concentrations, suggesting that the surface was saturated.

These data clearly illustrate the effect of type of functional group on adsorption of organic acids to oxide surfaces. It appears that the charge of the organic functions relative to the charge of the surface indicates the removal efficiency. Deprotonated groups, e.g., carboxylic functions, enhance adsorption to a positively charged surface, whereas neutral functional groups, e.g., undissociated phenolic groups, increase removal near the pH_{iep}. These results also show that functional groups other than those that are strongly acidic

play an important role in the adsorption of organic compounds. Davis (1982) suggested that carboxyl groups ($pK_a = 3 - 6$) are less important in surface complex formation than weakly acidic ($pK_a = 6 - 10$) and phenolic groups. His assertion may be correct, considering that at equimolar concentrations pyromellitic acid was better removed than pyrogallic acid only at pH < 6.5 in these experiments. (Note that other authors consider functional groups with $pK_a < 8$ carboxylic (Thurman, 1985). However, for this work, this difference is irrelevant because the pK_a of the organic acids used in this work are either less or very near 6 or greater than 8.)

The effects of these two compounds on the ζ-potential of the hydroxide particles is shown in Figure 4.25 and 4.26. Clearly, both polyprotic organic acids cause the ζ-potential to reverse, which indicative of inner-sphere complexation at the aluminum hydroxide surface. Pyrogallic acid decreased the pH_{iep} by roughly two pH units, whereas the adsorption of pyromellitic acid displaced the isoelectric point to pH < 6. However, pyrogallic acid exerted a greater influence on the ζ-potential at pH > 8 and had little effect near pH 5.

The ζ-potential of the $Al(OH)_3(s)$ particles decreased rapidly with increasing pH upon pyromellitic acid adsorption although removal stagnated or decreased between ph 5 and 6. This may have been due to deprotonation of one or two carboxyl groups (pK_a 4.92 and 6.23). These ionized functions may not form additional bonds to "neutralize" positively charged surface hydroxyl groups and therefore increase the negative surface charge. Thus, the greater removal of phthalic acid at the 0.20 mM dose indicated earlier may be a result of electrostatic repulsion and not (only) an effect of site saturation. Several authors found that additional functional groups in the *ortho* position lead to increased adsorption, whereas carboxyl groups in the *para* or *meta* positions may not participate in surface reactions and thus have little or no effect (Lefebvre and Legube, 1993; Rahni and Legube, 1996; Evanko and Dzombak, 1998). These findings suggest that the additional functions on the pyromellitic acid molecule acid are indeed not involved in surface complexation to aluminum hydroxide. Greater removal at low concentrations compared to phthalic acid may be due to the ability to form a bidentate or binuclear surface complex as shown in Figure 4.27. However, the greater charge density and acidity may be detrimental at higher adsorption density because the additional carboxyl groups are deprotonated and prevent adsorption of

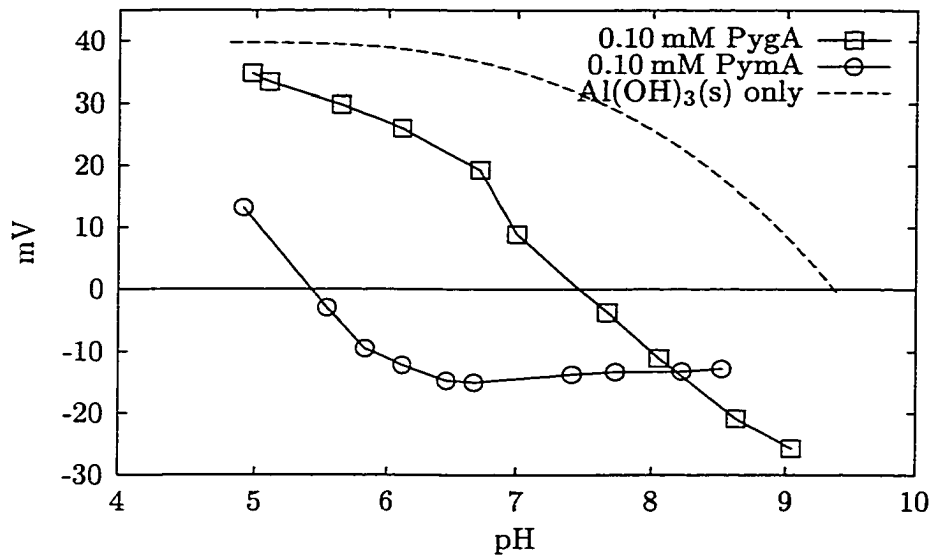

Figure 4.25. Effect of adsorption of pyromellitic and pyrogallic acid on ζ-potential as a function of pH (Total concentration of each acid = 0.10 mM).

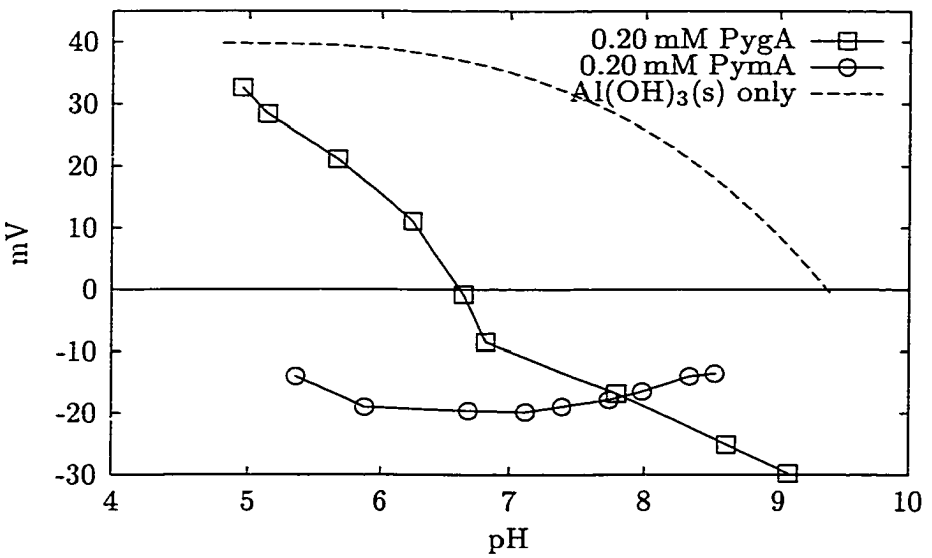

Figure 4.26. Effect of adsorption of pyromellitic and pyrogallic acid on ζ-potential as a function of pH (Total concentration of each acid = 0.20 mM).

additional molecules by electrostatic repulsion.

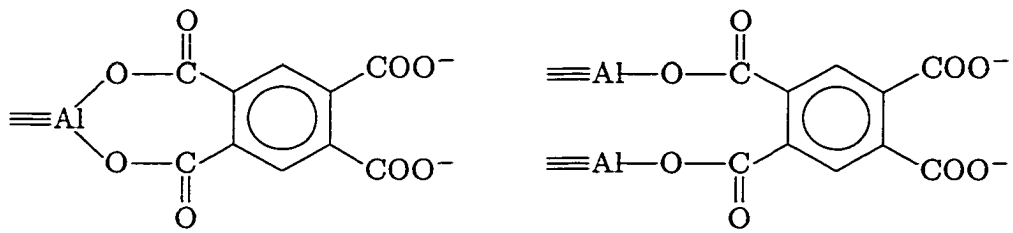

Figure 4.27. Possible surface structures for pyromellitic acid. Carboxylic functional groups are fully deprotonated.

The shape of the ζ-potential versus pH curve of pyrogallic acid suggests that this organic acid forms an uncharged surface complex near pH 5, which becomes negatively charged with increasing pH. The decrease in charge as measured by the ζ-potential may be caused by ionization of nonbonding phenolic groups as shown in Figure 4.28. The proposed reaction illustrates that the adsorption of pyrogallic acid must be accompanied by deprotonation of a phenolic group. Because of the high pK_a of 9.2, the proton release may not be favored at low pH and cause a decrease in adsorption as the experimental results show.

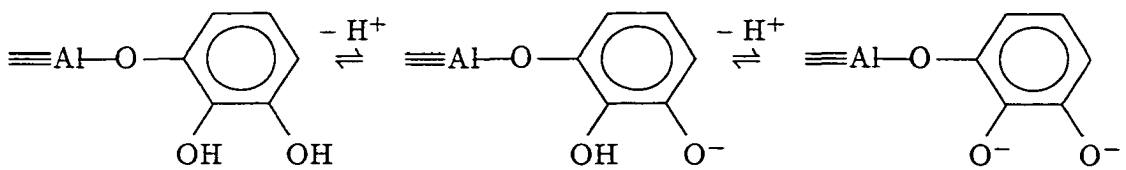

Figure 4.28. Possible surface structures for pyrogallic acid.

Further mechanistic interpretation of the experimental results is possible by calculating the decrease in charge per mol organic acid adsorbed from ζ-potential measurements as described previously. The results are shown in Figure 4.29 and the plot reveals that with the exception of pyromellitic acid, all simple organic acids exert a similar effect on the charge of the aluminum hydroxide particles. The decrease is proportional to the surface

concentration irrespective of whether the organic acid carries carboxylic or phenolic functional groups. Therefore, these compounds must form surface complexes of similar charge that are near neutral at low pH but cause the charge of the particles to decrease more with increasing pH. This apparent linear trend is not easily explained because the surface charge is proportional to the sum of the charges of surface hydroxyl groups and adsorbed ligands, and thus nonlinear in $[H^+]$ and pH. The change of surface charge due to pyromellitic acid adsorption is much greater and it also appears to be linearly correlated to pH. Because the plotted data are normalized to the adsorbed concentration, it is apparent that pyromellitic acid forms higher charged complexes than the other simple organic acids. The proposed surface structures for these adsorbates (Figures 4.19, 4.27, and 4.28) reflect this observation: Pyromellitic acid may form predominantly divalent surface complexes, whereas the other simple organic acids may result in singly charged complexes.

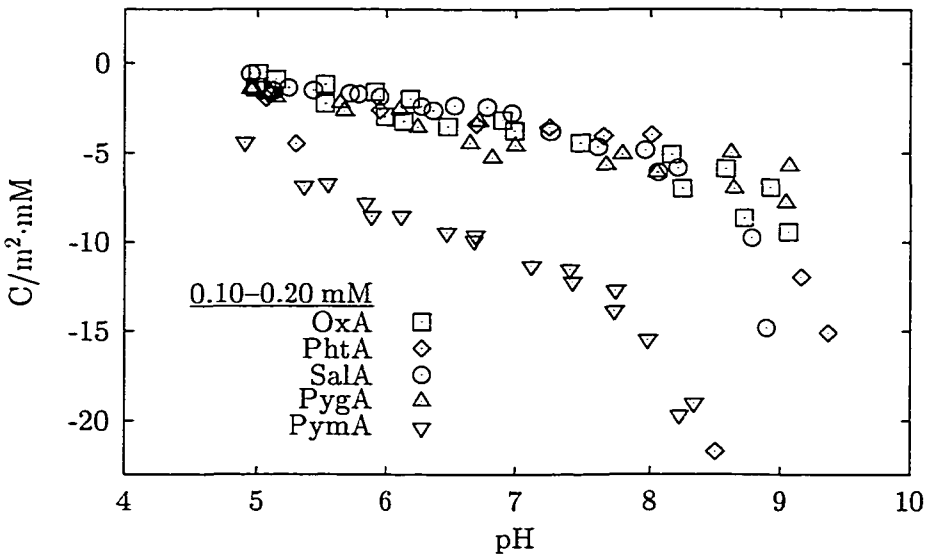

Figure 4.29. Change of surface charge per mM organic acid adsorbed as a function of pH.

4.3.5. Adsorption of Natural Organic Acids

The adsorption of two natural organic acids to aluminum hydroxide, Aldrich Humic acid and Dismal Swamp Organic Matter (DSOM) were examined in this work. Fractional removal of these substances and their effect on ζ-potential are shown in Figures 4.30 and 4.31.

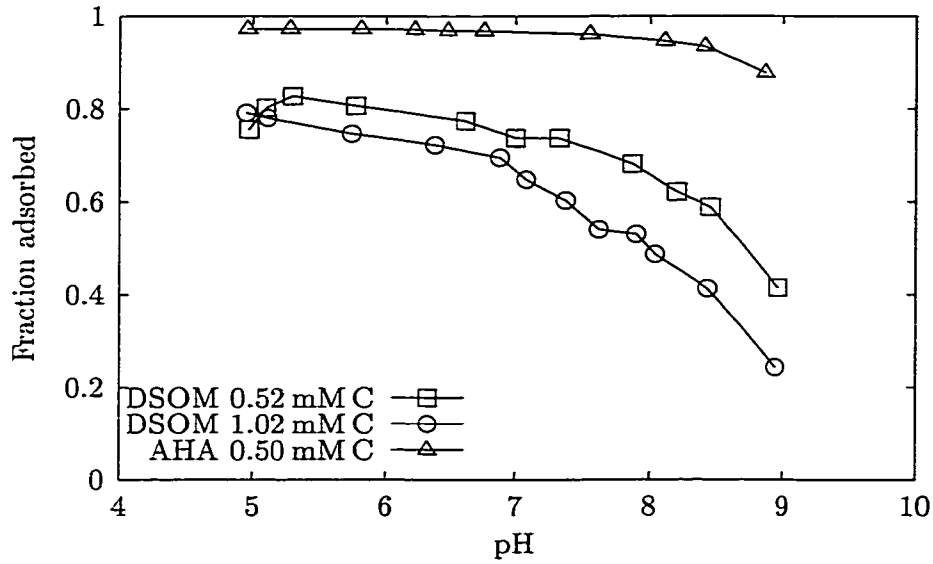

Figure 4.30. Fraction of DSOM and Aldrich Humic Acid adsorbed as a function of pH and total concentration.

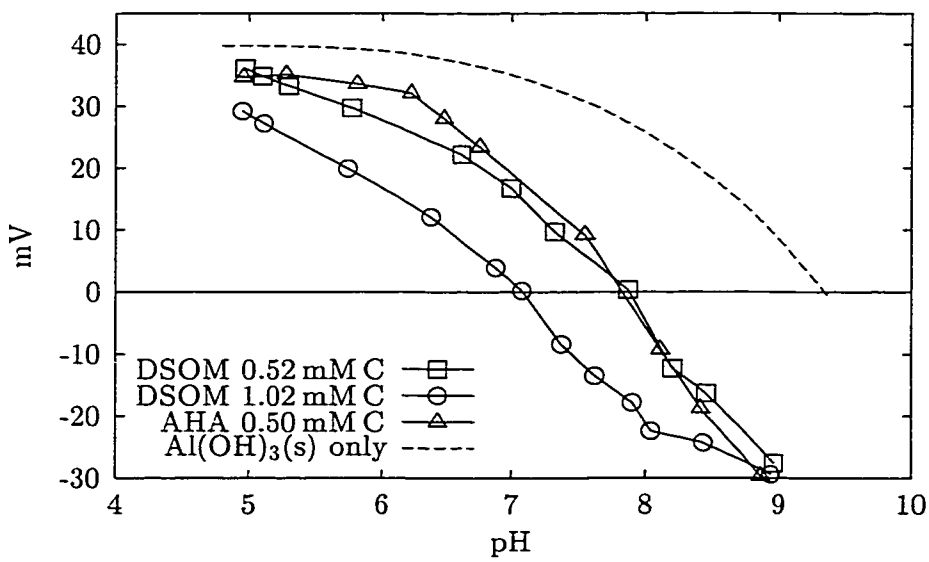

Figure 4.31. Effect of adsorption of Aldrich Humic acid and DSOM on ζ-potential as a function of pH and total concentration.

Generally, adsorption of these compounds decreased with increasing pH indicating the anionic character of these substances. However, compared to the simple organic acids examined in this work, the removal appears to be less pH dependent. Over the examined pH-range and at a similar total organic carbon concentration, humic acid removal exceeded that of DSOM greatly despite its lower charge density (Table 4.2) and similar ionizable functional groups. (Based on the model calculations, the pK_a of the functional groups of Aldrich humic acid and DSOM differ by less than one pH). These observations are consistent with the results of the work of Bose and Reckhow (1998) who found that natural organic matter fractions with charge densities higher than humic acid exhibited lower removal by adsorption to aluminum hydroxide. The reason for this behavior may be related to the differences in size between DSOM and Aldrich humic acid. According to Thurman (1985), humic acids are large aggregates that range in molecular weight from 2000 to 100000 and contain fewer functional groups than smaller molecules. Typically, natural dissolved organic acids are 1000 to 2000 in molecular weight and it is likely that DSOM falls within this range. Both the smaller size and the greater number of (ionizable) functional groups may render DSOM more soluble and this may in part be the cause for the difference in adsorption to Aldrich humic acid. In addition, Aldrich humic acid may contain various hydrophobic moieties, for example long-chain fatty acids (Thurman, 1985) that due to their limited solubility cause it to accumulate at the solid-water interfaces. Westall (1987) noted that the adsorption of higher molecular weight carboxylic acids even to polar surfaces appear to be dominated by the hydrophobic effect whereas lower molecular mass carboxylic acids adsorb to alumina surfaces primarily by ligand exchange. According to Thurman (1985), the ratio of carbon atoms per carboxyl groups is an important indicator for the hydrophobicity of humic substances. The C/COOH-ratio, which can be calculated from the model parameters in Table 4.2 (assuming the functional groups with $pK_a < 8$ are carboxylic groups), equals 3 for DSOM, whereas Aldrich humic acid has approximately 11 carbon atoms per carboxyl function and would therefore have much more hydrophobic character. In experiments with goethite, Evanko and Dzombak (1998) also attributed high adsorption densities of Aldrich humic acid to hydrophobic interactions.

Similar to the simple organic acids examined in this work, the adsorption of DSOM

decreases with increasing pH and dose. Near the pH_{iep} a significant fraction is still removed. The functional groups with a pK_a of 9.67 (Table 4.2) appear to be phenolic and seem to enhance removal at elevated pH. As with pyromellitic acid, the acidity of DSOM could also inhibit adsorption in the acidic region of the pH spectrum due to electrostatic repulsion by nonsorbing deprotonated functional groups. However, the ζ-potential measurements shown in Figure 4.31 suggest that at low pH the Al-DSOM surface complex is largely uncharged even at a total DSOM concentration of 1.02 mM C (12 mg/l).

Both natural organic acids caused the charge of the aluminum hydroxide particles to reverse. Therefore, functional groups of both substances may form inner-sphere complexes on the hydrous oxide surface. Based on the model calculations summarized in Table 4.2, Aldrich Humic acid and DSOM contain weakly acidic (carboxylic) functions that may react with surface hydroxyl groups similarly to mono- or dihydrogenphosphate ion. According to Hingston *et al.* (1972), the concurrent release of protons from weak acids allows exchange of surface hydroxyl groups and thus enables charge reversal. Therefore, the adsorption mechanisms for organic acids with weak acidic groups may be similar to those of weak inorganic acids and simple organic acids with phenolic functional groups. Actually, the graphs of ζ-potential versus pH in Figure 4.31 resemble those for orthophosphate and pyrogallic acid (Figure 4.12, 4.25, and 4.26) closely. No single simple organic acid appears to mimic the fractional removal of DSOM well, which is expected considering that natural organic matter is composed of a variety of individual organic acids. This substance may therefore be better represented by a mixture of two simple organic acids that contain carboxylic and phenolic groups with similar pK_a, e.g., phthalic and pyrogallic acid.

At approximately the same total organic carbon concentration of 0.50 mM C, DSOM and Aldrich humic acid exert an almost identical effect on the mobility on the aluminum hydroxide particles, although a greater amount of humic acid adsorbed. Therefore, DSOM must form more negatively charged complexes on the aluminum hydroxide surface than Aldrich Humic acid. A plot of the decrease in surface charge computed from the ζ-potential measurements per mol C adsorbed confirms this (Figure 4.32). The difference between the two natural organic acids appears to be small on a per mol C basis. However, because the humic acid molecules may be orders of magnitude greater in molecular weight than DSOM,

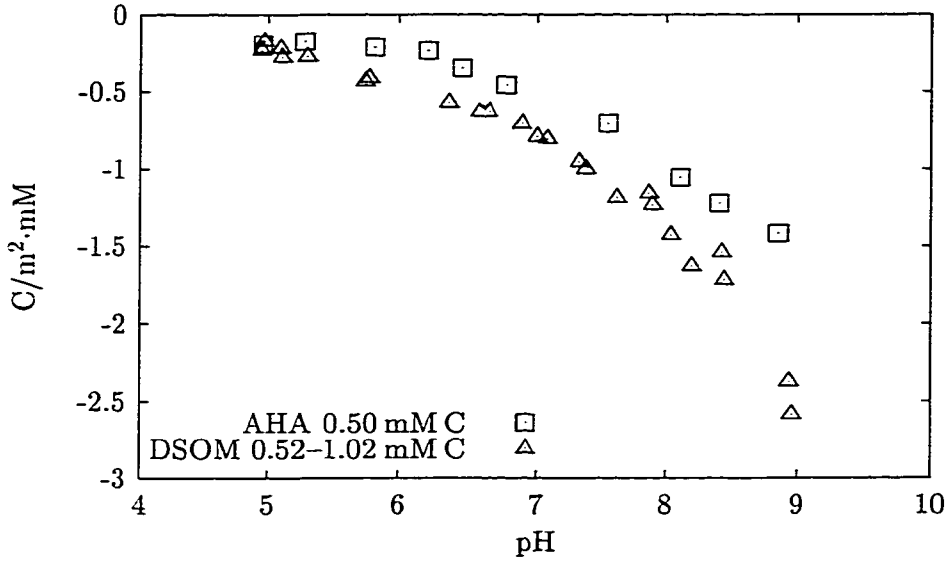

Figure 4.32. Change in surface charge per mM (as C) natural organic matter adsorbed as a function of pH.

the difference *per molecule* is likely to be significantly larger. Similar to the inorganic ions and the simple organic acids, both natural organic substances also caused a greater decrease in surface charge with increasing pH.

The preceding discussions illustrate that organic acids can exhibit different adsorption mechanisms which appear to depend largely on type and number of functional groups and also molecular size. These characteristics may also result in different responses to the presence of competing inorganic anions as examined in the following sections.

4.3.6. Effects of Sulfate on Adsorption of Organic Acids

To assess the effects of sulfate, aluminum hydroxide suspensions were dosed simultaneously with both sodium sulfate to result in concentrations of 0.10 mM, 0.50 mM, and 1 mM as SO_4 and either phthalic, salicylic, oxalic, pyromellitic acid (at 0.20 mM), Aldrich Humic acid (0.50 mM C, 6 mg C/l), or Dismal Swamp Organic Matter (1.02 mM C, 12 mg C/l).

Fractional adsorption of phthalic acid and sulfate and the ζ-potential of the suspensions as a function of pH are shown in Figures 4.33 to 4.35. These figures show that sulfate has a significant effect on the adsorption of phthalic acid, where a reduction in removal of greater than 50% occurred near pH 5 and at 1.00 mM SO_4. The impact diminished with increasing

pH, as would be expected, because sulfate was shown to adsorb more strongly at lower pH. Doubling the sulfate dose from 0.50 to 1.00 mM caused only a small incremental decrease on phthalic acid removal. As was observed in the absence of phthalic acid (Figure 4.9), the ζ-potential has decreased to less than 20 mV (Figure 4.34). At this point, lack of electrostatic attraction may limit sulfate adsorption and therefore competition with other anions. The effect of phthalic acid on sulfate adsorption is shown in Figure 4.35. When comparing these data with Figure 4.8, it appears that 0.2 mM of phthalic acid decreased fractional sulfate adsorption by approximately one half. A closer examination reveals that with increasing sulfate doses, the sum of molar concentrations of adsorbed sulfate and phthalic acid remains roughly constant up to $SO_4 = 0.50$ mM (Figure 4.36). This indicates that phthalic acid and sulfate mostly occupied and competed for the same adsorption sites on aluminum hydroxide. These data also show that if the adsorption of phthalic acid and sulfate is site-specific and the there is a 1:1 stoichiometry of surface hydroxyl groups and adsorbate ion, a minimum of approximately 0.2 mM of surface sites were available on the precipitate.

An estimate of the relative affinity of the adsorbate anions to the precipitate can be made when considering the ratio of fractional removals of sulfate and phthalic acid. At the 0.10 mM sulfate dose, the ratio of adsorbed sulfate to phthalic acid concentration averaged approximately 1 at pH < 7, which means that these ions adsorbed in proportion to their total concentrations, suggesting an equal affinity to the precipitate. The supporting data calculated from the (non-zero) surface concentrations and doses are summarized in Figure 4.37. A distinct trend can be observed at pH > 7, where the ratio increased above 1, indicating greater sulfate removal. However, because the adsorbed fractions were generally small, this may also be an analytical artifact. At higher sulfate doses, phthalic acid appeared to be removed at a greater proportion. Below pH 7, the ratio of fractional removals was 0.5, suggesting that phthalic acid has generally adsorbs more strongly to aluminum hydroxide than sulfate under these conditions. The dependence of the relative affinity of competing anions to the adsorbent on their total concentrations has also been observed in studies with ferric oxides (Mesuere and Fish, 1992; Ali and Dzombak, 1996a). These researchers concluded that the observed effects can be attributed to surface site heterogeneity, particularly at high sorbate/sorbent ratios. Accordingly, a small number of sites on

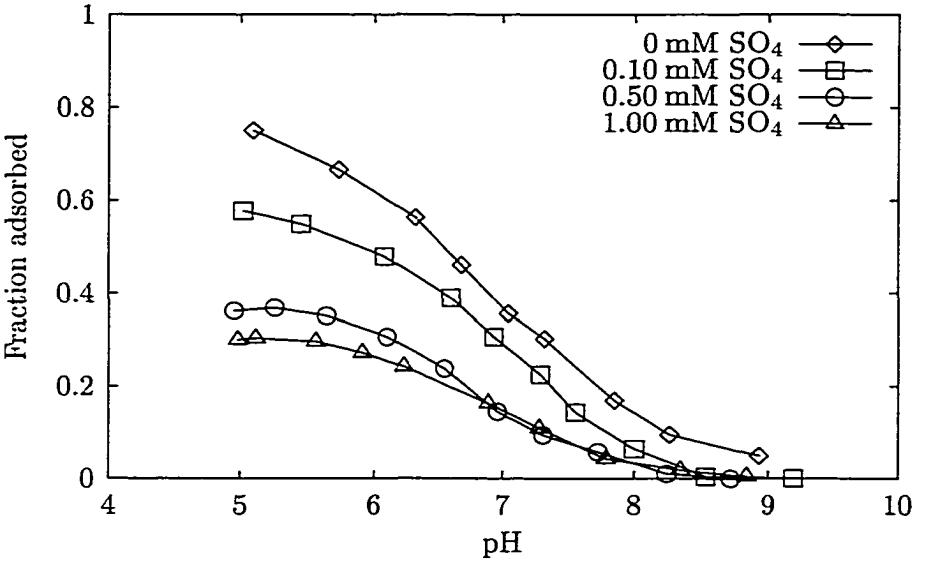

Figure 4.33. Fraction of phthalic acid adsorbed as a function of pH and total sulfate concentration. Total phthalic acid concentration = 0.20 mM.

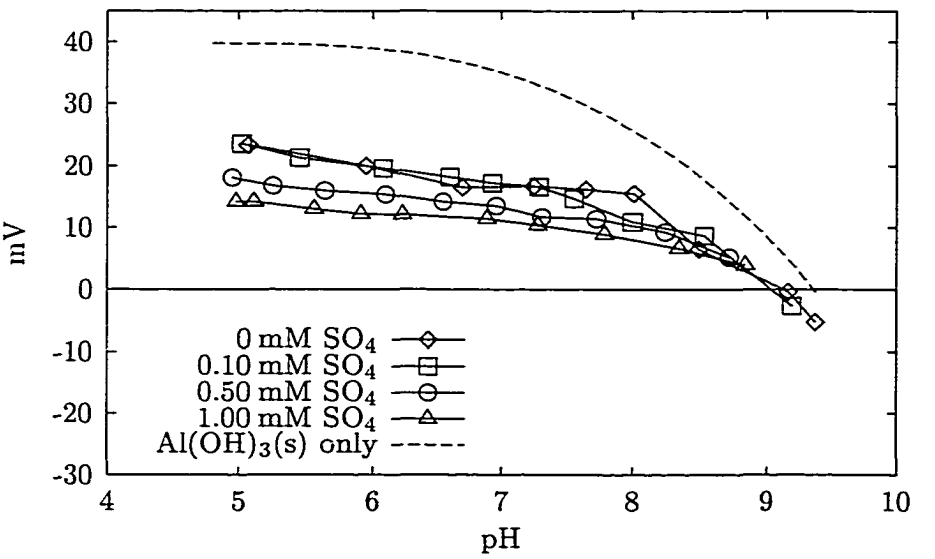

Figure 4.34. Effect of adsorption of phthalic acid on ζ-potential as a function of pH and total sulfate concentration. Total phthalic acid concentration = 0.20 mM.

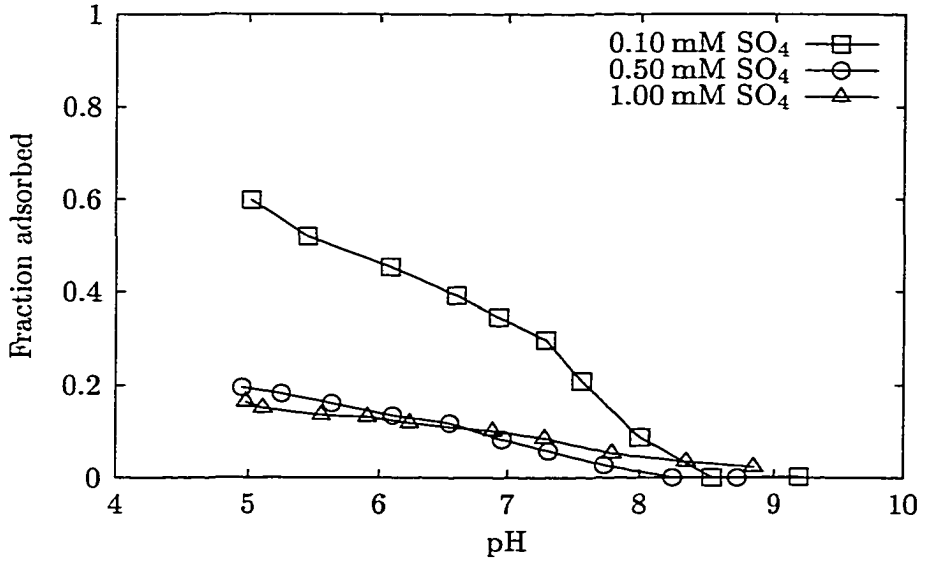

Figure 4.35. Fraction of sulfate adsorbed in the presence of 0.20 mM phthalic acid as a function of pH and total sulfate concentration.

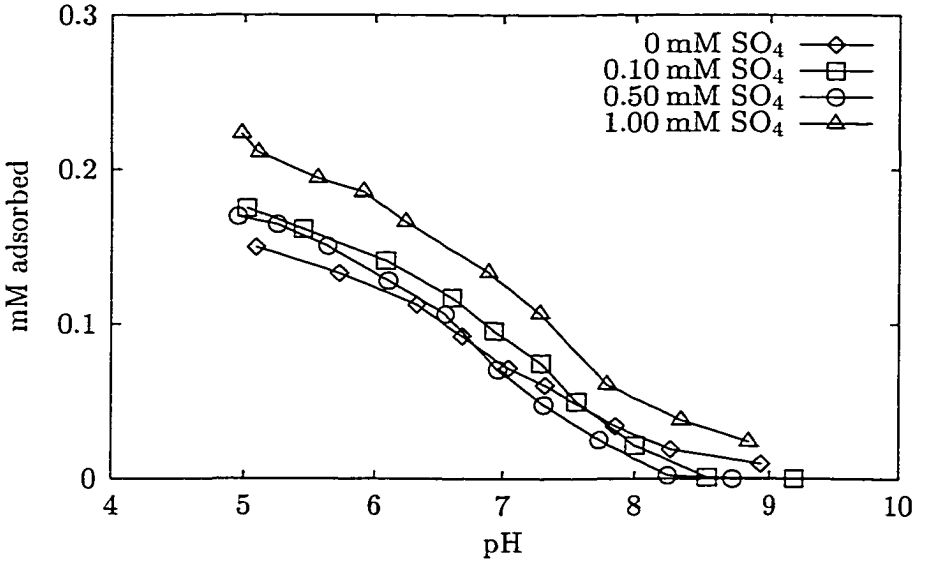

Figure 4.36. Sum of molar concentrations of sulfate and phthalic acid adsorbed as a function of pH and total sulfate concentration. Total phthalic acid concentration = 0.20 mM.

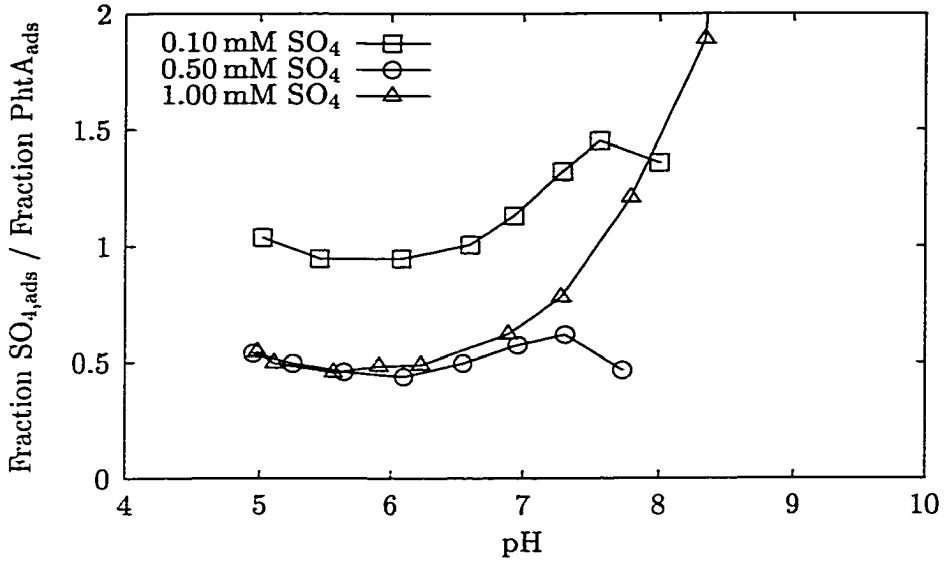

Figure 4.37. Ratio of fractions of sulfate and phthalic acid adsorbed as a function of pH and total sulfate concentration. Total phthalic acid concentration = 0.20 mM.

the aluminum hydroxide surface may be exclusively occupied by phthalic acid, resulting in greater adsorption compared to situations where sulfate and phthalic acid are present at similar concentrations and at low surface coverage. It is also possible that phthalic acid is less susceptible to electrostatic effects than sulfate. Because the ζ-potential decreased with increasing SO_4 doses, greater electrostatic repulsion of sulfate may have favored adsorption of phthalic acid.

Competitive adsorption in the binary salicylic acid – sulfate system exhibited largely the same trends as with phthalic acid. Sulfate at a total concentration of 0.50 mM caused a significant decrease (> 50%) in salicylic acid adsorption at pH < 7.5 (Figure 4.38) and the results were almost indistinguishable from the data of the experiment with the 1.00 mM SO_4 dose. Sulfate adsorption decreased correspondingly, i.e., it was affected most at the 0.50 mM dose (Figure 4.40, sulfate was not measured at the 0.10 mM dose). Based on the sum of the molar concentrations of the two adsorbates depicted in Figure 4.41, it appears that surface site saturation increased with increasing sulfate concentrations. Because the adsorbed salicylic acid concentration decreased, it can be concluded that sulfate occupied sites on the hydroxide surface in addition to those where salicylic acid was displaced.

The ratio of fractional removals of sulfate versus salicylic acid steadily decreased with

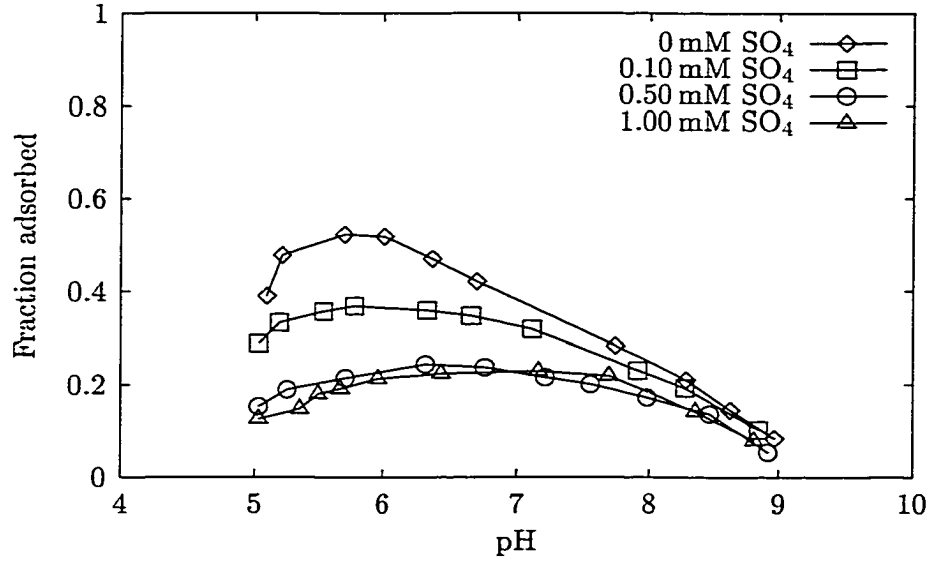

Figure 4.38. Fraction of salicylic acid adsorbed as a function of pH and total sulfate concentration. Total salicylic acid concentration = 0.20 mM.

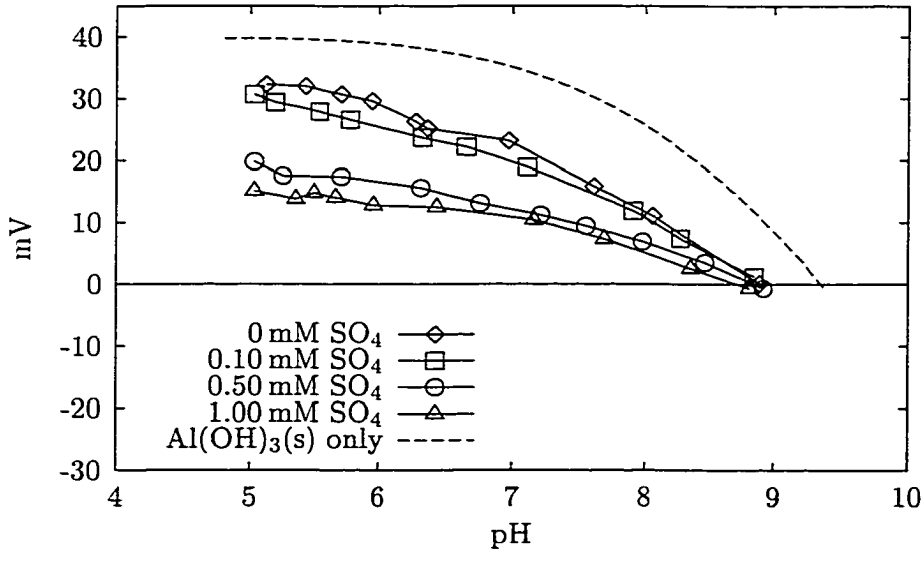

Figure 4.39. Effect of adsorption of salicylic acid on ζ-potential as a function of pH and total sulfate concentration. Total salicylic acid concentration = 0.20 mM.

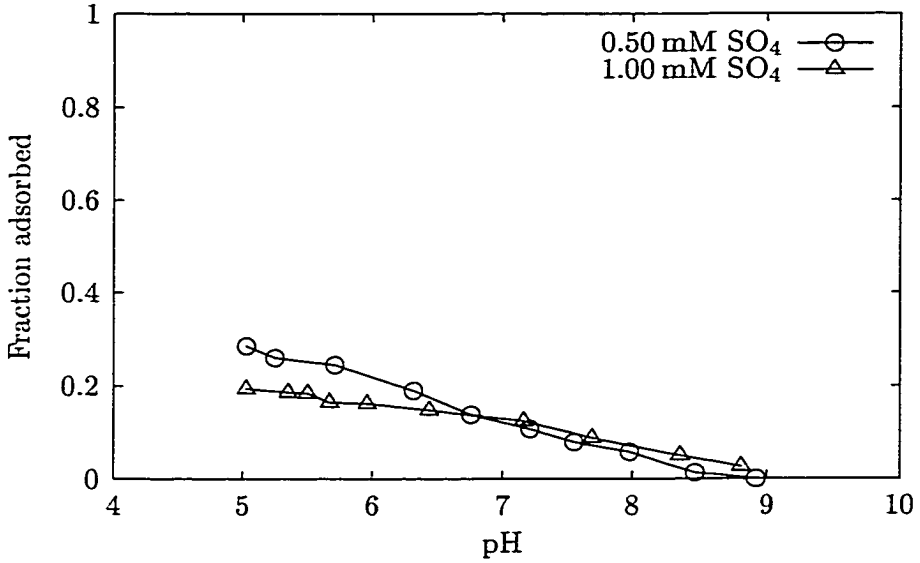

Figure 4.40. Fraction of sulfate adsorbed in the presence of 0.20 mM salicylic acid as a function of pH and total sulfate concentration.

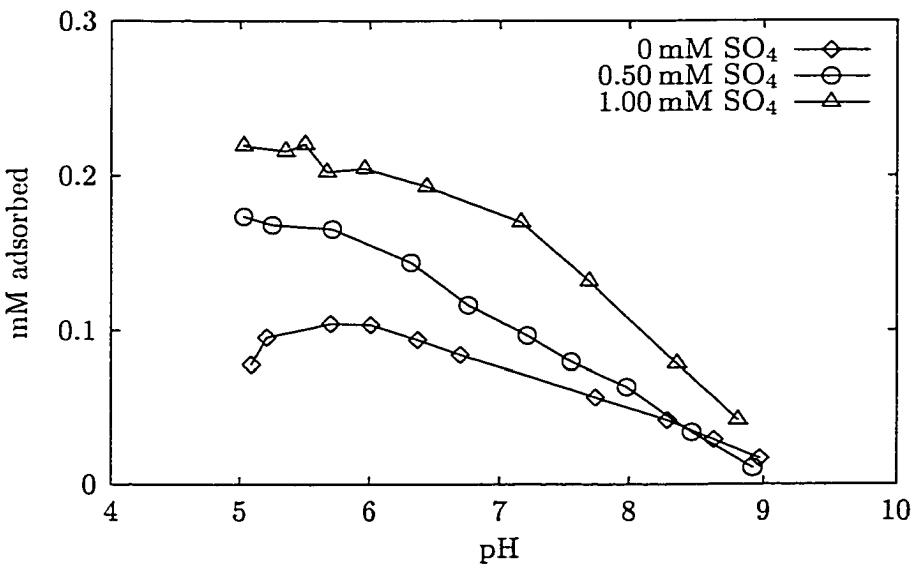

Figure 4.41. Sum of molar concentrations of sulfate and salicylic acid adsorbed as a function of pH and total sulfate concentration. Total salicylic acid concentration = 0.20 mM.

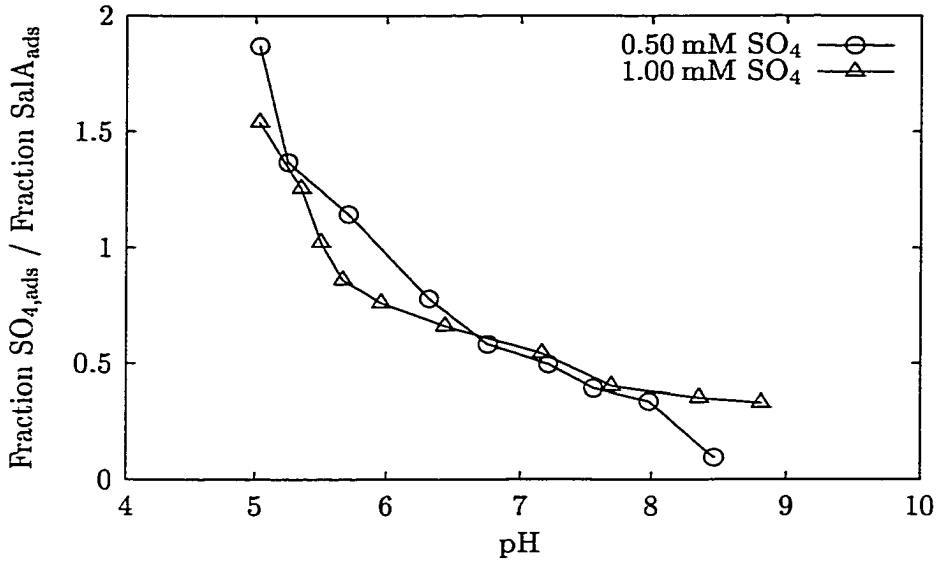

Figure 4.42. Ratio of fractions of sulfate and salicylic acid adsorbed as a function of pH and total sulfate concentration. Total salicylic acid concentration = 0.20 mM.

increasing pH as shown in Figure 4.42. At sulfate doses of 0.50 and 1.00 mM, a similar ratio was obtained at any given pH, which was also observed in the sulfate–phthalic acid system. This suggests that under these circumstances, the relative affinity of sulfate and salicylic acid to adsorb to aluminum hydroxide is independent of the total concentrations. At pH less than approximately 6, sulfate adsorbed more strongly than salicylic acid (ratio > 1) and the ratio of fractional adsorption approaches zero near the pH_{iep} where measurable amounts of salicylic are still removed (Figure 4.38). A comparison to the sulfate–phthalic acid system, where the fractional removal ratio seemed to increase with pH, clearly illustrates that the phenolic functional group influences the surface complexation of salicylic acid to aluminum hydroxide.

The effects of sulfate on oxalic acid adsorption are shown in Figures 4.43 through 4.46. These data indicate that sulfate competes with oxalic acid predominantly at pH < 7 and caused oxalic acid adsorption to exhibit a more pronounced maximum near pH 6.5. The ζ-potential measurements shown in Figure 4.44 indicate that sulfate caused a slight decrease in surface charge and that the influence of sulfate diminishes when the aluminum hydroxide particles carry a near neutral charge. Sulfate adsorption in the presence of oxalic acid was primarily affected in this pH range (Figure 4.45), which confirms the earlier finding

that sulfate interacts with aluminum hydroxide by electrostatic attraction to positively charged surface hydroxyl groups. The sum of molar concentrations of sulfate and oxalic acid at 1.00 mM SO_4 were approximately equal to the adsorbed oxalic acid concentration in the absence of sulfate (Figure 4.46). However, inexplicably, at 0.10 and 0.50 mM SO_4, a significantly greater amount of anions had adsorbed. When considering Figures 4.8 and 4.45, it becomes apparent that greater sulfate removal was achieved at pH > 8 in the presence of oxalate. Because this increase corresponds to lower dissolved sulfate concentrations, it was suspected that an analytical error occurred. A review of the particular chromatographic analysis showed that the instrument was calibrated for the range up to 1.00 mM SO_4 and that at dissolved sulfate concentrations below 0.20 mM, only 85% recovery was achieved. The quality control samples for oxalate were satisfactory.

The ratio of fractional adsorption of sulfate and oxalic acid as a function of pH is shown in Figure 4.47. The relative affinity of oxalic acid to adsorb to aluminum hydroxide increased with increasing sulfate doses. The potential reasons for this behavior may be related to surface site heterogeneity or electrostatic effects as discussed previously.

The effect of surface charge on the ability of sulfate to compete with organic acids becomes most evident when considering the effect on adsorption of pyromellitic acid. In these experiments, sulfate did not have a discernible effect on pyromellitic acid removal (Figure 4.48) or ζ-potential of the precipitate particles (Figure 4.49). Over the examined pH range, the aluminum hydroxide particles acquired a negative charge, and the resulting electrostatic repulsion must have hindered significant adsorption of sulfate and competition with pyromellitic acid. Sulfate adsorption data in these experiments confirmed this. At both sulfate doses only insignificant amounts were removed from solution (not shown). Therefore, this finding confirms that the interaction of sulfate and aluminum hydroxide is an electrostatic attraction of the negatively charged ion to positively charged surface groups.

Sulfate did not have any impact on the removal of Aldrich humic acid (Figure 4.50), although it clearly influenced the ζ-potential at pH < 7.5 where the particles where positively charged (Figure 4.51). As indicated earlier, near pH 5, humic acid did not noticeably decrease the ζ-potential of the precipitate. The effect in the binary system at pH < 7 is therefore predominantly due to sulfate adsorption. In fact, the measured ζ-potentials

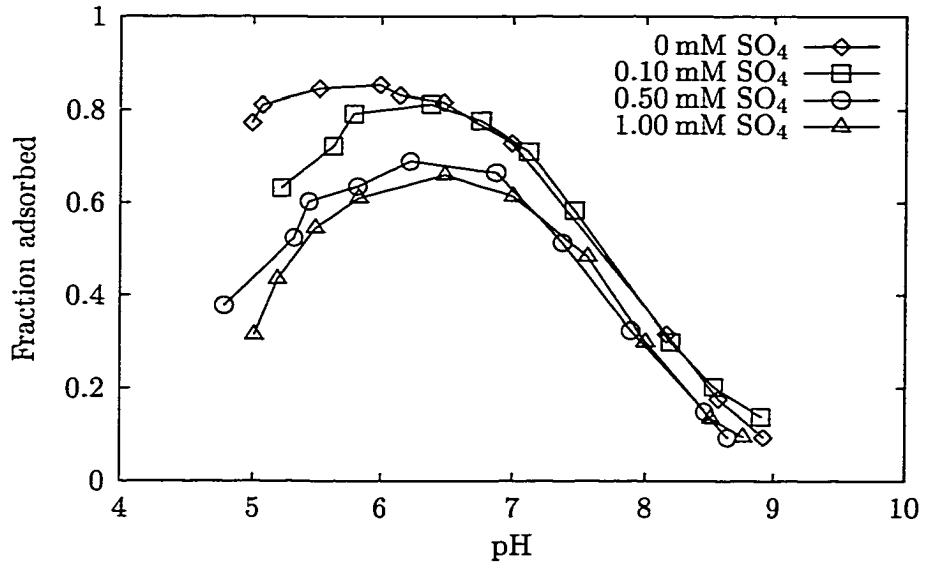

Figure 4.43. Fraction of oxalic acid adsorbed as a function of pH and total sulfate concentration. Total oxalic acid concentration = 0.20 mM.

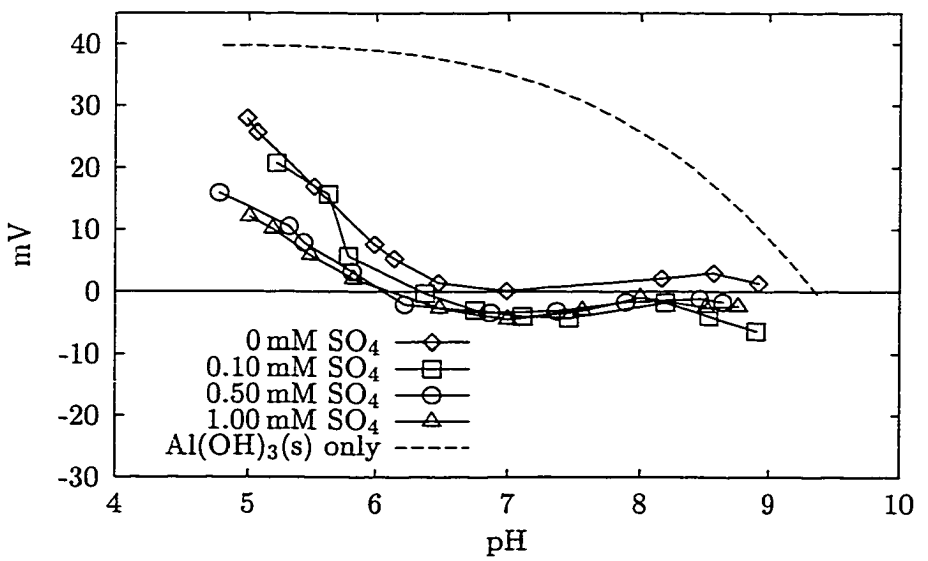

Figure 4.44. Effect of adsorption of oxalic acid on ζ-potential as a function of pH and total sulfate concentration. Total oxalic acid concentration = 0.20 mM.

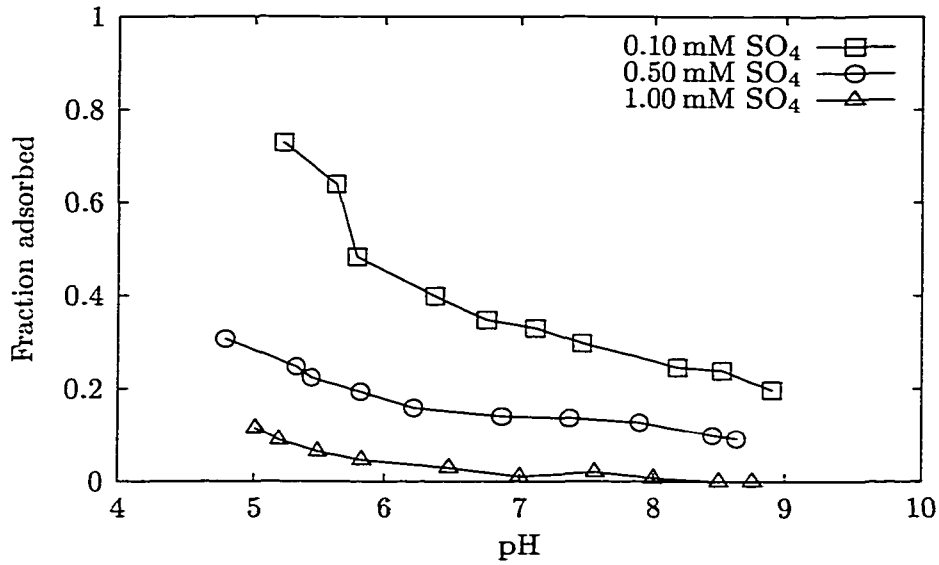

Figure 4.45. Fraction of sulfate adsorbed in the presence of 0.20 mM oxalic acid as a function of pH and total sulfate concentration.

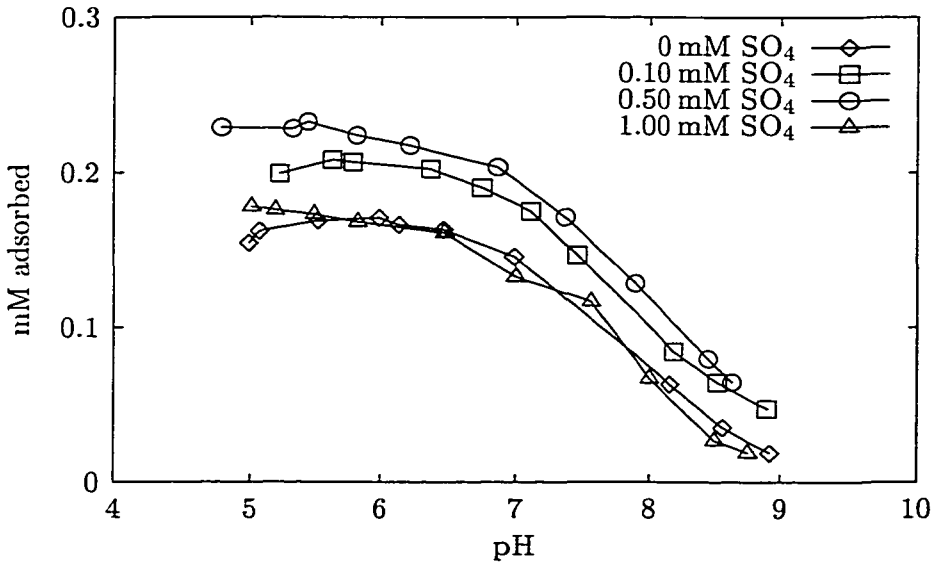

Figure 4.46. Sum of molar concentrations of sulfate and oxalic acid adsorbed as a function of pH and total sulfate concentration. Total oxalic acid concentration = 0.20 mM.

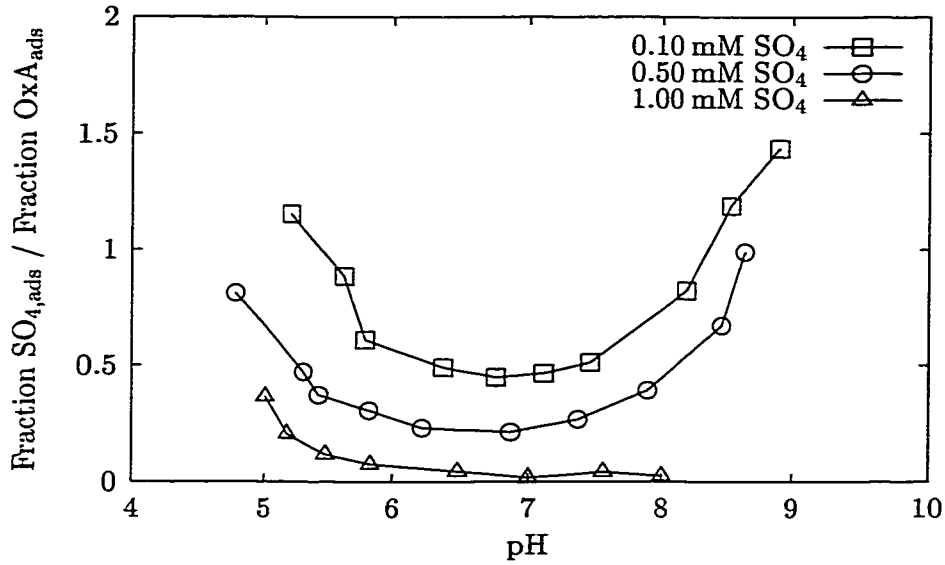

Figure 4.47. Ratio of fractions of sulfate and oxalic acid adsorbed as a function of pH and total sulfate concentration. Total oxalic acid concentration = 0.20 mM.

in this pH range are similar to the data from the single sorbate experiments with sulfate. Sulfate adsorption data (not shown) indicate that humic acid did not affect sulfate removal at all, suggesting that either excess surface hydroxyl groups were available in the presence of Aldrich humic acid or that the adsorbed organic molecules provided additional sites for sulfate to adsorb. It is also possible that Aldrich humic acid is removed from solution entirely by hydrophobic expulsion, in which case little competition with chemically adsorbing ions would be expected. However, chemical interaction (or electrostatic attraction) must contribute to natural organic matter adsorption to oxides, because removal efficiencies vary widely depending on the adsorbents, e.g., silica versus alumina (Davis, 1982).

DSOM adsorption was influenced to a small extent by sulfate, resulting in an approximately 20% decrease in removal near pH 5 at a sulfate dose of 1 mM (Figure 4.52). At pH > 7, sulfate had no discernible impact. The ζ-potential data collected during this experiment (Figure 4.53) indicate that in this pH range, DSOM caused charge reversal of the precipitate and thus inhibited sulfate adsorption. Comparison of the sulfate adsorption data with and without DSOM (Figure 4.8 and 4.54) shows that decreased sulfate removal occurred over the whole pH range but the competitive effects of DSOM are most noticeable at pH > 7. Although the effect on organic acid removal is much lower for DSOM than for

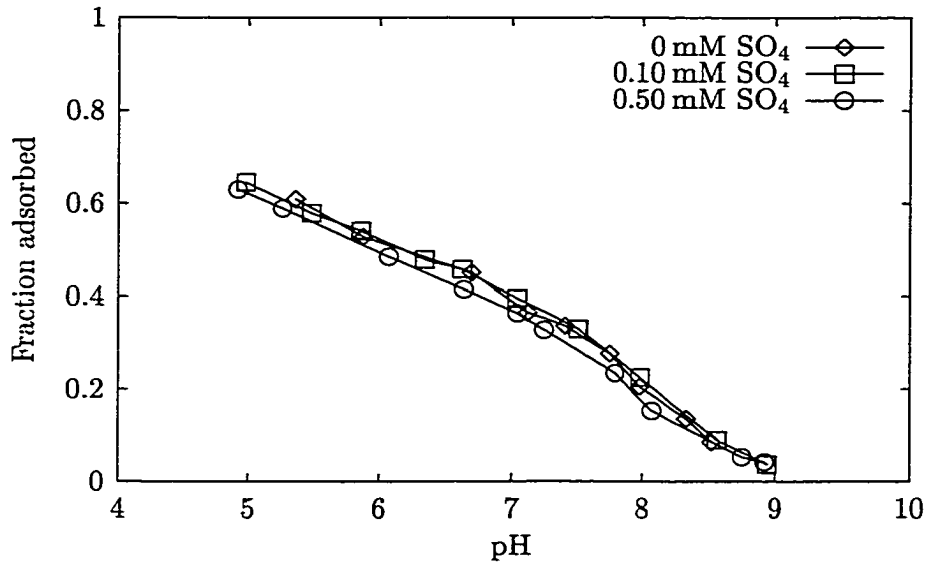

Figure 4.48. Fraction of pyromellitic acid adsorbed as a function of pH and total sulfate concentration. Total pyromellitic acid concentration = 0.20 mM.

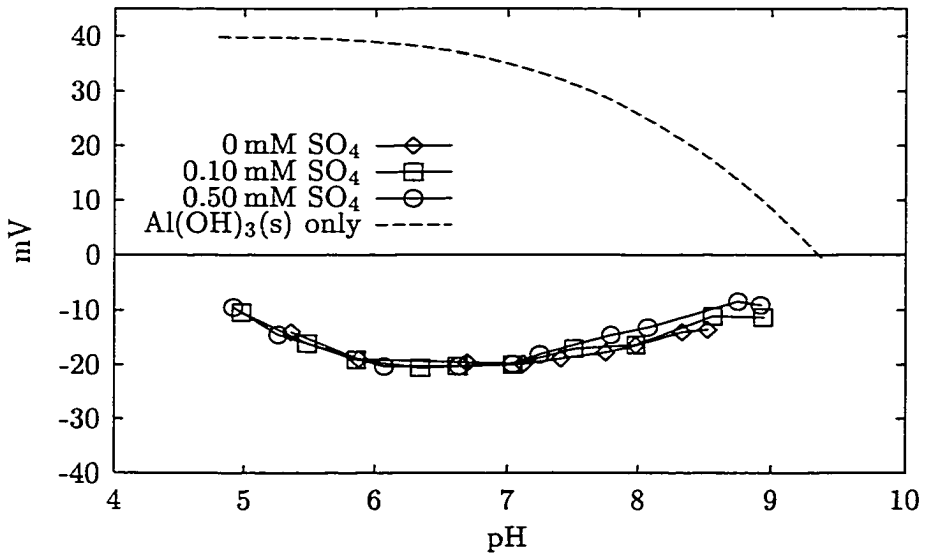

Figure 4.49. Effect of adsorption of pyromellitic acid on ζ-potential as a function of pH and total sulfate concentration. Total pyromellitic acid concentration = 0.20 mM.

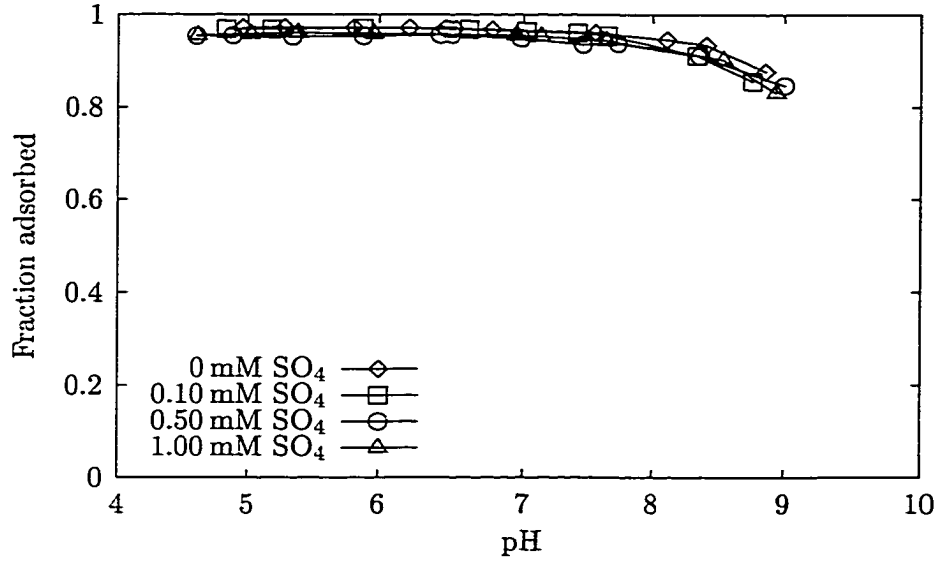

Figure 4.50. Fraction of Aldrich humic acid adsorbed as a function of pH and total sulfate concentration. Total Aldrich humic acid concentration = 0.50 mM as C.

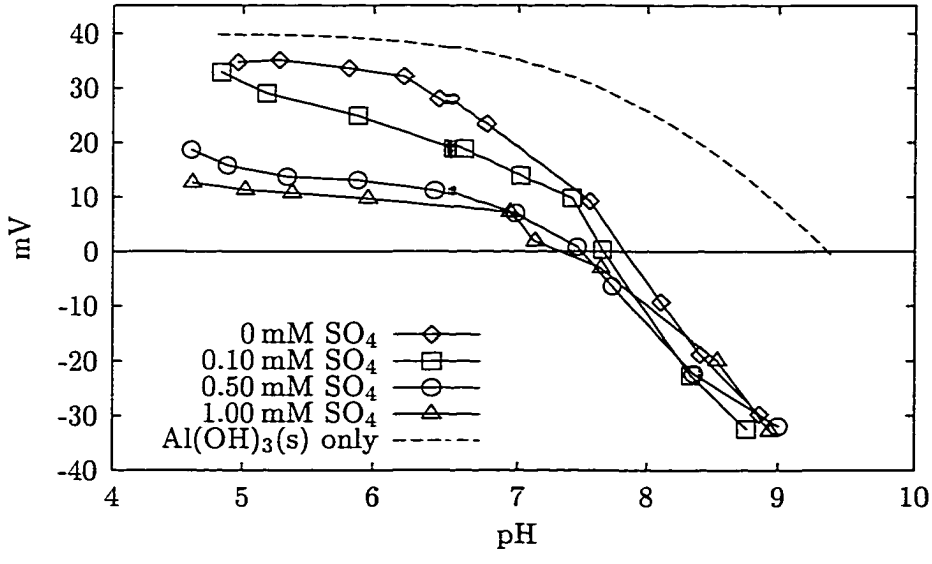

Figure 4.51. Effect of adsorption of Aldrich humic acid on ζ-potential as a function of pH and total sulfate concentration. Total Aldrich humic acid concentration = 0.50 mM as C.

the tested simple organic acids, the results suggest that natural organic matter adsorption to aluminum hydroxide responds in a similar fashion to the presence of elevated concentrations of sulfate. Therefore, if DSOM represents organic substances in natural waters, then simple organic acids may be better surrogates for evaluating the competitive effects of sulfate than Aldrich humic acid. However, pyromellitic acid may be an exception because although it may mimic the adsorption of NOM well (Evanko and Dzombak, 1998), its effects on electrophoretic mobility appear to be significantly different.

The most significant finding with respect to sulfate competition may be the fact that detrimental effects were generally encountered when the precipitate was positively charged, whereas if the organic acid caused charge reversal, only minimal sulfate removal and interference with organic acid adsorption occurred. In these experiments, charge reversal occurred typically at pH > 7. However, the conditions under which the precipitate reaches a near zero charge depend not only on pH, but also the amount of adsorbent, i.e.,the mass of aluminum hydroxide precipitate, which was held constant in this work. In conventional water treatment with metal salt coagulants, operators control pH and the "amount of adsorbent" by varying the coagulant dose to achieve a near-zero surface charge. At constant pH, the ζ-potential of particles in water treatment increases with increasing coagulant dose. Based on the results presented here, sulfate will not coadsorb as long as the isoelectric point has not been reached. When the precipitate acquires a positive charge, sulfate will adsorb due to electrostatic attraction with two consequences: 1. Sulfate will "quench" the surface charge and prevent restabilization that could lead to detrimental effects on turbidity removal and 2. Sulfate will compete with other anions for surface sites and cause a decrease in removal of organic anions. These effects are generally more pronounced at lower pH, e.g., pH 5–6, a range that water treatment plant operators may target under "enhanced coagulation" conditions using aluminum sulfate (alum). At the same time, organic acid removal is also a function of pH and acid or base addition and must therefore be carefully adjusted to minimize the interference by sulfate while maximizing organic acid removal. In addition, the solubility of the adsorbent and the ability of the organic acid to form soluble aluminum complexes can affect adsorption. Combined, these conditions can result in a situation where the optimum pH for the removal of two different organic acids differs by

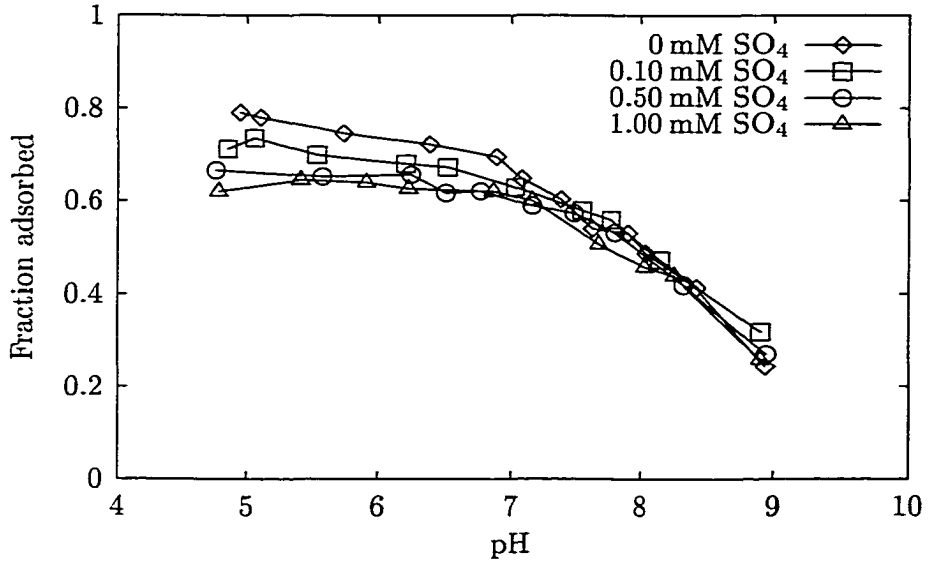

Figure 4.52. Fraction of DSOM adsorbed as a function of pH and total sulfate concentration. Total DSOM concentration = 1.02 mM as C.

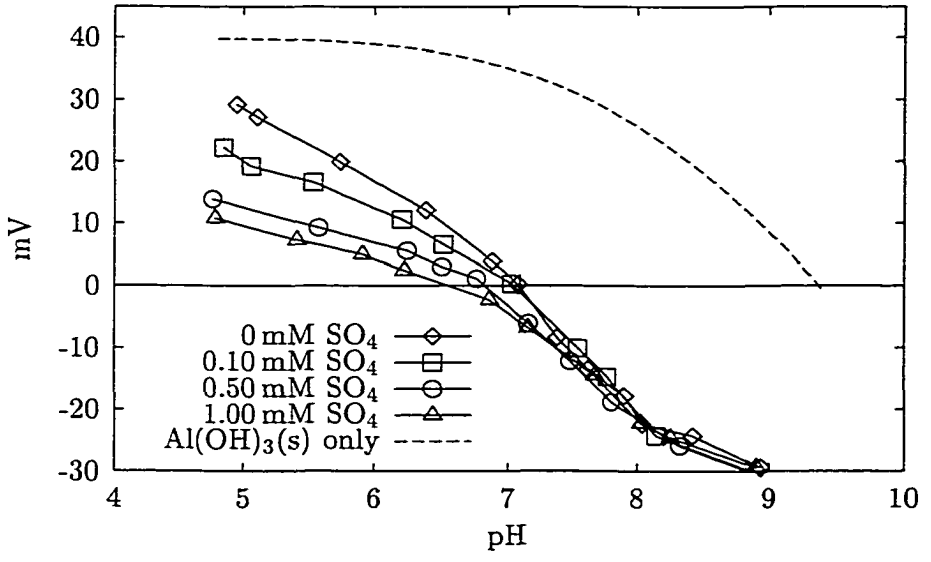

Figure 4.53. Effect of adsorption of DSOM on ζ-potential as a function of pH and total sulfate concentration. Total DSOM concentration = 1.02 mM as C.

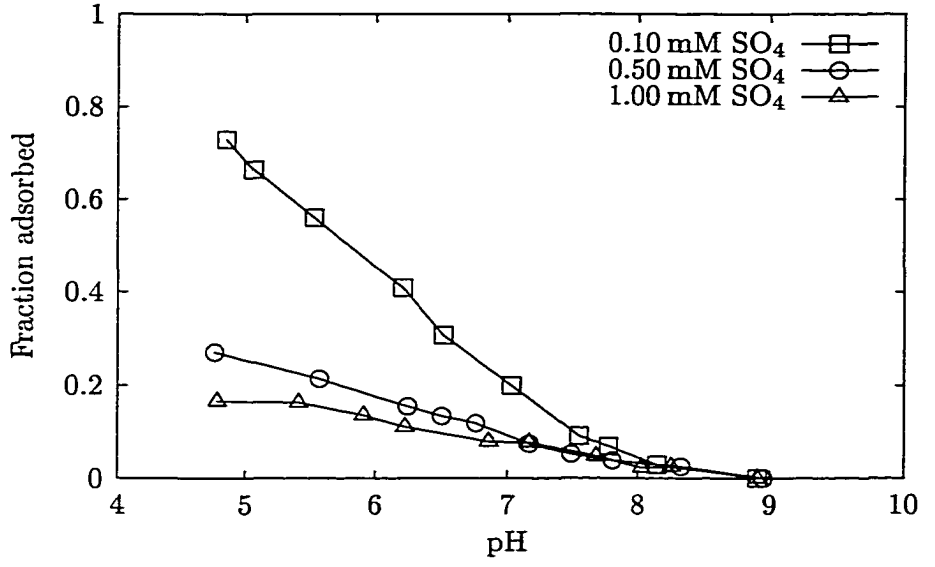

Figure 4.54. Fraction of sulfate adsorbed in the presence of 1.02 mM DSOM as a function of pH and total sulfate concentration.

almost two pH units. For instance, in the presence of sulfate, the optimum pH for removal of phthalic acid was at pH 5, whereas oxalic acid was most strongly adsorbed to $Al(OH)_3(s)$ near pH 7. Therefore, the optimization of coagulation processes which commonly involve pH and coagulant dose adjustment should also include testing the susceptibility of organic matter removal to the presence of sulfate. If organic matter removal is affected, then it may be advantageous to utilize non-sulfate based coagulants.

4.3.7. Effects of Orthophosphate on Adsorption of Organic Acids

The effect of orthophosphate on removal of phthalic, salicylic, oxalic, and Aldrich humic acid by adsorption to aluminum hydroxide was tested at 0.01 and 0.10 mM PO_4. Total organic acid concentrations were 0.20 mM (0.50 mM as C for AHA). The results of these experiments are shown in Figure 4.55 through 4.63. The effect of phosphate on the adsorption of phthalic acid is significantly stronger than the influence of sulfate (Figure 4.55). Almost no effect can be observed at 0.01 mM PO_4. At the 0.10 mM PO_4, phthalic acid adsorption was similar to that at a 0.50 mM sulfate dose, where a decrease in removal of greater than 30% occurred. This impact is significant considering that the total phthalic acid concentration was twice at high as the orthophosphate concentration. Based on the single sorbate experiments, where

orthophosphate was completely removed over a wide pH range, these results were expected and were likely due to the greater ability of phosphate to undergo ligand exchange by donating protons. Phthalic acid was largely deprotonated under tested conditions and had therefore a smaller affinity to replace surface hydroxyl groups. Orthophosphate adsorption in the presence of phthalic acid was not affected (not shown).

The ζ-potential measurements indicate that the surface charge is largely governed by the adsorption of phthalic acid at low pH (Figure 4.56), where phosphate may form an uncharged surface complex. At pH > 7, it is dominated by phosphate which caused charge reversal near pH 8. This provides further confirmation that the deprotonation of dihydrogen phosphate in solution affects the charge of the complex formed at the aluminum hydroxide–water interface. In the pH region where the precipitate was negatively charged, no phthalic acid was removed, which seems to support findings by other researchers that electrostatic attraction is the main adsorption mechanism for phthalic acid at higher pH (Person *et al.*, 1998).

A plot of the sum of molar concentrations of orthophosphate and phthalic acid is shown in Figure 4.57. The graph indicates that a significantly greater number of anions is adsorbed in the presence of 0.10 mM orthophosphate. At pH < 7, the difference is approximately 0.05 mM, accounting for half of the adsorbed orthophosphate (0.10 mM). Therefore, the remainder of 0.05 mM PO_4 adsorbed to sites that would have been occupied by phthalic acid in the absence of the competing anion. If the same surface sites were available for both anions, phthalic acid would have to occupy twice as many sites per adsorbed molecule than orthophosphate, for example by forming binuclear surface complexes. (E.g., the decrease in removal of phthalic acid by 0.05 mM created 0.10 mM of available sites for PO_4 to adsorb). However, the stoichiometry of the surface reactions cannot be estimated a priori and there is likely to be a difference in affinity to aluminum hydroxide which is a result of the ability of orthophosphate to complex charged and uncharged surface hydroxyl groups, whereas phthalic acid requires positively charged functions (i.e.,$\equiv AlOH_2^+$) to be electrostatically attracted.

Competitive adsorption in the salicylic acid–phosphate system shows similar trends (Figure 4.58), in that the lower phosphate dose of 0.01 mM PO_4 had little effect and the

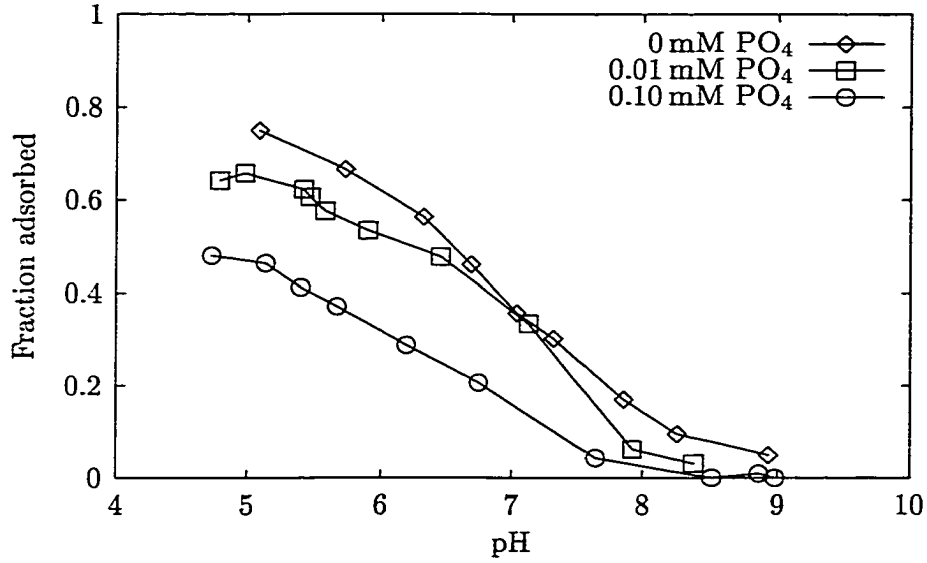

Figure 4.55. Fraction of phthalic acid adsorbed as a function of pH and total orthophosphate concentration. Total phthalic acid concentration = 0.20 mM.

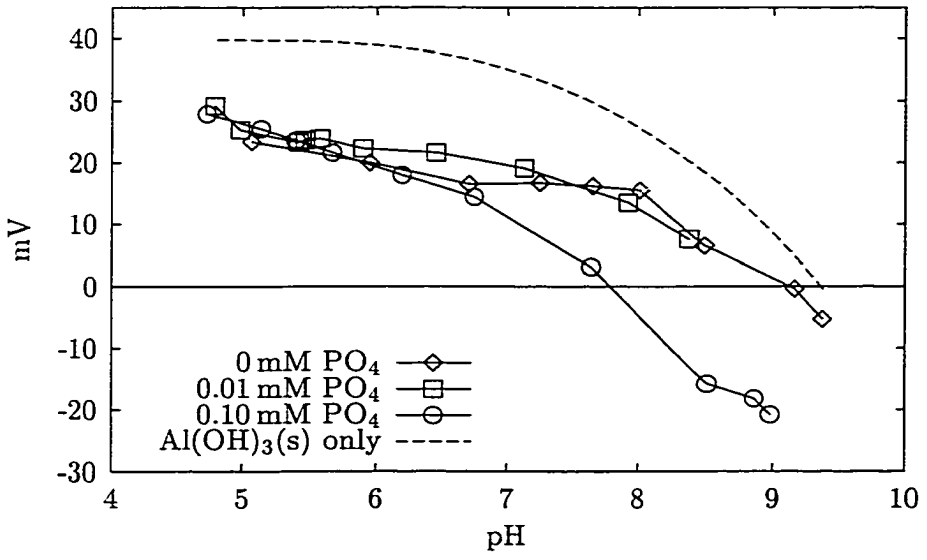

Figure 4.56. Effect of adsorption of phthalic acid on ζ-potential as a function of pH and total orthophosphate concentration. Total phthalic acid concentration = 0.20 mM.

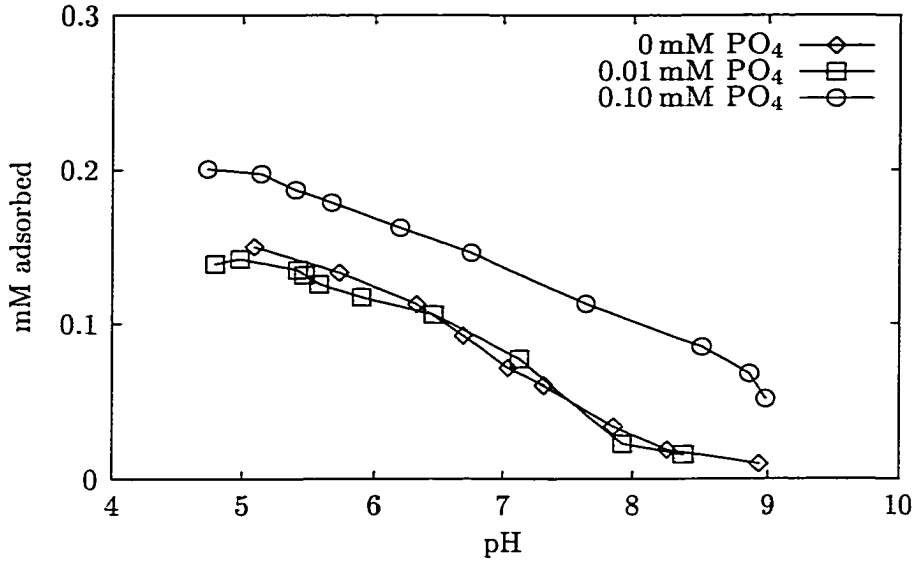

Figure 4.57. Sum of molar concentrations of orthophosphate and phthalic acid adsorbed as a function of pH and total orthophosphate concentration. Total phthalic acid concentration = 0.20 mM.

0.10 mM PO_4 dose resulted in a decrease in organic acid removal of up to approximately 0.05 mM. As in the single sorbate experiments, orthophosphate was completely removed from solution (not shown) and adsorption appeared to be sorbent-limited at pH > 8. Similarly to the experiment with phthalic acid (and likely for the same reasons), phosphate removal exceeded the decrease in salicylic acid adsorption on a molar basis, resulting in a greater amount of anions adsorbed than in the single-sorbate systems. A comparison of the adsorption data with the ζ-potential measurements in Figure 4.59 shows that significant adsorption of salicylic acid occurred despite the negative surface charge at pH > 7.5. This observation supports the contention that salicylic acid can form inner-sphere complexes at hydrous aluminum surfaces. It also seems to confirm that the phenolic group is involved in the adsorption reaction.

Removal of oxalic acid, which adsorbed most strongly at a given concentration among the simple organic acids in the single-sorbate system, was also affected by the presence of 0.10 mM phosphate (Figure 4.60). As with phthalic and salicylic acid, the decrease in fractional removal at 0.10 mM PO_4 appears to be roughly constant over the examined pH range, which is likely due to the fact that phosphate adsorption was limited by the amount added. The decrease was approximately 0.5 mol oxalic acid per mol PO_4 adsorbed, which,

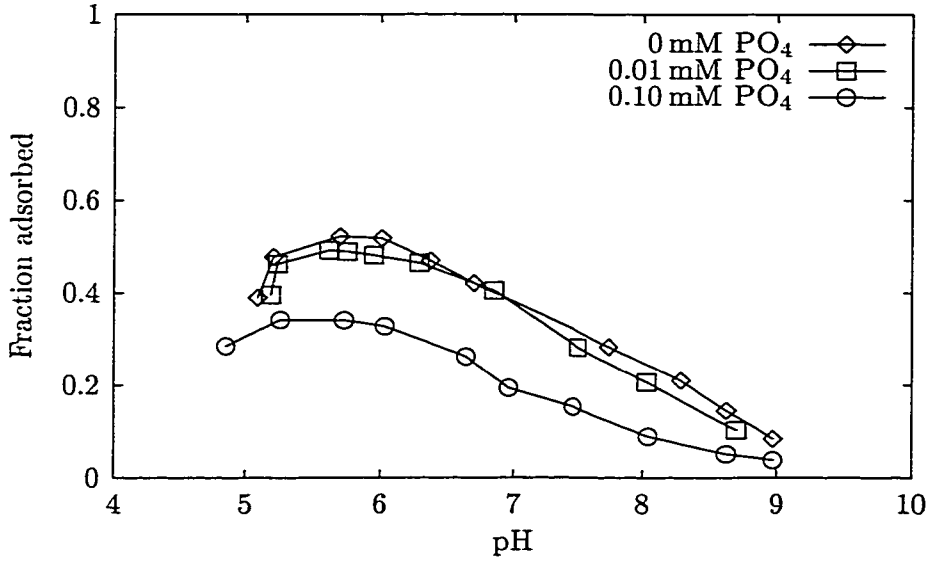

Figure 4.58. Fraction of salicylic acid adsorbed as a function of pH and total orthophosphate concentration. Total salicylic acid concentration = 0.20 mM.

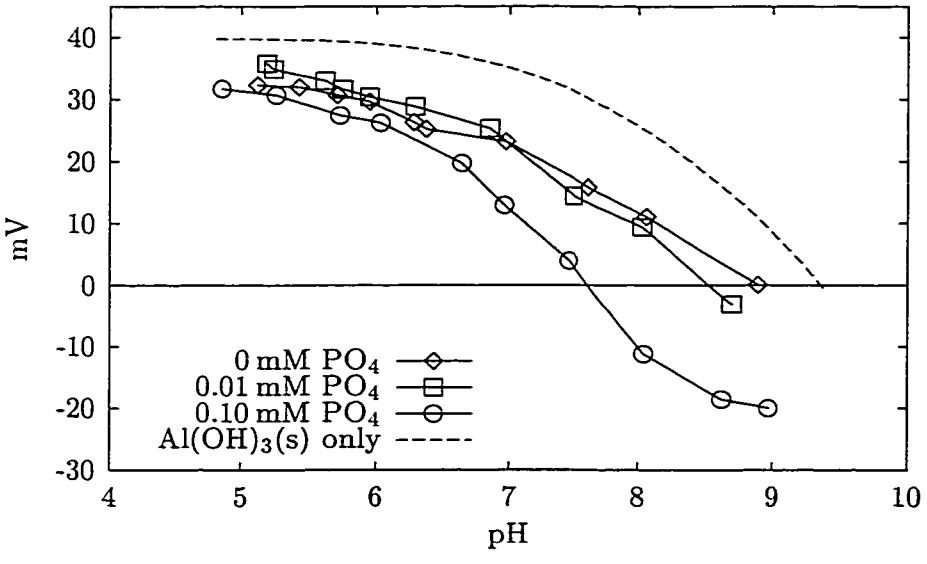

Figure 4.59. Effect of adsorption of salicylic acid on ζ-potential as a function of pH and total orthophosphate concentration. Total salicylic acid concentration = 0.20 mM.

as observed previously, may be the result of different adsorption reaction stoichiometries and the fact that phosphate can complex sites that are neutral or negatively charged. ζ-potential measurements show that at pH > 6, oxalic acid adsorbed to a slightly negatively charged surface. Despite its divalent charge, electrostatic interactions did not appear to influence the adsorption behavior of oxalic acid to the same extent as the other simple organic acids.

Fractional removal of Aldrich humic acid in the presence of orthophosphate is depicted in Figure 4.62. A perceptible decrease in adsorption of Aldrich humic acid occurred only at pH > 7.5. Below this pH, there is virtually no impact on either adsorption of humic acid or phosphate, which suggests that an excess of surface sites must have been present allowing both constituents to be completely removed. At pH > 8, the amount of precipitate decreased with increasing pH (Figure 4.6), limiting both humic acid and phosphate adsorption and resulting in the observed competitive effects in the binary system. Further evidence for surface sites excess at pH < 8 is provided by the ζ-potential measurements shown in Figure 4.63. In the single sorbate systems with either 0.10 mM PO_4 or 0.50 mM C humic acid, the pH_{iep} was near pH 8, whereas in the binary system it moved by one pH unit to approximately pH 7. It is apparent that charged orthophosphate and humic acid surface complexes exerted a much greater effect on the ζ-potential of the precipitate than the individual ions alone. The decrease in surface charge calculated from the ζ-potential measurements as described earlier clearly shows that at the concentrations used in this work, the effects of humic acid and orthophosphate (0.10 mM) were additive. Figure 4.64 indicates that both constituents had an identical effect on surface charge in the single adsorbate system. When added together, the change in charge expressed in C/m^2 was approximately twice as high at pH < 8.

Despite the limited results in the experiments with humic acid, the effect of orthophosphate on the adsorption or organic molecules was clearly perceptible. Even when added at half the molar concentration of the organic acid, orthophosphate caused a significant decrease in removal efficiency. At pH > 7, orthophosphate appears to form negatively charged surface complexes, which can cause reversal of the surface charge of aluminum hydroxide and lead to repulsion of anions that adsorb predominantly through electrostatic attraction.

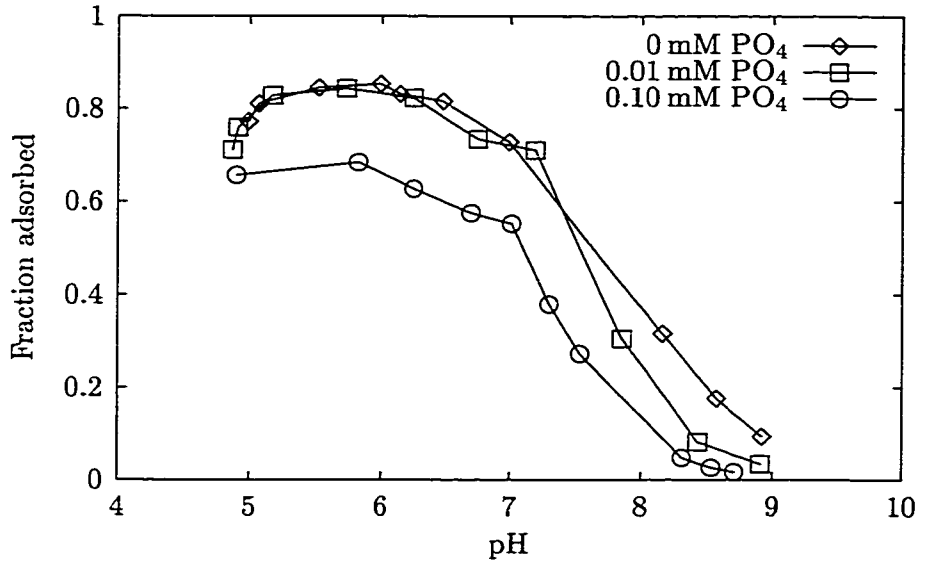

Figure 4.60. Fraction of oxalic acid adsorbed as a function of pH and total orthophosphate concentration. Total oxalic acid concentration = 0.20 mM.

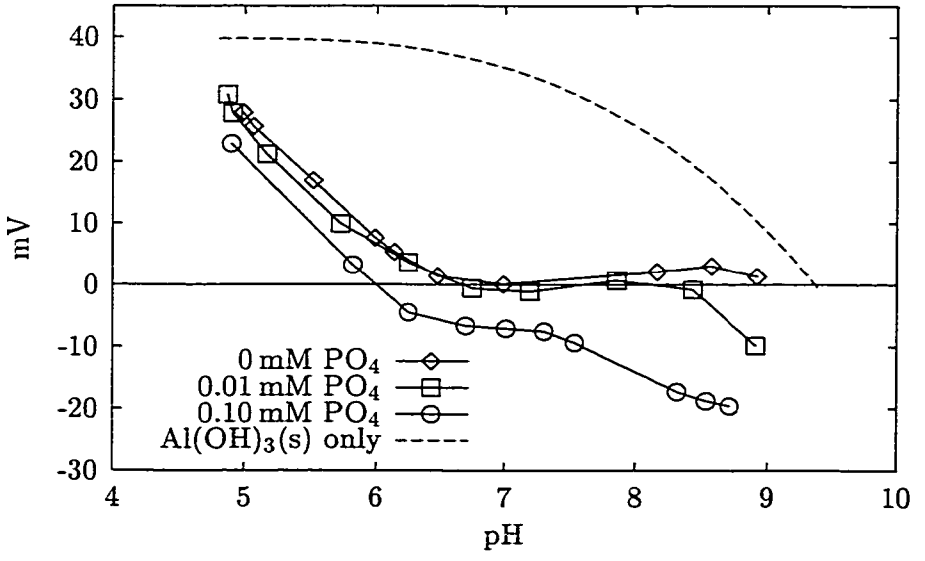

Figure 4.61. Effect of adsorption of oxalic acid on ζ-potential as a function of pH and total orthophosphate concentration. Total oxalic acid concentration = 0.20 mM.

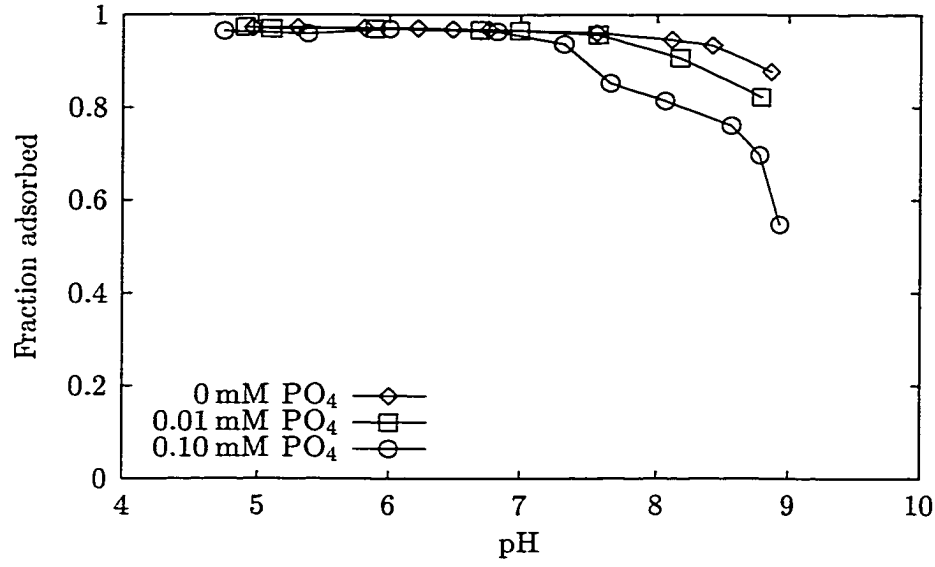

Figure 4.62. Fraction of Aldrich humic acid adsorbed as a function of pH and total orthophosphate concentration. Total Aldrich humic acid concentration = 0.50 mM as C.

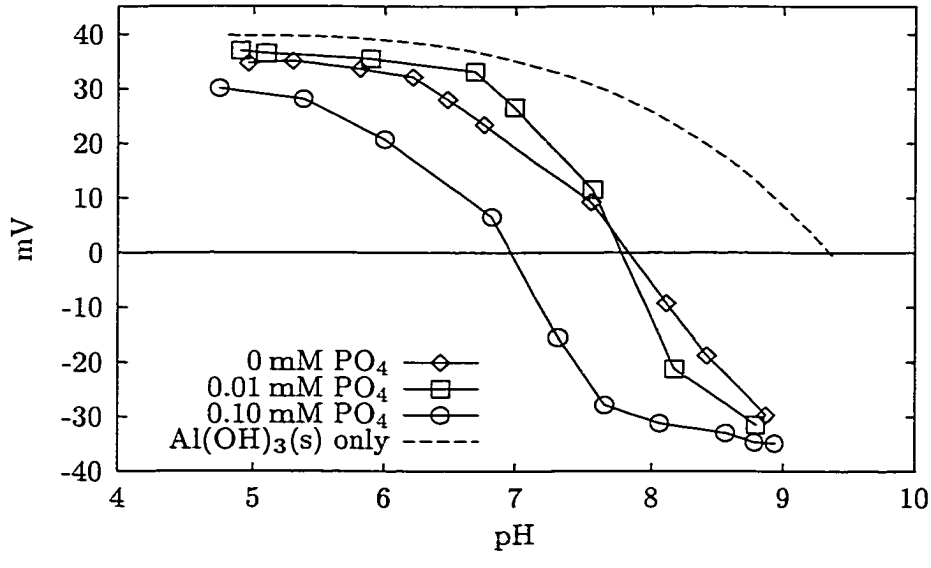

Figure 4.63. Effect of adsorption of Aldrich humic acid on ζ-potential as a function of pH and total orthophosphate concentration. Total Aldrich humic acid concentration = 0.50 mM as C.

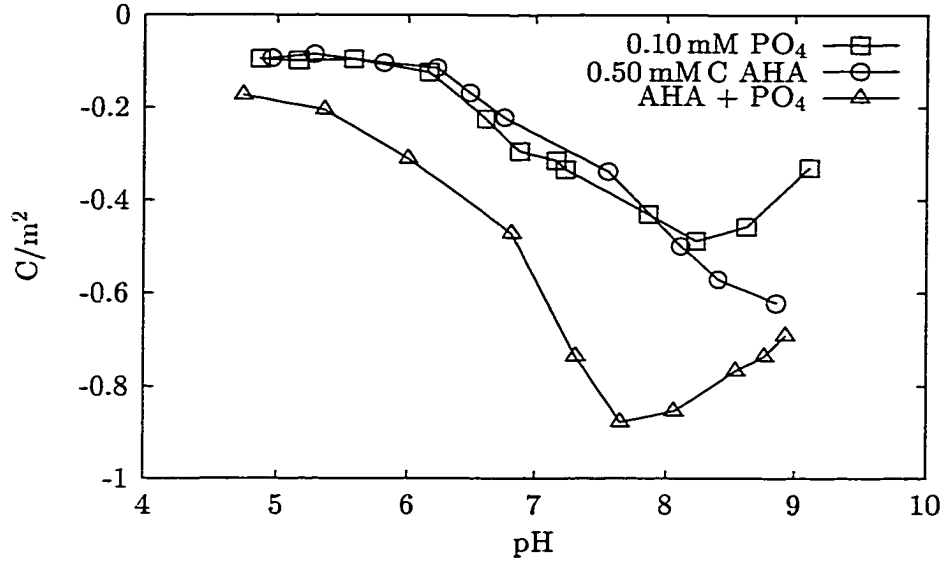

Figure 4.64. Decrease in surface charge in the presence of Aldrich humic acid and orthophosphate in the single and binary sorbate system as a function of pH.

4.3.8. Effects of Fluoride on Adsorption of Organic Acids

The effects of fluoride dosed at 0.05 and 0.16 mM on the adsorption of phthalic, salicylic, oxalic and Aldrich humic acid were tested at total organic acid concentrations of 0.20 mM (0.50 mM as C for AHA). The data from the experiments with phthalic acid are typical for the competition of fluoride with simple organic acids tested in this work. Fluoride dosed at 0.16 mM had a less substantial effect on phthalic acid adsorption (Figure 4.65) compared to the other inorganic anions. Actually, the impact was similar to the influence of 0.10 mM SO_4 on phthalic acid adsorption, despite the fact that the removal of fluoride exceeded that of sulfate (dosed at 0.10 mM) at pH > 6 in the single-sorbate system. The effect of fluoride on the ζ-potential of the precipitate particles in the binary system was barely perceptible (Figure 4.66), indicating that fluoride formed an uncharged surface complex and therefore did not affect the surface charge. Therefore, the greater influence of sulfate on phthalic acid removal may in part be due to a decrease in electrostatic attraction. In addition, the smaller impact of fluoride may also be related to the ion's adsorption to specific sites on $Al(OH)_3(s)$. This conclusion can be made when considering that the total number of sites occupied on the precipitate substantially increased with increasing fluoride concentrations

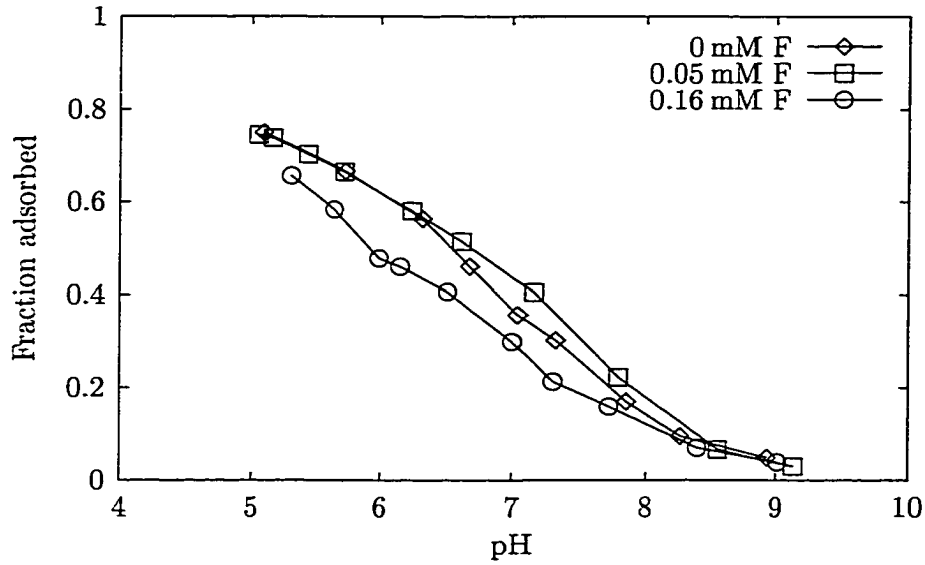

Figure 4.65. Fraction of phthalic acid adsorbed as a function of pH and total fluoride concentration. Total phthalic acid concentration = 0.20 mM.

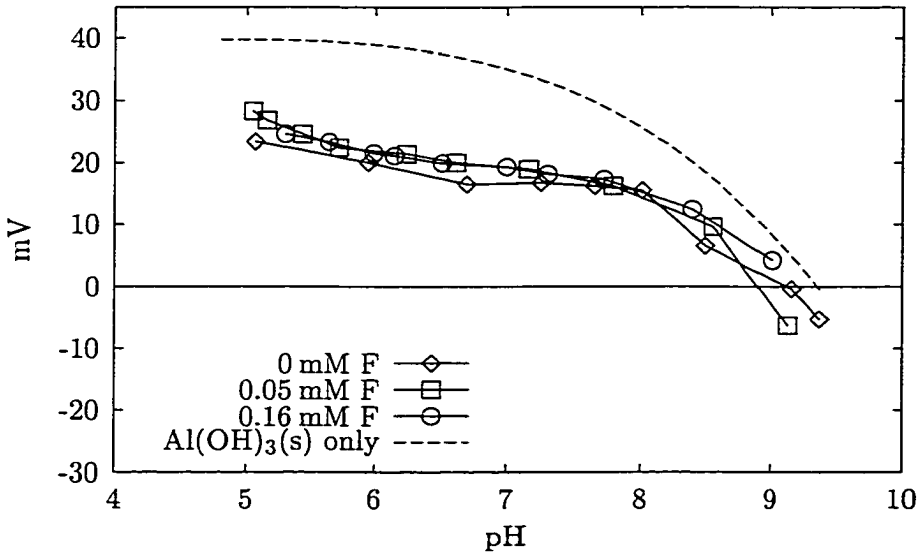

Figure 4.66. Effect of adsorption of phthalic acid on ζ-potential as a function of pH and total fluoride concentration. Total phthalic acid concentration = 0.20 mM.

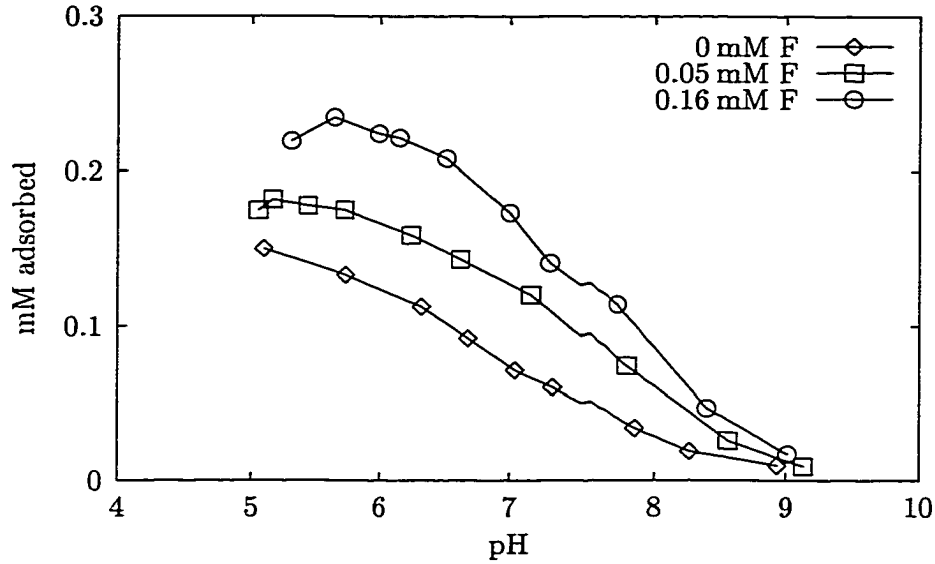

Figure 4.67. Sum of molar concentrations of fluoride and phthalic acid adsorbed as a function of pH and total fluoride concentration. Total phthalic acid concentration = 0.20 mM.

as shown in Figure 4.67. This plot indicates that over a wide pH range, the sum of molar concentrations of adsorbed fluoride and phthalic acid increased by approximately 0.04 and 0.10 mM while up to 80% (0.04 and 0.12 mM) of the added fluoride was removed at a dose of 0.05 and 0.16 mM F, respectively (Figure 4.68, 4.69). Therefore, although there was a small decrease in adsorption of both phthalic acid and flouride compared to the single-sorbate system, it appears that fluoride adsorbed under the test conditions predominantly to sites that are usually not occupied by phthalic acid.

Similar observations were also made in the experiments with salicylic acid. Fluoride did not affect organic acid adsorption to a large extent (Figures 4.70) when compared to the effects of sulfate or orthophosphate and only a negligible effect on ζ-potential due to F-adsorption was observed (not shown). There also seemed to be only a few "shared" surface sites as evident from the plot of the sum of molar concentrations of fluoride and salicylic acid versus pH (Figure 4.71). Similar to phthalic acid, salicylic acid caused fluoride removal to decrease by 10% (not shown).

In the binary fluoride-oxalic acid system, substantially greater competition occurred. Although there was only a small impact on oxalic acid removal (Figure 4.72), fluoride adsorption decreased by more than 20% (Figure 4.68, 4.69). Apparently, a greater number

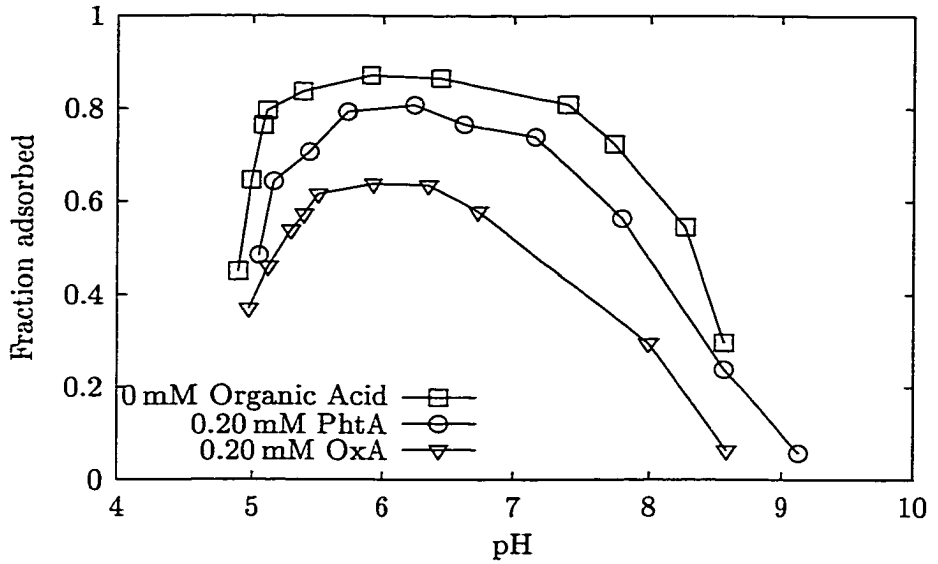

Figure 4.68. Fraction of fluoride adsorbed as a function of pH and organic acid concentration (Total fluoride concentration = 0.05 mM).

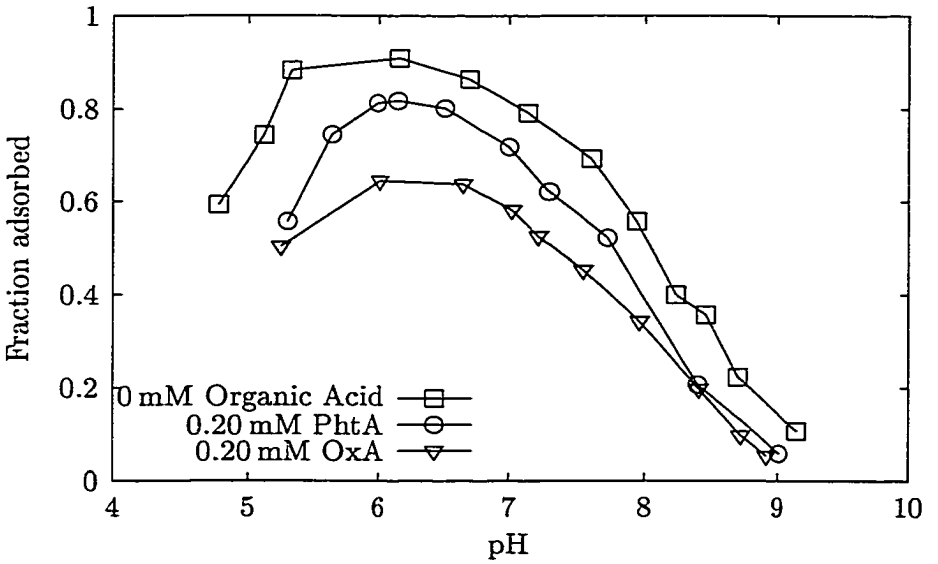

Figure 4.69. Fraction of fluoride adsorbed as a function of pH and organic acid concentration (Total fluoride concentration = 0.16 mM).

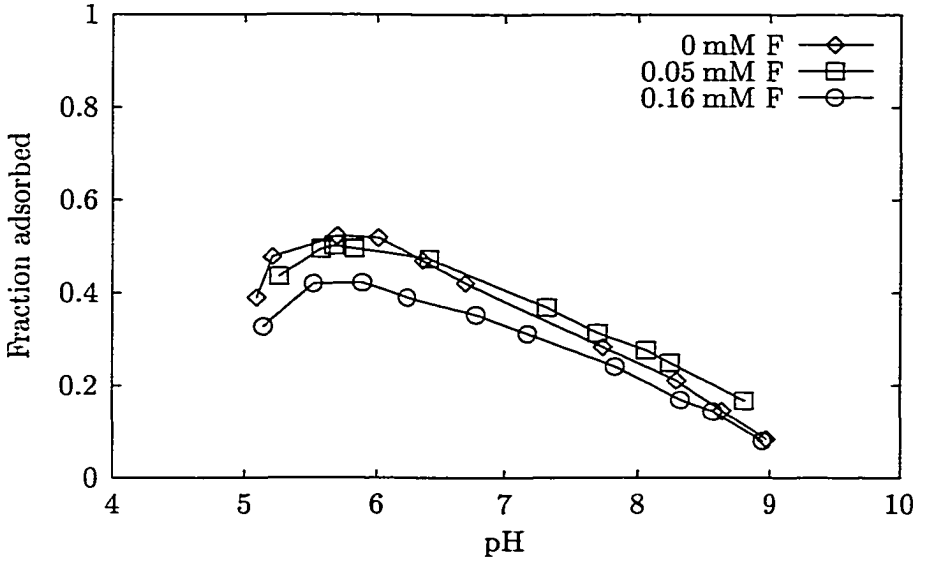

Figure 4.70. Fraction of salicylic acid adsorbed as a function of pH and total fluoride concentration. Total salicylic acid concentration = 0.20 mM.

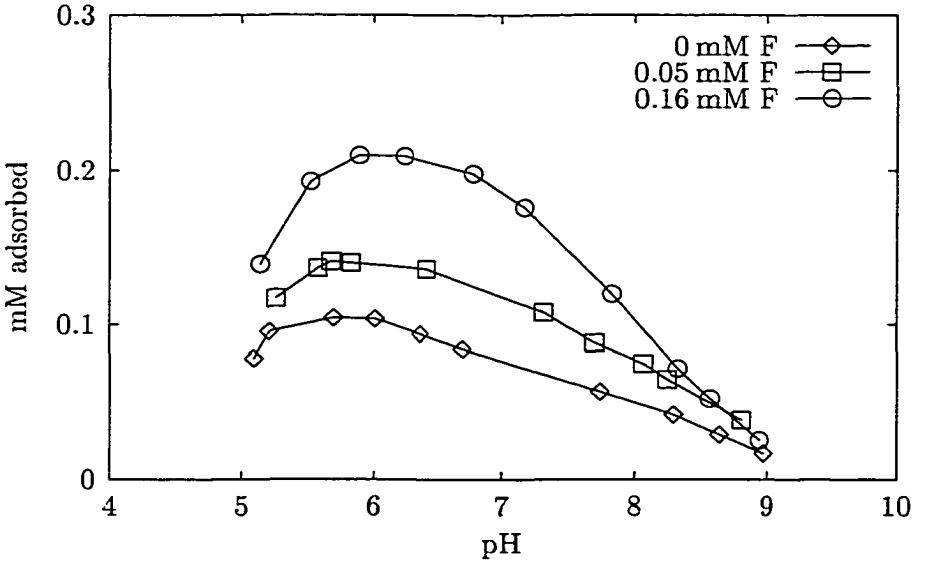

Figure 4.71. Sum of molar concentrations of fluoride and salicylic acid adsorbed as a function of pH and total fluoride concentration. Total salicylic acid concentration = 0.20 mM.

of fluoride adsorption sites on the aluminum hydroxide surface were accessible for oxalic acid than for phthalic or salicylic acid. The ζ-potential of the suspended particles was not affected (not shown).

Fluoride did not influence the removal of Aldrich humic acid (Figure 4.73). In this case, surface site saturation may have not been reached as observed previously with orthophosphate, which would have allowed fluoride to adsorb without competing with the organic molecules. However, Aldrich humic acid had a similar impact on fluoride adsorption as phthalic acid (not shown), causing a decrease in fractional adsorption by approximately 10%, which seems surprising considering that the removal of a more weakly adsorbing anion, sulfate, was essentially not affected by Aldrich humic acid. As with the other organic acids, differences in ζ-potentials of the precipitate particles in the presence and without fluoride were barely perceptible (not shown).

The observations gathered in the experiments with fluoride have two implications for water treatment. First, fluoride does not appear to greatly influence organic matter removal by alum coagulation through competition for available surface sites on aluminum hydroxide. Both adsorption to "fluoride-specific" sites and the inability to affect the surface charge of the precipitate may be the reason for this behavior. The interferences observed in bench- and pilot-scale studies (Section 2, 3) mainly resulted from the ability to form soluble complexes and thus decrease the amount of aluminum hydroxide precipitate that serves as a sorbent for organic molecules. Second, despite the ability of fluoride to form very strong complexes with aluminum, organic acids can successfully compete for adsorption sites on aluminum hydroxide. Therefore, where fluoride is a target contaminant to be removed from solution by adsorption to aluminum oxide (which is a common treatment method), the presence of organic matter can hamper treatment efficiency.

4.4. Summary and Conclusions

Single adsorbate experiments with inorganic anions showed that the adsorption of sulfate, orthophosphate, and fluoride to amorphous aluminum hydroxide is generally consistent with the findings of other researchers. Sulfate, which is fully dissociated in the pH range examined in this work, formed relatively weak bonds that appear to be dominated by electrostatic

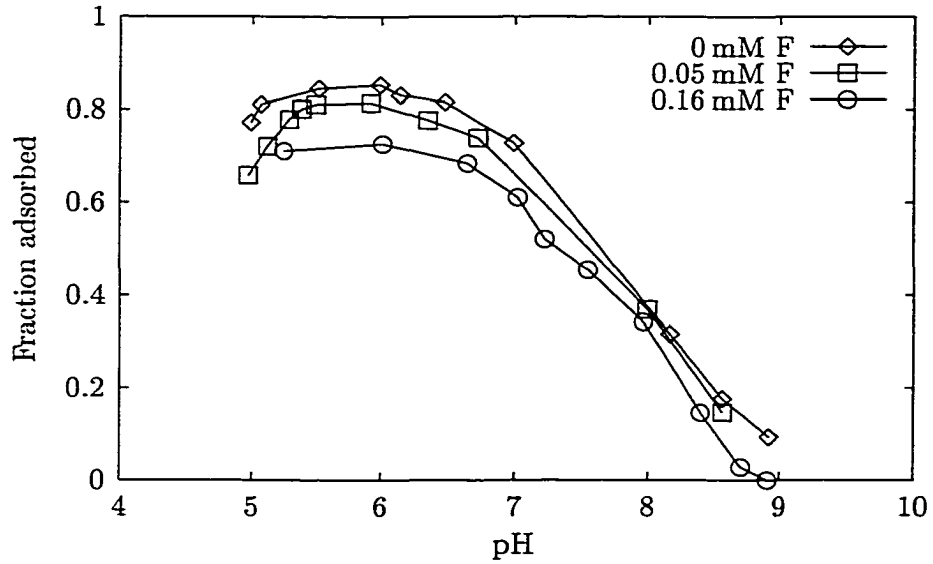

Figure 4.72. Fraction of oxalic acid adsorbed as a function of pH and total fluoride concentration. Total oxalic acid concentration = 0.20 mM.

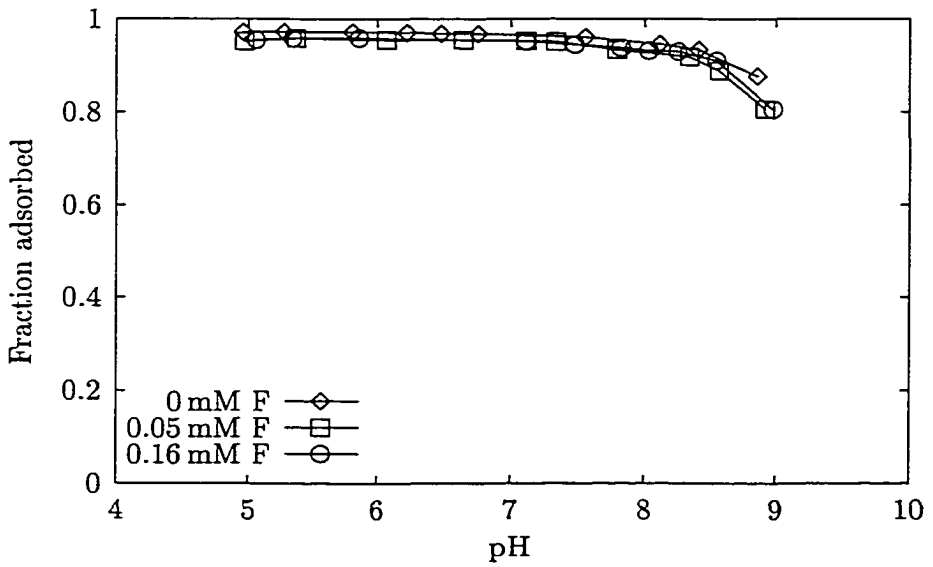

Figure 4.73. Fraction of Aldrich humic acid adsorbed as a function of pH and total fluoride concentration. Total Aldrich humic acid concentration = 0.50 mM as C.

attraction. This conclusion is based on the observation that sulfate was only removed from solution when the precipitate particles were positively charged. Orthophosphate adhered strongly to $Al(OH)_3(s)$ and caused charge reversal of the floc. The interaction is primarily a result of the formation of inner-sphere surface complexes which is favored because protonated orthophosphate ions allow the exchange of surface hydroxyl groups. Fluoride, which is well known to form strong bonds with aluminum in solution, also exhibited high removal rates. However, whereas sulfate removal increased with decreasing pH, optimum removal of fluoride by adsorption to $Al(OH)_3(s)$ occurred at intermediate pH values. It is suggested that the formation of soluble, non-adsorbable fluoroaluminum complexes caused decreased removal at pH < 6.

Organic acids containing low-pK_a acidic functional groups generally behaved like inorganic anions with adsorption maxima at low pH and decreasing removal with increasing pH. The adsorption of those that only carry carboxyl groups appears to be strongly influenced by the charge of the sorbent because they generally remained completely in solution near the pH_{iep} of $Al(OH)_3(s)$. Additional phenolic groups enhance removal at higher pH, whereas additional carboxylic groups do not necessarily improve adsorption at low pH. Pyromellitic acid contains additional weakly acidic functional groups that may facilitate ligand exchange reactions. However, ζ-potential measurements suggest that the functional groups in the *para* or *meta* position may remain uncomplexed at the solid-water interface and, if deprotonated, hamper adsorption by electrostatic repulsion. If only two adjacent carboxyl groups are present (oxalic and phthalic acid), the acidity of these groups may affect the strength and structure of the aluminum-carboxylate bond possibly resulting in bidentate complexes. However, a strong affinity to surface aluminum atoms is likely to correlate to the tendency to form dissolved aluminum complexes which can result in dissolution of the sorbent and negatively influence organic acid removal at low pH. Oxalic and salicylic acid exhibited this type of behavior. The experiments with pyrogallic acid showed that the presence of carboxylic functional groups is not necessary for strong adsorption to occur. Phenolic groups may deprotonate near the surface at neutral or higher pH to complex aluminum atoms, and additional weak attractive forces due to hydrogen bonding may be involved.

Despite the different affinities to aluminum hydroxide, oxalic, phthalic, salicylic, and pyrogallic acid exert the same effect on the surface charge of $Al(OH)_3(s)$ when the data calculated from ζ-potential measurements was normalized to the surface concentration of the adsorbate. It is concluded that these compounds form surface complexes of similar charge. Pyromellitic acid, which has four carboxylic functional groups exerts a significantly greater effect on surface charge. Among the simple organic acids, only the compounds that have functional groups with $5 < pK_a < 10$, pyromellitic and pyrogallic acid, clearly induced charge reversal.

The data gathered from experiments with Dismal Swamp organic matter (DSOM) showed that natural organic acids exhibit similar adsorption behavior and effects on ζ-potential as simple organic acids. The data obtained by titration of this natural organic acid indicate the presence of functional groups with acidity constants similar to carboxylic and phenolic groups. Comparison of the adsorption envelopes and ζ-potential measurements suggests that natural organic matter may be represented by a mixture of simple organic acids. However, more systematic research would be required, because the removal of very large natural organic molecules as represented by Aldrich humic acid was much higher than for DSOM despite the smaller amount of functional groups, and the adsorption may thus be affected by hydrophobic forces.

Competitive adsorption experiments revealed that sulfate can significantly decrease organic acid adsorption. The effect was most perceptible at low pH and when sulfate exceeded the organic acid concentration 2.5 times or higher, and it occurred only when the aluminum hydroxide particles were neutral or positively charged. These findings are important because not only are sulfate based coagulants widely used in water treatment, but "enhanced" coagulation at lower pH and at doses exceeding that required for charge neutralization is also a primary strategy to improve disinfection byproduct precursor removal. Orthophosphate exerted the greatest influence on the removal of simple organic acids. The effect was nearly independent of pH, which was due to the fact that phosphate adsorption was limited by the phosphate dose. It also affected removal of Aldrich humic acid at pH > 7.5, where phosphate adsorption appeared to be sorbent-limited. Despite the shortcoming due to the experimental conditions, the results unambiguously illustrate the negative effects

that orthophosphate can have when it is added during water treatment at a point upstream of coagulation or filtration processes and where aluminum based coagulants are used: It affects particle stability due to its ability to cause charge reversal and effectively competes strongly with organic matter for adsorption sites. In competitive adsorption experiments, fluoride removal exhibited a noticable decrease while only a moderate effect on organic acid removal was observed. Therefore, detrimental effects of fluoride in water treatment as observed in bench and pilot-studies are mainly a consequence of its ability to impair precipitate formation.

5. MODELING THE ADSORPTION OF INORGANIC AND ORGANIC LIGANDS ONTO ALUMINUM HYDROXIDE

5.1. Introduction

Utilizing surface complexation models in studying the adsorption of various inorganic and organic substances to oxides has long become a valuable research tool for geochemists and environmental scientists. In surface complexation modeling, discrete surface binding sites undergo reactions similar to solute-solute interactions. In addition, electrostatic surface complexation models allow surfaces to acquire electrical charge by adsorption. The accumulated charge at the surface has to be counterbalanced by a diffuse ion swarm in order to maintain electroneutrality. This spatial distribution of ions near the surface results in an electrostatic potential between the particle surface and the bulk solution and therefore causes a repulsive force when particles or ions with similar charge approach, whereas ions of opposite charge would be attracted.

Although electrostatic correction terms in surface complexation models have helped correctly predict the extent of adsorption of a substance, there appear to have been few efforts to verify whether the changes in electrokinetic properties of the solids upon adsorption can be predicted adequately at the same time. As a prerequisite, it has to be assumed that the predicted diffuse layer potential ψ_d is representative for the ζ-potential of the particles. Because of the importance of electrostatic forces in particle aggregation and removal, surface complexation modeling could gain a tremendous practical value in conventional, physicochemical water treatment, where multicomponent interactions between dissolved and solid substances are common. Because both optimum removal of contaminant solutes and particle destabilization are primary goals in conventional treatment, a theory-based model that could compute optimum treatment conditions for a given water and target contaminant would be a powerful tool for engineers, designers, and operators.

In this work, the results from well controlled laboratory studies (Section 4) were used to determine whether surface complexation modeling can adequately describe the competitive adsorption of inorganic (SO_4^{2-}, PO_4^{3-}, F^-) and organic anions (phthalic, salicylic,

oxalic, pyrogallic, pyromellitic, Aldrich humic acid, and Dismal Swamp organic matter) to aluminum hydroxide and the effect on the electrokinetic properties of the adsorbent.

5.2. Methods

5.2.1. Chemical Equilibrium Modeling Software

Currently, there are numerous software packages that allow numerical evaluation of chemical speciation including surface complexation modeling, such as FITEQL (Herbelin and Westall, 1996), MINEQL+ (Schecher and McAvoy, 1998), MINTEQA2 (Allison *et al.*, 1993), or PHREEQC (Parkhurst and Appelo, 1999). Most of these programs allow the selection of different conceptual representations of the interfacial structure, namely the Constant Capacitance Model (CCM), the Diffuse Double Layer Model (DDLM), and the Triple Layer Model (TLM). These different models were reviewed by Davis and Kent (1990). The TLM, which was employed in this work, divides the solid-water interface into three planes: A surface plane 0 for the adsorption of H^+, OH^- and strongly adsorbing ions, a near-surface plane β for weakly adsorbing ions, and a diffuse layer plane (d-plane), representing the closest distance of approach for the dissociated charge. Thus, coordinate (or inner-sphere) complexes would be placed into the 0-layer, whereas ions that remain hydrated and interact predominantly through electrostatic attraction would adsorb to the β-plane.

Among the mentioned software packages, only FITEQL is designed for the purpose of estimating parameters from experimental data. However, the program can only estimate concentrations and equilibrium constants, and it is not easily adapted to also optimize specific surface area, surface site density, or interfacial capacitances. Therefore, a chemical equilibrium solver similar to FITEQL was written in FORTRAN and incorporated in the public domain software package for weighted orthogonal distance regression, ODRPACK (Boggs and Rogers, 1989; Boggs *et al.*, 1992) as part of this study. The technique used for solving the chemical equilibrium problems is described in Appendix A. The computer program was tested with synthetic data generated using MINEQL+ (Schecher and McAvoy, 1998). The parameters estimated by ODRPACK and those used to generate the synthetic data in MINEQL+ were in excellent agreement. Because ODRPACK allows utilization

of a finite difference approximation to determine derivatives, the parameter estimation is not limited to equilibrium contants and concentrations. The chemical equilibrium solver was also enhanced to allow the surface site concentration to vary with the precipitation or dissolution of the solid. FITEQL lacks this feature which is important if there is a strong pH-dependency in solubility and the total sorbent concentration is low (as in water treatment with alum), or if an adsorbing ion has also the capability to dissolve the solid, e.g., fluoride. The parameter estimation routines implemented in ODRPACK can fit data both by weighted ordinary least squares (OLS) (utilized by FITEQL) or by weighted orthogonal distance regression (ODR). In OLS problems, model and experimental errors are attributed to the observations of the dependent variable. ODR minimizes the sum of squares of the weighted orthogonal distances between data points and the fitted curve and thus takes errors in the independent variables also into account. In this work, all problems were solved utilizing weighted ODR, unless numerical instabilities or nonconvergence was encountered. Similar to FITEQL, ODRPACK computes from the weighted sum of squares and the degrees of freedom the residual standard deviation of the regression, $\hat{\sigma}$, which was utilized as a measure for the goodness of fit. ODRPACK also computes the 95% confidence intervals of the best fit parameters.

5.2.2. Error Estimates

In order to compare the goodness of fit for different model runs, it was required to use realistic weighting factors. Boggs and Rogers (1989) recommend using reciprocal error variances as weights for the data points, $w_i = 1/\sigma_i^2$. The error variances σ_i^2 were estimated according to $\sigma_i = s_{\text{rel}} \cdot C_i + s_{\text{abs}}$, where s_{rel} and s_{abs} represent the relative and absolute standard deviation of the measured concentration C_i, respectively. A similar approach is used by FITEQL (Herbelin and Westall, 1996). Values for the relative standard deviation and detection levels found in the literature or derived from the actual analyses were used as estimates for s_{rel} and s_{abs}, respectively (Table 5.1).

The ζ-potential (or ψ_d) is not directly used in the computer model but transformed into the dummy variable PSID $= \exp\left(\frac{-\zeta F}{RT}\right)$. According the the law of error propagation, the estimated absolute error of 1 mV in ζ-potential equals a relative error in PSID of 0.04.

Table 5.1. Relative and absolute error estimates.

Variable	s_{rel}	s_{abs}	Estimated from
Hydrogen Ion (pH)	0.11	0	Eaton *et al.* (1995)
Phthalic Acid	0.05	3×10^{-7}M	"
Salicylic Acid	0.05	6×10^{-7}M	"
Aldrich Humic Acid	0.05	2×10^{-6}M as C	"
Pyromellitic Acid	0.05	10^{-6}M	"
Orthophosphate	0.05	2×10^{-7}	"
Fluoride	0.05	3×10^{-6}M	Experimental data
Aluminum	0.05	10^{-5}M	"
Sulfate	0.05	10^{-5}M	"
Oxalic Acid	0.05	10^{-5}M	"
Pyrogallic Acid	0.05	10^{-5}M	"
DSOM	0.05	5×10^{-5}M as C	"
PSID	0.04	0	"

Similarly, for an estimated absolute error in pH of 0.05 pH units (Eaton *et al.*, 1995), the relative error in $[H^+]$ is 0.11. For UV light absorption measurements, an absolute error of $0.002\,cm^{-1}$ and a relative error of 5% (Eaton *et al.*, 1995) was assumed. The absolute error in organic acid concentration was then computed from the molar extinction coefficients, ϵ, used in the analyses (refer to Section 4, Table 4.4).

5.2.3. Modeling Approach

In a first step during the modeling efforts, ODRPACK was used to determine the solubility constant of $Al(OH)_3(s)$ that was to be used for all subsequent model runs. In all simulations, the complexation constants for the hydrolysis of aluminum listed in Table 2.1 (Section 2) were used. Then, the equilibrium constants for the protonation and deprotonation of the surface hydroxyl groups and the electrolyte adsorption reactions were optimized to obtain a reasonable prediction of the ζ-potential of $Al(OH)_3(s)$ versus pH. The surface

acidity constants, which pertain to the protonation and deprotonation of the aluminum oxide/hydroxide surface hydroxyl groups, ≡AlOH, have been fairly well characterized. The reactions are written as

$$\equiv AlOH + H^+ \rightleftharpoons \equiv AlOH_2^+ \qquad \log K_+$$

$$\equiv AlOH \rightleftharpoons \equiv AlO^- + H^+ \qquad \log K_-$$

and they have been utilized by numerous researchers for surface complexation modeling of hydrous γ-Al_2O_3 (Hohl and Stumm, 1976; Kummert and Stumm, 1980; Hao and Huang, 1986; Person *et al.*, 1998) and amorphous aluminum hydroxide (Letterman and Iyer, 1985; Anderson and Benjamin, 1990a; Meng and Letterman, 1993b). Experimentally determined values for $\log K_+$ and $\log K_-$ span a fairly narrow range as indicated in Table 5.2.

Table 5.2. Literature values for surface acidity constants.

Solid	$\log K_+$	$\log K_-$	Reference
$Al(OH)_3$(s)	5.7	-11.5	Letterman and Iyer (1985)
$Al(OH)_3$(s)	6.8	-11.0	Anderson and Benjamin (1990a)
$Al(OH)_3$(s)	8.0	-10.2	Meng and Letterman (1993b)

Letterman and Iyer (1985) and Meng and Letterman (1993b) determined the acidity constants by fitting the TLM-predicted diffuse layer potential ψ_d to the ζ-potentials of aluminum hydroxide coated silica particles. Anderson and Benjamin (1990a) employed the constant capacitance model, not taking electrolyte adsorption into account. Therefore, the constants determined by Letterman and Iyer (1985) and by Meng and Letterman (1993b) were initially used during these modeling efforts.

The incorporation of electolyte adsorption to aluminum hydroxide allows mimicking the effect of ionic strength on surface complexation. The (outer-sphere) binding of the electrolyte ions is commonly incorporated in the TLM structure as follows:

$$\equiv AlOH + Na^+ \rightleftharpoons \equiv AlO^-Na^+ + H^+ \qquad \log K_{Na^+}$$

$$\equiv AlOH + Cl^- + H^+ \rightleftharpoons \equiv AlOH_2^+Cl^- \qquad \log K_{Cl^-}$$

In the notation for the reaction product, the charge of surface site and adsorbate are separated to indicate that the ion binds to the β-layer. Equilibrium constants for the adsorption of sodium and chloride have been reported by Iyer (1984) ($\log K_{Na^+} = 9.1$) and by Cheng and Huang (1996) ($\log K_{Na^+} = 9.1, \log K_{Cl^-} = -8.2$).

Other parameters required for input into the model that define the adsorbent in surface complexation models include surface area A_S, surface site concentration $T_{\equiv AlOH}$, and the solids concentration S. In addition, when using the TLM, the values for the capacitances of the inner and outer adsorption layer are needed for input. A value of $C_2 = 0.2\,F/m^2$ has been widely used for the outer layer capacitance of oxides (Hunter, 1981; Davis and Kent, 1990), whereas value of $C_1 = 1.4\,F/m^2$ has been utilized for the inner layer capacitance of hydrous aluminum surfaces (Iyer, 1984; Meng and Letterman, 1993b; Cheng and Huang, 1996). However, these values were not regarded as rigid constants in this work. C_1 can vary among different oxides and with ionic strength and the applicability of $C_2 = 0.2\,F/m^2$ to oxides may also be questionable (Lützenkirchen, 1998). Therefore, the sensitivity of the model fit to these surface parameters was evaluated. For the solids concentration S, the mass of precipitate ($Al(OH)_3(s)$, MW = 78 g/mol) computed by the chemical equilibrium solver was used.

Meng and Letterman (1993b) utilized the deuterium exchange method to determine the surface site concentration, $T_{\equiv AlOH}$, of aluminum hydroxide and obtained a value of 5 mmol of sites per 5 mmol of $Al(OH)_3(s)$. With the surface site density, ρ, and the molecular weight of aluminum hydroxide, the specific surface area, A_S, of the solid can be calculated according to

$$A_S = \frac{T_{\equiv AlOH}\ N_A}{MW_{Al(OH)_3(s)}\ \rho}$$

where N_A is Avogadro's Constant. Based on the value for site density used in that study of 8 sites per nm^2, aluminum hydroxide would have a specific surface area of approximately 965 m^2/g. In contrast however, Anderson and Benjamin (1990a) utilized in their model a surface area of only 41 m^2/g, which was based on BET-surface area measurements. Meng and Letterman (1993a) noticed descrepancies between site density values from the literature and that calculated by dividing the the surface site concentration (determined by deuterium

exchange) by the BET surface area. They concluded that many adsorption sites on aluminum hydroxide may not be accessible to N_2 in the BET surface area determination. Davis and Leckie (1978b) also discussed the discrepancies between the specific surface area values of iron hydroxide obtained by different analytical methods. They utilized a much higher value ($600\,m^2/g$) than determined by the BET technique or by negative adsorption, citing research where specific surface areas as high as $700\,m^2/g$ for similar solids were observed. In addition, the surface site density determination also relies on the correct molecular weight of the solid, i.e., aluminum hydroxide could also be expressed as $Al(OH)_3 \cdot nH_2O$. In this work, a site concentration of 1 mmol/mmol $Al(OH)_3(s)$ and a site density of 8 per nm^2 (corresponding to a specific surface area of $965\,m^2/g$) was used.

In the next step, it was attempted to fit the measured solution concentrations of the inorganic and organic adsorbates to the model output. The goal was to find a set of surface complexation reactions for each anion that minimize the residual standard deviation, $\hat{\sigma}$. In the model, the anions adsorbed either to the 0 or the β-layer. The following reactions were considered in the model for the adsorption of an n-valent ligand to the 0-layer:

$$\begin{aligned}
\equiv AlOH + L^{n-} &\rightleftharpoons \equiv AlOL^{(n+1)-} + H^+ \\
\equiv AlOH + L^{n-} &\rightleftharpoons \equiv AlOHL^{n-} \\
\equiv AlOH + H^+ + L^{n-} &\rightleftharpoons \equiv AlL^{(n-1)-} + H_2O \\
\equiv AlOH + 2H^+ + L^{n-} &\rightleftharpoons \equiv AlHL^{(n-2)-} + H_2O \\
&\vdots \\
\equiv AlOH + nH^+ + L^{n-} &\rightleftharpoons \equiv AlH_{n-1}L + H_2O
\end{aligned}$$

Only mononuclear, monodentate surface complexes were considered. This approach has been used for modeling the adsorption of several inorganic and organic anions on goethite (Ali and Dzombak, 1996b; Evanko and Dzombak, 1998). Mesuere and Fish (1992) also described the adsorption of oxalate to iron oxide with these reactions, but they acknowledged that some of them may not be realistic from a chemical standpoint. The author feels that the existence of $\equiv AlOL^{(n+1)-}$ or $\equiv AlOHL^{n-}$ may be questionable.

As an additional parameter that could improve the model fit, the number of surface sites "covered" by the adsorbate, $\bar{n}$, was also varied. This method has been implemented in

most chemical equilibrium software programs and it allows applying different stoichiometric coefficients to the mass action expression and the mass balance. That is, the mass action law could be written as a mononuclear adsorption reaction, whereas the mass balance would reflect the coverage of $\bar{n}$ sites. This approach has been used by other researchers to predict the adsorption envelope of sulfate to aluminum and iron hydroxides (Meng and Letterman, 1993b, 1996).

The complexation of the inorganic and organic ligands L^{n-} to the β-layer was also evaluated and implemented in the model similar to the electrolyte adsorption reactions:

$$\begin{aligned} \equiv AlOH + H^+ + L^{n-} &\rightleftharpoons \equiv AlOH_2^+L^{n-} \\ \equiv AlOH + 2H^+ + L^{n-} &\rightleftharpoons \equiv AlOH_2^+HL^{(n-1)-} \\ &\vdots \\ \equiv AlOH + nH^+ + L^{n-} &\rightleftharpoons \equiv AlOH_2^+H_{n-1}L^{(n-1)-} + H_2O \end{aligned}$$

The results from the single-sorbate modeling were subsequently used to predict the data collected in the binary-sorbate systems.

5.3. Results and Discussion

5.3.1. Solubility and Electrokinetic Properties of $Al(OH)_3(s)$

The solubility constant for $Al(OH)_3(s)$ was determined using the dissolved aluminum concentrations measured following the adsorption experiments with inorganic and organic ions. Although some anions, notably oxalic acid and fluoride, can significantly complex aluminum in solution, it was assumed that due to the high total aluminum concentration of 1 mM, the solubility was only influenced by hydroxoaluminum complexes (Section 2, Table 2.1). The best fit solubility constant of $\log K_S = 10.585$ (95%-confidence interval $10.566 - 10.604$, $\hat{\sigma} = 1.84$) agrees well with published literature values (Stumm and Morgan, 1996). Model-fitted and measured dissolved aluminum concentrations from all the experiments are displayed in Figure 5.1.

The results of the modeling efforts to mimic the ζ-potential of aluminum hydroxide particles are shown in Figure 5.2. The corresponding modeling parameters are shown in

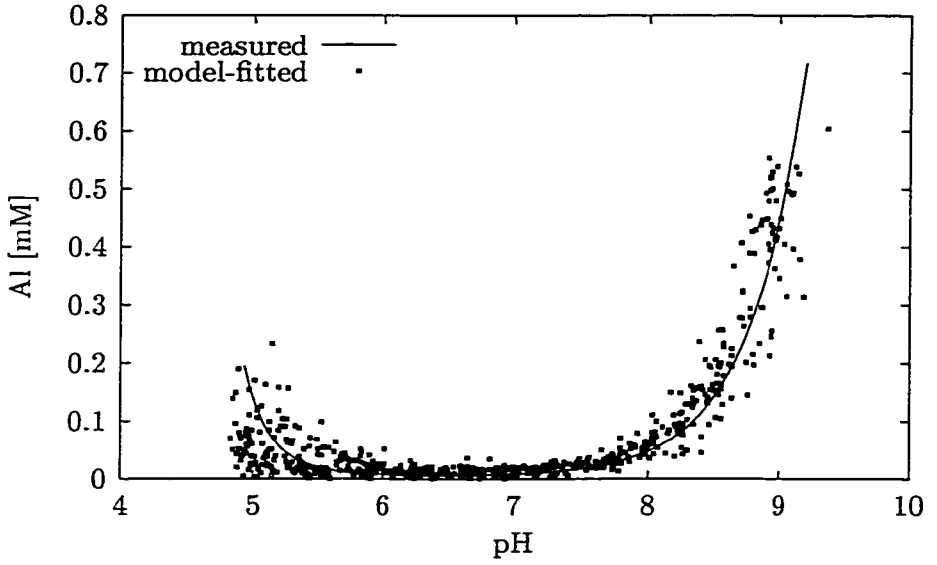

Figure 5.1. Model-fitted and measured dissolved aluminum concentration.

Table 5.3. The baseline data from Meng and Letterman (1993b) (K_{Na^+}, K_{Cl^-} from Cheng and Huang (1996)) overestimated the measured ζ-potential by almost 100%. The model fit did not substantially improve when the electrolyte adsorption constants from Meng and Letterman (1993b) ($\log K_{K^+} = -10.4, K_{NO_3^-} = 7.8$) were used. However, the model was most sensitive to K_{Cl^-} as a significantly better model fit was obtained when optimizing this parameter ($\hat{\sigma} = 2.684$, model fit 1). Optimizing more than two parameters at the same time did usually result in rank defiencies during calculation of the derivatives, indicating that some parameters did not improve the model fit and were "dropped" from further variation. Therefore, K_+, K_-, K_{Na}, and K_{Cl^-} were individually optimized until $\hat{\sigma}$ asymptotically approached 1.2 (model fit 2). Surprisingly, however, a similar good correlation of model-fitted to measured data was obtained when utilizing the baseline parameters and optimizing the specific surface area of the solid (model fit 3). The resulting value of $60\,m^2/g$ seems reasonable and is similar to that used by Anderson and Benjamin (1990a) in their modeling studies. An adequate fit was also achieved when either a surface site concentration of 18 mol per mol $Al(OH)_3(s)$, an inner layer capacitance C_1 of $0.15\,F/m^2$, or an outer layer capacitance C_2 of $0.09\,F/m^2$ was utilized (Table 5.3, model fit 4, 5, 6). These observations indicate that it is difficult, if not impossible, to obtain a unique set of parameters that adequately

Table 5.3. Best fit model parameters.

Parameter	Unit	Base	Fit 1	Fit 2	Fit 3	Fit 4	Fit 5	Fit 6
$\log K_+$	–	8.0	8.0	7.96	8.0	8.0	8.0	8.0
$\log K_-$	–	-10.2	-10.2	-10.72	-10.2	-10.2	-10.2	-10.2
$\log K_{Cl^-}$	–	8.2	9.095	9.63	8.2	8.2	8.2	8.2
$\log K_{Na^+}$	–	-9.1	-9.1	-8.80	-9.1	-9.1	-9.1	-9.1
A_S	m^2/g	965	965	965	60	965	965	965
$T_{\equiv AlOH}$	$\frac{mol}{mol\ Al(OH)_3(s)}$	1.0	1.0	1.0	1.0	16.4	1.0	1.0
C_1	F/m^2	1.4	1.4	1.4	1.4	1.4	0.135	1.4
C_2	F/m^2	0.2	0.2	0.2	0.2	0.2	0.2	0.079
$\hat{\sigma}$	–	3.604	2.684	1.203	1.094	1.120	1.729	2.675

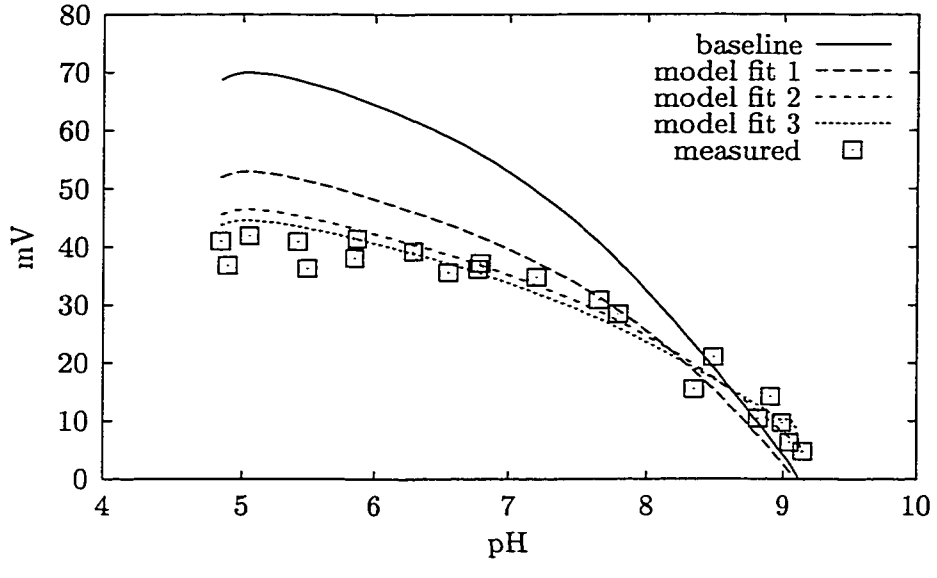

Figure 5.2. Best fit diffuse layer potential ψ_d and measured ζ-potential of aluminum hydroxide.

describes the ζ-potential of freshly precipitated $Al(OH)_3(s)$ particles as a function of pH.

For the remainder of this work, the parameters determined with model fit 2 were used. The speciation of the surface complexes on $Al(OH)_3(s)$ in the electrolyte solution is shown in Figure 5.3. These data indicate that uncharged $\equiv AlOH$ groups predominate over the whole pH range. The surface charge is therefore influenced by surface complexes that account for less than 10% of the total amount of hydroxyl groups. Chloride, which forms $\equiv AlOH_2^+Cl^-$, appears to suppress the positive surface charge that is imparted by $\equiv AlOH_2^+$. The plot also shows that at the pH_{iep} near pH 9, $[\equiv AlOH_2^+] \approx [\equiv AlO^-]$ and $[\equiv AlOH_2^+Cl^-] \approx [\equiv AlO^-Na^+]$. Therefore, the charge in both the 0-layer, σ_0, and the β-layer, σ_β, becomes zero, satisfying the charge balance at the pH_{iep}, i.e., the total charge within the diffuse layer $\sigma_d = -\sigma_0 - \sigma_\beta = 0$.

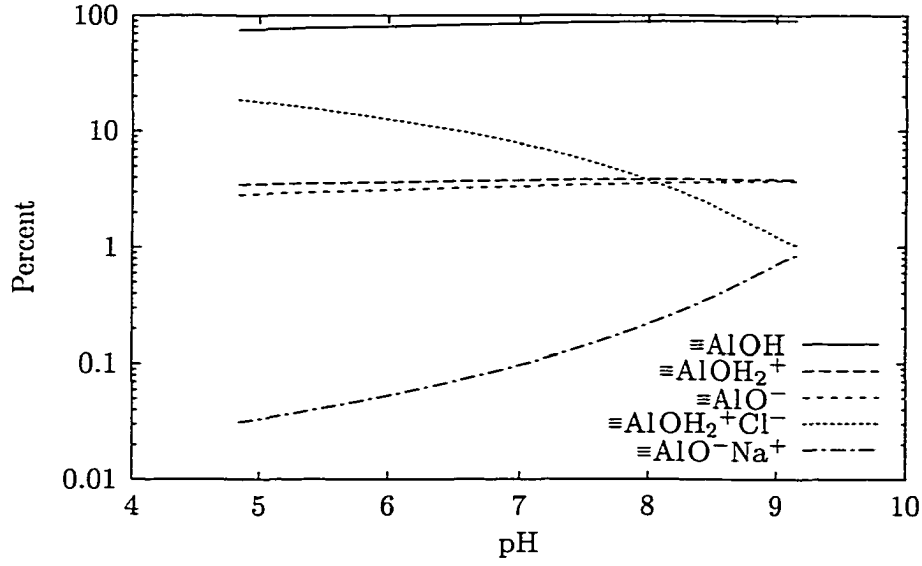

Figure 5.3. Speciation of surface complexes on $Al(OH)_3(s)$.

5.3.2. Adsorption of Inorganic Anions

Fitting measured dissolved sulfate concentrations to the model did usually not yield satisfactory results when considering complexes that adsorb to the β-layer ($\hat{\sigma} > 5$). Meng and Letterman (1993b) made a similar observation when modeling the adsorption of sulfate to aluminum hydroxide covered silica particles. It was also necessary to invoke multiple site coverage, i.e., to utilize stoichiometric coefficients $\bar{n} > 1$ (surface sites per sulfate ion) in

the mass balance equation. Depending on the selected surface complexation reactions, $\hat{\sigma}$ was at a minimum when either three, four or five surface hydroxyl groups were covered by one adsorbed sulfate ion. An adequate fit of the dissolved sulfate concentration could be achieved with almost any combination of reactions. However, sulfate surface complexes with a charge < -1 ($\equiv AlOSO_4^{3-}$, $\equiv AlOHSO_4^{2-}$) caused charge reversal in the examined pH range. The reactions

$$\equiv AlOH + H^+ + SO_4^{2-} \rightleftharpoons \equiv AlSO_4^- + H_2O \qquad \log K = 9.412$$

$$\equiv AlOH + 2H^+ + SO_4^{2-} \rightleftharpoons \equiv AlHSO_4^0 + H_2O \qquad \log K = 16.896$$

using a stoichiometric coefficient of $\bar{n} = 5$ in the mass balance resulted in $\hat{\sigma} = 1.10$. The model reactions illustrate that sulfate adsorption either needs to be accompanied by proton consumption or requires the presence of positively charged surface hydroxyl groups (Note that $\equiv AlOH + H^+ \rightleftharpoons \equiv AlOH_2^+$). A graphical comparison of the model-fitted and the measured variables is provided in Figures 5.4 and 5.5. At the extremes of the examined pH range, the fitted sulfate concentrations were generally higher than the measured values. The ψ_d values are in good agreement with the measured ζ-potentials.

In order to correctly model the adsorption of orthophosphate to aluminum hydroxide, the acid/base chemistry of PO_4^{3-} was included in the model according to the reactions shown below. The acidity constants were taken from the thermodynamic database of PHREEQC (Parkhurst and Appelo, 1999).

$$H^+ + PO_4^{3-} \rightleftharpoons HPO_4^{2-} \qquad \log K = 12.346$$

$$2H^+ + PO_4^{3-} \rightleftharpoons H_2PO_4^- \qquad \log K = 19.553$$

$$3H^+ + PO_4^{3-} \rightleftharpoons H_3PO_4 \qquad \log K = 21.7$$

Because the adsorption of orthophosphate appeared to be sorbent-limited, finding a unique set of reactions through optimization proved to be difficult. Nearly any combination of uncharged, mono-, di-, and trivalent surface complexes provided a satisfactory result ($\hat{\sigma} \approx 1$). It was also observed that in some cases, the optimum equilibrium constants depended on the initial guesses. Therefore, a solution was sought that adequately predicted the measured ζ-potentials and also converged independently of the initial guess. Only a

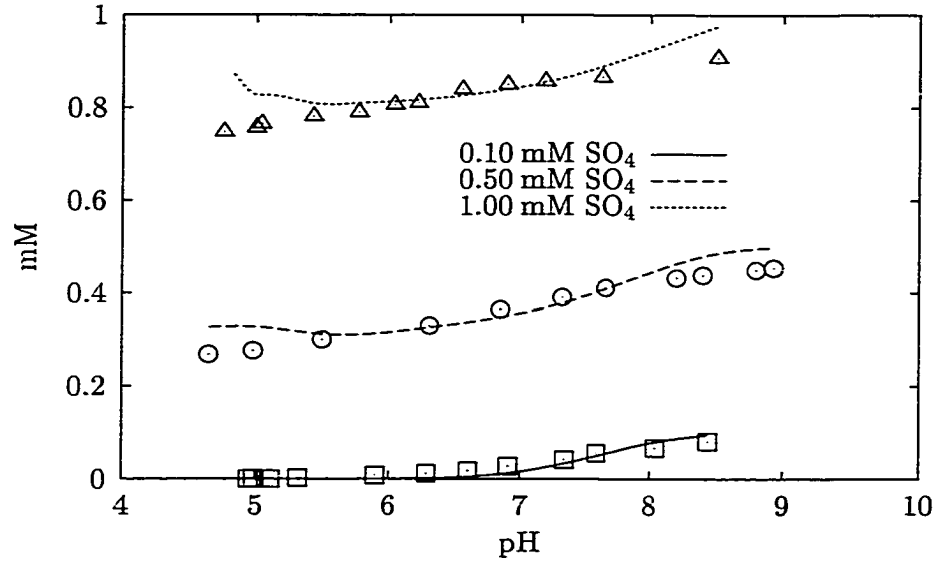

Figure 5.4. Model-fitted and measured dissolved sulfate concentration as a function of pH.

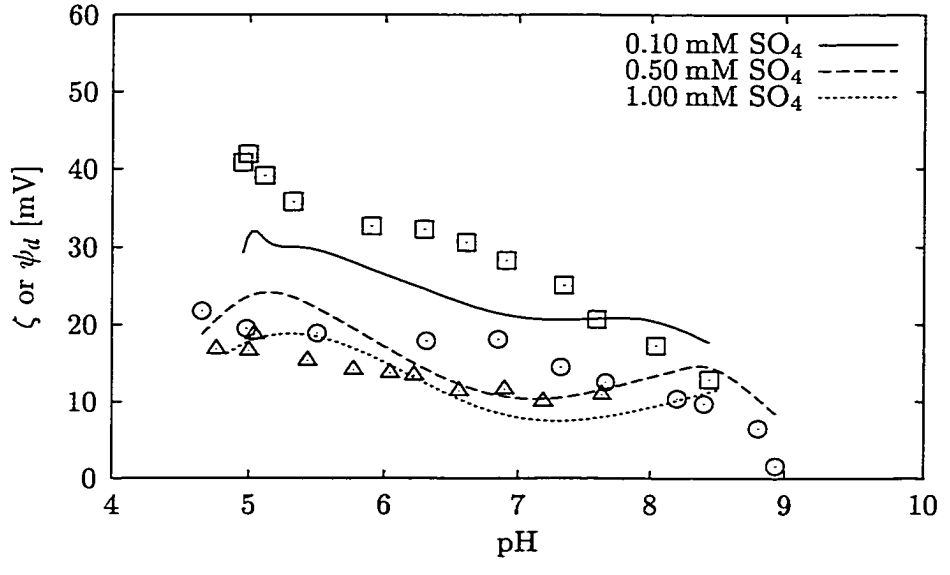

Figure 5.5. Model-predicted diffuse layer potential ψ_d and measured ζ-potential of aluminum hydroxide in the presence of sulfate as a function of pH.

single surface complexation reaction was necessary ($\hat{\sigma} = 1.989$):

$$\equiv AlOH + H^+ + PO_4^{3-} \rightleftharpoons \equiv AlPO_4^{2-} + H_2O \qquad \log K = 16.314$$

The stoichiometry of the mass balance did not require modification. The modeling results are shown in Figures 5.6 and 5.7. Although the pH_{iep} was predicted correctly, ψ_d was substantially lower than the measured ζ-potential at pH < 8, which may be a result of the absence of lower charged surface complexes. However, the addition of $\equiv AlHPO_4^-$ or $\equiv AlH_2PO_4^0$ to the model did not improve the fit. Although two orthophosphate solution species, HPO_4^{2-} and $H_2PO_4^-$, predominate in the examined pH range, a similar speciation may not occur at the aluminum hydroxide surface. It has also be recognized that a good correlation to the experimental data does not necessarily prove the existence or absence of a particular surface complex.

Modeling results for fluoride adsorption to aluminum hydroxide are shown in Figures 5.8 and 5.9. Similar to orthophosphate, a single reaction seemed to well describe the removal of fluoride from solution (Figure 5.8, $\hat{\sigma} = 1.558$):

$$\equiv AlOH + H^+ + F^- \rightleftharpoons \equiv AlF + H_2O \qquad \log K = 11.142$$

These figures also show that the model can accurately mimic the increase in dissolved fluoride concentration at pH < 6 due to the formation of fluoroaluminum complexes (Section 2, Table 2.1) and the negligible impact that the uncharged surface complex has on ζ-potential (Figure 5.9).

5.3.3. Adsorption of Simple Organic Acids

Fitting model-predicted concentrations of dissolved organic acids to the experimental data proceeded in the same manner as above. The acid/base reactions of these acids were included utilizing the acidity constants listed in Section 4 (Table 4.1). Where the thermodynamic data were available, the formation of organic acid–aluminum complexes was incorporated in the model. These included the complexes formed by phthalic, salicylic, and oxalic acid (refer to Section 4, Table 4.5).

Utilizing the mono- and the divalent surface complex to simulate the adsorption of phthalic acid to aluminum hydroxide yielded almost the same fit as the uncharged and

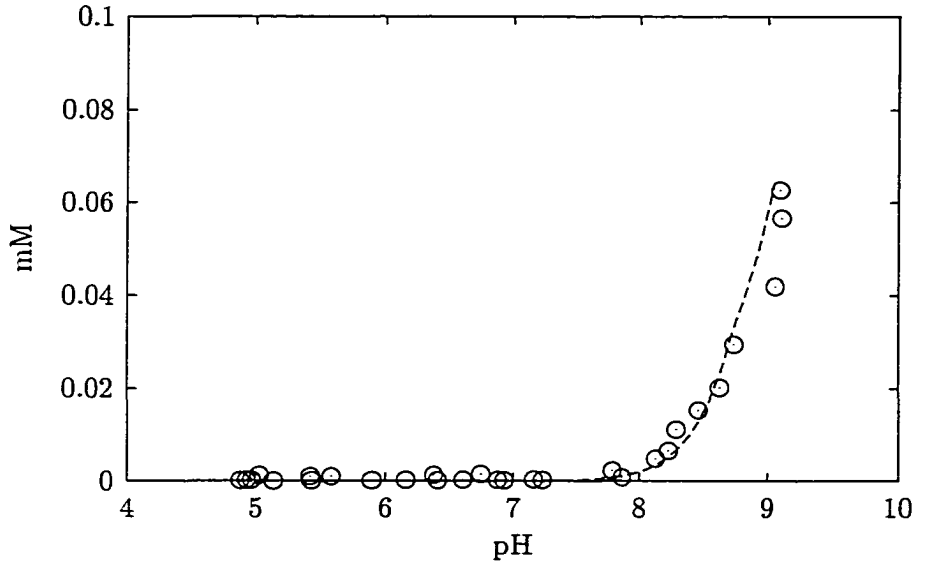

Figure 5.6. Model-fitted and measured dissolved orthophosphate concentration as a function of pH.

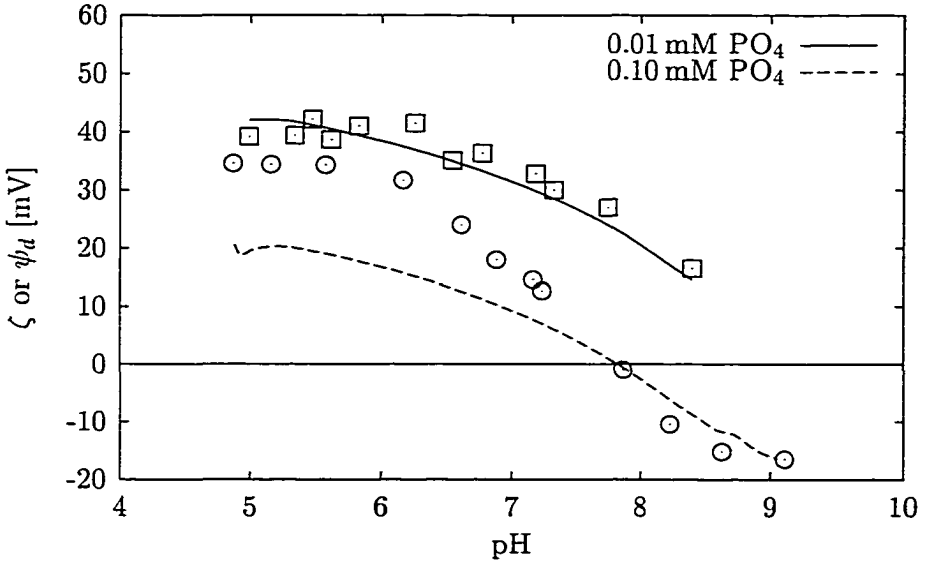

Figure 5.7. Model-predicted diffuse layer potential ψ_d and measured ζ-potential of aluminum hydroxide in the presence of orthophosphate as a function of pH.

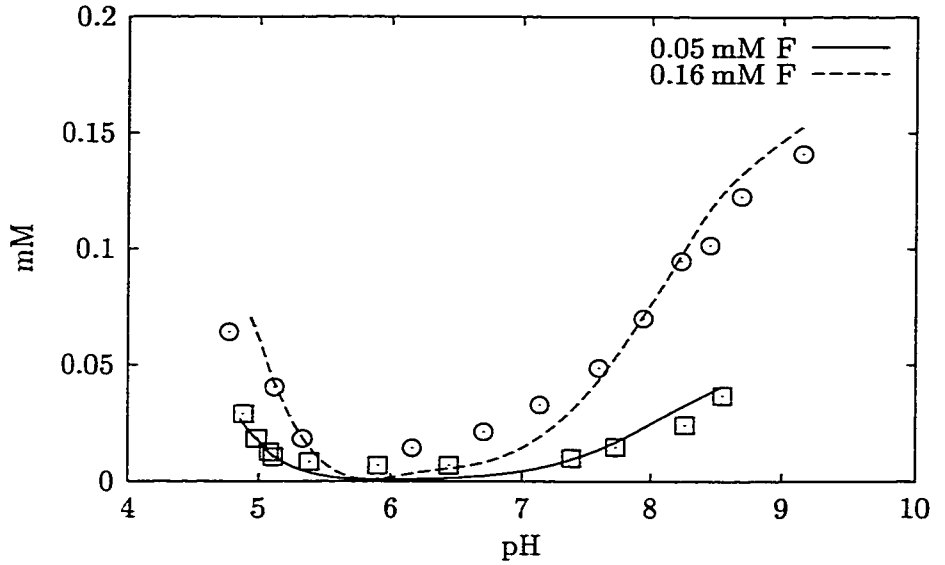

Figure 5.8. Model-fitted and measured dissolved fluoride concentration as a function of pH.

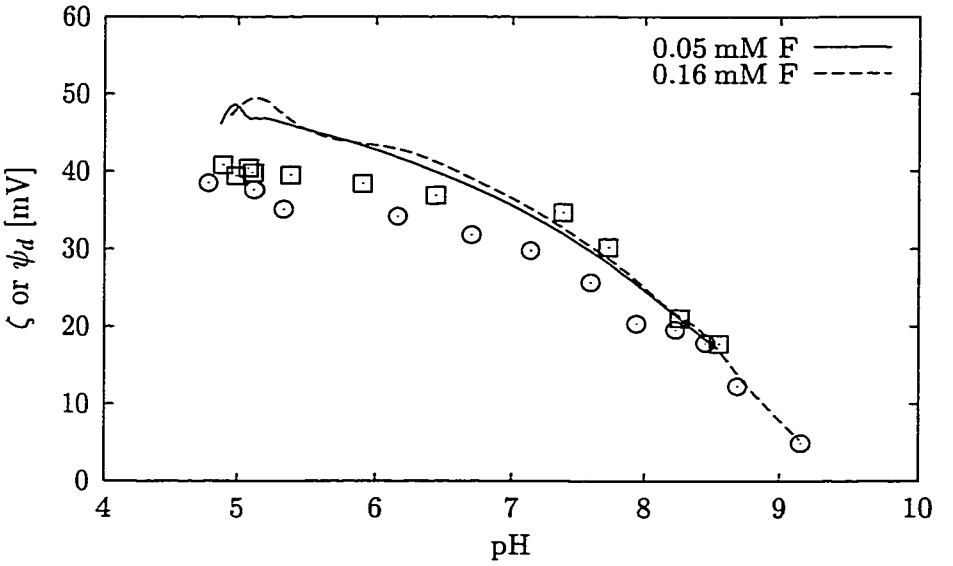

Figure 5.9. Model-predicted diffuse layer potential ψ_d and measured ζ-potential of aluminum hydroxide in the presence of fluoride as a function of pH.

divalent surface complex. The latter combination of surface complexes was also used by Ali and Dzombak (1996a), who investigated the adsorption of phthalic acid to goethite. The best-fit reactions and their associated equilibrium constants ($\hat{\sigma} = 2.543$, $\bar{n} = 2$) are shown below. Model-fitted concentrations and diffuse layer potentials and experimental data are graphically represented in Figures 5.10 and 5.11.

$$\equiv\mathrm{AlOH} + \mathrm{C_8H_4O_4^{2-}} \rightleftharpoons \equiv\mathrm{AlO\,C_8H_4O_4^{3-}} + \mathrm{H^+} \qquad \log K = -8.813$$

$$\equiv\mathrm{AlOH} + \mathrm{C_8H_4O_4^{2-}} \rightleftharpoons \equiv\mathrm{AlOH\,C_8H_4O_4^{2-}} \qquad \log K = -0.550$$

ζ-potential was not measured in the experiment with the 0.10 mM phthalic acid dose. Although the model slightly overpredicted the impact on ζ-potential, the model-fitted data illustrate that phthalic acid had little influence on the $\mathrm{pH_{iep}}$ as observed in the experiment.

Model-fitted and measured dissolved salicylic acid concentrations are shown in Figure 5.12 and these data are in excellent agreement ($\hat{\sigma} = 1.553$). Surface complexation was modeled according to the reaction below and using $\bar{n} = 3$.

$$\equiv\mathrm{AlOH} + \mathrm{C_7H_4O_3^{2-}} \rightleftharpoons \equiv\mathrm{AlOH\,C_7H_4O_3^{2-}} \qquad \log K = 6.414$$

A minimum in dissolved salicylic acid concentration, which corresponds to a maximum in surface concentration, can be observed between pH 5.5–6. The speciation calculated with the model (not shown) indicated that the decrease in removal from solution below pH 5.5 is predominantly due to the formation of soluble aluminum-salicylate complexes. Similar to the other anions, the impact of salicylic acid on ζ-potential is slightly overpredicted (i.e., the predicted ζ-potential is lower than the measured value).

The model also simulated the adsorption of oxalic acid well (Figure 5.14). Utilizing more than a single reaction did not result in further improvement of the model fit ($\hat{\sigma} = 0.609$, $\bar{n} = 4$).

$$\equiv\mathrm{AlOH} + \mathrm{H^+} + \mathrm{C_2O_2^{2-}} \rightleftharpoons \equiv\mathrm{AlC_2O_2^-} + \mathrm{H_2O} \qquad \log K = 10.296$$

With these parameters, the model-calculated diffuse layer potentials were in good agreement with the measured ζ-potentials (Figure 5.15). Although the predicted values were higher at the 0.20 mM dose between pH 6–8, the model seems to accurately simulate certain nuances

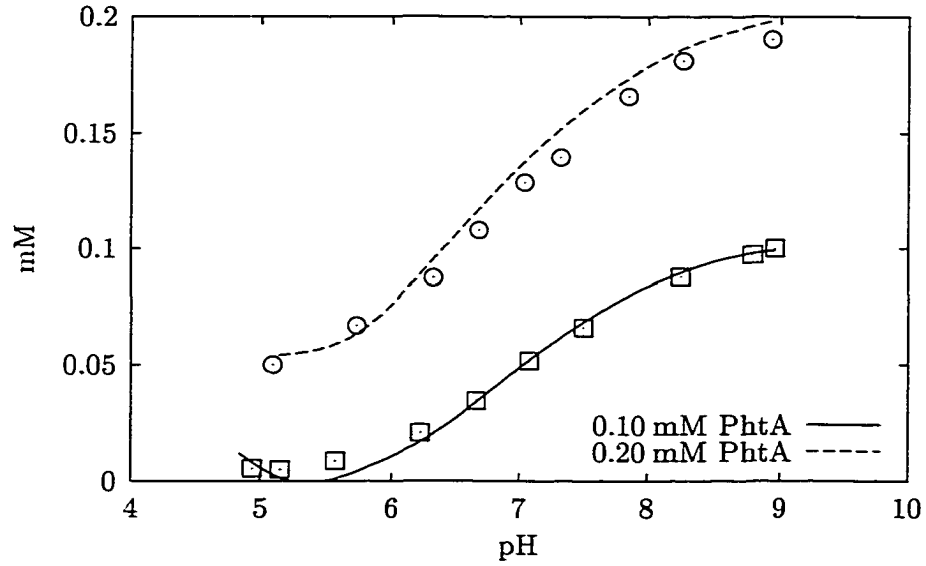

Figure 5.10. Model-fitted and measured dissolved phthalic acid concentration as a function of pH.

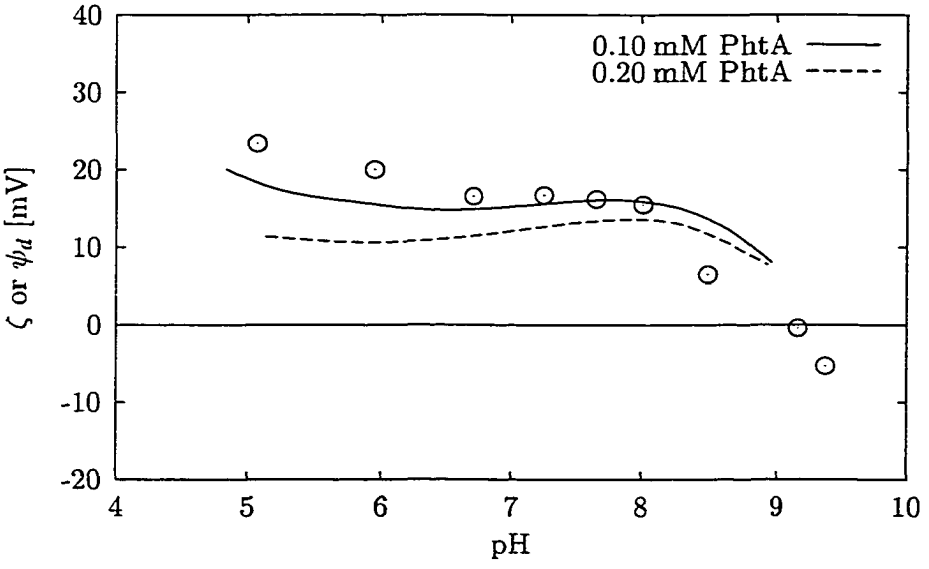

Figure 5.11. Model-predicted diffuse layer potential ψ_d and measured ζ-potential of aluminum hydroxide in the presence of phthalic acid as a function of pH.

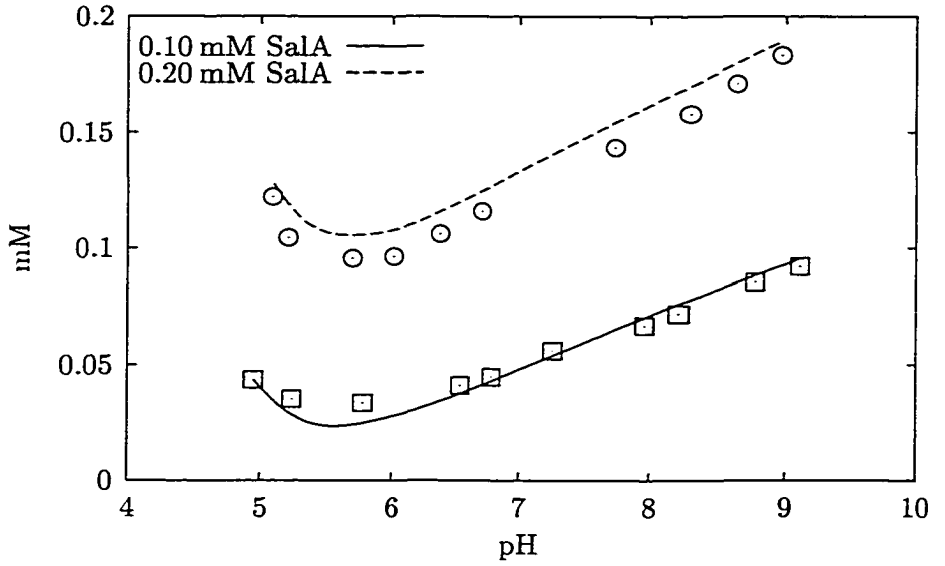

Figure 5.12. Model-fitted and measured dissolved salicylic acid concentration as a function of pH.

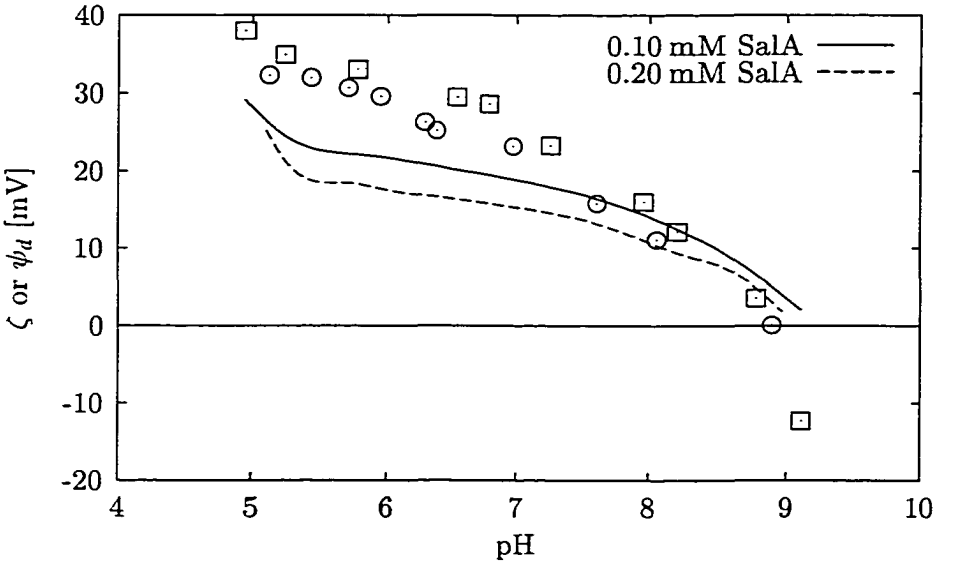

Figure 5.13. Model-predicted diffuse layer potential ψ_d and measured ζ-potential of aluminum hydroxide in the presence of salicylic acid as a function of pH.

in the observed ζ versus pH curve, e.g., the inflection near pH 8.5 and the nearly horizontal trend between pH 6–8.

In modeling the adsorption of pyrogallic acid to aluminum hydroxide, several types of surface complexes resulted in equally low residual standard deviations, $\hat{\sigma}$. Incorporating only the monocharged surface complex ($\equiv AlHL^-$) in the model provided an excellent fit ($\hat{\sigma} = 0.699$, $\bar{n} = 2$), but effect on the pH_{iep} was underpredicted. Using only $\equiv AlOHL^{3-}$ yielded $\hat{\sigma} = 0.880$, but in this scenario, all phenolic groups on the organic molecule would be ionized, which may be chemically unrealistic. Modeling the reaction

$$\equiv AlOH + H^+ + C_6H_3O_3^{3-} \rightleftharpoons \equiv AlC_6H_3O_3^{2-} + H_2O \qquad \log K = 22.253$$

provided a satisfactory correlation to the measured concentratons ($\hat{\sigma} = 0.669$, $\bar{n} = 2$, Figure 5.16) and also seemed to adequately mimic the measured trends in ζ-potential (Figure 5.17) including a shift in pH_{iep} to lower pH, i.e., charge reversal at pH > 7.5. Potentially, dissolved aluminum-pyrogallic acid complexes may exist. However, based on the good modeling results, including them is not likely to provide a better fit of dissolved concentrations, although they may be significant for predicting the effects on ζ-potential.

Determining best-fit parameters for the adsorption of pyromellitic acid was difficult because results exhibited a strong influence of initial guess for $\log K$. Despite this shortcoming, an acceptable solution modeling a single surface complexation reaction of the type

$$\equiv AlOH + C_{10}H_2O_4^{4-} \rightleftharpoons \equiv AlOC_{10}H_4O_4^{5-} + H^+ \qquad \log K = -8.922$$

was found ($\hat{\sigma} = 1.657$, $\bar{n} = 2$, Figure 5.18). As pointed out earlier, the chemical nature of this surface complex may be questionable as it would require the combination of fully ionized carboxyl groups ($-COO^-$) with a negatively charged surface hydroxyl group ($\equiv AlO^-$). However, based on the decrease in surface charge per mol adsorbed ion computed from ζ-potential measurements and surface concentrations, it was observed that pyromellitic acid has approximately twice the impact than the other simple organic acids examined in this work (Section 4). Accordingly, it was proposed that it forms higher negatively charged surface complexes. The modeling results seem to confirm this proposition.

The model also produced a poor prediction for the ζ-potentials (Figure 5.19). The ψ_d values are approximately 20 mV higher than ζ over a wide pH range. However, when

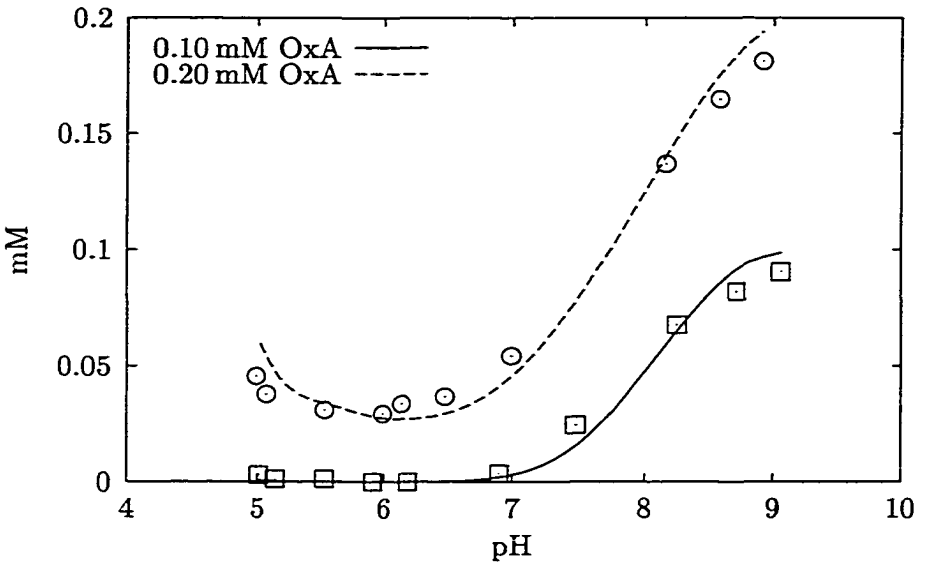

Figure 5.14. Model-fitted and measured dissolved oxalic acid concentration as a function of pH.

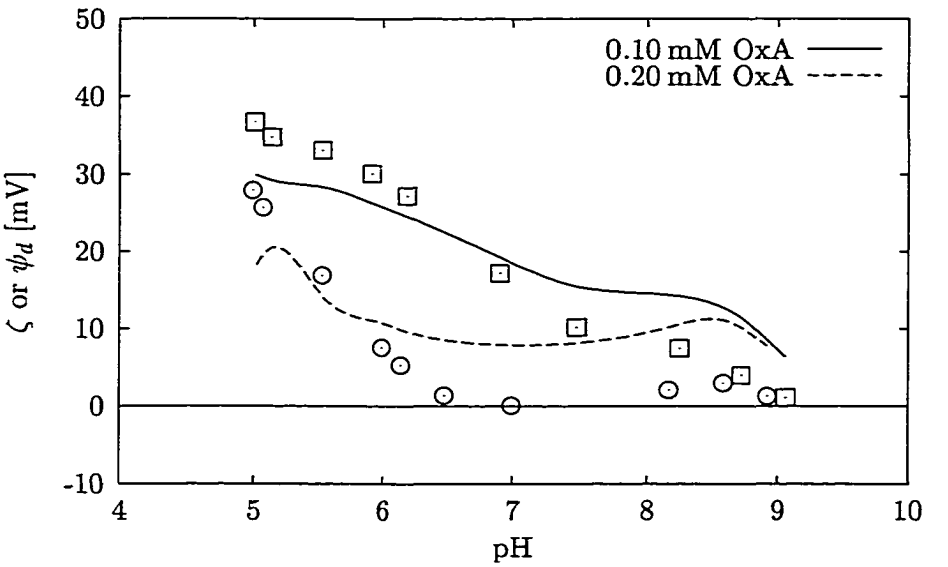

Figure 5.15. Model-predicted diffuse layer potential ψ_d and measured ζ-potential of aluminum hydroxide in the presence of oxalic acid as a function of pH.

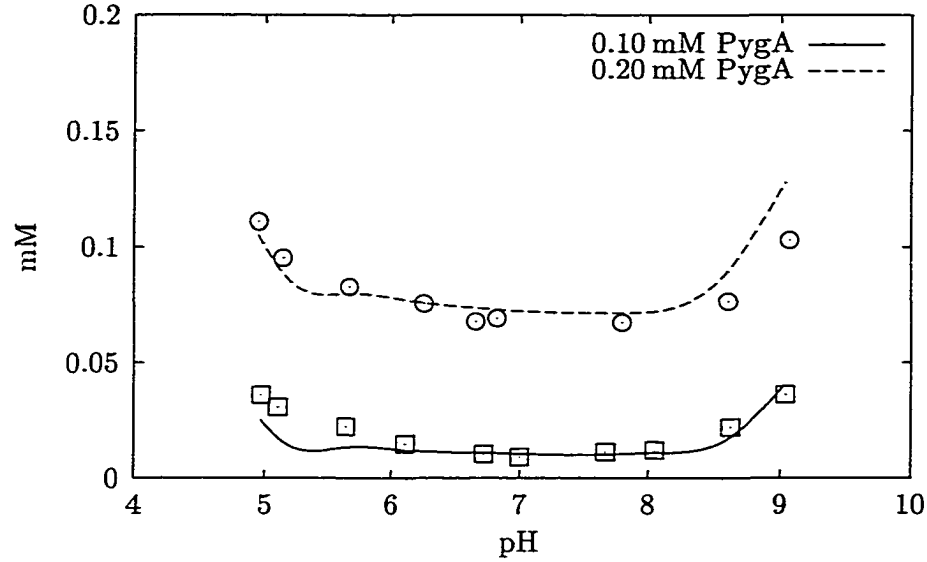

Figure 5.16. Model-fitted and measured dissolved pyrogallic acid concentration as a function of pH.

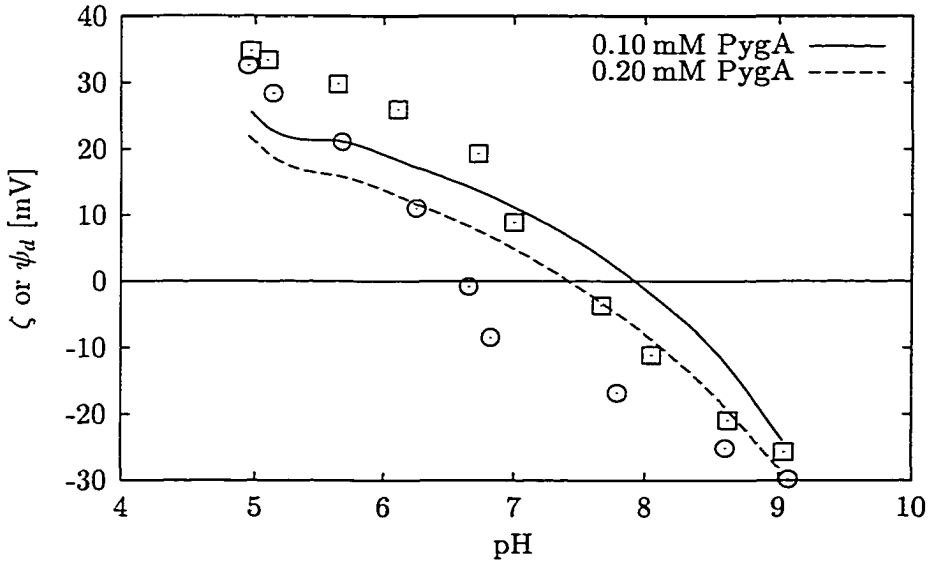

Figure 5.17. Model-predicted diffuse layer potential ψ_d and measured ζ-potential of aluminum hydroxide in the presence of pyrogallic acid as a function of pH.

vertically shifting the modelled data to more negative values, it can be observed that the predicted trend agrees with the measured data.

5.3.4. Adsorption of Natural Organic Acids

To model the adsorption of Aldrich humic acid and Dismal Swamp organic matter (DSOM) to aluminum hydroxide, the substances were represented as if they were composed of a mixture of three monoprotic acids (HL_1, HL_2, HL_3). The acidity constants and relative concentrations of the model acids representing Aldrich humic acid and DSOM have been previously evaluated using titration data (Section 4, Table 4.2). A reevaluation using ODRPACK yielded results that were in excellent agreement with those determined using FITEQL (Table 5.4). The doses of Aldrich humic acid and DSOM used in the experiments corresponded to model acid concentrations according to Table 5.5.

Similar to pyromellitic acid, modeling the adsorption of Aldrich humic acid also required careful selection of the initial guesses for the equilibrium constants of the adsorption reactions that are listed below.

$$\equiv AlOH + L_1^- \rightleftharpoons \equiv AlOHL_1^- \qquad \log K_1 = 4.014$$

$$\equiv AlOH + L_2^- \rightleftharpoons \equiv AlOHL_2^- \qquad \log K_2 = 5.073$$

$$\equiv AlOH + L_3^- \rightleftharpoons \equiv AlOHL_3^- \qquad \log K_3 = 3.506$$

Although it cannot be ascertained that the iteration converged to a global optimum for the weighted sum of squared residuals, the simple representation of this complex substance seems to have produced an acceptable result ($\hat{\sigma} = 1.209$, $\bar{n} = 1$, Figure 5.20). The resulting speciation indicated that the most acidic model compound with a $\log K_a$ of -4.173 was completely adsorbed at low pH and removal decreased with pH > 7, whereas HL_2 ($\log K_a$ = -6.206) was eliminated from solution over the whole pH range. Approximately 80% of the model acid with $\log K_a = -8.646$ was adsorbed and maximum removal occurred near pH 7 (90%). This observation seems to indicate that more acidic fractions are removed preferentially at low pH.

As the model reactions indicate, it was necessary to assume formation of a surface complex that may not exist in reality. However, it has been suggested that humic acid

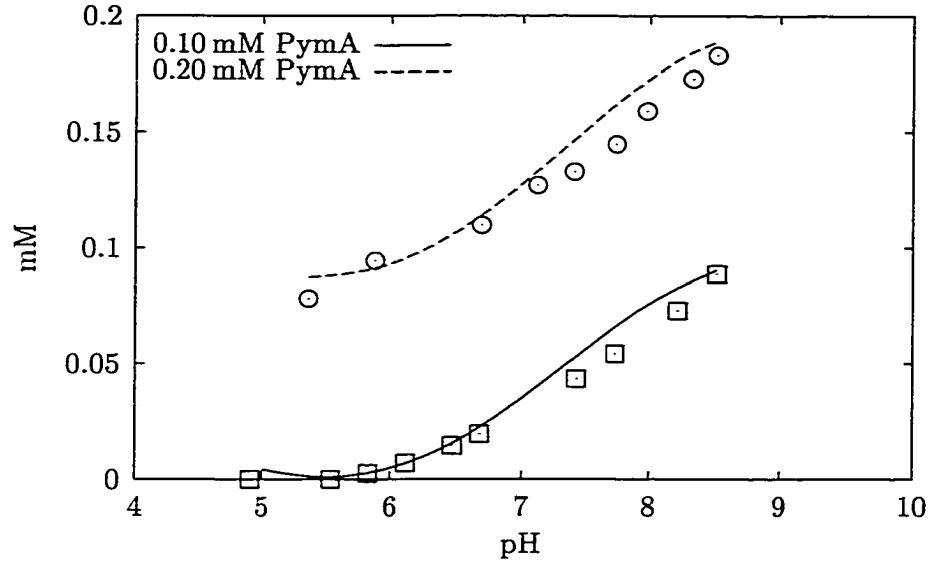

Figure 5.18. Model-fitted and measured dissolved pyromellitic acid concentration as a function of pH.

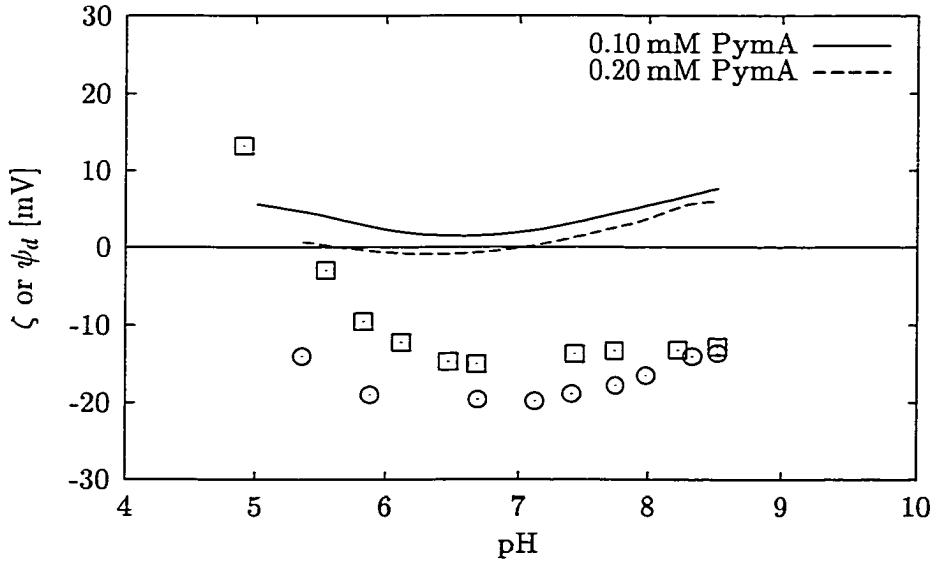

Figure 5.19. Model-predicted diffuse layer potential ψ_d and measured ζ-potential of aluminum hydroxide in the presence of pyromellitic acid as a function of pH.

Table 5.4. Model Parameters for Aldrich humic acid and Dismal Swamp organic matter extract represented as a mixture of three monoprotic acids.

NOM	Acidity [meq/g C]	$\log K_a$
DSOM	18.05	-3.250
	9.94	-5.986
	16.17	-9.650
HA	4.87	-4.173
	3.05	-6.206
	1.76	-8.646

Table 5.5. Total concentrations of Aldrich humic acid and Dismal Swamp organic matter as represented in the surface complexation model.

	Aldrich Humic acid	Dismal Swamp organic matter	
	0.50 mM C	0.52 mM C	1.02 mM C
T_{L_1} [meq/l]	0.029	0.110	0.220
T_{L_2} [meq/l]	0.018	0.061	0.121
T_{L_3} [meq/l]	0.010	0.097	0.197
Total [meq/l]	0.058	0.27	0.540

adsorption may involve hydrophobic interactions with the adsorbent and thus modeling this process assuming an association reaction may not be appropriate anyway.

Model-predicted diffuse layer potentials and measured ζ-potentials shown in Figure 5.21 did not agree well as the shift in pH_{iep} to lower pH due to adsorption is underestimated.

Convergence problems were also encountered when fitting the adsorption data of DSOM, although good agreement between modeled and measured values for both concentration and surface potentials was eventually achieved utilizing the reactions below ($\hat{\sigma} = 2.221$, $\bar{n} = 1$, Figures 5.22, 5.23).

$$\equiv AlOH + L_1^- \rightleftharpoons \equiv AlOHL_1^- \qquad \log K_1 = 3.253$$

$$\equiv AlOH + L_2^- \rightleftharpoons \equiv AlOHL_2^- \qquad \log K_2 = 0.516$$

$$\equiv AlOH + L_3^- \rightleftharpoons \equiv AlOHL_3^- \qquad \log K_3 = 23.390$$

The speciation of the adsorbed model acids indicated that HL_2 represented the portion of the natural organic matter that largely remained in solution. Both the more and the less acidic fraction ($\log K_a = -3.250, -9.650$) were removed to a greater extent. Therefore, conclusions based on these modeling results correlating acidity and adsorbability have to be made with caution.

5.3.5. Competitive Adsorption of Inorganic and Organic Anions

Results from the single-sorbate modeling were used to test whether the adsorption of both inorganic and organic anions to aluminum hydroxide can be adequately predicted. The best-fit reactions and their associated $\log K$ values were used in the model to compute dissolved adsorbate concentrations and diffuse layer potential. The computer model was set up to compute the weighted residual standard deviation of measured and predicted concentration, $\hat{\sigma}$; no iteration was performed to improve the goodness-of-fit.

The results from the binary adsorbate modeling are summarized in Table 5.6. These data indicate that the weighted residual standard deviations were significantly higher than in the single-sorbate systems, and extremely poor model predictions with $\hat{\sigma} > 10$ were obtained in some cases.

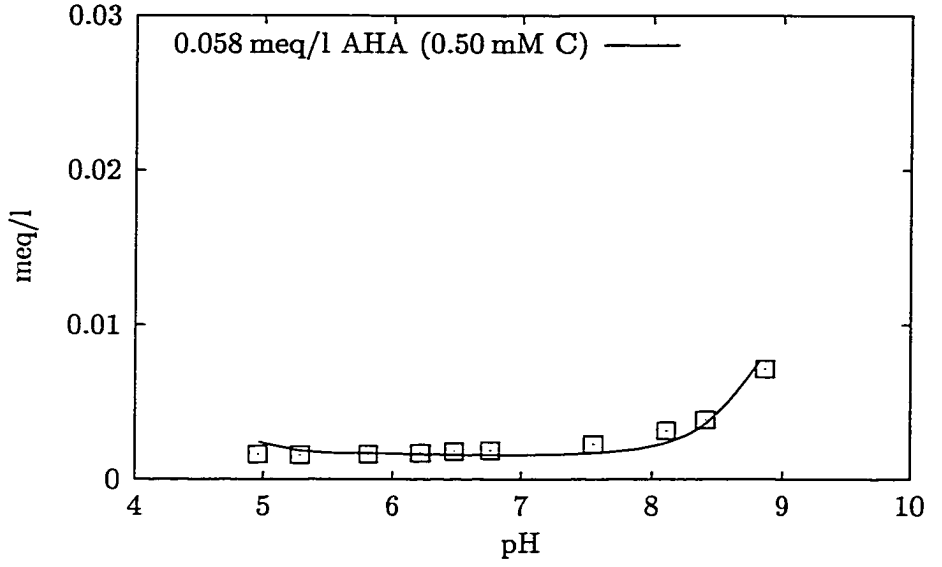

Figure 5.20. Model-fitted and measured dissolved Aldrich humic acid concentration as a function of pH.

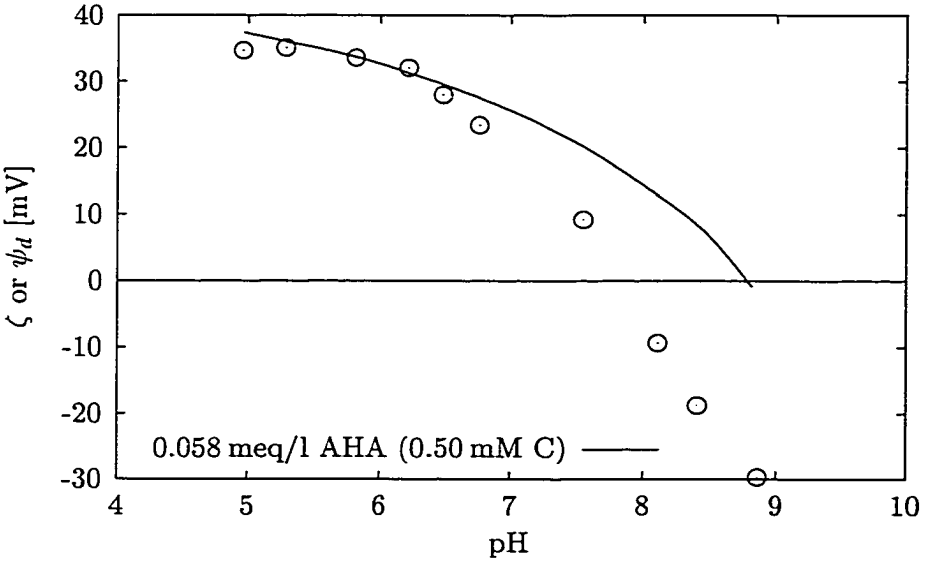

Figure 5.21. Model-predicted diffuse layer potential ψ_d and measured ζ-potential of aluminum hydroxide in the presence of Aldrich humic acid as a function of pH.

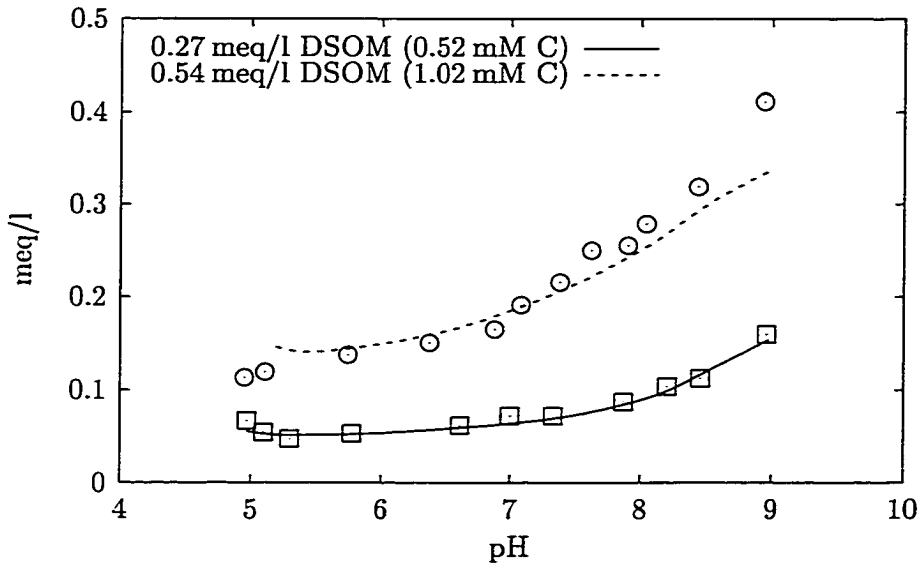

Figure 5.22. Model-fitted and measured dissolved DSOM concentration as a function of pH.

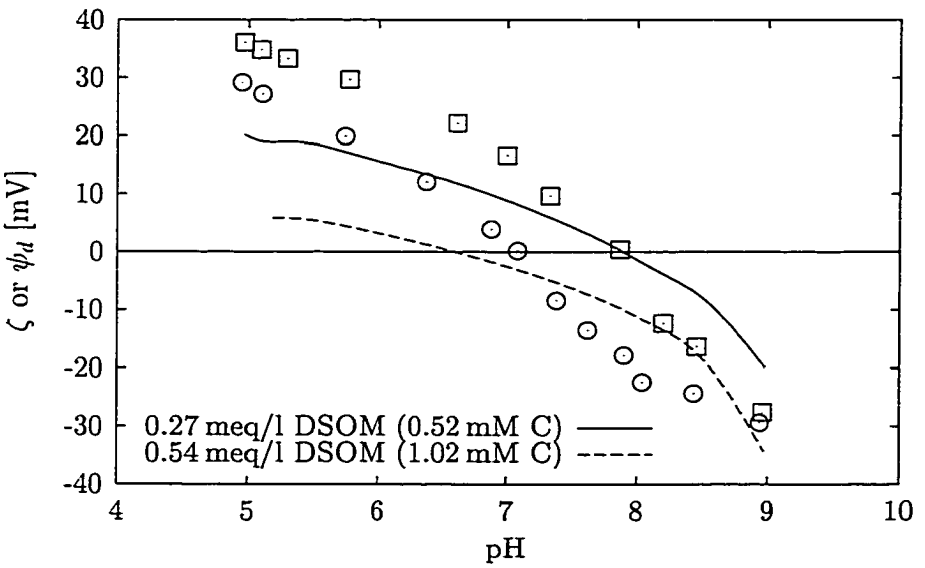

Figure 5.23. Model-predicted diffuse layer potential ψ_d and measured ζ-potential of aluminum hydroxide in the presence of DSOM as a function of pH.

Table 5.6. Weighted residual standard deviations in model predictions of competitive adsorption.

Inorganic Anion	Organic Acid	$\hat{\sigma}$
Sulfate	Phthalic Acid	7.569
	Salicylic Acid	5.341
	Oxalic Acid	5.132
	Pyromellitic Acid	12.93
	Aldrich Humic Acid	47.71
	Dismal Swamp O.M.	11.08
Orthophosphate	Phthalic Acid	45.28
	Salicylic Acid	4.474
	Oxalic Acid	34.97
	Aldrich Humic Acid	18.93
Fluoride	Phthalic Acid	3.864
	Salicylic Acid	3.296
	Oxalic Acid	3.658
	Aldrich Humic Acid	3.262

The ability of sulfate to suppress the removal of organic acids from solution was generally found to be greatly overestimated. Model-predicted and measured dissolved oxalic acid concentrations shown in Figure 5.24 provide an example. Although the experimental

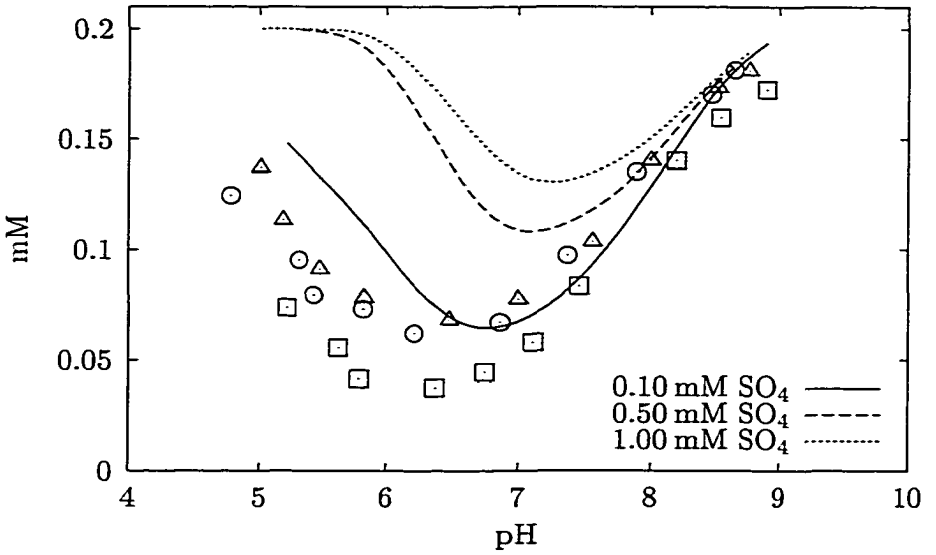

Figure 5.24. Model-predicted and measured dissolved oxalic acid concentration as a function of pH and total sulfate concentration. Total oxalic acid concentration = 0.20 mM.

data indicated that sulfate had only a small impact, the model suggests that oxalic acid adsorption is completely inhibited at lower pH and sulfate doses greater than 0.10 mM. Similar results were obtained for the other organic acids in the presence of sulfate. Due to the consistent overprediction of sulfate adsorption in the binary systems, it seems that the selected surface complexation reactions may not be appropriate. Ali and Dzombak (1996a) modeled the competitive adsorption of sulfate and simple organic acids to goethite, a well characterized, crystalline iron oxide. They incorporated a trivalent sulfate surface complex in the model in addition to those used in this work. However, they also found that the effect of sulfate was substantially exaggerated when it was added at doses greater than the organic acid concentration. They attributed this behavior to the heterogeneity of surface sites. To remediate the resulting discrepancies, it would be required to incorporate multiple (e.g., strong and weak) surface hydroxyl groups in the model as has been done by other researchers (Dzombak and Morel, 1990).

An argument can also made that sulfate does not adsorb to the same layer as the

organic acids, although this was concluded from the single-sorbate modeling studies. The possibility that sulfate adsorbs to the β-layer in the model was rejected based on ζ-potential measurements. Because the impact of adsorbed ions on the calculated diffuse layer potential depends on the interfacial capacitances, it is possible that varying these parameters could yield an adequate prediction of sulfate adsorption to the β-layer and good agreement of ζ and ψ_d potential. It is worth noting that Letterman and Iyer (1985) successfully modeled proton uptake and ζ-potential of aluminum hydroxide coated silica particles as a function of total sulfate concentration at pH 5. They utilized both $\equiv AlOH_2{}^+SO_4{}^{2-}$ and $\equiv AlOH_2{}^+SO_4{}^-$ in their model but did not verify whether sulfate concentrations were correctly calculated.

It was shown previously that different sets of surface parameters adequately fitted the measured ζ-potential of aluminum hydroxide. Therefore, further studies should be conducted to determine how sulfate adsorption can be incorporated in the model in order to achieve reasonable results when organic anions are included.

Model-predicted and measured concentrations of phthalic acid in the presence of orthophosphate are depicted in Figure 5.25, and the corresponding ζ-potential measurements are shown in Figure 5.26. These data illustrate that at pH $>$ 5, the model predicted the impact of orthophosphate on phthalic acid adsorption correctly. The high value for $\hat{\sigma}$ must have been caused by overestimating the effect at pH $<$ 5. In fact, when these data points are removed from the analysis, an acceptable value of $\hat{\sigma} = 2.880$ is obtained.

Similar to the single-sorbate modeling results for orthophosphate and phthalic acid, model-predicted diffuse layer potentials were lower than the measured ζ-potentials. However, at the 0.10 mM PO_4 dose, the pH_{iep} was estimated accurately.

Adequate predictions were also made for the effect of orthophosphate on the adsorption of salicylic and oxalic acid and the associated ζ-potential measurements (Figures 5.27 to 5.30). As with phthalic acid, the high residual standard deviation in the orthophosphate-oxalic acid system was mainly due to overpredicting the residual organic acid concentration at low pH. The concentrations of orthophosphate, which was removed completely and not affected by the presence of the simple organic acids, were also in good agreement with measured values (not shown).

The results from modeling the competitive adsorption of orthophosphate and Aldrich

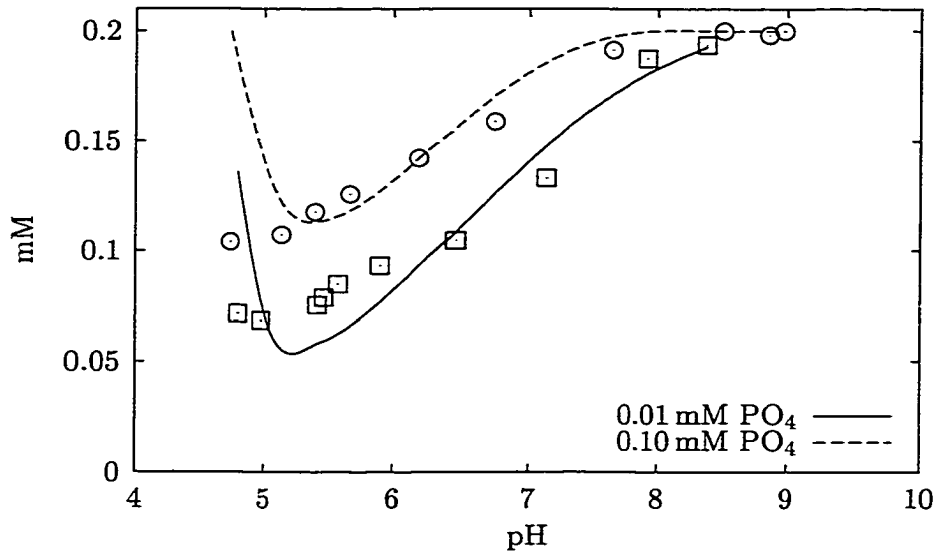

Figure 5.25. Model-predicted and measured dissolved phthalic acid concentration as a function of pH and total orthophosphate concentration. Total phthalic acid concentration = 0.20 mM.

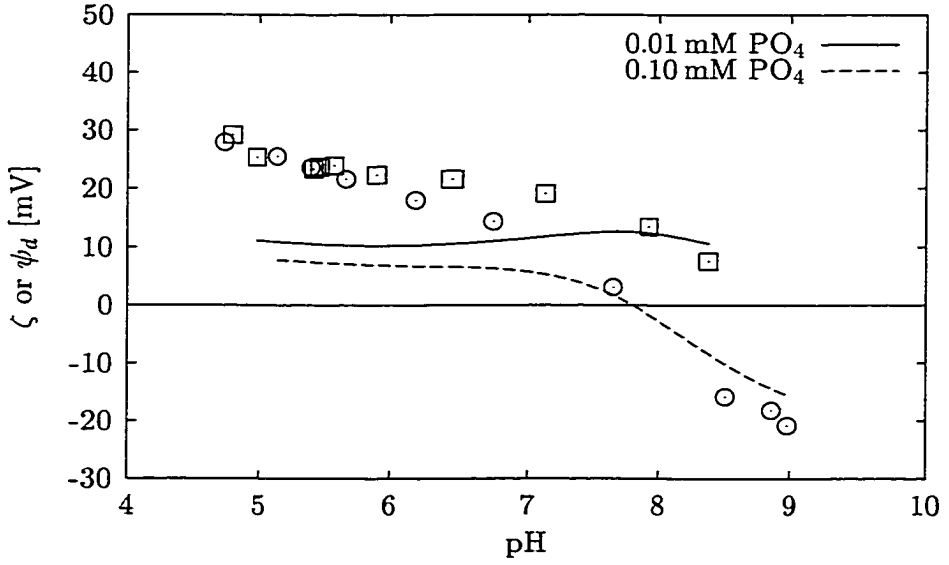

Figure 5.26. Model-predicted diffuse layer potential ψ_d and measured ζ-potential of aluminum hydroxide in the presence of orthophosphate and phthalic acid as a function of pH. Total phthalic acid concentration = 0.20 mM.

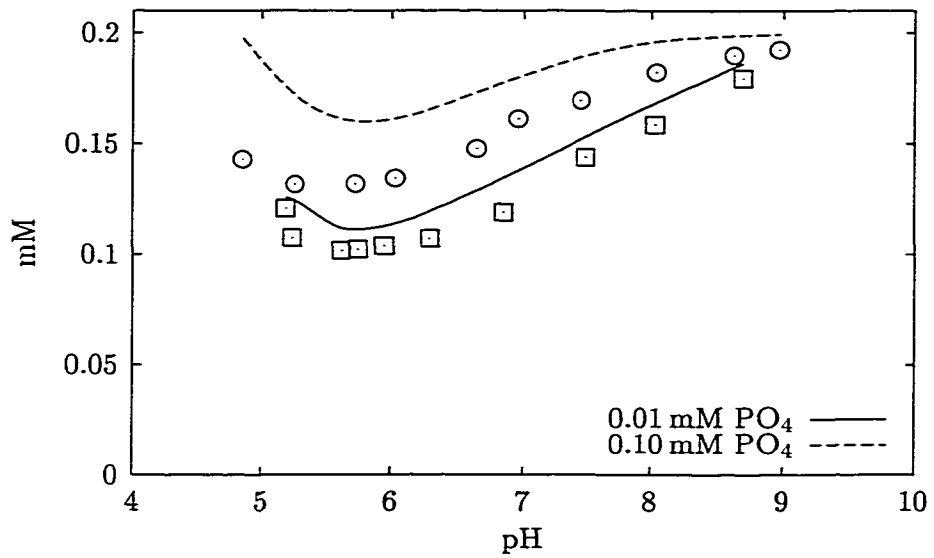

Figure 5.27. Model-predicted and measured dissolved salicylic acid concentration as a function of pH and total orthophosphate concentration. Total salicylic acid concentration = 0.20 mM.

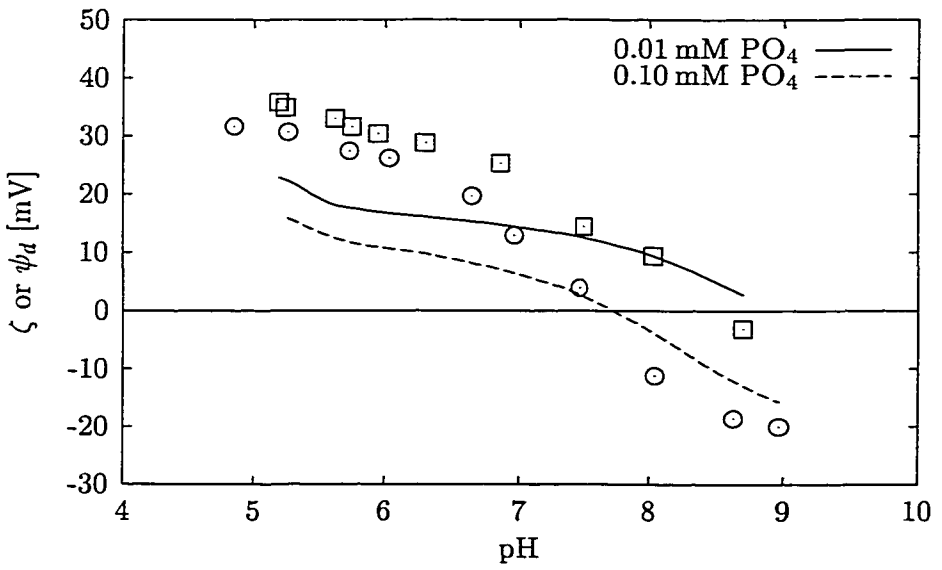

Figure 5.28. Model-predicted diffuse layer potential ψ_d and measured ζ-potential of aluminum hydroxide in the presence of orthophosphate and salicylic acid as a function of pH. Total salicylic acid concentration = 0.20 mM.

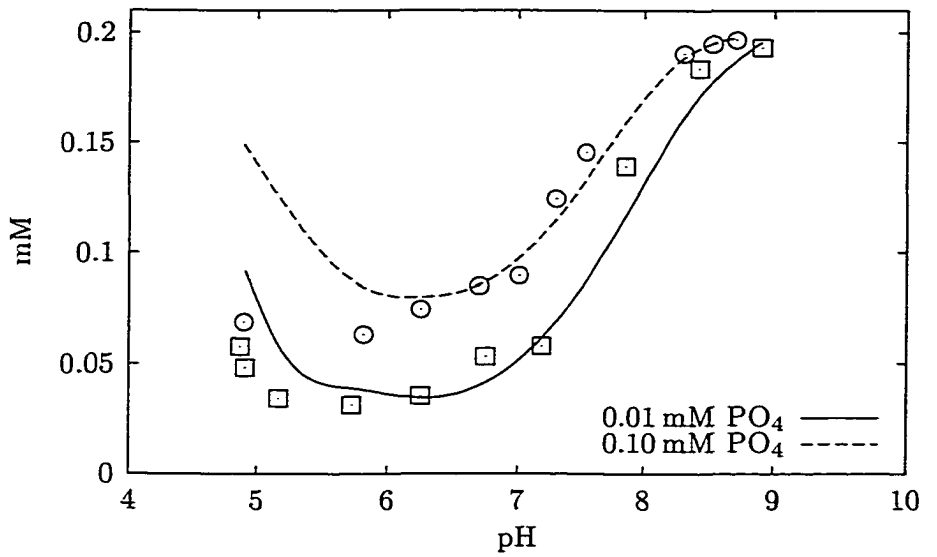

Figure 5.29. Model-predicted and measured dissolved oxalic acid concentration as a function of pH and total orthophosphate concentration. Total oxalic acid concentration = 0.20 mM.

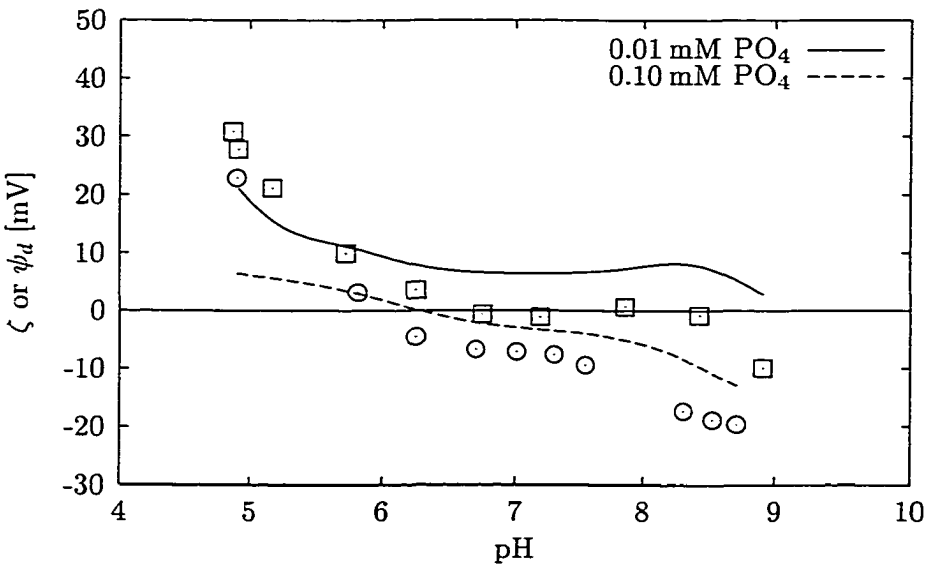

Figure 5.30. Model-predicted diffuse layer potential ψ_d and measured ζ-potential of aluminum hydroxide in the presence of orthophosphate and oxalic acid as a function of pH. Total oxalic acid concentration = 0.20 mM.

humic acid are shown in Figures 5.31 and 5.32. The predicted and measured concentrations agreed well only at the 0.01 mM PO_4 dose (where orthophosphate had little effect) and at pH > 7.5. At both doses, the computed pH_{iep} was approximately one pH unit higher than the experimentally obtained value.

Although the better predictions of competitive adsorption by orthophosphate compared to sulfate may indicate that the model reactions were more appropriate, it has to be kept in mind that sulfate doses were varied over a much greater range of (molar) concentrations. This also applies to the modeling results with fluoride and organic acids, where generally good agreement between predicted and measured values was achieved (Table 5.6). The computational results for phthalic acid, which are graphically shown in figures 5.33 and 5.34, were typical for the interaction of fluoride and organic acids with aluminum hydroxide. The chemical equilibrium computation adequately predicted the small impact that fluoride has on organic acid adsorption and that the ζ-potential was nearly unaffected by the presence of fluoride. At the same time, the experimentally observed impact that different organic acids have on fluoride adsorption, was in good agreement with the model predictions. Examples are provided in Figures 5.35 and 5.36.

5.4. Discussion

The model presented here has shown that to a certain extent, the competitive adsorption of some inorganic and organic anions to aluminum hydroxide can be adequately predicted. Even though the absolute values of the measured ζ-potentials did not always agree with the calculated diffuse layer potentials, ψ_d, the model often estimated correctly the impact on the pH_{iep}. The pH at which the particle charge (and thus electrostatic forces) becomes zero is important for water treatment with metal-salt coagulants. Therefore, the surface complexation modeling approach has the potential for predicting both particle and organic matter removal in multi-sorbate solutions, such as raw waters. However, as the results with sulfate showed, more research is needed. Although a nearly perfect fit was obtained when no competing ion was present, the data from the sulfate-organic acid systems suggested that the model reactions may be inappropriate. Therefore, a model-fit of adsorption and electrokinetic data alone is insufficient to determine the type and stoichiometry of a surface

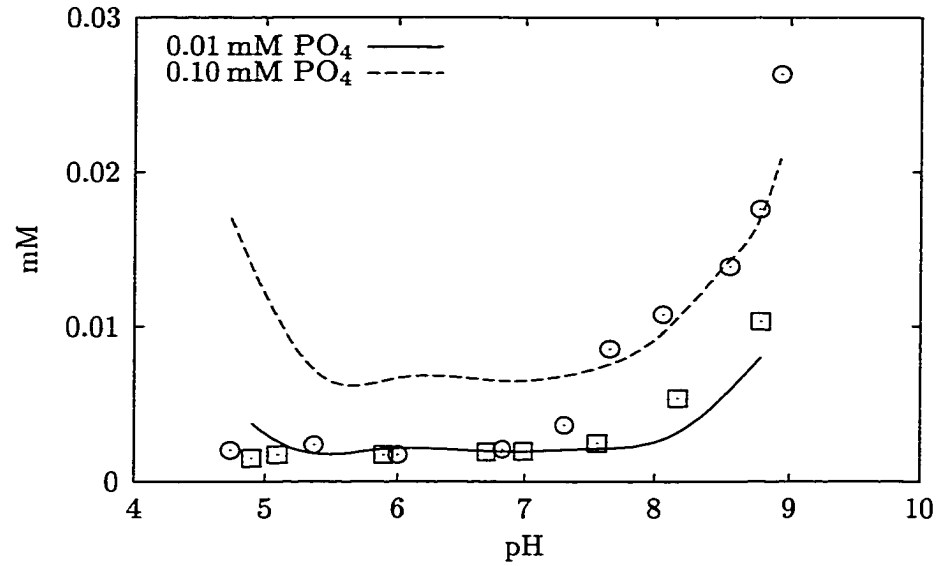

Figure 5.31. Model-predicted and measured dissolved Aldrich humic acid concentration as a function of pH and total orthophosphate concentration. Total Aldrich humic acid concentration = 0.20 mM.

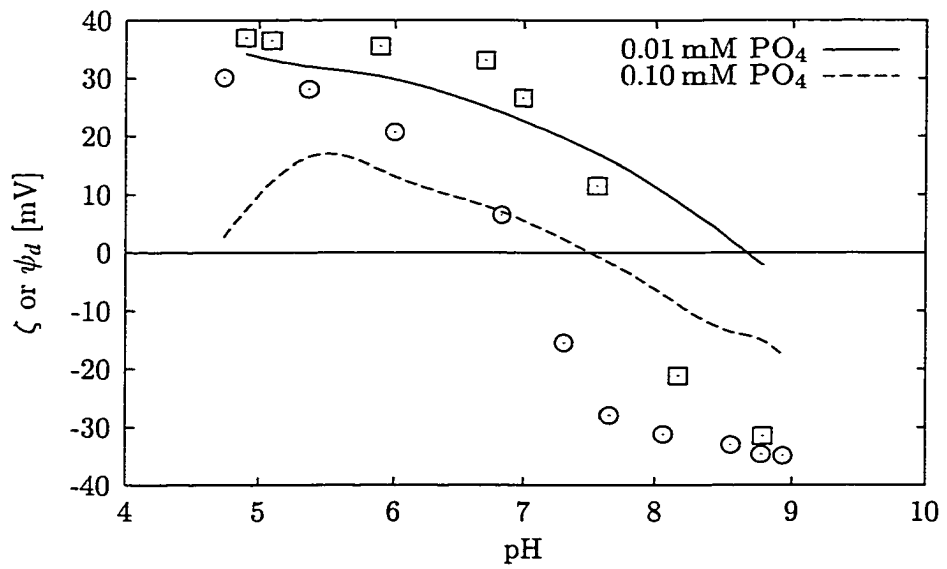

Figure 5.32. Model-predicted diffuse layer potential ψ_d and measured ζ-potential of aluminum hydroxide in the presence of orthophosphate and Aldrich humic acid as a function of pH. Total Aldrich humic acid concentration = 0.058 meq/l.

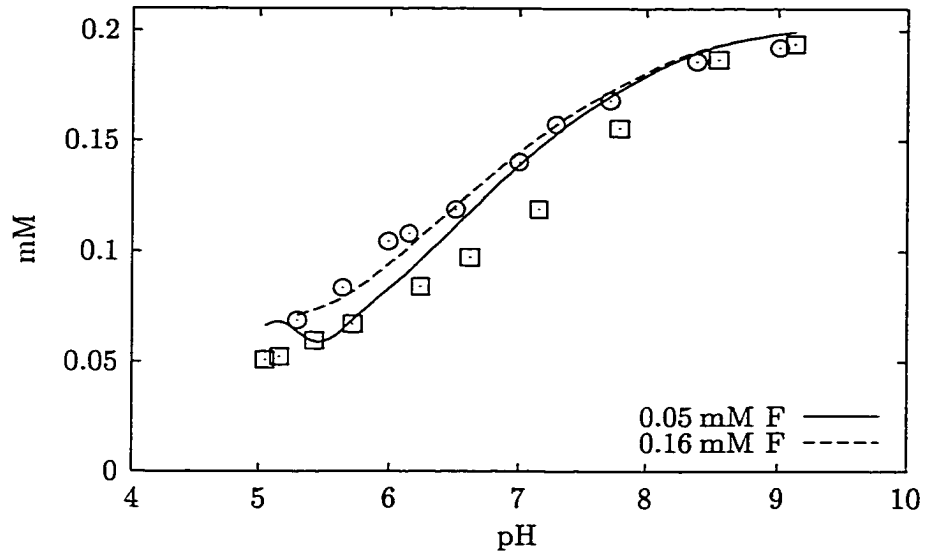

Figure 5.33. Model-predicted and measured dissolved phthalic acid concentration as a function of pH and total fluoride concentration. Total phthalic acid concentration = 0.20 mM.

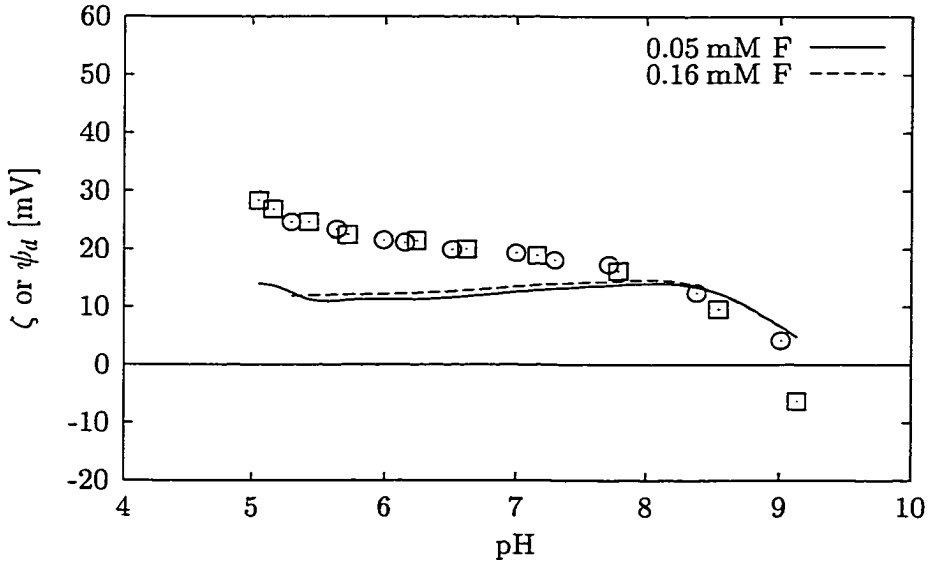

Figure 5.34. Model-predicted diffuse layer potential ψ_d and measured ζ-potential of aluminum hydroxide in the presence of fluoride and phthalic acid as a function of pH. Total phthalic acid concentration = 0.20 mM.

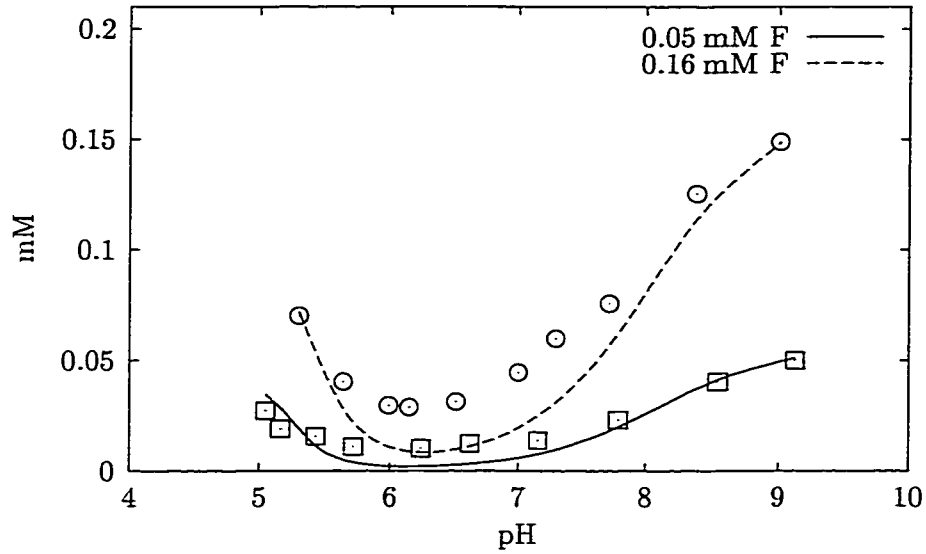

Figure 5.35. Model-predicted and measured dissolved fluoride concentration in the presence of 0.20 mM phthalic acid as a function of pH and total fluoride concentration.

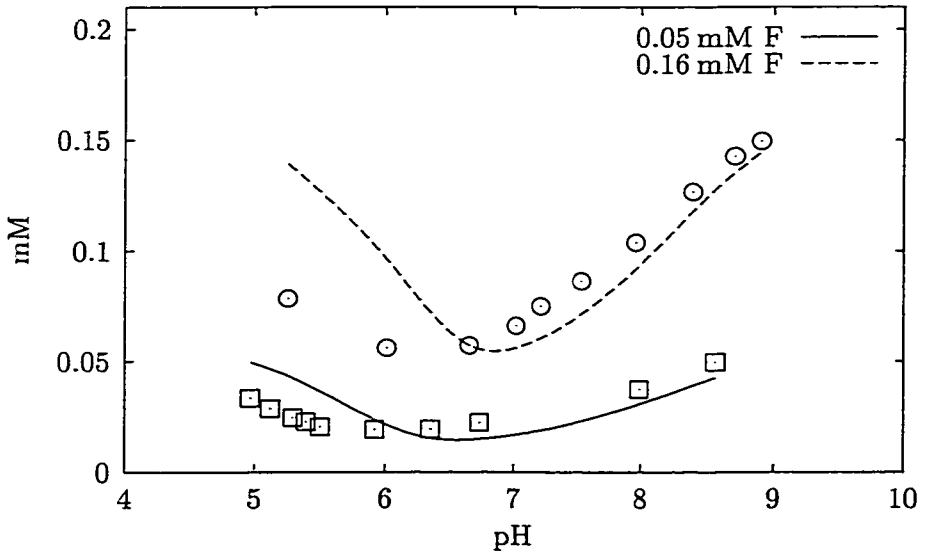

Figure 5.36. Model-predicted and measured dissolved fluoride concentration in the presence of 0.20 mM oxalic acid as a function of pH and total fluoride concentration.

complex. It may be necessary to supplement these data with other measurements, such as the proton uptake or release during the adsorption. Efforts are also being made by several researchers to characterize the nature of organic acid bonds on oxide surfaces by infrared spectroscopy (Biber and Stumm, 1994; Person *et al.*, 1998).

An additional difficulty in surface complexation modeling appears to be the considerable uncertainty with respect to the parameters that characterize the solid-water interface. A sensitivity analysis revealed that, for example, vastly different values for the specific surface area of the solid can yield a reasonable fit for given ζ-potential data. Part of this problem lies in the different methods that can be used to determine this parameter, e.g., BET-adsorption, negative adsorption, deuterium or tritium exchange. Davis and Leckie (1978b) pointed out that the values for A_S can span several hundred m^2/g. Thus, more than one value can be "right" as some of the modeling results in this work suggest.

A similar argument can be made regarding the interfacial capacitances, C_1 and C_2. The model-fitted diffuse layer potentials were fairly sensitive to the selection of these values, and it has also been pointed out that C_1 can vary among different oxides and with ionic strength and the applicability of $C_2 = 0.2\,F/m^2$ to oxides may also be questionable (Lützenkirchen, 1998).

Considering that natural waters have a more complex composition than the aqueous solutions examined in this work, the goal of being able to model such a system may seem far out of reach. However, it may only be necessary to achieve self-consistency, neglecting the uncertainties in some parameters as long as they remain unchanged.

5.5. Summary

Data obtained from single and binary adsorbate experiments were used to determine whether surface complexation modeling would adequately predict the competitive adsorption of inorganic and organic anions to aluminum hydroxide. Using literature values as initial guesses and electrokinetic data, surface acidity and eletrolyte adsorption constant were determined. However, the parameter estimation also indicated that these values are not necessarily unique, as the variation of interfacial capacitances, specific surface area, and surface site density also yielded an acceptable model fit.

The adsorption of single inorganic or organic adsorbates to aluminum hydroxide could be simulated well in most cases. In general, good agreement between model-predicted and measured pH_{iep} was also achieved. However, modeling the binary sulfate-organic acid system yielded the disconcerting result that the affinity of the inorganic ion was greatly overpredicted by the model. The competitive adsorption modeling of organic acids and fluoride or orthophosphate was not affected as strongly. However, these inorganic ions were added at much lower concentrations than sulfate. Despite these drawbacks, surface complexation modeling can potentially be used for predicting both adsorption to and electrokinetic properties of aluminum hydroxide particles and thus serve as a tool for estimating particle and natural organic matter removal by metal salt coagulation.

6. SUMMARY

With the development of more stringent regulations for drinking water quality, including lower limits for disinfection byproducts (DBPs), greater removal requirements for DBP precursor material, and enhanced elimination of chlorine-resistant, pathogenic microorganisms, utility operators, researchers, and engineers have recently focussed on implementing advanced treatment techniques to meet these new objectives. However, particularly smaller utilities that practice conventional treatment would often be faced with major capital investments if they pursued this avenue, and thus resort to making incremental changes to their processes. These may include switching to chloramination for residual disinfection to minimize DBP formation, decreasing the coagulation treatment pH to improve precursor removal, and applying organic polymers as coagulation and filtration aids. Although these treatment alterations are likely to be beneficial, during process optimization, more emphasis should be placed on the influence that some inorganic anions may have on the water chemistry and therefore on the overall treatment.

This work has focussed on examining the influence that fluoride, sulfate, and orthophosphate can have on the removal of organic substances by adsorption to amorphous aluminum hydroxide. These chemicals may be present at elevated levels in raw waters but they can also enter the treatment process where fluoridation, corrosion control, or coagulation with sulfate-based metal salts is practiced. Both electrokinetic measurements in batch adsorption experiments and bench- and pilot-scale testing also enabled to elucidate the effects on removal of particulate matter by metal salt coagulation.

Jar test results indicated that the efficiency of natural organic matter and particle removal by coagulation with alum is substantially decreased when fluoride is added to the raw water at concentrations typically used in water treatment plants. Based on equilibrium calculations, tests with iron-based coagulants, and variation of the point of addition, it was concluded that the observed detrimental effects were primarily due to the ability of fluoride to bond with aluminum *prior* to the formation of aluminum hydrolysis products, which are needed to destabilize particles and provide adsorption sites for natural organic matter. A

utility would therefore have to add higher alum doses in order to achieve the same removal rates that would be obtained in the absence of fluoride. If fluoride is added for dental caries prophylaxis, it may also be removed by adsorption to floc, incurring additional chemical costs. Pilot studies clearly confirmed these findings and also indicated that the addition of fluoride to the raw water at pH 6 results in a tenfold increase in finished water aluminum concentrations, which can not only cause operational problems within the water distribution system, but may also have implications on public health.

Batch adsorption experiments and surface complexation modeling showed that fluoride competes moderately with simple organic acids for adsorption sites on freshly precipitated aluminum hydroxide. Because fluoride forms uncharged surface complexes, it cannot directly impact particle charge and thus removal in water treatment, supporting the finding that its primary influence is the ability to form soluble complexes with aluminum.

The effects that sulfate has on coagulation with alum are more obscure. Although the batch adsorption experiments indicated that it can compete with organic acids for adsorption to positively charged aluminum floc, jar tests did not yield conclusive evidence that this ion has a considerable influence on turbidity and natural organic matter removal. The latter observation may have been due to the fact that alum (aluminum sulfate) was used in these tests. Thus, sites for adsorption of sulfate may have been saturated and any excess sulfate could not exert the effects observed in the batch adsorption experiments, where aluminum hydroxide was prepared from the chloride salt. Further research comparing sulfate versus non-sulfate based coagulants (e.g., ferric sulfate and ferric chloride) would probably help elucidate this influence. It has, however, been confirmed that sulfate has the ability to limit the positive charge of aluminum precipitates by adsorption. Therefore, sulfate can prevent the negative effects of particle restabilization due to overdosing the coagulant and help induce rapid floc formation.

The ability of orthophosphate to affect conventional treatment with alum was tested in batch adsorption experiments with preformed aluminum hydroxide and simple and natural organic acids. These results indicated that orthophosphate exerted the greatest influence among the inorganic anions on the removal of simple organic acids. Orthophosphate was found to form negatively charged surface complexes on aluminum hydroxide and thus affect

particle charge and stability. It also competed strongly with organic matter for adsorption sites, where both fluoride and sulfate at similar concentrations did not have any perceptible influence. Therefore, when it is present in raw waters or added during water treatment at a point upstream of coagulation or filtration processes and where aluminum based coagulants are used, significant detrimental effects on the removal of natural organic matter and particle removal can be expected. As with fluoride, these effects may be overcome by higher coagulant doses. However, hydrologic events, the occasional use of supplemental water sources, or recycling of spent backwash water can cause rapid changes in the ionic composition of the raw water, requiring the operator to immediately respond in order to avoid a risk to public health.

In this work, the foundation of a predictive, theory-based model was developed that could enable treatment plant operators to assess the effects that these anions may exert on coagulation with alum. Data obtained from experiments involving the competitive adsorption of inorganic and organic anions to preformed aluminum hydroxide floc were used for input into the model. Although good model fits were obtained for all anions in single adsorbate systems, only the model predictions in the binary systems with fluoride and orthophosphate yielded satisfactory results. Therefore, a reevaluation of the model with respect to sulfate is required before it can be further applied.

REFERENCES

Ali M. A. and Dzombak D. A. (1996a) Competitive sorption of simple organic acids and sulfate on goethite. *Environ. Sci. Technol.* **30**, 1061–1071.

Ali M. A. and Dzombak D. A. (1996b) Effects of simple organic acids on sorption of Cu^{2+} and Ca^{2+} on goethite. *Geochim. Cosmochim. Acta* **60**, 291–304.

Allison J. D., Brown D. S. and Novo-Gradac K. J. (1993) *MINTEQA2 / PRODEFA2: A Geochemical Assessment Model for Environmental Systems*. Environmental Research Laboratory, Office of Research and Development, U.S. EPA, Athens, Georgia.

American Dental Association (1995) California Fluoride Bill Becomes Law. Dental News Digest.

Amirtharajah A. and O'Melia C. R. (1990) Coagulation processes: Destabilization, mixing, and flocculation. In *Water Quality and Treatment – A Handbook of Community Water Supplies* (Edited by F. W. Pontius), 4th ed. McGraw-Hill, New York.

Anderson P. R. and Benjamin M. M. (1990a) Modeling adsorption in aluminum-iron binary oxide suspensions. *Environ. Sci. Technol.* **24**, 1586–1592.

Anderson P. R. and Benjamin M. M. (1990b) Surface and bulk characteristics of binary oxide suspensions. *Environ. Sci. Technol.* **24**, 692–698.

Balistrieri L. S. and Murray J. W. (1987) The influence of the major ions of seawater on the adsorption of simple organic acids by goethite. *Geochim. Cosmochim. Acta* **51**, 1151–1160.

Bar-Yosef B., Afik I. and Rosenberg R. (1988) Fluoride sorption by montmorillonite and kaolinite. *Soil Science* **145**, 194–200.

Biber M. V. and Stumm W. (1994) An in-situ ATR-FTIR study: The surface complexation of salicylic acid on aluminum and iron(III) oxides. *Environ. Sci. Technol.* **28**, 763–768.

Black A. P. and Willems D. G. (1961) Electrophoretic studies of coagulation for removal of organic color. *J. Am. Water Works Assoc.* **53**, 589–604.

Boggs P. T., Byrd R. H., Rogers J. E. and Schnabel R. B. (1992) *User's Reference Guide for ODRPACK Version 2.01 Software for Weighted Orthogonal Distance Regression*. Computing and Applied Mathematics Laboratory, National Institute of Standards and Technology, Gaithersburg, MD. NISTIR 4834.

Boggs P. T. and Rogers J. E. (1989) *Orthogonal Distance Regression*. Tech. Rep. NISTIR 89–4197, Computing and Applied Mathematics Laboratory, National Institute of Standards and Technology, Gaithersburg, MD. Revised July, 1992.

Boisvert J.-P., To T. C., Berrak A. and Jolicoeur C. (1997) Phosphate adsorption in flocculation processes of aluminum sulphate and poly-aluminum-silicate-sulphate. *Water Res.* **31**, 1939–1946.

Boller M. A. (1984) Chemical optimization of tertiary contact filters. *J. Environ. Eng.* **110**, 263–276.

Bose P. and Reckhow D. A. (1998) Adsorption of natural organic matter on preformed aluminum hydroxide flocs. *J. Environ. Eng.* **124**, 803–811.

Bottero J. Y. and Bersillon J. L. (1989) Aluminum and iron(III) chemistry: Some implications for organic substances removal. In *Aquatic Humic Substances: Influence on Fate and Treatment of Pollutants* (Edited by I. Suffet and P. MacCarthy). American Chemical Society, Washington, DC.

Bower C. A. and Hatcher J. T. (1967) Adsorption of fluoride by soils and minerals. *Soil Science* **103**, 151–154.

Bowers A. R. and Huang C. P. (1987) Role of Fe(III) in metal complex adsorption by hydrous solids. *Water Res.* **21**, 757–764.

Cathalifaud G., Ayele J. and Mazet M. (1997) Etude de la complexation de ions aluminium par des molécules organiques: Constantes et stœchiométrie des complexes. application au traitement de potabilisation des eaux. *Water Res.* **31**, 689–698.

Cheng W. P. and Huang C. (1996) Adsorption characteristics of iron-cyanide complex on γ-Al_2O_3. *J. Colloid Interface Sci.* **181**, 627–634.

Choi W. W. and Chen K. Y. (1979) The removal of fluoride from waters by adsorption. *J. Am. Water Works Assoc.* **71**, 562–570.

Chowdhury Z. K., Amy G. L. and Bales R. C. (1991) Coagulation of submicron colloids in water treatment by incorporation into aluminum hydroxide floc. *Environ. Sci. Technol.* **25**, 1766–1773.

Cleasby J. L. (1990) Filtration. In *Water Quality and Treatment – A Handbook of Community Water Supplies* (Edited by F. W. Pontius), 4th ed. McGraw-Hill, New York.

Corey R. B. (1981) Adsorption vs precipitation. In *Adsorption of Inorganics at Solid-Liquid Interfaces* (Edited by M. Anderson and A. Rubin). Ann Arbor Science, Ann Arbor, Michigan.

Crawford R. J., Harding I. H. and Mainwaring D. E. (1996) The zeta potential of iron and chromium hydrous oxides during adsorption and coprecipitation of aqueous heavy metals. *J. Colloid Interface Sci.* **181**, 561–570.

Crozes G., White P. and Marshall M. (1995) Enhanced coagulation: Its effects on NOM removal and chemical costs. *J. Am. Water Works Assoc.* **87**, 78–89.

Dalang F., Buffle J. and Haerdi W. (1984) Study of the influence of fulvic substances on the adsorption of copper(II) at the kaolinite surface. *Environ. Sci. Technol.* **18**, 135–141.

Davis J. A. (1982) Adsorption of natural dissolved organic matter at the oxide/water interface. *Geochim. Cosmochim. Acta* **46**, 2381–2393.

Davis J. A. and Kent D. B. (1990) Surface complexation modeling in aqueous geochemistry. In *Mineral-water Interface Geochemistry* (Edited by M. F. Hochella Jr and A. F. White). The Mineralogical Society of America, Washington, DC.

Davis J. A. and Leckie J. O. (1978a) Effect of adsorbed complexing ligands on trace metal uptake by hydrous oxides. *Environ. Sci. Technol.* **12**, 1309–1315.

Davis J. A. and Leckie J. O. (1978b) Surface ionization and complexation at the oxide/water interface. II. Surface properties of amorphous iron oxyhydroxide and adsorption of metal ions. *J. Colloid Interface Sci.* **67**, 90–107.

Dempsey B. A. (1989) Reactions between fulvic acid and aluminum: Effects on the coagulation process. In *Aquatic Humic Substances: Influence on Fate and Treatment of Pollutants* (Edited by I. H. Suffet and P. MacCarthy). American Chemical Society, Washington, DC.

Doren A., Lemaitre J. and Rouxhet P. G. (1989) Determination of the zeta potential of macroscopic specimens using microelectrophoresis. *J. Colloid Interface Sci.* **130**, 146–156.

Driscoll C. T. and Letterman R. D. (1988) Chemistry of Al(III) in treated drinking water. *J. Environ. Eng.* **114**, 21–37.

Dzombak D. A. and Morel F. M. M. (1990) *Surface Complexation Modeling: Hydrous Ferric Oxide*. John Wiley and Sons, New York.

Eaton A. D., Clesceri L. S. and Greenberg A. E., editors (1995) *Standard Methods for the Examination of Water and Wastewater*. 19th ed. American Public Health Association, Washington, D.C.

Edwards M. A. (1997) Predicting DOC removal during enhanced coagulation. *J. Am. Water Works Assoc.* **89**, 78–89.

Edzwald J. K., Becker W. C. and Wattier K. L. (1985) Surrogate parameters for monitoring organic matter and THM precursors. *J. Am. Water Works Assoc.* **77**, 122–132.

Evanko C. R. and Dzombak D. A. (1998) Influence of structural features on sorption of NOM-analogue organic acids to goethite. *Environ. Sci. Technol.* **32**, 2846–2855.

Evanko C. R. and Dzombak D. A. (1999) Surface complexation modeling of organic acid sorption to goethite. *J. Colloid Interface Sci.* **214**, 189–206.

Fox K. R. and Lytle D. A. (1996) Milwaukee's crypto outbreak: Investigation and recommendations. *J. Am. Water Works Assoc.* **88**, 87–94.

Hall E. S. and Packham R. F. (1965) Coagulation of organic color with hydrolyzing coagulants. *J. Am. Water Works Assoc.* **57**, 1149–1166.

Hanna G. P. and Rubin A. J. (1970) Effect of sulfate and other ions in coagulation with aluminum(III). *J. Am. Water Works Assoc.* **62**, 315–321.

Hansmann D. D. and Anderson M. A. (1985) Using electrophoresis in modeling sulfate, selenite, and phosphate adsorption onto goethite. *Environ. Sci. Technol.* **19**, 544–551.

Hao O. J. and Huang C. P. (1986) Adsorption characteristics of fluoride onto hydrous alumina. *J. Environ. Eng.* **112**, 1054–1069.

Hawke D., Carpenter P. D. and Hunter K. A. (1989) Competitive adsorption of phosphate on goethite in marine electrolytes. *Environ. Sci. Technol.* **23**, 187–191.

Hayden P. L. (1971) *Aqueous Chemistry of Aluminum(III) and the Solubility and Colloidal Stability of Its Precipitates*. Ph.D. thesis, The Ohio State University.

Herbelin A. L. and Westall J. C. (1996) *FITEQL: A Computer Program For Determination of Chemical Equilibrium Constants From Experimental Data. Version 3.2*. Department of Chemistry, Oregon State University, Corvallis. Report 96-01.

Hingston F. J., Posner A. M. and Quirk J. P. (1972) Anion adsorption by goethite and gibbsite. *J. Soil Sci.* **23**, 177–192.

Hohl H. and Stumm W. (1976) Interaction of Pb^{2+} with hydrous γ-Al_2O_3. *J. Colloid Interface Sci.* **55**, 281–288.

Hsu P. H. (1975) Precipitation of phosphate from solution using aluminum salt. *Water Res.* **9**, 1155–1161.

Hunter R. J. (1981) *Zeta Potential in Colloid Science*. Academic Press, London.

Ioannou A. and Dimirkou A. (1997) Phosphate adsorption on hematite, kaolinite, and kaolinite-hematite (k-h) systems as described by a constant capacitance model. *J. Colloid Interface Sci.* **192**, 119–128.

Iyer D. R. (1984) *Modeling the Effects of Adsorbed Aluminum Hydrolysis Products and Solution Chemistry on Colloid Stability and Flocculation Kinetics*. Ph.D. thesis, Syracuse University.

Jekel M. R. (1986) Interactions of humic acids and aluminum salts in the flocculation process. *Water Res.* **20**, 1535–1542.

Julien F., Gueroux B. and Mazet M. (1994) Comparaison de l'élimination de molécules organiques par coagulation-floculation et par adsorption sur flocs d'hydroxyde métallique préformes. *Water Res.* **28**, 2567–2574.

Kosmulski M. (1997a) Adsorption of trivalent cations on silica. *J. Colloid Interface Sci.* **195**, 395–403.

Kosmulski M. (1997b) Comments on "The Zeta Potential of Iron and Chromium Hydrous Oxides during Adsorption and Coprecipitation of Aqueous Heavy Metals." *J. Colloid Interface Sci.* **198**, 516.

Kosmulski M. and Matijević E. (1992) Zeta potential of anatase (TiO_2) in mixed solvents. *Colloids Surf.* **64**, 57–65.

Kummert R. and Stumm W. (1980) The surface complexation of organic acids on hydrous γ-Al_2O_3. *J. Colloid Interface Sci.* **75**, 252–266.

Lefebvre E. and Legube B. (1993) Coagulation-floculation par le chlorure ferrique de quelques acides organique et phénols en solution aqueuse. *Water Res.* **27**, 433–447.

Letterman R. D. and Driscoll C. T. (1994) *Control of Residual Aluminum in Filtered Water*. American Water Works Association Research Foundation, Denver, Colorado.

Letterman R. D. and Iyer D. R. (1985) Modeling the effects of hydrolyzed aluminum and solution chemistry on flocculation kinetics. *Environ. Sci. Technol.* **19**, 673–681.

Letterman R. D. and Vanderbrook S. G. (1983) Effect of solution chemistry on coagulation with hydrolyzed Al(III): Significance of sulfate ion and pH. *Water Res.* **17**, 195–204.

Letterman R. D., Vanderbrook S. G. and Sricharoenchaikit P. (1982) Electrophoretic mobility measurements in coagulation with aluminum salts. *J. Am. Water Works Assoc.* **74**, 44–51.

Lijklema L. (1980) Interaction of orthophosphate with iron(III) and aluminum hydroxides. *Environ. Sci. Technol.* **14**, 537–541.

Lin C.-F., Chang K.-S., Tsay C.-W., Lee D.-Y., Lo S.-L. and Yasunaga T. (1997) Adsorption mechanisms of gallium (III) and indium (III) onto γ-Al_2O_3. *J. Colloid Interface Sci.* **188**, 201–208.

Lützenkirchen J. (1998) Parameter estimation for the triple layer model. analysis of conventional methods and suggestion for alternative possibilities. *J. Colloid Interface Sci.* **204**, 119–127.

Martell A. E. and Smith R. M. (1977) *Critical Stability Constants*, vol. 3: Other Organic Ligands. Plenum Press, New York.

Martell A. E. and Smith R. M. (1982) *Critical Stability Constants*, vol. 5: First Supplement. Plenum Press, New York.

Matijević E., Kratohvil S. and Stickels J. (1969) Counterion complexing and sol stability I: Coagulation effects of aluminum salts in the presence of fluoride ions. *J. Phys. Chem.* **73**, 564–570.

Matijević E., Mangravite F. J. and Cassell E. A. (1971) Stability of colloidal silica: IV. The silica-alumina system. *J. Colloid Interface Sci.* **35**, 560–568.

Maulding J. S. and Harris R. H. (1968) Effect of ionic environment and temperature on the coagulation of color-causing organic compounds with ferric sulfate. *J. Am. Water Works Assoc.* **60**, 460–477.

Mazet M., Angbo L. and Serpaud B. (1990) Adsorption de substances humique sur flocs d'hydroxyde d'aluminium préformés. *Water Res.* **24**, 1509–1518.

Meng X., Bang S. and Korfiatis G. (2000) Effects of silicate, sulfate, and carbonate on arsenic removal by ferric chloride. *Water Res.* **34**, 1255–1261.

Meng X. and Letterman R. D. (1993a) Effect of component oxide interaction on the adsorption properties of mixed oxides. *Environ. Sci. Technol.* **27**, 970–975.

Meng X. and Letterman R. D. (1993b) Modeling ion adsorption on aluminum hydroxide modified silica. *Environ. Sci. Technol.* **27**, 1924–1929.

Meng X. and Letterman R. D. (1996) Modeling cadmium and sulfate adsorption by $Fe(OH)_3/SiO_2$ mixed oxides. *Water Res.* **30**, 2148–2154..

Mesuere K. and Fish W. (1992) Chromate and oxalate adsorption on goethite 2 : Surface complexation modeling of competitive adsorption. *Environ. Sci. Technol.* **26**, 2365–2370.

Montgomery J. M. (1985) *Water Treatment Principles and Design*. John Wiley and Sons, New York.

Morel F. M. M. and Hering J. G. (1993) *Principles and Applications of Aquatic Chemistry*. John Wiley and Sons, New York.

Narkis N. and Rebhun M. (1977) Stoichiometric relationship between humic and fulvic acids and flocculants. *J. Am. Water Works Assoc.* **69**, 325–328.

Nowack B. and Sigg L. (1996) Adsorption of EDTA and metal-EDTA complexes onto goethite. *J. Colloid Interface Sci.* **177**, 106–121.

Oliver B. G., Thurman E. M. and Malcolm R. L. (1983) The contribution of humic substances to the acidity of colored natural waters. *Geochim. Cosmochim. Acta* **47**, 2031–2035.

Parkhurst D. L. and Appelo C. A. J. (1999) *User's Guide to PHREEQC (Version 2)*. U.S. Geological Survey, Lakewood, Colorado. Water-Resources Investigations Report 99-4259.

Person P., Nordin J., Rosenqvist J., Lövgren L., Öhman L.-O. and Sjöberg S. (1998) Comparison of the adsorption of o-phthalate on boehmite (γ-AlOOH), aged γ-Al_2O_3, and goethite (α-FeOOH). *J. Colloid Interface Sci.* **206**, 252–266.

Rahni M. and Legube B. (1996) Mécanisme de la précipitation de l'acide salicylique par coagulation par le fer ferrique. *Water Res.* **30**, 1149–1160.

Rakotonarivo E., Tondre C., Bottero J. Y. and Mallevialle J. (1989) Complexation de l'aluminium(III) polymérisé et hydrolysé par les ions salicylate. Etude cinétique et thermodynamique. *Water Res.* **23**, 1137–1145.

Randtke S. J. (1988) Organic contaminant removal by coagulation and related process combinations. *J. Am. Water Works Assoc.* **80**, 40–56.

Roberson C. E. and Hem J. D. (1969) *Solubility of Aluminum in the Presence of Hydroxide, Fluoride and Sulfate*. U.S. Geological Survey, Washington, DC. Water Supply Paper 1827-C.

Rohmann U. and Sontheimer H. (1982) Mechanismen bei der Sorption organischer Säuren an Aluminiumoxid. *Vom Wasser* **58**, 143–164.

Schafran G. C. and Driscoll C. T. (1987) Temporal and spatial variation in the aluminum chemistry of a dilute acid lake. *Biogeochemistry* **3**, 105–119.

Schecher W. D. and McAvoy D. C. (1998) *MINEQL+: A Chemical Equilibrium Modeling System, Version 4.0 for Windows*. Environmental Research Software, Hallowell, Maine.

Schindler P. W. (1981) Surface complexes at oxide-water interfaces. In *Adsorption of Inorganics at Solid-Liquid Interfaces* (Edited by M. Anderson and A. Rubin). Ann Arbor Science, Ann Arbor, Michigan.

Semmens M. J. and Fields T. K. (1980) Coagulation: Experiences in organics removal. *J. Am. Water Works Assoc.* **72**, 476–483.

Sikora F. J. and McBride M. B. (1989) Aluminum complexation by catechol as determined by ultraviolet spectrophotometry. *Environ. Sci. Technol.* **23**, 349–356.

Snodgrass W. J., Clark M. M. and O'Melia C. R. (1984) Particle formation and growth in dilute aluminum(III) solutions. *Water Res.* **18**, 479–488.

Snoeyink V. L. and Jenkins D. (1980) *Water Chemistry*. John Wiley and Sons, New York.

Sricharoenchaikit P. and Letterman R. D. (1987) Effect of Al(III) and sulfate ion on flocculation kinetics. *J. Environ. Eng.* **113**, 1120–1138.

Stumm W. and Morgan J. J. (1996) *Aquatic Chemistry: Chemical Equilibria and Rates in Natural Waters*. 3rd ed. John Wiley and Sons, New York.

Sung W. and Rezania S. (1985) The effect of pH and fluoride on the soluble fraction of aluminum in water coagulated with alum. *Environ. Technol. Lett.* **6**, 20.

Thurman E. M. (1985) *Organic Geochemistry of Natural Waters*. M. Nijhoff/Dr. W. Junk Publishers, Dordrecht, Netherlands.

U.S. Environmental Protection Agency (1996) National primary drinking water regulations: Monitoring requirements for public drinking water supplies; final rule. *Federal Register* **61**, 24353–24388.

U.S. Environmental Protection Agency (1998) National primary drinking water regulations: Disinfectants and disinfection byproducts; final rule. *Federal Register* **63**, 69389–69476.

U.S. Environmental Protection Agency (2000) National primary drinking water regulations: Long term 1 enhanced surface water treatment and filter backwash rule; proposed rule. *Federal Register* **65**, 19045–19094.

Van Benschoten J. E. and Edzwald J. K. (1990a) Chemical aspects of coagulation using aluminum salts I : Hydrolytic reactions of alum and polyaluminum chloride. *Water Res.* **24**, 1519–1526.

Van Benschoten J. E. and Edzwald J. K. (1990b) Chemical aspects of coagulation using aluminum salts II : Coagulation of fulvic acid using alum and polyaluminum chloride. *Water Res.* **24**, 1527–1535.

Varner J. A., Jensen K. F., Horvath W. and Isaacson R. L. (1998) Chronic administration of aluminum-fluoride or sodium-fluoride to rats in drinking water: Alterations in neuronal and cerebrovascular integrity. *Brain Res.* **784**, 284–298.

Venema P., Hiemstra T. and van Riemsdijk W. H. (1997) Interaction of cadmium with phosphate on goethite. *J. Colloid Interface Sci.* **192**, 94–103.

Virginia Department of Health (1995) Waterworks regulations.

Westall J. C. (1980) Chemical equilibrium including adsorption on charged surfaces. In *Particulates in Water: Characterization, Fate, Effects, and Removal* (Edited by M. C. Kavanaugh and J. O. Leckie), vol. 189 of *Advances in Chemistry*. American Chemical Society.

Westall J. C. (1987) Adsorption mechanisms in aquatic surface chemistry. In *Aquatic Surface Chemistry: Chemical Processes at the Particle-Water Interface* (Edited by W. Stumm). John Wiley and Sons, New York.

White M. C., Thompson J. D., Harrington G. W. and Singer P. C. (1997) Evaluating criteria for enhanced coagulation compliance. *J. Am. Water Works Assoc.* **89**, 64–77.

Zachara J. M., Girvin D. C., Schmidt R. L. and Resch C. T. (1987) Chromate adsorption on amorphous iron oxyhydroxide in the presence of major groundwater ions. *Environ. Sci. Technol.* **21**, 589–594.

Appendix

A. COMPUTER PROGRAMS FOR CALCULATING CHEMICAL EQUILIBRIA

There are numerous computer programs available for calculating the speciation of elements in aqueous solution. Those used in this work, FITEQL (Herbelin and Westall, 1996), MINEQL+ (Schecher and McAvoy, 1998), and PHREEQC (Parkhurst and Appelo, 1999), although designed for different purposes, all rely on the same mathematical formulation describing the association of ions in aqueous solutions as described below.

Among the programs used in this work, FITEQL has the most simple chemical equilibrium solver and the ability to simulate precipitation and dissolution of solids and charge balance calculations is limited. However, FITEQL has algorithms implemented to estimate parameters from experimental data by weighted, nonlinear, ordinary regression. PHREEQC and MINEQL+ lack this feature, but these programs include advanced charge balance and phase transformation algorithms. PHREEQC has additional capabilities for batch-reaction and transport calculations, ion-exchange, kinetically controlled reactions, mixing and temperature changes, and inverse modeling. Despite this rich set of features, the triple layer surface complexation model, which was utilized in this work, is not incorporated in PHREEQC. Both MINEQL+ and PHREEQC are also supplied with a thermodynamic database containing equilibrium constants of several hundred inorganic and organic species. Although the use of these tables can be convenient, there is no assurance of consistency among the data derived from various sources.

The computer programs have in common that any chemical species is described in terms of "master species" (or "components") representing an element or element valence state. For example, the aqueous chemistry of calcium carbonate can be described as a combination of the "free" concentrations of the components Ca^{2+}, H^+, and $CO_3{}^{2-}$ and knowing the necessary equilibrium constants, K. Therefore, the concentration of bicarbonate would be $[HCO_3^-] = [H^+][CO_3^{2-}]K$, or similarly, a hydroxocalcium complex $[CaOH^+] = [Ca^{2+}][H^+]^{-1}[H_2O]K$. Typically, for computational purposes, these equations are transformed in their logarithmic forms, in which they can be manipulated through linear algebra. In PHREEQC, chemical reactions can be input in symbolic form, whereas the

coefficients of the logarithmic terms have to be entered directly in FITEQL and MINEQL+ using a tableau. The above examples would be entered as

Species	H^+	Ca^{2+}	CO_3^{2-}	H_2O	$\log K$
H^+	1	0	0	0	0
Ca^{2+}	0	1	0	0	0
CO_3^{2-}	0	0	1	0	0
HCO_3^-	1	0	1	0	10.33
$CaOH^+$	-1	1	0	1	-12.78

Morel and Hering (1993) have extensively discussed expressing mole balance equations in this manner. Precipitation and dissolution, effects of ionic strength, and surface complexation can essentially all be incorporated in this framework, of which an overview is provided below.

A.1. Precipitation and Dissolution

In the most simple way, a solid can be incorporated in the existing framework, by incorporating the phase as a "component" with a fixed "free" concentration (or activity) that corresponds to the solubility product. All relevant solution species are then written in terms of this component. For example, the aluminum master species would be $Al(OH)_3(s)$ (not Al^{3+}) having a fixed free concentration of $10^{10.4}$ M. The activity of the solution species Al^{3+} would then be given as

$$\begin{aligned} \log\{Al^{3+}\} &= \log\{Al(OH)_3(s)\} + 3\log\{H^+\} - 3\log\{H_2O\} + \log K = \\ &= 10.4 - 3\log\{H^+\} \end{aligned}$$

Note that the activity of water is assumed to be 1. MINEQL+ and PHREEQC have more sophisticated routines to compute solid phases. A description of these algorithms can be found in the respective manuals (Schecher and McAvoy, 1998; Parkhurst and Appelo, 1999).

A.2. Calculation of the Equilibrium Speciation

The concentration C_i of any solution species $i = 1, \ldots n_s$ can be expressed as a function of the free concentrations X_j of independent components $j = 1, \ldots n_c$, and it can be written

in the general form:

$$\log C_i = \log K_i + \sum_{j=1}^{n_c} a_{ij} \log X_j \tag{A.1}$$

or in matrix notation:

$$\log \boldsymbol{C} = \log \boldsymbol{K} + A \log \boldsymbol{X} \tag{A.2}$$

where a_{ij} represent the stoichiometric coefficients in the mass action expression. In common equilibrium problems, the vector of free concentrations $\boldsymbol{X}$ is generally not known, usually only the total (or analytical) concentration T_j of the component j is readily measurable. Given initial guesses for X_j, the total concentration for component j can be calculated using

$$T_j(\boldsymbol{X}) = \sum_{i=1}^{n_s} b_{ij} C_i \tag{A.3}$$

or in matrix notation

$$\boldsymbol{T} = B\ \boldsymbol{C} \tag{A.4}$$

where b_{ij} represent the stoichiometric coefficients in the mass balance expression, which are usually equal to a_{ij}. The goal of the equilibrium calculation is to find a set of X_j so that the differences r_j in calculated and observed total concentrations for all components j become zero (or less than an arbitrarily selected value, e.g., the machine precision):

$$r_j(\boldsymbol{X}) = T_j(\boldsymbol{X}) - T_j = 0 \tag{A.5}$$

The system of nonlinear equations represented by (A.5) can usually not be solved analytically. These problems can be evaluated iteratively using the Newton-Raphson method, which essentially involves approximating $r_j(\boldsymbol{X})$ by a Taylor series expansion, neglecting second and higher order terms, $O(\delta \boldsymbol{X}^2)$, and setting $r_j(\boldsymbol{X} + \delta \boldsymbol{X})$ to zero:

$$r_j(\boldsymbol{X}) + \sum_{k=1}^{n_c} \frac{\partial r_j(\boldsymbol{X})}{\partial X_k} \delta X_k = 0 \tag{A.6}$$

After rearranging, (A.6) can be written in matrix notation:

$$J\ \delta \boldsymbol{X} = -\boldsymbol{r}$$

which can be solved for $\delta \boldsymbol{X}$ using any of the available solution techniques for systems of linear algebraic equations (e.g., Gauss elimination, LU-decomposition, etc.). After updating

the free concentrations, i.e., $\boldsymbol{X}^{(i+1)} = \boldsymbol{X}^{(i)} + \delta\boldsymbol{X}$, the procedure started in (A.1) can be repeated until a suitable stopping criterion is met.

The elements of the Jacobian matrix J can be evaluated by replacing $T_j(\boldsymbol{X})$ in equation (A.5) and differentiation with respect to X_k:

$$\frac{\partial r_j}{\partial X_k} = \frac{\partial}{\partial X_k}\left(\sum_{i=1}^{n_s} b_{ij}C_i - T_j\right) = \sum_{i=1}^{n_s} b_{ij}\frac{\partial C_i}{\partial X_k} \tag{A.7}$$

The differentiation of (A.1) with respect to X_k results in

$$\begin{aligned} \frac{\partial \log C_i}{\partial X_k} &= \sum_{j=1}^{n_c} a_{ij} \underbrace{\frac{\partial \log X_j}{\partial X_k}}_{=0,\ \text{if } j \neq k} \\ \Rightarrow \frac{1}{C_i}\frac{\partial C_i}{\partial X_k} &= a_{ik}\frac{1}{X_k} \end{aligned}$$

which can be rearranged and substituted in (A.7) to yield the final expression for the derivatives in J :

$$\frac{\partial r_j}{\partial X_k} = \sum_{i=1}^{n_s} \frac{b_{ij}a_{ik}C_i}{X_k}$$

A.3. Calculating Effects of Ionic Strength

To compensate for the effects of ionic strength, the chemical equilibrium computer programs used in this work utilize activity coefficients, γ_i, that relate the concentration of a species to its activity, $\{C_i\} = \gamma_i C_i$. These are computed from the ionic charge, Z, and the ionic strength, I, using Davies' equation (Morel and Hering, 1993):

$$-\log\gamma_i = AZ_i^2\left(\frac{\sqrt{I}}{1+\sqrt{I}} - bI\right)$$

where A and b are constants and the ionic strength is computed by

$$I = \frac{1}{2}\sum_i Z_i^2 C_i$$

In FITEQL, activity coefficients are incorporated into the model by introducing ionic strength as a "dummy component," I. This special component is defined the by its "free" concentration, X_I and computed from an initial guess for I:

$$\log X_I = -A\left(\frac{\sqrt{I}}{1+\sqrt{I}} - bI\right) \tag{A.8}$$

Thus, a mass action law can be written as follows, for example:

$$\begin{aligned}\log[\mathrm{HCO_3^-}] &= 10.33 + \log[\mathrm{H^+}] + \log[\mathrm{CO_3^{2-}}] + \log\gamma_{\mathrm{CO_3^{2-}}} + \log\gamma_{\mathrm{H^+}} - \log\gamma_{\mathrm{HCO_3^-}} \\ &= 10.33 + \log[\mathrm{H^+}] + \log[\mathrm{CO_3^{2-}}] + (Z^2_{\mathrm{CO_3^{2-}}} + Z^2_{\mathrm{H^+}} - Z^2_{\mathrm{HCO_3^-}})\log X_I\end{aligned}$$

Recognizing that the ionic charge of a "derived" species, e.g., $\mathrm{HCO_3}^-$, can be calculated from the charge of the components and their stoichiometric coefficients, equation (A.1) can be written more generally as

$$\log C_i = \log K_i + \sum_{j=1}^{n_c} a_{ij}\log X_j + \left(\sum_{j=1}^{n_c} a_{ij}Z_j^2 - (\sum_{j=1}^{n_c} a_{ij}Z_j)^2\right)\log X_I$$

Similarly, the ionic strength, i.e., the total "concentration" of I, is calculated using

$$T_I = I = \sum_{i=1}^{n_s} \frac{Z_i^2}{2} C_i$$

Therefore, computing the ionic strength corrected concentrations of a species requires that a column be added to matrix A in equation (A.2) containing the coefficients $\sum_{j=1}^{n_c} a_{ij}Z_j^2 - (\sum_{j=1}^{n_c} a_{ij}Z_j)^2$ for the component X_I. A column added to matrix B in equation (A.4) containing the coefficients $Z_i^2/2 = \frac{1}{2}(\sum_{j=1}^{n_c} a_{ij}Z_j)^2$ facilitates computing the total ionic strength for use in (A.8).

The residuals $r_j(\boldsymbol{X})$ can be calculated as usual (Equation A.5), but the elements $\partial r_j/\partial X_I$ of the Jacobian J have to be modified:

$$\frac{\partial r_j}{\partial X_I} = \sum_{i=1}^{n_s} \frac{b_{ij}a_{ik}C_i}{X_k}\frac{\partial X_I}{\partial I}; j = 1, \ldots, n_c$$

and

$$\frac{\partial r_I}{\partial X_I} = \sum_{i=1}^{n_s} \frac{b_{iI}a_{iI}C_i}{X_I}\frac{\partial X_I}{\partial I} - 1$$

The derivative $\partial X_I/\partial I$ equals

$$\begin{aligned}\frac{\partial X_I}{\partial I} &= -AX_I \ln 10 \frac{\partial\left(\frac{\sqrt{I}}{1+\sqrt{I}} - bI\right)}{\partial T_I} = \\ &= -AX_I \ln 10 \left(\frac{1}{2\sqrt{I}(1+\sqrt{I})^2} - b\right)\end{aligned}$$

The iteration result δX_I is subsequently used to update I (not X_I).

A.4. Surface Chemistry

The association of solutes with surface functional groups can be incorporated into chemical equibrium models without further modification. However, if the effects of surface charge are to be considered, some adaptations are required to account for electrostatic effects.

To accomplish this, the free energy of the chemical interaction ΔG^0_{chem} has to be increased by the electrostatic (i.e., coulombic) work to bring a mol of solute from the bulk solution to the surface (Stumm and Morgan, 1996).

$$\Delta G^0 = \Delta G^0_{\text{chem}} + \Delta G^0_{\text{coul}}$$

The apparent equilibrium constant of a surface complexation reaction can thus be expressed as

$$K_{\text{app}} = \exp\left(-\frac{\Delta G^0_{\text{chem}} + \Delta G^0_{\text{coul}}}{RT}\right) = K^{\text{int}} \exp\left(\frac{-\Delta G_{\text{coul}}}{RT}\right)$$

R and T are the molar gas constant and the temperature in Kelvin, respectively. Like with solute-solute interactions, K^{int} represents an "intrinsic" complexation constant, that is independent of ionic strength effects. The coulombic term can be evaluated when realizing that the electrostatic work to bring a mol of solute to the surface equals the change in the ionic charge of the surface group multiplied by the electrostatic potential at that adsorption layer, l:

$$\Delta G^0_{\text{coul}} = F \sum_l \Delta Z_l \psi_l$$

Therefore,

$$\begin{aligned} \log K_{\text{app}} &= \log K^{\text{int}} + \log \exp\left(\frac{-F \sum_l \Delta Z_l \psi_l}{RT}\right) \\ &= \log K^{\text{int}} + \sum_l \Delta Z_l \log \exp\left(\frac{-F\psi_l}{RT}\right) \end{aligned}$$

where F represents Faraday's constant. In the triple-layer surface complexation model, three special "components," representing the layers $l = 0, \beta, d$, can be introduced to substitute the exponential term with X_{ψ_l}:

$$\begin{aligned} X_{\psi_l} &:= \exp\left(\frac{-\psi_l F}{RT}\right) \\ \Rightarrow \log K_{\text{app}} &= \log K^{\text{int}} + \sum_{l=0,\beta} \Delta Z_l \log X_{\psi_l} \end{aligned}$$

For example, consider the following surface complexation reaction:

$$\equiv \mathrm{AlOH} + \mathrm{NO_3^-} + \mathrm{H^+} \rightleftharpoons \equiv \mathrm{AlOH_2^+NO_3^-}$$

Assume that the proton (H^+) adsorbs to the 0-layer, where it increases the charge ΔZ_0 by +1. The adsorption of the nitrate ion NO_3^- to the β-layer results in a decrease of the β-layer charge, i.e., $\Delta Z_\beta = -1$. Therefore the concentration of the surface species $\equiv AlOH_2^+NO_3^-$ can be written as:

$$\begin{aligned} \log[\equiv \mathrm{AlOH_2^+NO_3^-}] &= \log[\equiv \mathrm{AlOH}] + \log[\mathrm{H^+}] + \log[\mathrm{NO_3^-}] \\ &\quad + \log X_{\psi_0} - \log X_{\psi_\beta} + \log K^{\mathrm{int}} \end{aligned}$$

Note that in the triple layer model, no specific adsorption occurs at the d-layer.

Similar to the corrections for activity coefficients, the modifications for electrostatic effects at the solid-water interface can be incorporated by adding a column in arrays A and B for each adsorption layer. The total "analytical concentrations," T_l, of the special surface components, which are utilized to compute the residuals r_j in Equation (A.5), are not given by the user but computed recursively from charge balance considerations (Westall, 1980). In the triple layer model, these terms equate to

$$\begin{aligned} T_0 &= -\frac{A_S S}{F} C_1 \frac{RT}{F} (\log X_{\psi_0} - \log X_{\psi_\beta}) \\ T_d &= -\frac{A_S S}{F} C_2 \frac{RT}{F} (\log X_{\psi_d} - \log X_{\psi_\beta}) \\ T_\beta &= -T_0 - T_d \end{aligned}$$

where A_S and S represent the specific surface area and concentration of the adsorbent, respectively. The values for $T_0(\boldsymbol{X})$ and $T_\beta(\boldsymbol{X})$ in (A.5) are computed conventionally using Equation (A.3), where b_{i0} and $b_{i\beta}$ are given by ΔZ_l for that surface complex. $T_d(\boldsymbol{X})$ is replaced by the following equation derived from Gouy and Chapman's theory:

$$T_d(\boldsymbol{X}) = -\frac{A_S S}{2F} \sqrt{8RT\epsilon\epsilon_0 I 10^3} \left(\frac{1}{\sqrt{X_{\psi_d}}} - X_{\psi_d} \right)$$

The elements in the Jacobian matrix $\partial r_m / \partial X_{\psi_l} (l, m = 0, \beta, d)$ also require some modification. A listing of these terms can be found in Westall (1980).

The concepts presented here were also incorporated in the chemical equilibrium solver that was used in this work in conjunction with the weighted orthogonal regression software ODRPACK (Boggs and Rogers (1989); Boggs *et al.* (1992), refer to Section 5).

B. ANALYTICAL METHODS

All instrumental analyses conformed with Standard Methods (Eaton *et al.*, 1995) if applicable. All chemicals used in the preparation of standards and reagents were supplied by Fisher Scientific unless otherwise noted.

B.1. Turbidity

A bench top nephelometer MONITEK TA-1 was used exclusively for turbidity measurements of grab samples. Calibration and measurement procedures strictly adhered to the manufacturer's operating instructions. The instrument was always allowed to warm up for at least one hour before calibration or sample analysis. Lenses, light source, and glass cuvettes were kept meticulously clean. The sample cuvettes were acid washed periodically and stored in an inverted position between uses.

The turbidimeter was calibrated daily with secondary standards covering the expected range in turbidity. A primary turbidity standard was prepared periodically by dissolving 1.000 g of hydrazine sulfate $N_2H_4 \cdot H_2SO_4$ in deionized, distilled water and diluted to 100 ml in a volumetric flask. In a second flask, 10.00 g of hexamethylenetetramine, $(CH_2)_6N_4$, were dissolved in deionized, distilled water and diluted to 100 ml. Equal volumes of the hydrazine sulfate solution and the hexamethylenetetramine solution were combined in a clean flask. The mixture was allowed to stand for at least 48 hours at room temperature before use. Secondary standards were prepared by appropriate dilution of this 4000 NTU standard.

Sample cells were always filled with great care to avoid entrainment of gas bubbles. After the cuvette was filled and capped, the outside surface was dried with a clean, lint-free wipe. A single sample cuvette was used for calibration and all measurements to minimize the variability due to imperfections between cells. The cuvette was inserted in the turbidimeter with the same orientation each time it was used.

B.2. Particle Size Distribution

Particle size distribution analyses were performed immediately after the experiment with a multichannel particle counter (Coulter Multisizer II). This instrument determined the number and size of suspended particles using the electrical impedance method. For the analysis, a 50 μm orifice tube was selected to cover a nominal particle size range of 1.0 to 30 μm, and the data were accumulated in 128 channels. The aperture was calibrated with 9.90 μm latex particles suspended in an electrolyte solution (ISOTON II, Coulter Corporation). To obtain sufficient statistical accuracy a sample volume of 2000 μl was selected.

Because high particle concentrations may lead to coincidence effects, samples required dilution by a suitable ratio so that the coincidence loss was between 5% and 10%. As a calibration blank and for dilution, a commercially available electrolyte solution (ISOTON II), which had been twice filtered through a 0.2 μm polycarbonate membrane, was used. The blank count was always subtracted from the sample count and was always less than 5% of the total count in each channel. At least one sample out of twenty was split and spiked with latex particles of a known size to verify the calibration. Multiple replicates were run for each sample. Glassware that came in contact with the sample was scrupulously brushed and rinsed with filtered distilled, deionized water and filtered electrolyte solution.

B.3. Sulfate and Oxalate by Ion Chromatography

The determination of sulfate and oxalate was performed utilizing a DIONEX 4500i Ion Chromatograph. This instrument was equipped with a gradient pump module, a conductivity detector, and an anion exchange column specifically designed for the rapid analysis of inorganic anions including oxyhalides (DIONEX IonPac AS12A or AS14A). An IonPac Guard Column was placed in-line prior to the analytical column to prevent sample contaminants from eluting onto the analytical column. For enhanced sensitivity, the eluent was pumped through an anion suppressor (DIONEX ASRS-I) before delivery to the conductivity detector.

A personal computer with the manufacturer's supplied software (DIONEX PeakNet Version 4.3) was utilized to setup and operate the instrument and modules and to perform the

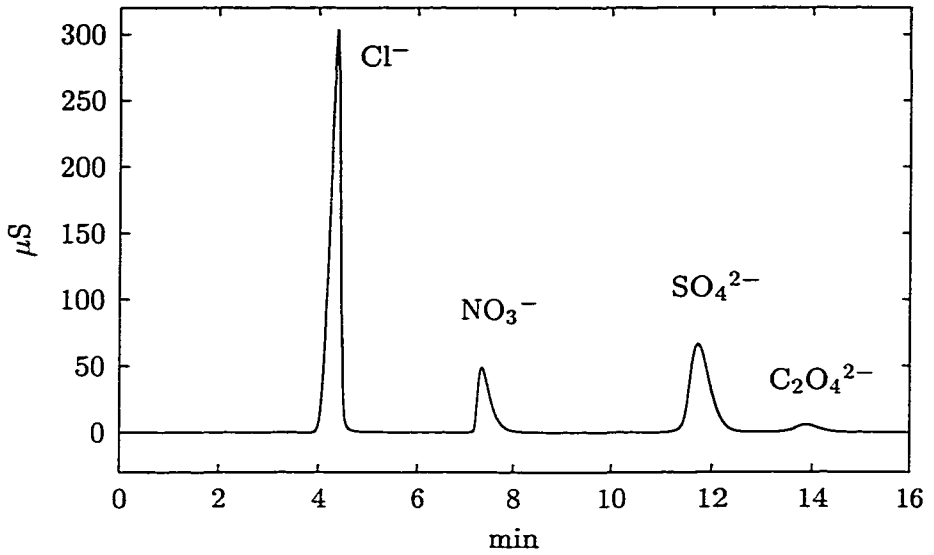

Figure B.1. Typical ion chromatogram.

integration of the chromatograms. Aside from the noise-filtering capabilities of the software, none of the special integration modes were needed.

The anions were always eluted isocratically at a flow rate of 1.0 ml/min utilizing a carbonate/bicarbonate eluent. The eluent was prepared according to the manufacturer's recommendations (AS12A: 2.7 mM Na_2CO_3, 0.3 mM $NaHCO_3$, AS14A: 3.5 mM Na_2CO_3, 1.0 mM $NaHCO_3$). Primary stock solutions of 0.5 M Na_2CO_3 and 0.5 M $NaHCO_3$ were made up from reagent grade chemicals.

At least five calibration standards were freshly prepared for each run by appropriate dilution of primary standards to cover the expected range of concentrations. The primary standards were made up from reagent grade sodium sulfate or sodium oxalate (Fisher Scientific) at a concentration of 0.5 M. Usually, three replicate injections were made for each sample. For both analytes, the relative standard deviation rarely exceeded two percent. Figure B.1 shows a typical chromatogram.

B.4. Electrophoretic Mobility, Zeta(ζ)-Potential

B.4.1. Linear Tracking Method

Electrophoretic mobility was analyzed with a Zeta Meter ZM-77 according to the manufacturer's operating instructions. Particular care was taken when filling the sample cell to avoid entrainment of gas bubbles that could influence the flow field in the channel. Usually, a voltage of 150 V was used. This potential was never applied for longer than 30 seconds to avoid heating of the sample. After a brief pause the polarity was reversed and the measurement resumed. To obtain reproducible results, at least ten particles were tracked.

The instrument was calibrated utilizing silica particles (MIN-U-SIL 5, U.S. Silica) suspended in a 1 mM potassium chloride solution. The mobility value of -4.3 μm cm/(V s) obtained from this calibration was well reproducible ($\sigma < 0.1\,\mu$m cm/(V s)).

B.4.2. Laser Doppler Velocimetry

Laboratory analyses of particle electrophoretic mobility were also conducted using a laser doppler velocimeter (Delsa 440, Coulter Corporation). This instrument utilizes the Doppler principle to measure the frequency distribution for the velocities of charged particles moving through an electrolyte solution due to an externally applied electric field. The supplied software converts electrophoretic mobility u_E (velocity/electric field) to ζ-potential based on Smoluchowski's equation (Hunter, 1981):

$$u_E = \frac{\epsilon_0 D}{\eta}\zeta$$

where ϵ_0 is the permittivity of free space ($8.854 \cdot 10^{-12}$ F/m). D and η are temperature dependent and represent the dielectric constant and the viscosity of water, respectively. Kosmulski (1997b) recently pointed out that "ζ-potentials of polydispersed, irregularly shaped and porous particles of unknown size distribution cannot be calculated from electrophoretic mobilities." For the purpose of this work, however, electrophoretic mobility was expressed as ζ-potential. Because during the analysis, the sample temperature was held constant at 25°C using the instruments' built-in thermostat, the ζ-potential values reported in this work can be easily converted to electrophoretic mobilities.

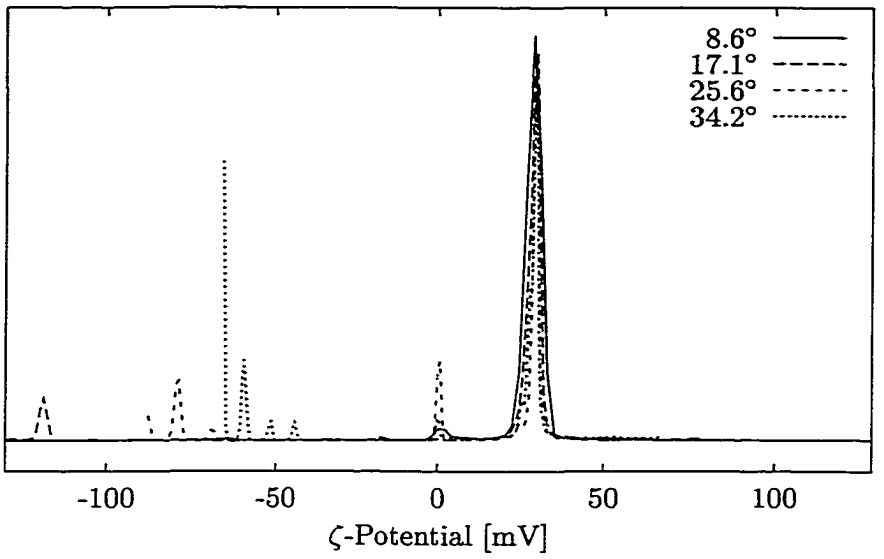

Figure B.2. Typical ζ-potential distribution for aluminum hydroxide particles ($\zeta = 29.2 \pm 1.8$ mV).

Prior to testing and after every cleaning of the sample cell, the conductivity detector of the instrument was calibrated using standard potassium chloride solutions. The instrument was tested for analytical bias using standard polystyrene latex particles supplied by the instrument manufacturer. Typically, the instrument was setup to measure for up to 60 s. The polarity was reversed every 2.5 s after a 0.5 s pause. All analyses were made at a constant current of 0.7 A. The instrument was set up to measure the scattered light intensity at four different angles. Arithmetic means and standard deviations of the four resulting mobility peaks were averaged for subsequent data analysis. Generally, all angles produced similar ζ-potential distributions as shown in Figure B.2.

To minimize errors due to large velocity gradients at the stationary layer and to compensate for potentially asymmetric mobility profiles due to particle attachment to the cell walls, at least five measurements at different depths of the channel were conducted. Consecutive measurements of the same sample were made without refilling the cell. In this work, there was no evidence of mobility shifts to lower values due to this practice, although these problems were seen in samples treated with ferric chloride and at higher ionic strength. Similar observations were reported by Kosmulski and Matijević (1992).

The ζ-potential of the particles in the sample was determined from the profile of appar-

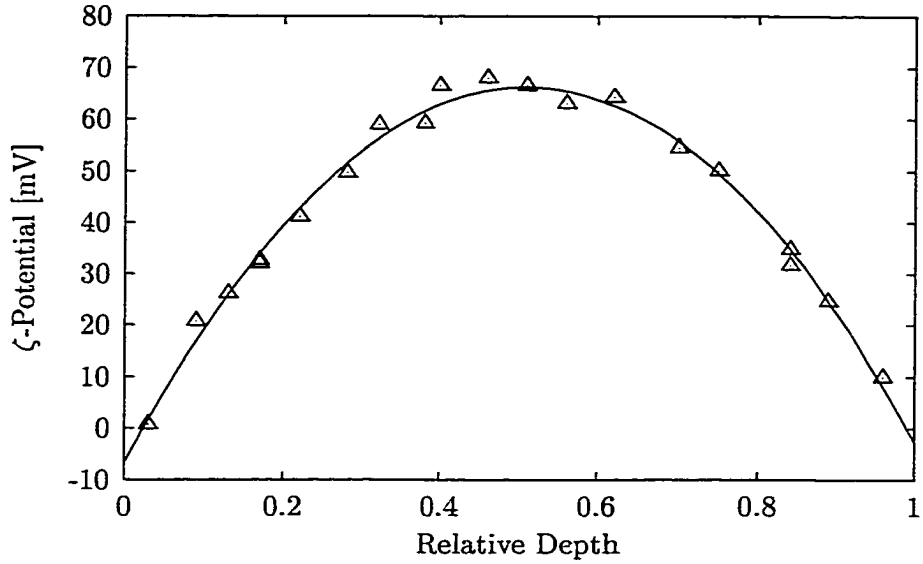

Figure B.3. Typical mobility profile for aluminum hydroxide particles (pH 6.8, $\zeta = 39.0 \pm 0.6$ mV).

ent mobility versus depth using the method outlined by Doren *et al.* (1989). This method basically involved fitting a second-order polynomial to the data and comparing the resulting regression coefficients with those in a theoretical expression for the apparent velocity distribution in the channel. The analysis was performed assuming that the velocities near the walls of the cells were similar. A cell height of 1.02 mm and width-to-height ratio of 3.18 were used in the calculations. The standard error in the calculated ζ-potential due to regression was generally less than the standard deviation of an individual measurement (< 2 mV). Typical mobility profiles are shown in Figures B.3 and B.4. In the first example, the profile was slightly asymmetrical; the stationary layers were determined to be at 0.18 and 0.86 relative cell depth, respectively.

B.5. Aluminum

Total and dissolved concentrations of aluminum were determined utilizing an atomic absorption spectrometer (Perkin Elmer 2100) at a wavelength of 309.3 nm. Sample aliquots were acidified with trace metal grade nitric acid to pH < 2 at least 12 hours prior to analysis. Analyses were conducted using either the flame or the graphite furnace technique depending on the metal concentrations in the sample. When using flame atomic absorption spectrom-

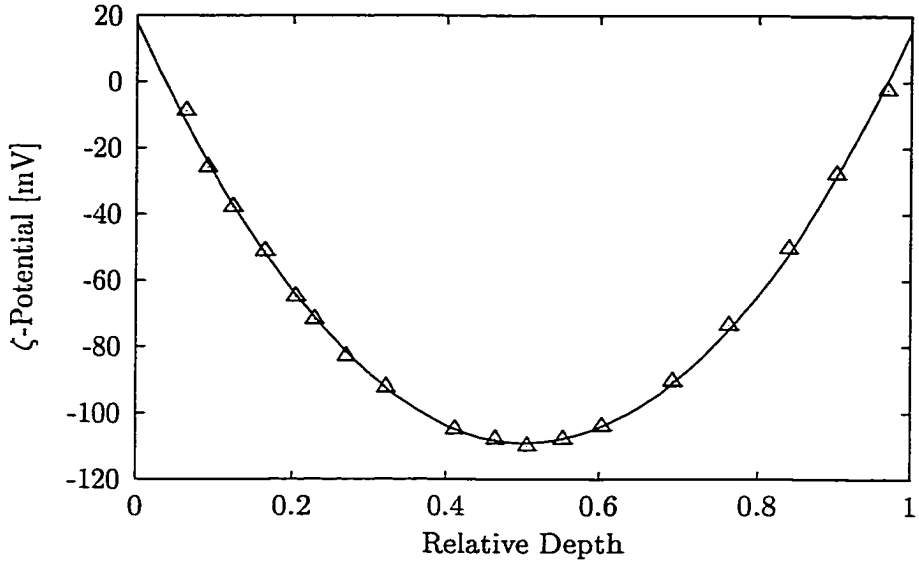

Figure B.4. Typical mobility profile for kaolin particles (pH 9.5, $\zeta = -51.0 \pm 1.0\,\mathrm{mV}$).

etry, the acidified sample was directly aspirated into a nitrous oxide - acetylene flame. The graphite furnace (Perkin Elmer HGA 700) was used if the concentration of the metal was below the detection limit for flame analysis ($\approx 0.3\,\mathrm{mg/l}$ as Al, $10\,\mu\mathrm{M}$). The instrument was calibrated for each run using standards made up from a commercially available aluminum reference solution. This primary standard was diluted to concentrations that covered the expected range of metal concentrations in the sample. At least three measurements were conducted per sample. The procedure was repeated if the relative standard deviation of the replicate measurements exceeded 10%.

B.6. pH

pH was measured using a glass electrode (Orion 8104) connected to a digital millivolt meter (Orion 920A). A three-point calibration of the pH-meter was performed before each set of samples using commercial standard buffer solutions (pH 4, 7, 10, Fisher Scientific). Between samples, the electrode was rinsed with deionized distilled water. When not in use, the probe was stored in a pH 7 phosphate buffer.

B.7. Non-Purgeable Organic Carbon

Non-purgeable organic carbon was analyzed with a Shimadzu TOC-5000 utilizing the combustion-infrared method. All samples were acidified to pH 2 with hydrochloric acid prior to analysis. A 1000 mg C/l organic carbon stock solution was prepared by dissolving reagent grade potassium hydrogen phthalate in carbon dioxide-free water. The instrument was calibrated using a series of dilutions of the stock solution that covered the expected range of organic carbon concentrations in the samples. The instrument was set up to sparge the acidified samples with synthetic air for seven minutes prior to injection to remove carbonate and volatile organics. Replicates of each sample were measured up to eight times or until the relative standard deviation met the preset maximum value of 2%.

B.8. Ultraviolet Absorbance

Ultraviolet light absorption at wavelengths of 220 to 390 nm were measured with a single-beam spectrophotometer (Milton Roy Spectronic 1201) with 10 and 50 mm quartz cells. For UV-scans, the data were resolved at wavelength intervals of 2 nm and automatically recorded through a computer interface. The spectrophotometer was zeroed for the selected wavelength region using deionized, distilled water, or, if the sample composition was known, a solution containing the same background electrolyte. Under the experimental conditions in this work and in the wavelength region of interest, sulfate, chloride and/or aluminum solutions were not distinguishable from distilled, deionized water. Nitrate, however, interfered considerably at lower wavelengths.

B.9. Fluoride

Fluoride was determined potentiometrically utilizing an ion selective combination electrode (ORION 9409) and a voltmeter with an expanded millivolt scale (ORION 920A). An equal amount of a decomplexing agent and ionic strength adjustment buffer was added to the samples and standards at least eight hours prior to analysis. The fluoride buffer was prepared by dissolving 4.0 g cyclohexylenediaminetetraacetic acid (CDTA, trans-1,2-Diaminocyclohexane-N,N,N',-tetraacetic acid monohydrate, Aldrich Chemical Company)

and 58 g of NaCl in a mixture of approximately 500 ml of distilled water and 57 ml of glacial acetic acid. After cooling, the solution was adjusted to pH 5.4 by addition of approximately 125 ml 6 N NaOH and diluted to 1000 ml with distilled, deionized water.

The Nernstian slope of the instrument was determined using a series of dilutions of a stock solution prepared from reagent grade sodium fluoride. Preliminary experiments using known fluoride standards showed that the measured fluoride concentration decreased by 5% at a total aluminum concentration of 100 μM Al. Because this analytical method is only capable to measure free fluoride, it was suspected that the reagent added to the sample did not effectively decomplex aluminum. Therefore, where aluminum concentrations were known to be in excess of 40 μM ($\approx$ 1 mg/l), a single known addition technique was employed. When this variation of the method was utilized, no analytical bias was observed. The necessary calculations were performed by the microprocessor controlled voltmeter.

B.10. Orthophosphate

Orthophosphate was analyzed utilizing the ascorbic acid reduction method (Eaton *et al.*, 1995). For this procedure, a potassium antimonyl tartrate solution was prepared by dissolving 1.3715 g of $K(SbO)C_4H_4O_6 \cdot \frac{1}{2}H_2O$ in 400 ml distilled, deionized water. An ammonium molybdate solution was made up from 20 g of $(NH_4)_6Mo_7O_{24} \cdot 4\,H_2O$ and 500 ml distilled, deionized water. A 0.1 M ascorbic acid solution was prepared weekly by dissolving 1.76 g of the pure chemical in distilled water. Five ml potassium antimonyl tartrate solution, 15 ml of the ammonium molybdate solution, and 30 ml of the ascorbic acid solution were sequentially combined with 50 ml 5 N H_2SO_4. Four ml of the combined reagent were added to 25 ml of sample or standard in an acid-washed flask and mixed thoroughly. After a reaction time of ten minutes but less than 30 minutes, the light absorbance at 880 nm was measured utilizing a spectrophotometer (Milton Roy Spectronic 1201) and a 10 mm quartz cell.

Four standards at concentrations up to approximately 20 μM (2 mg/l as PO_4^{3-}) were prepared from reagent grade anhydrous potassium phosphate, monobasic. Samples exceeding the calibration range were appropriately diluted with distilled, deionized water prior to the addition of the combined reagent. This analytical procedure was highly reproducible; the minimum detectable concentration was approximately 0.1μM.

VITA

for
Peter Pommerenk

DEGREES:

Master of Science (Environmental Engineering),
Old Dominion University, Norfolk, Virginia,
December 1996

Diplom Ingenieur (univ.) (Luft- und Raumfahrttechnik),
Universität der Bundeswehr München, Neubiberg (Germany)
December 1989